Università
Ca'Foscari
Venezia

PhD program in
Environmental Science

37° cycle

Research Thesis

in collaboration with GreenPropulsion Laboratory,
VERITAS spa

# Biological hydrogen production through Dark and Photo Fermentation and its applications for $CO_2$ bio-methanation

SSD: ICHI-02/A (formerly ING-IND/25)


**PhD coordinator**
Prof. Enrico Bertuzzo

**Supervisor**
Prof. Cristina Cavinato

**Company Supervisor**
Dr. Graziano Tassinato

**PhD candidate**
Marco Biasiolo
839245


**Year of dissertation**
2025

# Table of Contents

# Index of Figures

# Index of Tables

# Abbreviations

5-ALA – 5-aminolevulenic acid

AD – Anaerobic Digestion

AAD – Aldehyde Alcohol Dehydrogenase

ACK – Acetate Kinase

ADC – Acetoacetate Decarboxylase

ATP – Adenosine Triphosphate

AY – Acidification Yields

BA – Basic Anaerobic medium

BA-C – Basic Anaerobic medium, without carbonates

BChl *a* – Bacteriochlorophyll *a*

BCD – Butyryl-CoA Dehydrogenase

BM – Biological Methanation

BUK – Butyrate Kinase

COD – Chemical Oxygen Demand

CoQ10 – coenzyme Q10

DAD – Diode Array Detector

DF – Dark Fermentation

DFE – Dark Fermentation Effluent

DW – Dry Weight

FB – Fermentative Broth medium

$Fd_{ox}$ – Oxidized Ferredoxin

$Fd_{rd}$ – Reduced Ferredoxin

FW – Food Waste

GC – Gas Chromatography

HBD – β-Hydroxybutyryl-CoA Dehydrogenase

HC – Hydrodynamic Cavitation

HPB – Hydrogen-Producing Bacteria

HPLC - High Performance Liquid Chromatography

HPR – Hydrogen Production Rate

HRT – Hydraulic Retention Time

HY – Hydrogen production Yield

HYD – Hydrogenase

LAB – Lactic Acid Bacteria

LEDs – Light-Emitting Diodes

LDH – Lactate Dehydrogenase

MECs – Microbial Electrolysis Cells

NADH – Nicotinamide Adenine Dinucleotide

NDIR – Non-Dispersive Infrared

NFOR – NADH: Ferredoxin Oxidoreductase

OL – Organic Loading

OLR – Organic Loading Rate

PF – Photo Fermentation

PFOR – Pyruvate: Ferredoxin Oxidoreductase

PFL – Pyruvate: Formate Lyase

PNSB – Purple Non-Sulfur Bacteria

PPB – Purple Phototrophic Bacteria

PSB – Purple Sulfur Bacteria

PTA – Phosphotransacetylase

SHMA – Specific Hydrogenotrophic Methanogenic Activity

SHP – Specific Hydrogen Production

SGP – Specific Gas Production

SMP – Specific Methane Production

SRB – Sulfate-Reducing Bacteria

sCOD – soluble Chemical Oxygen Demand

THL – Thiolase

TS – Total Solids

TVS – Total Volatile Solids

VFAs – Volatile Fatty Acids

WAS – Waste Activated Sludge

WWTP – Wastewater Treatment Plant

# Abstract (ENG)

Hydrogen has been widely recognized as a promising energy vector to address global warming problems, offering a carbon-free and environmentally friendly alternative to fossil fuels. However, hydrogen production is nowadays almost entirely fossil-based and associated with intense carbon emissions. Reconceptualizing hydrogen production and utilization in an environmentally sustainable manner is imperative for it to become a viable clean energy source in a zero-carbon society. Among sustainable hydrogen production methods, biological processes have gained a lot of interest in recent years, allowing the conversion of organic waste into hydrogen under mild operative conditions and with minimal net greenhouse emissions. The objective of the thesis is i) to evaluate hydrogen production from food wastes and waste activated sludge by coupling Dark and Photo fermentation, and to assess its scalability from laboratory to pilot scale, and ii) to exploit hydrogen for e-fuel production through biological methanation. In Dark Fermentation, the best results were obtained under semi-continuous laboratory scale, while at pilot scale the process resulted in lower stability and yields. The coupling of the process with Photo Fermentation resulted feasible when mutated strains of bacteria, more tolerant to ammonia concentration, were involved. The $CO_2$ bio-methanation tests demonstrated the feasibility of the process, although satisfactory conversion yields were unattained.

**Keywords**: Hydrogen, Waste Treatment, Dark Fermentation, Photo Fermentation, Bio-Methanation

# Abstract (ITA)

L'idrogeno è riconosciuto come un promettente vettore energetico utile ad affrontare i problemi del riscaldamento globale, offrendo un'alternativa sostenibile ai combustibili fossili tradizionali. Tuttavia, la produzione di idrogeno ad oggi è quasi interamente basata sulla conversione di combustibili fossili, ed è associata a significative emissioni di carbonio in atmosfera. Reimmaginare lo scenario di produzione ed utilizzo dell'idrogeno è essenziale affinché questo possa diventare una valida fonte di energia pulita per una società a zero emissioni. Tra i metodi sostenibili di produzione di idrogeno, i processi biologici stanno guadagnando molto interesse negli ultimi anni, in quanto permettono la conversione di rifiuti organici ad idrogeno, in condizioni operative energeticamente favorevoli e con minime emissioni nette di gas serra. L'obiettivo della tesi è i) valutare la produzione di idrogeno da rifiuti alimentari e fanghi di supero tramite accoppiamento dei processi di *Dark Fermentation* e *Photo Fermentation*, valutandone la scalabilità da scala di laboratorio a quella pilota, e ii) sfruttare l'idrogeno prodotto per la produzione di e-fuel tramite metanazione biologica. Nella *Dark Fermentation*, i migliori risultati sono stati ottenuti in semicontinuo su scala da laboratorio, mentre lo *scale-up* a pilota ha evidenziato una diminuzione delle rese e della stabilità del processo. L'accoppiamento con la *Photo Fermentation* è risultato praticabile grazie all'uso di ceppi batterici mutati più tolleranti all'azoto ammoniacale. Nella bio-metanazione della $CO_2$, è stata evidenziata la fattibilità del processo, pur con rese di conversione non ancora ottimali.

# 1. Introduction

## 1.1. Energy transition: an urgent need

The climate crisis is undoubtedly one of the most critical challenges of our age, and it is escalating at a concerning pace, mainly boosted by the rising global temperature. The IPCC has repeatedly highlighted the problem in the last three decades, presenting concrete data and alarming future projections through successive reports, but a shift in direction still appears to be far off, despite its urgency. In the Sixth Assessment Report (AR6), IPCC states that human activities have driven a global surface temperature rise of 0.99–1.65 °C between 1750 and 2019 (IPCC, 2021) and, according to the current and inadequate climate policies in places, we are on track to maintain this increasing trend (UNEP, 2023). This could lead to temperatures rising above 3 °C by 2100, resulting in further and irreversible damage to our ecosystems, and exacerbating environmental degradation, natural disasters, weather extremes, food and water insecurity, economic disruption, as well as conflict and terrorism (IPCC, 2023; Lynas et al., 2021). Tackling global emissions and managing the reliance of our society on fossil fuels surely can play an important role in addressing this issue, achieving future energy sustainability and ensuring global security. To achieve these ambitious goals, it is crucial to identify secure, affordable, and sustainable alternative sources of energy.

Currently, fossil fuels (such as oil, coal, and natural gas) provide roughly 80% of the total primary energy consumed globally and are responsible for approximately 75 % of all global greenhouse gas emissions (Ritchie & Rosado, 2020). The remaining portion of the energy mix consists of low-carbon energy sources and is led by hydroelectric (6 % of the total) and nuclear power (4 %), with biofuels and all other renewables still representing a minor fraction of the total (bp p.l.c., 2024). Despite the use of renewable energy rising in the last years (+ 0.85 % in the global energy mix between 2019 and 2023, Ritchie & Rosado, (2020)), the transition is still currently too slow. Following this trajectory, the cumulative $CO_2$ emissions will keep rising and will exceed by the early 2040s the carbon budget set by IPCC as the threshold that should not

be crossed to limit global temperature rises below 2 °C (bp p.l.c., 2024). Keeping current emission levels will have further repercussions on all major climate system components, leading to irreversible changes on centennial to millennial time scales, with greater impacts as global warming intensifies (IPCC, 2023). This means that the effect of the choices and actions implemented in this decade will last long and that it is essential to implement urgent, effective, and fair mitigation and adaptation actions to prevent threats to ecosystems and ensure a viable future for the generations to come.

In the context of energy transition, hydrogen ($H_2$) can have a significant role in the shift from a fossil-based to a zero-carbon society and has been widely recognized as a promising tool to address global warming problems. The main assets hydrogen can provide in the race for energy transition consist of: (I) producing energy with no direct carbon emissions, (II) storing within its molecule the surplus energy from intermittent renewable sources, and (III) converting captured carbon dioxide back to an energy-rich substance by the production of e-fuels (Beyazit, 2025; Segovia-Hernández, 2025).

However, the role hydrogen can play in this framework is significantly limited by its current production methods, which in the vast majority of cases are fossil-based and associated with carbon emissions, and by its applications, which are often shifted to industrial manufacture more than to sustainable efforts. Thus, for hydrogen to become a viable clean energy source for a zero-carbon future society both its production methods and utilization must be re-evaluated. This can only be achieved by developing a deeper understanding of the available green production pathways, such as biological anaerobic fermentation, and advancing the scale-up of these processes, which are not yet widely implemented nor frequently developed beyond the pilot scale.

Among biological production processes, Dark Fermentation (DF) of organic waste stands out as one of the most sustainable green hydrogen production technologies. The sustainability of the process is mainly boosted by: (I) the lower carbon footprint, associated with the emission of biogenic rather than fossil-derived $CO_2$; and (II) the exploitation of energy-rich compounds

found in organic waste, which might otherwise not be efficiently valorized in traditional treatment and disposal pathways. One of the main issues of DF is that a significant fraction of the influent organic compounds is not converted to hydrogen, but to other byproducts, such as alcohols and acids (Rai & Singh, 2016), limiting the overall hydrogen production yield to roughly 33% of the maximal theoretical yield (Hitit et al., 2017). This limits the specific hydrogen production achievable through this sole process and impacts its economic feasibility (Magdalena et al., 2024). To overcome this issue, it is necessary to couple DF with secondary processes to improve yields and remove the residual carbon and energy contained in the effluent (Niño-Navarro et al., 2020). One of the possible technologies to be coupled with this process is Photo Fermentation (PF). PF consists of the exploitation of purple phototrophic bacteria (PPB) ability to grow photoheterotrophically under anaerobic conditions, metabolizing short-chain organic molecules and producing hydrogen as byproduct. The metabolism of dark and photo fermentative bacteria is then complementary to each other, as the volatile fatty acids produced as a byproduct during DF could serve as a substrate for PPB during PF (Rai & Singh, 2016). By coupling DF and PF, the residual carbon and energy contained in the effluent after DF can be further converted into hydrogen, increasing the overall yield of the process and, possibly, its economic feasibility. Although the integration of DF and PF theoretically enables the production of biological hydrogen at maximal yield (12 $mol_{H2}$ $mol_{glucose}^{-1}$) (Niño-Navarro et al., 2020), practical implementation is hindered by several constraints. Among all, the high ammonium concentration of Dark Fermentation Effluents (DFE) stands out as one of the main issues to face when the two processes are coupled, as even relatively low concentrations of ammonium (above 80 $mg_{NH4+}$ $L^{-1}$) can severely inhibit hydrogen production by PPB, repressing the activity of *nitrogenase* enzyme (Ghosh et al., 2017). Moreover, not all organic acids are efficiently converted into hydrogen by PPB. For the coupled system to work efficiently, DFE should be optimized to produce specific organic acids (particularly acetate, lactate, and butyrate, Lo et al., (2011)), and this can be challenging to control, especially when feeding real organic waste as substrates instead of synthetic growth media (Niño-Navarro et al., 2020).

## 1.2. Thesis objectives and structure

The thesis aimed to scale up a DF process from laboratory to pilot scale, coupling the system with photo fermentative hydrogen production. The main goal was to maximize the conversion to hydrogen of the organic matter contained in waste streams and then exploit it for the production of e-fuels through a biological methanation process. Food Waste (FW) and Waste Activated Sludge (WAS) were the main substrates tested for DF, with food waste acting as the main fermentable organic source and the waste activated sludge as both a carbon source and a pH buffer. Moreover, given their year-round availability, these substrates are a suitable feedstock for a scaled-up process.

The thesis is structured in seven chapters. In this first chapter (**Chapter 1**), a general overview of the topic covered in this work is presented, along with the motivations and objectives of the study, and details of its structure. **Chapter 2** mainly focuses on a literature review of hydrogen production methods, prioritizing biological fermentations (dark, photo, and coupled systems) and targeting hydrogen conversion to e-fuels. In the last section of the chapter, food waste generation and available valorization technologies are briefly summed up. **Chapter 3** describes the material and methods employed in this work, with details on all the experiments and analyses performed. **Chapter 4** presents the results of the DF tests conducted. Overall, four different experiments were set up, starting from batch laboratory scale and progressively moving through semicontinuous pilot scale tests. All the tests performed focused on the valorization of Food Waste and Waste Activated Sludge through mixed consortia. In the first test, food waste and waste activated sludge were fermented in batch conditions on laboratory-scale reactors. In the second test, Hydraulic Cavitation (HC) pretreatment of the influent feedstock was tested, to evaluate its effectiveness in enhancing the production yields. In the third test, the same reactor was tested in semi-continuous, to evaluate the stability of the process on a smaller scale. Finally, in the fourth test, a pilot scale reactor was employed in semi-continuous mode. In this last phase, the fermentate produced was directed to a pilot-scale anaerobic digestion process, to manage the abundant volumes generated. In the other ones, the fermentate was characterized and further valorized in PF processes, as

described in **Chapter 5**. This chapter describes the results of the two main tests performed. In the first PF test, two different wild type strains (*Rhodopseudomonas palustris* and *Rhodospirillum rubrum*) were employed and tested for the production of hydrogen using the metabolites present in the DFE as the main carbon source. In the second one, mutated strains of *Rps*. *palustris* were tested with the same goal. The mutated strains tested were characterized by a greater tolerance to high ammonium concentrations, one of the main issues when DF and PF are coupled, and by alteration of the metabolic pathways that optimized hydrogen generation. **Chapter 6** describes the results of the bio-methanation tests performed to produce methane by the biological conversion of hydrogen and carbon dioxide. Finally, **Chapter 7** provides an overview of the general conclusions of this work.

## 1.3. References

Beyazit, N. I. (2025). Journey to a sustainable future: The importance of renewable hydrogen in industrial and domestic applications. In *International Journal of Hydrogen Energy* (Vol. 99, pp. 836–851). Elsevier Ltd. https://doi.org/10.1016/j.ijhydene.2024.12.065

bp p.l.c. (2024). *Energy Outlook 2024*.

Ghosh, S., Dairkee, U. K., Chowdhury, R., & Bhattacharya, P. (2017). Hydrogen from food processing wastes via photofermentation using Purple Non-sulfur Bacteria (PNSB) – A review. In *Energy Conversion and Management* (Vol. 141, pp. 299–314). Elsevier Ltd. https://doi.org/10.1016/j.enconman.2016.09.001

Hitit, Z. Y., Zampol Lazaro, C., & Hallenbeck, P. C. (2017). Increased hydrogen yield and COD removal from starch/glucose based medium by sequential dark and photo-fermentation using Clostridium butyricum and Rhodopseudomonas palustris. *International Journal of Hydrogen Energy*, *42*(30), 18832–18843. https://doi.org/10.1016/j.ijhydene.2017.05.161

IPCC. (2021). *Climate Change 2021: The Physical Science Basis. Contribution of Working Group I to the Sixth Assessment Report of the Intergovernmental Panel on Climate Change*.

IPCC. (2023). *Climate Change 2023: Synthesis Report. Contribution of Working Groups I, II and III to the Sixth Assessment Report of the Intergovernmental Panel on Climate Change*. (P. Arias, M. Bustamante, I. Elgizouli, G. Flato, M. Howden, C. Méndez-Vallejo, J. J. Pereira, R. Pichs-Madruga, S. K. Rose, Y. Saheb, R. Sánchez Rodríguez, D. Ürge-Vorsatz, C. Xiao, N. Yassaa, J. Romero, J. Kim, E. F. Haites, Y. Jung, R. Stavins, … C. Péan, Eds.). https://doi.org/10.59327/IPCC/AR6-9789291691647

Lo, Y. C., Chen, C. Y., Lee, C. M., & Chang, J. S. (2011). Photo fermentative hydrogen production using dominant components (acetate, lactate, and butyrate) in dark fermentation effluents. *International Journal of Hydrogen Energy*, *36*(21), 14059–14068. https://doi.org/10.1016/j.ijhydene.2011.04.148

Lynas, M., Houlton, B. Z., & Perry, S. (2021). Greater than 99% consensus on human caused climate change in the peer-reviewed scientific literature. In *Environmental Research Letters* (Vol. 16, Issue 11). IOP Publishing Ltd. https://doi.org/10.1088/1748-9326/ac2966

Magdalena, J. A., Perez-Bernal, M. F., Rodero, M. del R., Roslan, E., Lanfranchi, A., Dabestani-Rahmatabad, A., Mahieux, M., Capson-Tojo, G., & Trably, E. (2024). Bioprocesses coupling for biohydrogen production: applications and challenges. In V. Alcaraz Gonzalez, R. A. Flores Estrella, A. Haarstrick, & V. Gonzalez Alvarez (Eds.), *Wastewater exploitation* (pp. 273–304). Springer Nature Switzerland. https://doi.org/10.1007/978-3-031-57735-2

Niño-Navarro, C., Chairez, I., Christen, P., Canul-Chan, M., & García-Peña, E. I. (2020). Enhanced hydrogen production by a sequential dark and photo fermentation process: Effects of initial feedstock composition, dilution and microbial population. *Renewable Energy*, *147*, 924–936. https://doi.org/10.1016/j.renene.2019.09.024

Rai, P. K., & Singh, S. P. (2016). Integrated dark- and photo-fermentation: Recent advances and provisions for improvement. In *International Journal of Hydrogen Energy* (Vol. 41, Issue 44, pp. 19957–19971). Elsevier Ltd. https://doi.org/10.1016/j.ijhydene.2016.08.084

Ritchie, H., & Rosado, P. (2020). *Energy Mix*. OurWorldInData.org

Segovia-Hernández, J. G. (2025). Advancing E-fuels production through process intensification: overcoming challenges and seizing opportunities for a sustainable energy future - A critical review. In *Chemical Engineering and Processing - Process Intensification* (Vol. 208). Elsevier B.V. https://doi.org/10.1016/j.cep.2024.110107

UNEP. (2023). *Emissions Gap Report 2023: Broken Record – Temperatures hit new highs, yet world fails to cut emissions (again)*. United Nations Environment Programme. https://doi.org/10.59117/20.500.11822/43922

# 2. Literature Review

This chapter provides a comprehensive review of the current state of the art of hydrogen production, primarily focusing on emerging biological pathways such as Dark Fermentation and Photo Fermentation. By comparing the available technologies on the market, the chapter aims to highlight the potential of biological methods over the traditional ones, along with their current limitations. Although promising, biological processes for hydrogen production require further research to boost yields, that are currently not competitive with traditional production methods. Among the various biological processes for hydrogen production, Dark Fermentation and Photo Fermentation have emerged as the most suitable for scale-up and industrialization. Moreover, the coupling of these two processes was identified as a promising approach for effluent valorization and enhancing process yields. Finally, the potential of utilizing hydrogen for carbon dioxide conversion to e-fuels has been highlighted, with a focus on the available biological processes.

## 2.1. Hydrogen

Under standard conditions, hydrogen is a gas made up of diatomic hydrogen molecules. It is a colorless, odorless, tasteless, non-toxic, and flammable gas. In its atomic form, it is the simplest element of the periodic table, consisting of an atom with just a single proton and one electron. One of its earliest recognized chemical properties is its capacity to burn with oxygen to produce water; in fact, the term hydrogen derives from the Greek “water” (*húdōr*) and “forming” (*gennáō*) meaning “maker of water.” It is this feature that makes hydrogen a valuable alternative to traditional fossil fuels, as its combustion generates energy with no carbon emissions (Eq. 1, Keçebaş & Kayfeci, (2019)).

$$H_2 + {}^1/_2\, O_2 \rightarrow H_2O \qquad \Delta H^0_{C\,(25°C)} = -286\, {}^{kJ}/_{mol} \qquad \text{Eq. 1}$$

Moreover, hydrogen combustion does not release SOx and NOx into the atmosphere, unlike fossil fuels like coal and oil (Qureshi et al., 2023). The growing interest in $H_2$ is driven not only

by the sustainability of its utilization, as no carbon is emitted by its combustion, but also by its energy density, almost three times higher than that contained in traditional fuels (120.1 MJ $kg^{-1}$ for hydrogen, compared to 40–50 MJ $kg^{-1}$ for traditional fuels). However, as shown in Table 1, the considerably lower density of hydrogen leads to a significant decline in its volumetric energy content, both for gaseous and liquid hydrogen.

*Table 1, Comparison of the energy content and carbon emissions of hydrogen and traditional fuels*

| Fuel | density [kg $m^{-3}$] | Gravimetric Energy Density [MJ $kg^{-1}$] | Volumetric Energy Density [MJ $L^{-1}$] | Specific $CO_2$ emission [$kg_{CO2}$ $kg_{fuel}^{-1}$] |
|---|---|---|---|---|
| Gaseous Hydrogen [25 °C, 1 bar] | 0.081[a] | 120.1[a] | 0.01 | 0 |
| Pressurized Hydrogen [25 °C, 350 bar] | 23.3[b] | 120.1[a] | 2.80 | 0 |
| Pressurized Hydrogen [25 °C, 700 bar] | 39.3[b] | 120.1[a] | 4.72 | 0 |
| Liquid Hydrogen [-253 °C, 1 bar] | 70.8[a] | 120.1[a] | 8.50 | 0 |
| Compressed Natural Gas (CNG) [15 °C, 250 bar] | 167.4[d] | 47.1[c] | 7.88 | 2.75[c] |
| Gasoline [15 °C, 1 bar] | 737[c] | 46.4[c] | 34.20 | 3.30[c] |
| Diesel [15 °C, 1 bar] | 846[c] | 45.7[c] | 38.66 | 3.15[c] |

a (F. Wang et al., 2023)

b (Q. Cheng et al., 2024)

c (The Engineering ToolBox, 2009)

d calculated by approximating the molecular weight to that of methane, 16.04 g $mol^{-1}$

Despite being by far the most abundant element in the universe, hydrogen is rarely found in its molecular form on Earth, as its low density prevents it from being retained in the atmosphere. However, it is extensively present in its bound form as water, and in a multitude of organic compounds. As a consequence, unlike natural gas and other natural resources, hydrogen cannot be directly extracted from the environment but must be produced from the compounds that contain it. Nowadays, hydrogen is mostly produced for industrial applications and is usually generated on-site due to its transportation hazards (American Chemistry Society, 2020). It is mainly used for the production of ammonia and in the hydrogenation processes of carbon monoxide and organic compounds, with a global demand of around 70 million tons per year (International Energy Agency, 2019). Other possible applications include fuel cells for clean electricity generation (Shaker et al., 2024), production of bioplastics (Rogers et al., 2021), organic chemistry (Reed-Berendt et al., 2021), synthesis of methanol (Tedeeva et al., 2024), steel industry (W. Liu et al., 2021), heating system (Yu et al., 2023), and transportation (Halder et al., 2024).

Hydrogen is usually referred to as an “energy vector” instead of an “energy carrier”, as it is an energy-rich substance that not only allows the transformation of energy from one form to another but also its translocation in time and/or space (Abdin et al., 2020).

Due to its characteristics, hydrogen has the potential to play a significant role in the transition to low-carbon energy system, by: (I) serving as a storage medium for intermittent renewable energy and facilitating their large-scale integration into the existing infrastructure, (II) developing a more resilient energy system that delivers accessible, reliable, safe, clean and affordable energy across all sectors and regions, (III) offering a cleaner feedstock and energy source for industrial applications, and (IV) providing a cleaner alternative for transportation through fuel cells and hydrogen-fueled engines (Acar & Dincer, 2019). However, achieving these benefits heavily depends on the production method employed, as relying on high-carbon processes for its production clearly hinders these goals.

## 2.2. Overview of traditional hydrogen production methods

There are several different production pathways for hydrogen production, each using different technologies, feedstocks (biological or non-biological), and energy sources (renewable or non-renewable) (European Biogas Association, 2023), and each characterized by different production costs and carbon emissions (Ajanovic et al., 2022). To simplify the complexity of the different hydrogen production methods, these technologies are often classified with different colors, summarized in Table 2.

Currently, grey and brown/black hydrogen are the leading production methods, making global hydrogen production strongly dependent on fossil fuels. The main non-renewable fuels used as feedstock for hydrogen production are natural gas (Stolten & Emonts, 2016) and oil (Dou et al., 2019) via steam-reforming processes, and coal (International Energy Agency, 2019) through gasification processes, with approximately 6 % of global natural gas and 2 % of coal being consumed for this purpose. Moreover, since carbon capture, utilization, and storage (CCUS) technologies are rarely applied, all these processes result in significant $CO_2$ emissions, undermining the use of hydrogen as a sustainable energy source. International Energy Agency, (2019) reported that, at the time the report was written, less than 0.7 % of the hydrogen production came from renewables or fossil fuel plants equipped with CCUS, making its production responsible for 830 Mt/yr of $CO_2$, equivalent to the annual $CO_2$ emissions of the whole Southern Europe (Global Carbon Budget, 2023).

Grey hydrogen (i.e., Steam Methane Reforming (SMR) of natural gas) is the most applied technology in hydrogen production, with a global daily production of around 500,000 $kg_{H2}$/day (Vita & Italiano, 2019). With a production cost of less than 2 €/$kg_{H2}$ (Ajanovic et al., 2022), SMR is currently the cheapest and most established option in hydrogen production. In this process, natural gas is first pretreated to remove hydrogen sulfide and prevent catalyst poisoning, then converted at high pressure (25–30 bar) and temperature (700–1000 °C) to hydrogen, most commonly using $Ni/Al_2O_3$-based catalyst (Vita & Italiano, 2019). The reactions taking place in this process are summarized in Eq. 2 – Eq. 4 (Vita & Italiano, 2019).

*Table 2, Hydrogen categories and production pathways. Adapted from Incer-Valverde et al., (2023)*

| Type of hydrogen | Feedstock | Energy source | Process | $CO_2$ emissions [$kg_{CO2eq}$ $kg_{H2}^{-1}$] | Production price [$\$_{US}/kg_{H2}$] | % global production[a] |
|---|---|---|---|---|---|---|
| Brown/Black | Coal/Lignite | Coal | Gasification | 18 – 25 | 1.3 – 2.5 | 19 % |
| Grey | Natural gas | Natural gas | SMR | 7.5 – 25[d] | 0.7 – 2.3 | 62 % |
| Blue | Natural gas | Natural gas | SMR + CCS | 3.97 – 6.87[d] | 1.4 – 3.2 | 0.7 % |
| Turquoise | Natural gas | Natural gas | Pyrolysis | 3.94 – 9.91[d] | 1.6 – 3.4 | - |
| Red | Water | Nuclear power | Catalytic water splitting | 0.1 – 0.6[d] | 2.2 – 2.6 | - |
| Purple/Pink | Water | Nuclear power | Electrolysis | 0.1 – 0.6[d] | 3.8 – 7 | - |
| Orange | Water | Mix of electricity grid | Electrolysis | Depends on the electricity mix | 3.3 – 3.6 | - |
| Green | Water | Renewable electricity | Electrolysis | ~ 0[d] | 1.9 – 8.2 | 0.04 % |
| | Biomass[b] | Biomass derived energy | Biological processes | Biogenic $CO_2$ emissions[b] | 2.6 – 2.8[c] | - |

[a] remaining amount being produced as a byproduct in the chemical industry

[b] (European Biogas Association, 2023)

[c] (Nikolaidis & Poullikkas, 2017)

[d] (Hammi et al., 2024)

$$CH_4 + H_2O \leftrightarrow CO + 3H_2 \qquad \Delta H^0_{C\,(25°C)} = -206\,{}^{kJ}/_{mol} \qquad \text{Eq. 2}$$

$$CH_4 + CO_2 \leftrightarrow 2CO + 2H_2 \qquad \Delta H^0_{C\,(25°C)} = -247\,{}^{kJ}/_{mol} \qquad \text{Eq. 3}$$

$$CO + H_2O \leftrightarrow CO_2 + H_2 \qquad \Delta H^0_{C\,(25°C)} = 41\,{}^{kJ}/_{mol} \qquad \text{Eq. 4}$$

The gaseous steam produced after these reactions is then subjected to CO cleanup and hydrogen purification through a pressure swing adsorption process, that separates the produced hydrogen from the residual $H_2O$ and $CO_2$ present in the steam.

The second most spread production process is coal gasification, known as brown hydrogen, which is particularly prevalent in China due to its large reserve of coal and the higher cost of natural gas (Ajanovic et al., 2022). In this process, dry pulverized coal reacts at temperatures over 900 °C with oxygen and steam, generating hydrogen and $CO_2$ (Ajanovic et al., 2022).

The hydrogen produced by SMR can become less carbon-intensive if the emission of $CO_2$, up to 7.05 $kg_{CO2}/kg_{H2}$ (Yukesh Kannah et al., 2021), is mitigated through the use of CCUS technologies, in which case the hydrogen is labeled as blue hydrogen. The carbon intensity and cost of blue hydrogen depend strongly on the type and quantity of CCUS technologies applied (Incer-Valverde et al., 2023), with physical and chemical absorption being proposed as the most applicable methods (Vita & Italiano, 2019). Despite being reported as technically and economically feasible (Vita & Italiano, 2019) and as a potential bridge between highly carbon-intensive technologies and clean hydrogen ones (Woody & Carlson, 2020), blue hydrogen is still not sufficiently integrated into the global market (as evidenced in Table 2), accounting for less than 0.7 % of the worldwide total production. Large-scale and well-established CCUS systems are not yet a reality (Incer-Valverde et al., 2023) but, driven by carbon and greenhouse emissions targets set by several countries, the market of blue hydrogen is expected to growth considerably in the next decades (Precedence Research, 2024), as several traditional gray hydrogen production plants are being retrofitted or are planned to be converted soon to blue hydrogen (International Energy Agency, 2020).

A more extensive transition to blue hydrogen will positively impact carbon emissions but will hardly completely be carbon-free. The $CO_2$ is only partially captured, depending on the type, quantity, and cost of the employed CCUS systems. In most cases, only high-pressure and high-concentrated $CO_2$ streams are treated, as treating diluted $CO_2$ streams is much more expensive, resulting in a capture efficiency that rarely exceeds 85 – 90 % (International Energy Agency, 2020). While aiming at capturing 100 % of the emitted $CO_2$ is usually not thermodynamically feasible, capture rates of 98 % or above are technically achievable, when the trade-offs in terms of energy consumption and cost of the process are accepted (International Energy Agency, 2020). Investing in technologies that provide high carbon capture rates will be an important step in moving towards a net-zero emissions future.

An alternative strategy to limit the carbon intensity of hydrogen production could be to focus on technologies that, from the outset, do not result in $CO_2$ emissions. Among those methods, green hydrogen stands out as one of the most promising approaches for achieving sustainable hydrogen production. Green hydrogen commonly refers to hydrogen produced by electrolysis using renewable energy, such as solar, wind, or hydroelectric (Incer-Valverde et al., 2023). This process consists of splitting water molecules into hydrogen and oxygen using electricity, with no direct $CO_2$ emissions (Eq. 5 – Eq. 7, (Agyekum et al., 2022)).

$$\text{Anode:} \quad H_2O \rightarrow {}^{1}/_{2}\, O_2 + 2H^+ + 2e^- \qquad \text{Eq. 5}$$

$$\text{Cathode:} \quad 2H^+ + 2e^- \rightarrow H_2 \qquad \text{Eq. 6}$$

$$\text{Overall:} \quad H_2O \rightarrow H_2 + {}^{1}/_{2}\, O_2 \qquad \text{Eq. 7}$$

However, it is currently energy-intensive and costly. The expense is driven by the high capital investment required for electrolyzers and the cost of renewable energy, which makes this production route less competitive with traditional methods (Ajanovic et al., 2022). At present, only 0.04 % of global hydrogen is produced by combining electrolysis and renewable energy sources. However, the decreasing costs of both electrolyzers and renewable electricity

suggest that green hydrogen may have a significant role in future energy systems (International Energy Agency, 2023).

Besides electrolytic green hydrogen, $CO_2$-free hydrogen can be also produced from biomass, in which case it's referred to as bio-hydrogen. Biomass is a renewable primary energy source derived from plant and animal materials, which capture and store solar energy in their chemical bonds during their growth. Biomass materials include forest residues, crops, microalgae, municipal solid waste, or animal byproducts, all of which can be considered significant potential biological fuels and chemical feedstocks (Qureshi et al., 2023). Biomass already plays a crucial role in the global energy supply, currently accounting for about 14% of total energy generation (Qureshi et al., 2023), and it is projected that by 2050 it will contribute to more than 25% of global energy demand (Faye et al., 2022).

Currently, biomass is converted to hydrogen in processes such as biomass gasification, biogas reforming, bio-photocatalysis, microbial electrolysis, and anaerobic Dark Fermentation and Photo Fermentation (European Biogas Association, 2023; Hammi et al., 2024; Jiao et al., 2024). The main advantage of these processes is that the $CO_2$ emitted during hydrogen production is fixed during biomass formation, leading to a net balance of carbon emissions. Moreover, biomass can have a higher hydrogen-to-carbon ratio compared to some of the fossil fuels used for hydrogen production. For example, pure cellulose has a 1.7 ratio, higher compared to that of 0.8 for bituminous coal (black hydrogen, coal gasification), leading to lower $CO_2$ emissions (Agyekum et al., 2022).

Biomass gasification and biogas reforming are similar in principle to their fossil-based counterparts, though they typically require more intensive feedstock pretreatment and result in fluctuations in $H_2$ yields due to the complexity, composition, and origin of the involved biomass (Agyekum et al., 2022; Dou et al., 2019).

## 2.3. Biological hydrogen production

Biological hydrogen production methods, including fermentations, photo-biological processes, and bio-electro-chemical systems, leverage microbial metabolic pathways that are capable of breaking down organic substrates or water into hydrogen. In Figure 1, the main processes for biological hydrogen production are summarized.

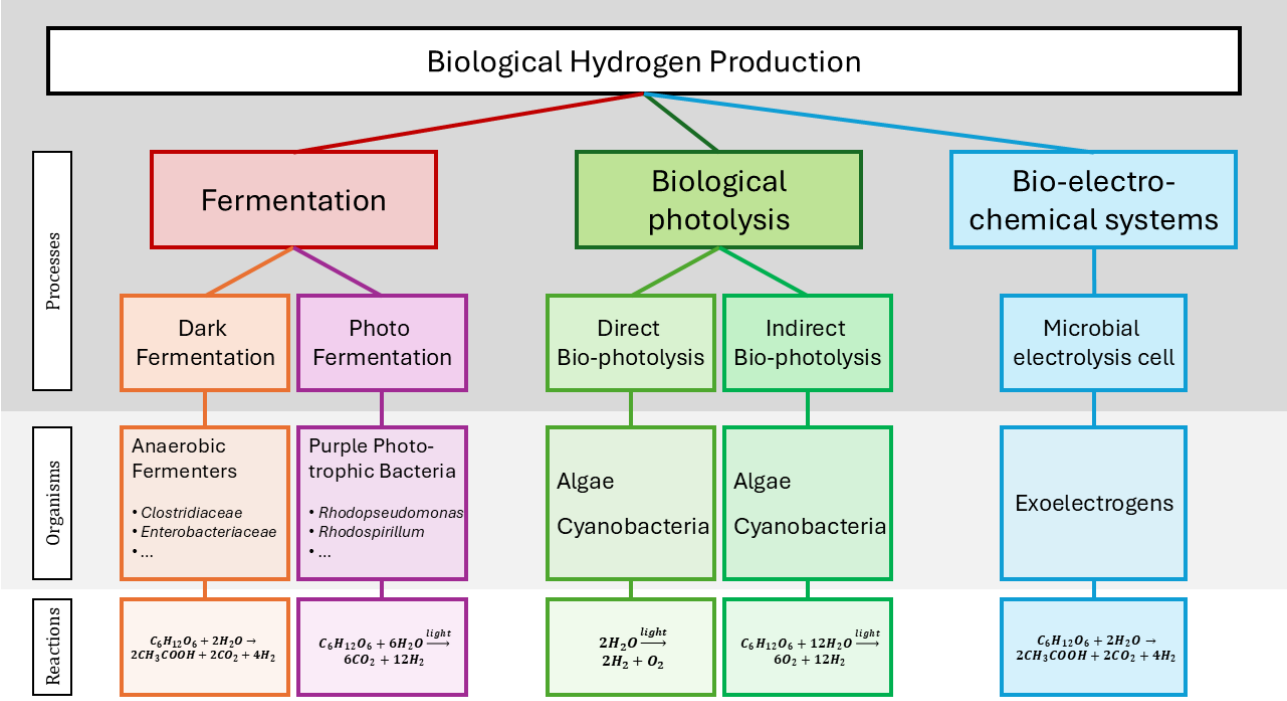


*Figure 1, Overview of biological hydrogen production processes (adapted and modified from Gopalakrishnan et al., 2019)*

A key advantage of these methods over their thermochemical counterpart (e.g., gasification, pyrolysis, biogas reforming) is that they operate at ambient temperature and pressure conditions, thereby potentially simplifying the complexity of reactor design and lowering the energy input requirements.

Non-fermentative biological hydrogen production methods include biological photolysis and bio-electro-chemical systems. Bio-photolysis can be classified into two categories: direct and indirect bio-photolysis, depending on whether light is irradiated during the hydrogen production process or not. The mechanism of direct biological photolysis closely resembles the photosynthetic process that occurs in plants and microalgae. In this case, green microalgae under strict anaerobic conditions utilize light to split water molecules into oxygen, protons, and electrons, subsequently generating hydrogen via the hydrogenase enzyme (Jiao et al., 2024). Bio-photolysis has gained significant interest among researchers due to its potential to produce a clean, carbon-neutral energy source using only water and sunlight. However, direct bio-photolysis faces several challenges, including its extreme sensitivity to oxygen, the need for complex bioreactor design with large surface areas for efficient light capturing, and the overall low $H_2$ conversion yields (Anjum et al., 2023; Jiao et al., 2024). Indirect bio-photolysis offers a promising strategy to overcome some of the challenges faced by direct photolysis. In this process, hydrogen production happens in two separate steps. Initially, microalgae convert solar energy into chemical energy through photosynthesis, synthetizing organic compounds, then, the produced organic compounds are metabolized by hydrogenase enzymes under anaerobic conditions to produce hydrogen. By separating in two steps the reactions linked to oxygen evolution and hydrogen production, this process mitigates the oxygen sensitivity issue associated with bio-photolysis, leading to enhanced hydrogen production and improved productivity (Sharma & Arya, 2017; Vargas et al., 2018). However, both direct and indirect bio-photolysis yield relatively low amounts of hydrogen, mostly due to hydrogen consumption by uptake hydrogenase (Akhlaghi & Najafpour-Darzi, 2020), thus hindering the industrialization of these processes (Chen et al., 2023).

Bio-electro-chemical systems (BES) offer another promising approach to biological hydrogen production, utilizing electroactive microorganisms to drive hydrogen evolution through electrochemical reactions. In these systems, exo-electrogenic microorganisms transfer electrons between substrates and electrodes, enabling the conversion of chemical energy into electricity or vice versa (Jayathilake et al., 2024). These systems find their application for hydrogen production in the Microbial Electrolysis Cells (MECs), where the application of an

external small voltage is used for microbial conversion of organic substrates, either synthetic or derived from wastewaters, into hydrogen or other products of commercial interest like methane or acetate (Corona-Martínez et al., 2025). In MECs, exo-electrogenic microorganisms oxidize the supplied substrates in the anodic chamber, leading electrons to flow through an external circuit to the cathodic chamber, where the hydrogen generation occurs (Corona-Martínez et al., 2025). Despite these systems offering a promising alternative for wastewater treatment and sustainable hydrogen generation, several challenges hinder their large-scale development. Their high capital and operational costs, low efficiency for large-scale applications, the occurrence of undesired electrode fouling, and limited process stability (Tan et al., 2021) are some critical aspects that are limiting the application of this technology.

## 2.4. Dark Fermentation

### 2.4.1. Process overview and metabolic pathways

Dark Fermentation (DF) is a robust biological process in which carbohydrate-rich substrates are broken down anaerobically by Hydrogen Producing Bacteria (HPB) in a chain of reactions that leads to the evolution of molecular hydrogen. HPB are a broad group of facultative or obligate anaerobic microorganisms that, primarily through hydrogenase enzymes, dispose of the excess electrons generated during the oxidation of organic substrates (C. Li & Fang, 2007). Under anaerobic conditions, the accumulation of reduced compounds such as volatile fatty acids and alcohols caused by the oxidation of organic substrates is neutralized by $H^+$ protons, which act as electron acceptors to restore the redox balance within the cell, eventually resulting in the production of hydrogen (Gopalakrishnan et al., 2019). There is a wide variety of microorganisms able to produce hydrogen via DF. These microorganisms are typically classified according to their tolerance to oxygen (obligate or facultative anaerobes) and their temperature requirements (mesophiles, thermophiles, and extremophiles). Among these, facultative anaerobes are usually selected over obligate ones as they are easier to cultivate and maintain under laboratory and industrial conditions. Thermophiles are reported to be able to achieve the maximum theoretical hydrogen yield of 4 $mol_{H2}$ $mol_{glucose}^{-1}$, due to the reduced

thermodynamic barrier in their metabolic processes. However, the high-energy input required to sustain the higher operative temperatures hinders the practical application of these microorganisms at a larger scale (Das, 2009). DF can be carried out by single organisms or by a microbial consortium. For large-scale hydrogen production, relying on microbial consortia certainly offers significant advantages, as it allows the process to operate under non-sterile conditions, enabling the use of unsterilized organic waste as substrates, thereby limiting operational costs (Correa-Villa et al., 2024; Gopalakrishnan et al., 2019). Moreover, this approach can improve the system's efficiency in converting complex substrates, given the greater metabolic flexibility and robustness of the microbiome. However, the presence of alternative metabolic pathways or non-hydrogen-producing microorganisms such as hydrogenotrophic methanogens, can compromise the overall yield of the process by limiting the conversion of organic compounds to hydrogen or consuming the one already produced (Correa-Villa et al., 2024). Therefore, it is essential to monitor and manage microbial diversity to optimize process efficiency (Gopalakrishnan et al., 2019).

All microorganisms in the microbial consortium cooperate in a complex biochemical pathway to degrade organic compounds. A schematic representation of DF is presented in Figure 2.

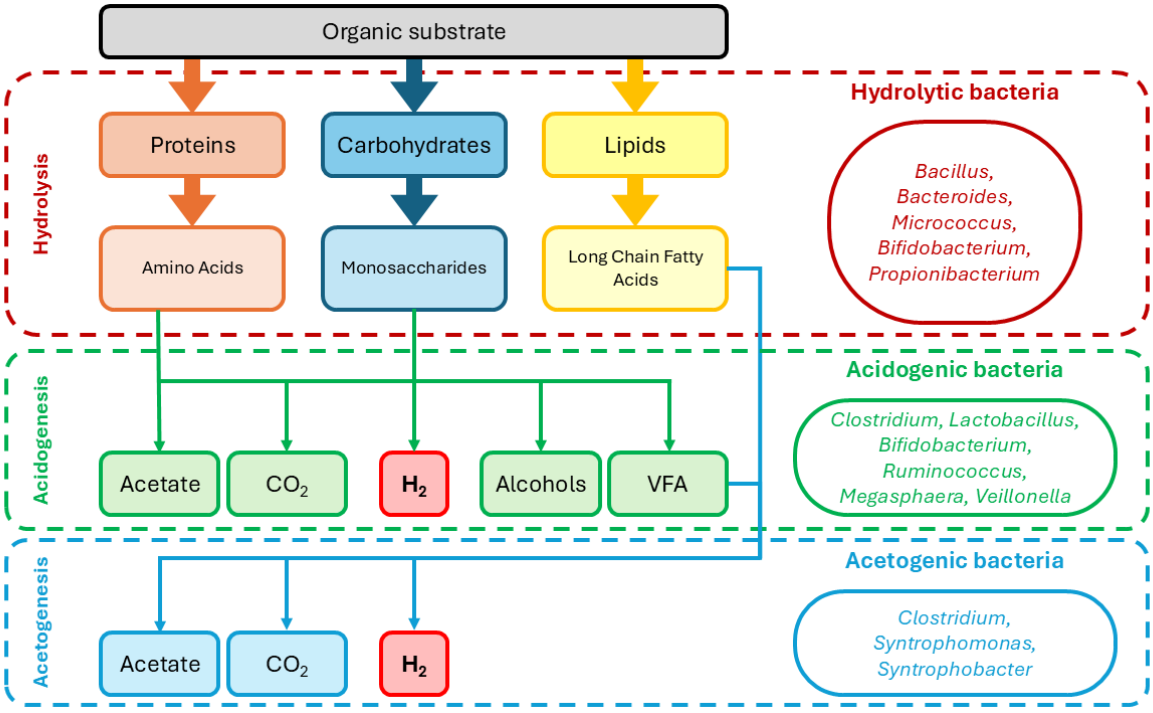


*Figure 2, Biodegradation and microbiological pathways involved in the breakdown of waste biomass through Dark Fermentation (adapted and modified from Villanueva-Galindo et al., 2023).*

Along with hydrogen, DF results in the production of a mixture of fermentative metabolites, such as acetate, butyrate, propionate, and other compounds (Moscoviz et al., 2018). Acetate (Eq. 8) and butyrate (Eq. 9) are the most common products resulting from DF (Hawkes et al., 2007). Metabolic pathways that lead to acetate as the primary metabolite result in the highest stoichiometric yield, reaching 4 $mol_{H2}\ mol_{glucose}^{-1}$, while when butyric acid is the main end-product this yield decreases to 2 $mol_{H2}\ mol_{glucose}^{-1}$. However, in a DF process with a mixed microbial community, the actual hydrogen yield of the overall process is typically lower than the maximum theoretical yields mentioned. This occurs because: i) a portion of the available organic substrates may be metabolized by alternative metabolic pathways with lower or no hydrogen evolution (e.g., ethanol, propionate, or lactate production, Eq. 10 – Eq. 13), ii) a part of the supplied organic compounds can be utilized for microbial biomass production (Palanivel et al., 2025), and iii) the presence of some undesired microorganism such as hydrogenotrophic

methanogens, homoacetogens, and sulfate-reducing bacteria can consume the produced hydrogen (Eq. 14 – Eq. 16) (Ghimire, 2015).

| | | |
|---|---|---|
| Acetic acid: | $C_6H_{12}O_6 + 2H_2O \rightarrow 2CH_3COOH + 2CO_2 + 4H_2$ | Eq. 8 |
| Butyric acid: | $C_6H_{12}O_6 \rightarrow CH_3CH_2CH_2COOH + 2CO_2 + 2H_2$ | Eq. 9 |
| Acetic acid and ethanol: | $C_6H_{12}O_6 + 2H_2O \rightarrow CH_3COOH + CH_3CH_2OH + 2CO_2 + 2H_2$ | Eq. 10 |
| Ethanol | $C_6H_{12}O_6 \rightarrow 2CH_3CH_2OH + 2CO_2$ | Eq. 11 |
| Propionic acid | $C_6H_{12}O_6 + 2H_2 \rightarrow 2CH_3CH_2COOH + 2H_2O$ | Eq. 12 |
| Lactic acid: | $C_6H_{12}O_6 \rightarrow CH_3CHOHCOOH + 2CO_2$ | Eq. 13 |
| Hydrogenotrophic methanogens | $CO_2 + 4H_2 \rightarrow CH_4 + 2H_2O$ | Eq. 14 |
| Homoacetogens | $2CO_2 + 4H_2 \rightarrow CH_3COOH + 2H_2O$ | Eq. 15 |
| Sulfate Reducing Bacteria | ${SO_4}^{2-} + 4H_2 + H^+ \rightarrow HS^- + 4H_2O$ | Eq. 16 |

The predominant metabolic pathways of the process are critical in determining the efficiency of the system and are greatly influenced by different variables, including the initial inoculum and its pretreatments, the substrate type and the complexity of its organic compounds, the reactor design, and the operative parameters like pH, HRT, and OLR (Ghimire, 2015; Palanivel et al., 2025). The activity of undesired hydrogen consumers can be controlled by inoculum pretreatments (Rafieenia et al., 2018) or by operative parameters (Guo et al., 2010). Hydrogenotrophic methanogens, for instance, are considered the primary hydrogen-consuming microorganisms in DF systems (Weijma et al., 2002), but their presence can be controlled through various strategies, including pretreating the inoculum with heating or acidic conditions, maintaining an operative pH below 6, or applying short HRT (typically in a range between 3 to 48 h, based on the complexity of the fermented substrate) to wash out the methanogens from the reactor (Guo et al., 2010). In contrast, sulfate-reducing bacteria (SRB) exhibit a higher tolerance to short HRT, even at retention times below 2 h. When sulfate is

abundant in the supplied substrate, these microorganisms can significantly reduce the process yields, as sulfate and nitrate reduction with hydrogen are thermodynamically more favorable. Under these conditions, operating at a pH lower than 6, combined with a short HRT, has been shown to significantly inhibit SRB activity and limit their impact on the process yields (Lin & Chen, 2006). Another category of undesirable bacteria that can affect process efficiency is homoacetogens. These bacteria are capable of producing acetate from hydrogen and carbon dioxide. In contrast to SRB and hydrogenotrophic methanogens, these bacteria cannot be removed by inoculum pretreatment, as some of them are spore-forming and can thereby survive the harsh environmental conditions of the pretreatment. Moreover, they have an optimum pH that falls in the range of 5.0 – 6.0 (Hussy et al., 2003), thus overlapping the optimal one for HPB. The best option for limiting homoacetogens' activity is working at a pH lower than 5.0 (Hussy et al., 2003), or at thermophilic conditions with an initial pH of 5.5 (G. Luo et al., 2011) or reducing the partial pressure of hydrogen and carbon dioxide by removing these compounds from the headspace of the reactor (Diekert & Wohlfarth, 1994; Park et al., 2005). Other undesired microorganisms are lactic acid bacteria (LAB), which are commonly associated with lower productivity and instability in the DF process (Detman et al., 2021). These microorganisms can outcompete HPB by consuming the supplied organic substrates, leading to lactate accumulation instead of hydrogen production. Moreover, excessive lactate accumulation can lower the pH of the fermentation medium at values below 4 (pKa = 3.79, Song et al., 2022), which is generally undesirable for hydrogen production. Their presence in a DF system is usually difficult to control, especially when operating with unsterilized substrates, as they are indigenous of various organic waste, including food waste (Guo et al., 2010), and at mesophilic conditions (X. Wang & Zhao, 2009). Their activity can be inhibited only by a combination of thermophilic conditions and short HRTs (Guo et al., 2010). However, the literature is not unanimous on LAB effect on DF, and some studies suggest that their presence may contribute to the stability of the system and be beneficial for the overall hydrogen yield, due to their contribution to pH regulation, substrate hydrolysis, oxygen depletion, microbial inhibition, and the possibility of recovering the produced lactate as substrate for hydrogen production (Correa-Villa et al., 2024; Dzulkarnain et al., 2022; Sikora et al., 2013).

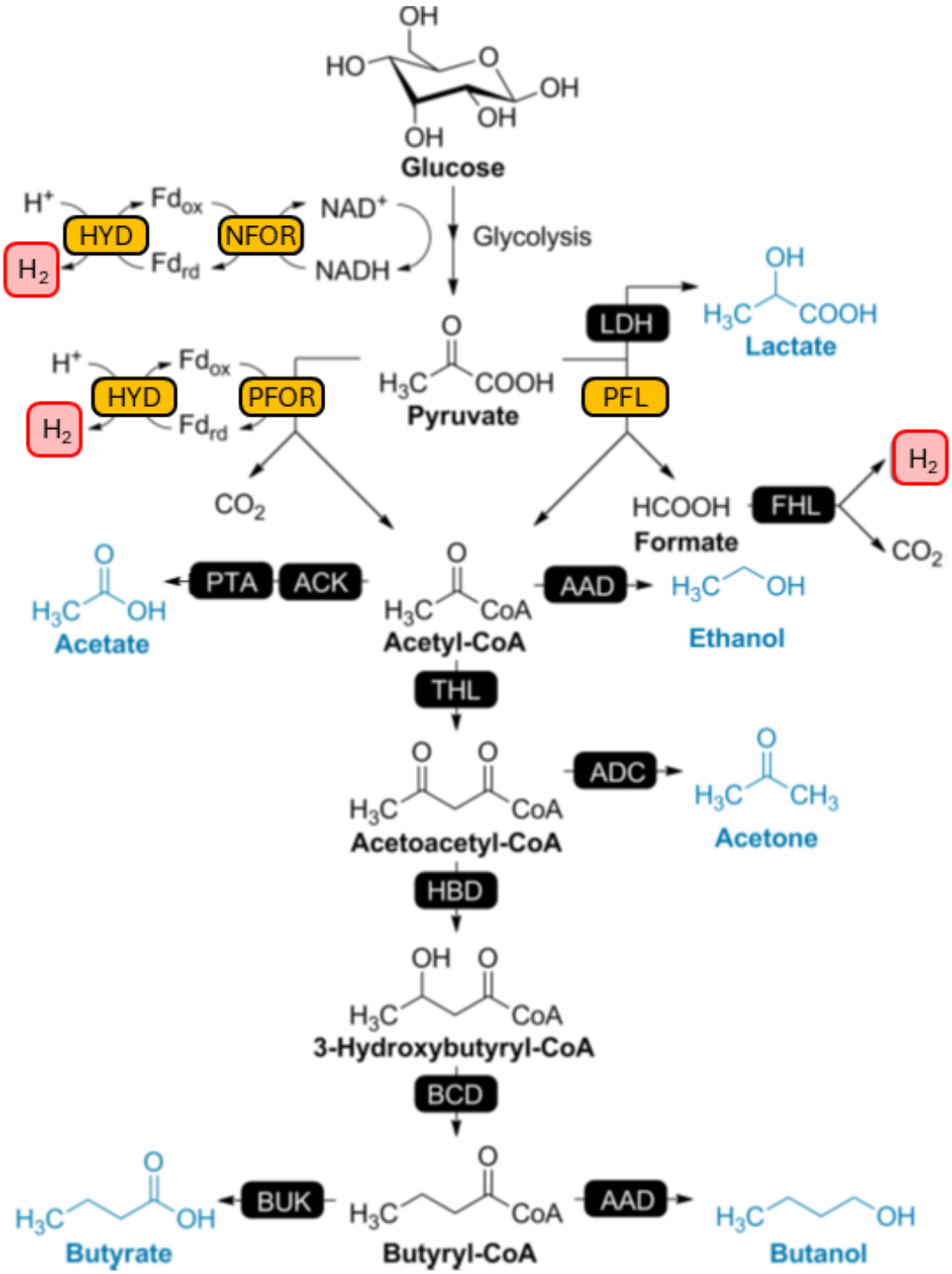


*Figure 3, Scheme of the key metabolic pathways involved in DF. In orange, the main enzymes involved in the biological hydrogen production. PFL reactions (on the right) are employed by facultative anaerobes. PFOR and NFOR pathways (on the left) are utilized by strict anaerobes and are catalyzed by HYD. In blue, alternative metabolites that can be synthetized alongside hydrogen during the DF process. Abbreviations: NFOR, NADH: ferredoxin oxidoreductase; HYD, hydrogenase; PFOR, pyruvate: ferredoxin oxidoreductase; ACK, acetate kinase; PTA, phosphotransacetylase; LDH, lactate dehydrogenase; PFL, pyruvate: formate lyase; FHL, formate: hydrogen lyase complex; AAD, aldehyde alcohol dehydrogenase; THL, thiolase; ADC, acetoacetate decarboxylase; HBD, $\beta$-hydroxybutyryl-CoA dehydrogenase; BCD, butyryl-CoA dehydrogenase; BUK, butyrate kinase; $Fd_{ox}$ and $Fd_{rd}$, oxidized and reduced ferredoxin. (adapted and modified from Cao et al., 2022)*

Figure 3 shows the currently known metabolic pathways involved in biological hydrogen production through DF. The process begins with the catabolism of glucose (or the other carbon sources supplied to the system) through the glycolysis pathway, leading to the formation of pyruvate. Then, hydrogen production may occur through three main metabolic pathways: the pyruvate: formate lyase (PFL), the pyruvate: ferredoxin oxidoreductase (PFOR), and the NAD(P)H: ferredoxin oxidoreductase (NFOR) pathways (Figure 3, labeled in orange). In PFL, pyruvate is first converted to formate, and then the formate is split into hydrogen and carbon dioxide by formate: hydrogen lyase. This pathway typically occurs in facultative anaerobes (Y. Cao et al., 2022). In strict anaerobes, instead, hydrogen production is primarily driven by the PFOR pathway, where pyruvate oxidation leads first to the reduction of ferredoxin, and then to its oxidation by hydrogenase. Hydrogenase is responsible for the reversible reaction of conversion of molecular hydrogen into two protons and two electrons (Gopalakrishnan et al., 2019). However, hydrogenases are highly sensitive to oxygen, in whose presence they do not lead to hydrogen production (Y. Cao et al., 2022). In NFOR, similarly to the PFOR pathway, hydrogen is produced when hydrogenase oxides ferredoxin, while ferredoxin is reduced at the expense of the NAD(P)H generated during microbial catabolism. As depicted in Figure 3, apart from biological hydrogen production, the energy retrieved during glycolysis can be used for the synthesis of a variety of reduced metabolites, such as acetate, butyrate, lactate, ethanol, and butanol (Hallenbeck et al., 2009), depending on the composition of the fermentative microbial consortium and the operative conditions.

### 2.4.2. Factors affecting DF yields

Hydrogen production through DF is the consequence of a complex system where different microorganisms with different metabolic pathways interact following syntrophic, competitive, or antagonistic patterns. In this complex system, operative parameters such as pH, temperature, hydrogen partial pressure, HRT, and OLR play a crucial role in regulating metabolic pathways and determining process efficiency (Ghimire, 2015).

pH

The pH value is one of the most important parameters to consider when managing DF, as it affects the microbial community composition, the enzyme expression and activity, and, consequently, possible shifts in metabolic pathways (Zhao et al., 2024). Optimal values drop typically in a pH range of 5.2–6.0, both for pure strains and mixed consortia (Qureshi et al., 2023), as at these values biohydrogen production can occur, while competitive microorganisms (i.e., methanogens) are inhibited (Khanal et al., 2004). Values of pH below 5, however, could inhibit the hydrogenase activity, thereby affecting substrate degradation and hydrogen production (Bao et al., 2013). Below this value, some HPB such as *Clostridium* sp. shift their metabolic pathway to solventogenesis, resulting in the production of ethanol, butanol, and acetone instead of hydrogen (Argun & Kargi, 2011). When pH falls at even lower values, microbial growth can be strongly inhibited. In fact, in these conditions, the concentration of the undissociated forms of carboxylic acids ($pKa_{(acetic\ acid)}$ = 4.75, $pKa_{(butyric\ acid)}$ = 4.80) increases consistently (Elbeshbishy et al., 2017). Undissociated organic acids, being more liposoluble, are more permeable to bacterial cells. When they diffuse into the cytoplasm, given the neutral internal pH, they dissociate, releasing protons and leading to a decrease in the intracellular pH of the bacteria, causing their inhibition (Lund et al., 2020). The optimal pH for DF is strongly dependent also on the type of substrate being fermented. For FW, the most suitable pH range appears to be between 5.0 and 6.0 (S. H. Kim et al., 2004), while it can vary from neutral values for animal manure (Ziara et al., 2019) and corn straw (Guo et al., 2010) to values between 4.0 and 5.5 for rice waste (Sattar et al., 2016).

Temperature

Temperature is another fundamental parameter in a DF process, as it directly influences microbial activity and community composition. The most employed temperature ranges in DF are mesophilic (25 – 40 °C), thermophilic (40 – 65 °C), and hyper-thermophilic (over 80 °C) (Argun & Kargi, 2011). Each microorganism species and carbon source has an optimal temperature range in DF (Ziara et al., 2019). Therefore, when working with mixed consortia and

complex substrates, it is crucial to ensure that the chosen operative temperature range is suitable for the overall specific process. Besides its impact on microbial communities, temperature strongly affects the hydrolysis rate, which is particularly important when treating complex and not easily degradable substrates (Ghimire, 2015). When lignocellulosic materials are present in the fermented feedstock, higher operative temperatures may result in better hydrolysis, and therefore, enhance the process yields (Guo et al., 2010). On the contrary, when the substrate is easily degradable, mesophilic conditions may be favored for an optimal hydrogen yield (Ghimire, 2015). The primary drawback of operating under higher temperatures is the increased energy demand associated with heating and maintaining the target operative conditions (Jain et al., 2024). However, higher temperatures can offer a significant advantage by inhibiting competitive microorganisms, such as those involved in propionogenesis and homoacetogenesis, which are difficult to control under mesophilic conditions (Palanivel et al., 2025).

Hydrogen partial pressure

Operating under high hydrogen partial pressure is a restrictive factor during DF, while a lower partial pressure helps in maintaining optimal conditions for biohydrogen production. The oxidation of LCFA has a positive Gibbs free energy and is therefore thermodynamically unfavorable and extremely sensitive to hydrogen concentration in the medium (Dong et al., 2009). When hydrogen partial pressure rises in the reactor, dissolved hydrogen in the liquid medium increases, and the bacterial metabolic reactions that result in hydrogen production are inhibited (Dong et al., 2009). While hydrogen production is thermodynamically unfavored, a metabolic shift toward solventogenesis may occur, leading to ethanol, butanol, and acetone accumulation instead of hydrogen (Argun & Kargi, 2011). Moreover, the activity of all those microorganisms that use hydrogen as a substrate, such as hydrogenotrophic methanogens and homoacetogens, is favored when more dissolved hydrogen is available, further reducing the performance of the process. One of the most easily applicable techniques for decreasing hydrogen partial pressure in the medium is increasing the mixing (Guo et al., 2010). Other strategies may be directly decreasing the internal pressure of the reactor by employing a

vacuum pump or sparging the fermenter with nitrogen or carbon dioxide to strip the dissolved hydrogen (Ghimire, 2015). Both options, however, increase the operational costs of the process, on one side due to the energy demands of the vacuum pump, and on the other due to the dilution of the produced hydrogen and the consequent increase of the cost related to the downstream processes (Ghimire, 2015). Submerged hollow-fiber membranes provide an alternative energy-effective strategy for hydrogen partial pressure management. However, membranes could be difficult to operate due to the formation and accumulation of biofilm over time, which may eventually favor the proliferation of methanogens (Guo et al., 2010). Temperature regulation can assist in managing the partial pressure, as operating at lower temperatures reduces the partial pressure of gasses within the reactor system. Therefore, from this perspective, working under mesophilic conditions may result as a preferable option rather than thermophilic conditions (Zhao et al., 2024). Another energy-effective solution is to work with lower liquid-to-gas volume proportions (Junghare et al., 2012).

Hydraulic Retention Time (HRT)

HRT is a fundamental parameter that helps in governing hydrogen production by shaping the microbial community and its metabolic activity. It determines the average residence time of microorganisms in the reactor, directly affecting microbial selection and byproduct production, based on growth rates and substrate consumption kinetics (García-Depraect et al., 2021). It is one of the key parameters to consider for limiting the proliferation of competitive microorganisms, such as methanogens, which growth at much lower rates compared to HPB and therefore are washed out from the system when short HRTs are employed (Palanivel et al., 2025). Typically, short HRTs in the range of 8 to 14 h are the optimal setpoint to achieve excellent hydrogen generation (Qureshi et al., 2023). However, like other parameters, this parameter strongly depends on the type of substrate fermented, as more complex substrates often require longer HRTs to become bioavailable for the HPB. Insufficient HRT can lead to incomplete hydrolysis of these compounds, resulting in reduced hydrogen yields (Ghimire, 2015). For complex substrates like OFMSW and FW, optimal hydrogen production yields can be achieved at HRTs of 3 to 5 days (D. Liu et al., 2008; Martins et al., 2022).

Organic Loading Rate (OLR)

The OLR defines the availability of substrate for the microbial community and is calculated as the ratio between its concentration in the feeding inflow and its residence time in the reactor. Usually, higher hydrogen productivity is associated with higher OLR values, which can be obtained by either shortening the HRT or increasing the substrate concentration in the inflow (Palanivel et al., 2025). It's worth mentioning, however, that a trade-off between hydrogen production rate and yield could be necessary. Increasing the OLR typically optimizes the hydrogen production rate (defined as the volume of hydrogen produced per unit of reactor volume and unit of time) while decreasing the production yield (volume of hydrogen produced per unit of substrate consumed) (García-Depraect et al., 2021; X. Wang & Zhao, 2009). Depending on the type of substrate fed, optimal OLRs typically range between 100 and 200 $g_{COD}$ $L^{-1}$ $d^{-1}$, as long as there is no inhibition due to substrate overload, biomass washout, or over-acidification (García-Depraect et al., 2021).

Inoculum pretreatment

One possible way to manage a microbial consortium and drive it to hydrogen production is to pretreat it to inhibit hydrogen-consuming bacteria, such as hydrogenotrophic methanogens, homoacetogens, lactic acid bacteria, propionate-producing bacteria, and sulfate reducers (Rafieenia et al., 2018). Inoculum pretreatment technologies rely on the ability of hydrogen producers to sporulate when they are subjected to harsh conditions (pH, temperature, irradiation, chemicals) (Rafieenia et al., 2018). These spores allow them to survive in the generated extreme environments, while non-sporulating hydrogen consumers are destroyed. When the environmental conditions become favorable again, the sporulating bacteria can reactivate, resulting in an inoculum enriched in HPB (Ren et al., 2008). Among the available inoculum pretreatments, heat shock and acidic or alkaline pretreatments have shown the greatest potential for enriching hydrogen producers (L. Luo et al., 2022). Another promising pretreatment strategy is inoculum repeated-aeration, which involves increasing the oxidation-reduction potential of the inoculum by subsequent aeration steps, maintaining

dissolved oxygen concentrations below 0.5 mg $L^{-1}$. This pretreatment method has been proved to effectively enrich the HPB in the inoculum while preserving a higher microbial diversity, as it can eliminate methanogens without adversely affecting non-spore-forming hydrogen producers (Ren et al., 2008). However, none of these pretreatments can completely and permanently suppress hydrogen-consuming microorganisms, especially when operating under unsterile continuous conditions, since other external microorganisms may enter the reactor and proliferate (Rafieenia et al., 2018).

Substrate pretreatment

When complex feedstocks are treated, substrate pretreatments may be required to enhance their biodegradability (Rafieenia et al., 2018). The goal of these pretreatments is to increase the soluble fraction of organic compounds and break down the structure of the organic materials, increasing the surface area available for microbial degradation and, therefore, enhancing the hydrolysis phase (Ghimire, 2015). Pretreatments are particularly necessaries when treating substrates rich in lignocellulose, hemicellulose, and cellulose (Saratale et al., 2008). These compounds are mainly composed of glucose monomers, making them theoretically an ideal substrate for DF. However, their crystalline structure makes them inaccessible to fermentative bacteria (Gopalakrishnan et al., 2019; Rafieenia et al., 2018). Traditional pretreatments of the substrate include physical (e.g., mechanical grinding or thermal pretreatment), chemical (e.g., acid or alkaline pretreatment), or biological methods to increase its biodegradability (Zhao et al., 2024). Most of these pretreatments, however, are highly energy intensive and despite actually increasing the hydrogen yields, can negatively affect the economic viability of the overall process (Rafieenia et al., 2018). An effective pretreatment technology should enhance the biodegradability of the substrate and improve hydrogen yields, without incurring excessive energy consumption, and thus not compromising the economic feasibility of the process (Gbiete et al., 2024). A promising energy-efficient alternative pretreatment for DF substrates can be Hydrodynamic Cavitation (HC). Cavitation technologies consist of exploiting the localized high energy release caused by the collapse of cavitation bubbles. In HC, cavitation bubbles are generated by pressure variations that a liquid incurs while passing through a

hydrodynamic cavitation reactor. When these bubbles collapse, high pressure (~ 1000 bar), high temperature (~ 5000 K), and strongly oxidizing conditions (•OH, $•O_2$, •OOH) are generated in the surrounding environment (Prado et al., 2022). The sum of these extreme conditions promotes the breakdown of complex organic matter, thereby improving hydrolytic kinetics, solubilizing organic compounds, and enhancing the bioavailability of the substrates (Sun et al., 2024). Lanfranchi et al., (2022) investigated the effect of HC pretreatment on the acidogenic co-fermentation of FW and WAS, reporting an 83 % increase in the soluble COD after pretreatment. Other authors explored the use of this process, primarily for its application as lignocellulosic biomass pretreatment (Bimestre et al., 2022). The main advantage of HC over other comparable technologies, including ultrasonic and laser-generated cavitation, lies in its short application time and its versatility for integration with other treatments such as alkali or acid pretreatments (Prado et al., 2022).

### 2.4.3. Food Waste and Waste Activated Sludge as potential substrates for fermentative biohydrogen production

HPB can efficiently metabolize a wide variety of organic compounds. However, selecting an appropriate substrate is crucial for optimizing hydrogen yield, production rate, and the overall economic viability of the process (Gopalakrishnan et al., 2019). While pure organic compounds such as glucose, sucrose, and starch can be effectively converted to hydrogen by HPB, the high operational cost of their utilization severely hinders their practical application for large-scale processes (Akhlaghi & Najafpour-Darzi, 2020). Additionally, since simple carbohydrates like glucose, sucrose, and lactose are often used in food products or animal feeds, their use for producing biofuels (such as biohydrogen) is controversial (Łukajtis et al.).2018). The broad metabolic capabilities of HPB, however, enable them to utilize organic waste as substrate, and this can substantially enhance the economic feasibility of the process. The use of organic waste materials as substrate for DF can represent a virtuous solution, as it ensures on one hand the production of bio-hydrogen and VFA as byproducts, and on the other, serves as a

biological treatment for these wastes, reducing their volume and stabilizing them (Ghimire, 2015). For them to be a viable option for biohydrogen production, these organic waste materials need to be abundant, easily available, cheap, and highly biodegradable (Guo et al., 2010). Among the various types of biomasses available, Food Waste (FW) meets these requirements and can be exploited as a substrate for DF hydrogen production (Carmona-Cabello et al., 2018; Gopalakrishnan et al., 2019). The Food Waste Index Report 2024 (United Nations Environment Programme, 2024) states that FW is generated globally in massive amounts, with 1.05 billion tons generated only in 2022, and that they are ubiquitous worldwide, despite significant differences between high-income and low-income countries. Annual food waste generation in Italy amounts to approximately 1.62 million tons, corresponding to around 3.82 million tons of $CO_{2eq}$ and an economic impact of about 10 billion euros per year (Antonelli et al., 2024). Currently, FW is primarily treated through biological processes, with anaerobic digestion for biogas production and aerobic oxidation for organic compost generation as the most widely implemented treatment strategies (United Nations Environment Programme, 2024), while a portion of the waste is still sent to landfill disposal (Alexandropoulou et al., 2018). While not currently applied at full-scale, DF can effectively serve as an alternative valorization pathway for FW treatment (Villanueva-Galindo et al., 2023). One of the main challenges of using FW on a large-scale is its complexity and heterogeneity, as well as its seasonal variability (Chu et al., 2012; Łukajtis et al., 2018). FW may include both easily degradable and recalcitrant compounds, as well as carbohydrate-rich materials with high hydrogen potentials and proteins and lipid-rich materials with low hydrogen potentials. Seasonal variation in FW composition can significantly affect hydrogen yields (Alibardi & Cossu, 2015; Mateus et al., 2020), especially under mono-fermentation (Karki et al., 2021). Besides seasonal variability, FW is often characterized by a limited amount of trace elements (Carmona-Cabello et al., 2018; Xu et al., 2018), which are indispensable cofactors for several enzymes, including hydrogenase and formate hydrogen lyase (Gopalakrishnan et al., 2019). To overcome these constraints, one possible strategy is to rely on FW co-fermentation, especially when an increase in the C:N ratio of the second feedstock is desirable, as for Waste Activated Sludge (WAS) (X. Liu et al., 2013). Co-fermentation of FW and WAS results in several

advantages, including balancing the C:N and C:P ratios, providing buffer capacity to the system, and improving substrate utilization efficiency (Vidal-Antich et al., 2021; D. Zhang et al., 2020). Several authors studied the co-fermentation of FW and WAS to determine the optimal operative parameters and reactor configuration, highlighting the advantages of this approach over mono-fermentation. Table 3 and Table 4 provide some examples of batch and continuous DF tests for the co-fermentation of FW and WAS. Under batch mode systems, the co-fermentation of FW and WAS generally results in higher process yields compared to the mono-fermentation of FW alone, typically with better performances when FW is present in higher proportions than WAS. This improvement is attributed to a synergistic effect between the two substrates, in which FW provides a carbohydrates-rich and easily degradable carbon source and WAS contributes to the buffer capacity of the system, balances the C:N ratio, and provides micronutrients such as Fe and Ca, known to be beneficial for DF fermentation (D. H. Kim et al., 2011). Under continuous-mode operations, the proportion between FW and WAS is usually adjusted to increase WAS dosage, to ensure adequate buffering capacity to the system and avoid over-acidification. Optimal results are associated with HRT values of 3 – 4 days, with performance decreasing as HRT increases (Gottardo et al., 2023; Martins et al., 2022). A further decrease of HRT to shorter values may instead result in a decline in substrate conversion efficiency, due to the slow solubilization of the organic particulate materials present in FW (Redondas et al., 2012).

*Table 3, Examples of batch mode DF tests comparing FW mono-fermentation and co-fermentation of FW and WAS*

| Co-substrate ratio | Pretreatments * | T (°C) | pH | OL ($g_{VS}$ $L^{-1}$) | $H_2$ (%) | $H_2$ yield ($L_{H2}$ $kg_{VS}^{-1}$) | Reference |
|---|---|---|---|---|---|---|---|
| FW:WAS 87:13 [c] | I (90 °C, 90 min) | - | 5.0 – 6.0 | 32.5 $g_{COD}$ $L^{-1}$ | - | 122.9 $L_{H2}$ $kg_{COD}^{-1}$ | (S. H. Kim et al., 2004) |
| FW<br>FW:WAS 90:10 [d] | S (90 °C, 20 min) | 35<br>35 | 6<br>6 | 15.3<br>21.8 | -<br>- | 147<br>162 | (D. H. Kim et al., 2011) |
| FW<br>FW:WAS 80:20 [b] | WAS (dried 85 °C + alkali treatment) | 37<br>37 | 5.5<br>6.0 – 7.0 | 64.7<br>58.1 | 48.01<br>62.40 | 51<br>60 | (Z. Li et al., 2018) |
| FW<br>FW:WAS 90:10 [c] | I (105 °C, 24 h) | 37<br>37 | 7<br>7 | 10<br>10 | 51<br>65 | -<br>- | (Moreno-Andrade et al., 2023) |
| FW<br>FW:WAS 1:1.67 [a] | FW (dried 105 °C), WAS (UC 3.17 W/mL, 30 min + 121 °C, 20 min) | 55<br>55 | 4.5<br>5.0 | 15.6<br>15.9 | -<br>- | 34<br>192 | (Yang et al., 2025) |

[a] substrates mixed on a FM basis
[b] substrates mixed on a TS basis
[c] substrates mixed on a VS basis
[d] substrates mixed on a COD basis
* I = inoculum pretreatment, S = substrate pretreatment, UC = Ultrasonic Cavitation pretreatment

*Table 4, Examples of continuous mode DF tests comparing FW mono-fermentation and co-fermentation of FW and WAS*

| Co-substrate ratio | Pretreatments * | T (°C) | pH | HRT (d) | OLR ($g_{VS}$ $L^{-1}$ $d^{-1}$) | $H_2$ (%) | $H_2$ yield ($L_{H2}$ $kg_{VS}^{-1}$) | HPR ($L_{H2}$ L $d^{-1}$) | Reference |
|---|---|---|---|---|---|---|---|---|---|
| OFMSW | none | 37 | 5.0 | 4 | 23.6 | 25 | 8.48 | 0.20 | (Martins et al., 2022) |
| OFMSW | | 37 | 5.2 | 5 | 18.0 | 32 | 18.2 | 0.32 | |
| FW:WAS 1:1 [c] | S (70 °C, 8 h) | 55 | 4.8 – 5.3 | 4 | 4.6 | 34.4 | 46 | - | (Gottardo et al., 2023) |
| FW:WAS 1:1 [c] | | 55 | 4.8 – 5.3 | 6 | 3.1 | 28.0 | 35 | - | |
| FW | I (105 °C, 30 min) | 37 | 5.52 | 3 | 14.2 | 22.9 | 12.6 | - | (Baldi et al., 2019) |
| FW:WAS 1:5 [a] | | 37 | 5.54 | 3 | 14.6 | 18.4 | 8.6 | - | |
| OFMSW:WAS 1:5 [a] | none | 55 | 4.75 | 3 | 16.0 | 36 | 29 | 0.432 | (Zahedi et al., 2016) |
| FW:WAS 9:1 [c] | I (105 °C, 24 h) | 37 | 5.5 | 12 h | 15.0 | - | 9.3 | 0.364 | (Moreno-Andrade et al., 2023) |
| FW:WAS 9:1 [c] | | 37 | 5.5 | 8 h | 22.0 | - | 15.6 | 0.733 | |
| FW:WAS 9:1 [c] | | 37 | 5.5 | 4 h | 45.0 | - | 2.8 | 0.383 | |

[a] substrates mixed on a FM basis
[b] substrates mixed on a TS basis
[c] substrates mixed on a VS basis
* I = inoculum pretreatment, S = substrate pretreatment

## 2.5. Photo Fermentation

### 2.5.1. Process overview and metabolic pathways

Photo Fermentation (PF) is a promising biological hydrogen production method. One of the main differences with DF is the energy source that drives the process. While HPB in DF break down organic substrates to generate the reducing power needed for their metabolism, in PF light energy is harnessed in a photoautotrophic process that, under anoxygenic conditions, results in the photolysis of the organic substrate and the evolution of hydrogen (Rupprecht et al., 2006). Similarly to DF, the organic substrates utilized in PF systems may derive from waste streams, thereby providing a valorization option for their treatment and diminishing the operational costs of the process (K. Cao et al., 2020). The microorganisms responsible for PF are Purple Phototrophic Bacteria (PPB), a heterogeneous group of anoxygenic facultative anaerobes (Capson-Tojo et al., 2020) that thrive in a variety of natural environments (Adessi & De Philippis, 2012). They are generally categorized based on their tolerance and utilization of sulfide as Purple Sulfur Bacteria (PSB) and Purple Non-Sulfur Bacteria (PNSB) (Madigan & Jung, 2009). PSB are predominantly photoautotrophic microorganisms that rely on reduced sulfur compounds as electron donors. Their metabolism is less flexible compared to that of PNSB, and they usually require sulfur to grow (Madigan & Jung, 2009). Moreover, they can accumulate intracellular sulfur and generally better tolerate reduced sulfur species in the growth medium, although PNSB can as well thrive at low sulfide levels (Madigan & Jung, 2009). PNSB, in contrast, show a remarkable metabolic versatility, including photoautotrophy, photoheterotrophy, anaerobic fermentation (in the absence of light), and aerobic respiration (in the presence of oxygen) (Capson-Tojo et al., 2020). It is indeed this metabolic flexibility that makes PPB highly attractive for a broad range of biotechnological applications, including biohydrogen production. Among the broad spectrum of metabolic pathways PPB can perform, the one leading to hydrogen production is the one that occurs in the presence of light and absence of oxygen, with organic compounds serving as both electron donors and carbon sources (Adessi & De Philippis, 2012). PPB can utilize a diverse range of organic carbon compounds, such as pyruvate and acetate, various organic acids (propionate, butyrate,

malate, glutamate, succinate, lactate), amino acids, alcohols, and carbohydrates (Adessi & De Philippis, 2012; Capson-Tojo et al., 2020). Short-chain organic acids are the preferred organic substrates for PPB in hydrogen production, as they can easily enter the microbial carbon metabolism through the tricarboxylic acid (TCA) cycle, which is very active during photoheterotrophic growth (Adessi & De Philippis, 2012). PPB can also carry out nitrogen fixation, a process strictly related to hydrogen production (Adessi & De Philippis, 2012). The key enzyme in this reaction is nitrogenase, present both in PPB and all other nitrogen-fixating prokaryotes (Adessi & De Philippis, 2012). In the presence of molecular nitrogen, nitrogenase catalyzes its reduction to ammonia, resulting in the production of one mole of hydrogen, as in Eq. 17. When molecular nitrogen is absent, nitrogenase catalyzes an alternative reaction (Eq. 18) as a mechanism to dissipate the excess reducing power generated by the organism (Adessi & De Philippis, 2012). With four moles of hydrogen generated with the same ATP consumption, it's easy to spot why the latter reaction is the most advantageous when hydrogen production is the primary goal (Ghosh et al., 2017).

$$N_2 + 8H^+ + 8e^- + 16ATP \rightarrow 2NH_3 + H_2 + 16ADP + 16P_i \qquad \text{Eq. 17}$$

$$8H^+ + 8e^- + 16ATP \rightarrow 4H_2 + 16ADP + 16P_i \qquad \text{Eq. 18}$$

In these reactions, the required ATP is generated mainly by anoxygenic photosynthesis, while the reducing power is derived from the catabolism of organic acids (Adessi & De Philippis, 2014). However, nitrogenase is extremely sensitive to oxygen, which leads to its irreversible inactivation (Androga et al., 2012). Thus, to enhance hydrogen production, it is crucial to ensure the absence of both oxygen and nitrogen. Moreover, since the reaction is highly energy-intensive for the microorganism, it is strictly regulated by the accumulation of ammonium ions, which act as a key regulatory signal in the enzyme regulation mechanism, inhibiting nitrogenase expression and shifting the metabolism to ammonium assimilation and biomass growth rather than hydrogen production (Adessi & De Philippis, 2014). Therefore, the presence or accumulation of ammonium ions should be avoided in the reaction environment when hydrogen production Is the main objective (Androga et al., 2012).

Other key enzymes associated with PPB's hydrogen production are hydrogenases. Hydrogenases found in PPB are similar in cofactor structure and function to those found in HPB but are not phylogenetically related (Xuan et al., 2023). As in HPB, these enzymes catalyze the reversible reaction of conversion of molecular hydrogen into two protons and two electrons (Mohanraj et al., 2019). In PPB, hydrogenases generally function in close association with nitrogenase (Adessi & De Philippis, 2012), ensuring the uptake of the produced hydrogen and the maintenance of the redox balance required for cellular metabolism (Tsygankov & Khusnutdinova, 2015). For this reason, they are typically referred to as uptake hydrogenases and their activity is generally undesirable in hydrogen production processes, as they consume the produced hydrogen, reducing the process yields (Adessi & De Philippis, 2012). Hydrogenase expression is induced when molecular hydrogen is present in the growth environment, while it is significantly inhibited by oxygen (Xuan et al., 2023).

Under appropriate reaction conditions, PPB can metabolically convert organic compounds to hydrogen at near-theoretical yields, as the energy required in the process is derived from light and the substrate can be converted nearly stoichiometrically to carbon dioxide and hydrogen (Ghosh et al., 2017). The equations (Eq. 19 – Eq. 24) illustrate the photoheterotrophic conversion of some of the most commonly utilized organic compounds in PF (Ghosh et al., 2017; Reungsang et al., 2018).

| | | |
|---|---|---|
| Glucose: | $C_6H_{12}O_6 + 6H_2O \xrightarrow{light} 12H_2 + 6CO_2$ | Eq. 19 |
| Acetic acid: | $CH_3COOH + 2H_2O \xrightarrow{light} 4H_2 + 2CO_2$ | Eq. 20 |
| Propionic acid: | $CH_3CH_2COOH + 4H_2O \xrightarrow{light} 7H_2 + 3CO_2$ | Eq. 21 |
| Butyric acid: | $CH_3CH_2CH_2COOH + 6H_2O \xrightarrow{light} 10H_2 + 4CO_2$ | Eq. 22 |
| Lactic acid: | $CH_3CH(OH)COOH + 3H_2O \xrightarrow{light} 6H_2 + 3CO_2$ | Eq. 23 |
| Malic acid: | $COOHCH_2CH(OH)COOH + 3H_2O \xrightarrow{light} 6H_2 + 4CO_2$ | Eq. 24 |

It can be observed from the reactions in Eq. 19 – Eq. 24 that the maximum hydrogen yields obtainable in the process is dependent on the organic carbon source treated. However, these reaction yields are theoretical, as part of the substrate can be utilized for microbial growth, or some other limiting factors may occur in the system (Adessi & De Philippis, 2012). Generally, malate and lactate are considered more suitable substrates for hydrogen production, while acetate and butyrate tend to redirect the metabolic pathway toward polyhydroxyalkanoate (PHA) accumulation rather than hydrogen production (Hustede et al., 1993; D. H. Kim et al., 2012). However, this general observation may vary based on the specific PPB employed in the process, as some authors reported better hydrogen yields when acetate or butyrate was used as main carbon source rather than lactate or malate (Assawamongkholsiri et al., 2019; Barbosa et al., 2001; Fang et al., 2005; Govindaraju et al., 2019; Hu et al., 2018; Lo et al., 2011).

### 2.5.2. Factors affecting PF and strategies to enhance hydrogen production

Photofermentative hydrogen production depends on several operative parameters, which should be carefully considered to optimize the process yields. These parameters include, for instance, pH and temperature, ratio of carbon and nitrogen source, light intensity, and reactor design (Basak et al., 2014). Low pH values (below 5.5) strongly inhibit the hydrogen production process through PF. High pH values, instead, do not show a similar effect, likely due to an adaptation of PPB to organic acid consumption, which generally leads to a pH increase (Capson-Tojo et al., 2020). The optimal pH range for hydrogen production maximization, however, is around near-neutral values ranging between 6.5 to 7.4 (Capson-Tojo et al., 2020). Regarding temperature, PPB generally thrive at mesophilic conditions, showing optimal yields for temperatures between 31 and 35 °C, and a significant decrease for temperatures above 40 °C (Capson-Tojo et al., 2020). In contrast, temperatures below 25 °C do not have a similar inhibitory effect on the hydrogen yields (Capson-Tojo et al., 2020). This is of fundamental importance when considering outdoor cultivation, as avoiding reactor heating can have a substantial impact on process energy requirements. Hülsen et al., (2016), for instance,

examined the potential use of PPB for outdoor wastewater treatment, reporting efficient growth rate at around 10 °C. The supplied carbon source and its concentration can also play a crucial role in influencing the favorable metabolic pathways, thereby driving the process either towards hydrogen evolution, biomass production, or synthesis of other metabolites. Under limited nutrient conditions and with excessive organic substrate available, PPB tend to metabolize the supplied carbon as polyhydroxyalkanoates (PHA) as storage compounds (Moscoviz et al., 2018). The synthesis of such storage material has the same function of electron sinks as photofermentation, directly competing with this pathway, thereby should be avoided when aiming for hydrogen production (Adessi & De Philippis, 2012). When substrates are supplied at concentrations over 2 – 4 $g_{COD}$ $L^{-1}$, hydrogen yields tend to decrease significantly (Capson-Tojo et al., 2020), in many cases imposing the need for dilution when the process is applied for waste stream treatment. The dilution of the treated waste may be needed also to ensure the system with proper light distribution. Light, being the main energy source of PF, is a critical parameter to consider (Q. Zhang et al., 2017), particularly in terms of its intensity, quality, sources, and distribution (Adessi & De Philippis, 2014). Optimal light intensities for hydrogen production were reported within a range of 4,000 to 5,000 lux (Verma et al., 2025), When excessive light is provided to the system (above 8,000 lux), photo-inhibition phenomena occur, disrupting the photosynthetic process and drastically reducing its efficiency (Hitam & Jalil, 2023). Various artificial light sources can be employed in PF systems, including halogen lamps, fluorescent tubes, light-emitting diodes (LEDs), and optical fibers (Verma et al., 2025). However, when aiming for scaled-up photofermentative hydrogen production, the natural solar light is a more cost-effective light source compared to artificial ones (Adessi & De Philippis, 2014), which would otherwise negatively impact the process's economics (Capson-Tojo et al., 2020). The pigments used by PPB in their light-harvesting complexes are carotenoids and bacteriochlorophylls, whose combination enables PPB to cover a broad range of the visible spectrum (Swainsbury et al., 2023). Carotenoids absorb light between 450 and 550 nm, while bacteriochlorophylls in the near-infrared region, with peaks typically around 800, 850, and 880 nm (Swainsbury et al., 2023). The ability to absorb in the near-infrared region is a peculiarity almost exclusive to PPB (Madigan & Jung, 2009). This feature can promote the development of

large-scale PPB applications, as providing an appropriate light filter, like UV-VIS absorbing foils (Allegue et al., 2020) or colored filter glass (Fradinho et al., 2021), would enable the selective enrichment of PPB under unsterile conditions, preventing the growth of other photosynthetic microorganisms such as microalgae and cyanobacteria (Capson-Tojo et al., 2022). Another important factor to consider in optimizing the process is the photobioreactor (PBR) geometry, as it plays a crucial role in ensuring sufficient light distribution, optimal culture mixing and gas exchange, and scalability of the process (Adessi & De Philippis, 2014). Many different PBR geometries have been tested for photofermentative hydrogen production, with tubular and flat panel bioreactors as the generally preferred ones (Adessi & De Philippis, 2014).

Leveraging metabolic engineering and genetic manipulation is yet another promising approach for driving the PF process toward higher yields. In natural strains, photobiological hydrogen production is inherently constrained by several factors, including hydrogen consumption by uptake hydrogenases, nitrogenase inhibition by ammonium, limitations of the light-harvesting complexes, and the presence of alternative metabolic pathways like PHA production and carbon dioxide fixation that redirect electrons to non-hydrogen evolving reactions (Adessi, 2013). Since uptake hydrogenases directly contribute to hydrogen consumption, several studies have explored their inactivation by deletion of *hup* genes involved in their synthesis, reporting significant increases in total hydrogen production (Kars & Gündüz, 2010). However, one of the main challenges in wastewater treatment via PF is that these waste streams typically contain ammonium at concentrations above the nitrogenase inhibition threshold, necessitating ammonium removal pretreatment or the application of high dilution rates. Genetically engineered PPB can help in solving this issue. Modifications in the *nif*A gene can result in PPB exhibiting ammonium insensitivity, making nitrogenase constitutively active despite ammonium levels (D. Cheng et al., 2022). Another common approach for boosting hydrogen yields is the suppression of PHA production pathways, which has been observed to benefit hydrogen production by directing all the cells' reducing power to photofermentation (Kars & Gündüz, 2010). Some PPB can produce significant amounts of PHA (Monroy & Buitrón, 2020), directly competing with hydrogen production for excess reducing power dissipation (Adessi, 2013). Another pathway in competition with nitrogenase for electrons is carbon

dioxide fixation. Its reduction has been explored in several studies by inactivating, for instance, some of its key enzymes, such as RuBisCO and phosphoribulokinase (McCully & McKinlay, 2016).

### 2.5.3. Coupled Dark-Photo Fermentation systems

A promising approach for enhancing the overall process yield is the integration of Dark and Photo Fermentation (DF–PF). One of the main limits associated with DF processes is the relatively low hydrogen yields achievable, hindered by the concomitant accumulation of VFA along the process. The theoretical maximum glucose conversion efficiency achievable by the sole DF process, when acetate is the main metabolite generated, is stoichiometrically limited to 4 $mol_{H2}$ $mol_{glucose}^{-1}$, as in Eq. 8 (Hawkes et al., 2007). Therefore, a substantial portion of the supplied organic compounds remains in the DFE as VFA, requiring the effluent to undergo further treatments before its release into the environment (Rai & Singh, 2016). PPB's capability to convert a broad range of short-chain organic acids into hydrogen provides a unique opportunity for process improvement, as coupling the two processes in a two-phase sequential approach allows for further valorization of DF organic byproducts. When acetate is the main metabolite present in the DFE, PPB can theoretically convert it completely to hydrogen and carbon dioxide, as in Eq. 20, yielding 4 $mol_{H2}$ $mol_{acetate}^{-1}$ (Ghosh et al., 2017). Operating a sequential DF–PF process, the complete conversion of glucose to hydrogen and carbon dioxide is theoretically achievable, yielding an overall maximum conversion efficiency of 12 $mol_{H2}$ $mol_{glucose}^{-1}$, as in Eq. 25 (Argun & Kargi, 2011).

DF: $C_6H_{12}O_6 + 2H_2O \rightarrow 2CH_3COOH + 2CO_2 + 4H_2$ Eq. 8

PF: $CH_3COOH + 2H_2O \xrightarrow{light} 4H_2 + 2CO_2$ Eq. 20

DF–PF $C_6H_{12}O_6 + 6H_2O \rightarrow 12H_2 + 6CO_2$ Eq. 25

However, these reaction yields are theoretical, and real yields of combined DF–PF systems are generally much lower, due to: i) the production of a mixture of VFAs and other organic compounds as byproduct during the DF phase (Eq. 8 – Eq. 13, section 2.4.1); ii) the lower efficiency of PPB in converting these organic compounds to hydrogen during the PF phase (Eq. 21 – Eq. 24, section 2.5.1); iii) the utilization of part of the supplied substrate for microbial growth (Adessi & De Philippis, 2012); or the presence of other inhibitory factors within the two systems (D. Cheng et al., 2022; Elbeshbishy et al., 2017). Additionally, the integration of the two processes needs to consider their differences in production rates. Although PF yields higher conversion efficiencies when comparted to DF, it is generally characterized by substantially lower production rates (Ghosh et al., 2018). This outcome is due to: i) the lower biomass concentration achievable in PF systems, limited by light distribution constraints, compared to that of DF ones (Moscoviz et al., 2018), and ii) the main enzyme responsible for PPB's photoheterotrophic hydrogen evolution, nitrogenase, which catalyzes hydrogen production at a much slower rate than the hydrogenases utilized by HPB in DF (Xuan et al., 2023).

DF and PF can be integrated following single-stage or two-stage approaches. In single-stage DF–PF, the two processes occur simultaneously in one reactor, which is inoculated with both dark fermentative HPB and PPB in a single environment (Ghosh et al., 2018). Under this configuration, the VFAs generated during the DF phase are directly available for PPB for hydrogen evolution, reducing the capital and operative cost of operating two different reactors. Moreover, since VFA are immediately consumed by PPB as soon as they are generated, their accumulation in the system and the consequent excessive acidification is prevented, decreasing the risk of substrate inhibition and the need for external pH adjustments (Rai & Singh, 2016). However, relying on a single reactor for both processes does not allow them to be carried out under their respective optimal conditions (Akhlaghi & Najafpour-Darzi, 2020). Reduced light availability, in particular, may hinder PPB hydrogen production, limiting their role in the overall process (Rai & Singh, 2016). In a sequential two-stage DF–PF, the processes are carried out in two separate reactors, allowing each stage to operate under its respective optimal conditions (D. Cheng et al., 2022). Of course, this approach involves certain trade-offs,

such as the increased process complexity associated with operating two separate reactors and the necessity for cost-intensive pretreatments of the DFE before the PF phase, such as autoclaving, centrifugation, dilution, the addition of nutrients, etc (Ghosh et al., 2018). Several authors studied the efficiency of sequential two-stage DF–PF processes to determine the optimal operative parameters and reactor configuration, highlighting the advantages of these approaches over the single DF or PF process. As previously discussed for single-stage DF and PF process, one of the main advantages of DF–PF is the possibility of exploiting organic waste as a carbon source, with a substantial positive impact on the process economics (Hay et al., 2013). However, while extensive studies have explored the potential of FW valorization through DF, to the best of our knowledge, only a limited number have investigated its application in DF-PF coupled systems. Table 5 and Table 6 provide some examples of DF–PF batch and continuous treatments of organic waste. Hydrogen production yields are substantially boosted when the two processes are coupled, mainly due to the higher process efficiency of PF, generally ranging between 600 and 800 $mL_{H2}\ g_{COD}^{-1}$ (Table 5). In the study conducted by Niño-Navarro et al., (2020), for example, a DF–PF system was implemented for the concomitant treatment of FW and Cheese whey powder. The process was specifically designed to maximize lactate production during the DF phase rather than hydrogen production, resulting in a yield of 12.5 $mL_{H2}\ g_{COD}^{-1}$ for this first phase, significantly lower than the yields reported in the literature for similar substrates. For instance, S. H. Kim et al., (2004) reported a nearly 10-fold higher yield (122.95 $mL_{H2}\ g_{COD}^{-1}$) for the DF of FW and WAS. However, the subsequent integration of a PF performed by Niño-Navarro et al., (2020), enabled a more efficient conversion of the organic compounds into hydrogen, resulting in an overall yield of 793.7 $mL_{H2}\ g_{COD}^{-1}$, way higher than the one possibly achievable by the sole DF. A similar trend is generally reported also by other authors, with PF consistently enhancing the process yields (Laurinavichene et al., 2010; Su et al., 2010; Zong et al., 2009).

*Table 5, Examples of batch mode DF-PF tests treating organic waste*

| Substrate | DFE Pretreatments | T (°C)<br>DF \| PF | pH<br>DF \| PF | $H_2$ yield<br>($mL_{H2}$ $g_{COD}^{-1}$) | HPR<br>($mL_{H2}$ $L_{reactor}^{-1}$ $h^{-1}$) | Reference |
|---|---|---|---|---|---|---|
| FW + Cheese whey powder | Centrifugation, sterilization, 1:10 dilution | 35 \| 30 | 5.5 \| 6.8 | 12.5 (DF)<br>781.1 (PF)<br>793.7 (DF-PF) | 52.7 (PF)<br>62.8 (DF-PF) | (Niño-Navarro et al., 2020) |
| FW (potatoes) | - | 37 \| 28 | - | 82 (DF)<br>572 (PF)<br>654 (DF-PF) | 18.75 (PF) | (Laurinavichene et al., 2010) |
| FW | Centrifugation, 1:2 dilution | 37 \| 30 | 6.8 \| 7.0 | 206 (DF)<br>423 (PF)<br>629 (DF-PF) | 165 (DF)<br>116 (PF) | (Zong et al., 2009) |
| Water hyacinth hydrolysate | Centrifugation, sterilization, dilution | 35 \| 30 | 7.0 \| 7.0 | 73.5 (DF) *<br>522.6 (PF) *<br>596.1 (DF-PF) * | 59.7 (DF)<br>8.2 (PF) | (Su et al., 2010) |

* $mL_{H2}$ $g_{TVS}^{-1}$

*Table 6, Examples of continuous mode DF-PF tests treating organic waste*

| Substrate | DFE Pretreatments | T (°C) DF \| PF | pH DF \| PF | HRT (h) DF \| PF | OLR ($g_{COD}$ $L^{-1}$ $d^{-1}$) DF \| PF | $H_2$ yield ($mL_{H2}$ $g_{COD}^{-1}$) | HPR ($L_{H2}$ $L_{reactor}^{-1}$ $d^{-1}$) | Reference |
|---|---|---|---|---|---|---|---|---|
| Synthetic lignocellulosic hydrolysate | 1:2 dilution | 35 \| 32 | 6.0 \| 7.5 | 84 | 0.76 | 484 (DF)<br>275 (PF)<br>516 (DF-PF) | 0.5 (DF-PF) | (Zagrodnik & Duber, 2024) |
| Corn stover hydrolysate | - | 4.5 \| 7.0 | 35 \| 30 | 16 \| 48 | 15 | 500 (DF) | 7.5 (DF)<br>4.7 (PF)<br>5.42 (DF-PF) | (Q. Zhang et al., 2018) |
| Corn stover hydrolysate | NH4+ removal (zeolites), 1:1.5 dilution | 5.5 \| 7.0 | 40 \| 30 | 12 \| 24 | 10 | - | 4.70 (DF)<br>4.60 (PF)<br>6.45 (DF-PF) | (Y. Li et al., 2021) |
| WAS | VFA separation membrane | 5.5 \| 7.0 | 35 \| 30 | 72 \| 120 | 3.37 | 0 (AF) [a]<br>160.5 (PF) | 0 (AF) [a]<br>0.1 (PF) | (Jeong et al., 2007) |

[a] AF: acidogenic fermentation phase designed for VFA accumulation rather than hydrogen production

## 2.6. Converting hydrogen into e-fuels

Renewable hydrogen is expected to play an important role in decarbonizing the energy sector (Beyazit, 2025), particularly through its application in e-fuels generation. E- fuels are synthetic hydrocarbon fuels derived from the reaction of renewable hydrogen with either carbon dioxide or nitrogen (Nemmour et al., 2023). The term “e-fuels” derives from “electro” fuels, as they primarily refer to energy carriers produced by the conversion of electrical renewable power to hydrogen via water electrolysis (green hydrogen, section 2.2), followed by its transformation into gaseous or liquid fuels (Viscardi et al., 2021). However, beyond electrolysis-derived hydrogen, other forms of renewable hydrogen can serve as feedstocks for e-fuel production, such as Dark Fermentation, Photo Fermentation, and biomass gasification (Segovia-Hernández, 2025). Regardless of the specific pathways involved in hydrogen production and the different types of end-products, all e-fuels share the common feature of coming from renewable sources and being carbon-neutral (Viscardi et al., 2021). Additionally, their sustainability is further reinforced by their potential compatibility with existing infrastructure and vehicle fleet, facilitating their integration into the current energy and transport systems without extensive modifications (Viscardi et al., 2021). Liquid e-fuels include ammonia, methanol, ethylene, propylene, and high-carbon fuels like kerosene, petrol, diesel, and other derivates (dena, 2021). E-ammonia is produced via the Haber-Bosch process (Eq. 26) combining green hydrogen and nitrogen separated from the air through cryogenic distillation, membrane separation, or pressure swing adsorption (Nemmour et al., 2023). E-methanol is synthesized through the catalytical hydrogenative conversion of captured carbon dioxide and renewable hydrogen to methanol, as described in Eq. 27 (Nemmour et al., 2023). E-methanol can then be catalytically converted to propylene and ethylene using the methanol-to-olefins process (dena, 2021) or higher-carbon fuels using the Fisher-Tropsch process (Segovia-Hernández, 2025).

$$3H_2 + N_2 \rightarrow 2NH_3 \quad \text{Eq. 26}$$

$$3H_2 + CO_2 \rightarrow CH_3OH + H_2O \quad \text{Eq. 27}$$

Gaseous e-fuels include hydrogen itself and low-carbon fuels like methane, ethane, and propane (Segovia-Hernández, 2025). Focusing on methane production, the reaction can occur through a catalytic or biological process, in either case, based on the Sabatier reaction reported in Eq. 14 (Chatzis et al., 2024).

$$4H_2 + CO_2 \rightarrow CH_4 + 2H_2O \quad \text{Eq. 14}$$

Catalytic methanation typically occurs at high temperatures (200 – 550 °C) and pressures (1 – 100 bar) and is mediated by metal-based catalysts such as nickel, ruthenium, rhodium, or cobalt (Ghaib & Ben-Fares, 2018). In contrast, biological methanation is catalyzed by hydrogenotrophic methanogens, microorganisms that can biologically perform Sabatier reaction under mild conditions, at temperatures generally ranging between 35 to 70 °C and pressures from ambient values up to approximately 10 bar (Chatzis et al., 2024). These mild reaction conditions are one of the key aspects that make biological methanation an attractive alternative for e-methane production compared to the catalytic method. Additionally, biological methanation is more tolerant to gas impurities and intermittent hydrogen supply, while the catalytic process is less flexible, requiring a steady and high-purity gas feeding (Chatzis et al., 2024). However, biological methanation also faces challenges, primarily due to the lower production rates (approximately 50 times lower than those of catalytic methanation) and the low solubility of hydrogen in water (Chatzis et al., 2024). This limitation necessitates the implementation of specific strategies to improve gas-liquid mass transfer efficiency, thereby enhancing hydrogen bioavailability for the microbial community (Ngu et al., 2023). For the biological process to become competitive with the catalytic counterpart, therefore, further advancement in terms of theoretical knowledge on microbial kinetics, along with process and bioreactor design optimization, is needed (Kofoed et al., 2021).

### 2.6.1. Bio-methanation and Specific Hydrogenotrophic Methanogenic Activity

Biological Methanation (BM) is the phase in which, during AD, the metabolites generated as byproducts in the previous steps are converted into methane. According to their substrate utilization for methane production, methanogens are classified as: i) hydrogenotrophic methanogens, which convert carbon dioxide and hydrogen into methane; ii) acetoclastic methanogens, which utilize acetate as main substrate; and iii) methylotrophic methanogens, which metabolize methanol and other methyl compounds (Conrad, 2020). BM typically refers to systems in which hydrogenotrophic methanogen activity is prioritized, aiming to maximize the conversion of carbon dioxide and hydrogen into methane. While AD produces biogas, typically composed of 60 – 65 % methane with the remaining being mostly carbon dioxide (Metcalf & Eddy, 2014), BM can yield biomethane with methane concentration exceeding 96 % (Chatzis et al., 2024), thereby meeting the 95 % purity required for the natural gas grid by many countries (Angelidaki et al., 2018). Depending on the process configuration, BM is classified into two categories: in-situ and ex-situ methanation. In in-situ BM, hydrogen is fed directly into an AD reactor, thus promoting the conversion of the carbon dioxide naturally present in the biogas and increasing the overall methane content. In ex-situ configuration, instead, carbon dioxide and hydrogen are fed into a separate reactor, allowing for setting optimal conditions specifically for BM (Chatzis et al., 2024). Ex-situ BM can serve as a biogas upgrading strategy, when biogas and hydrogen are injected into the reactor, or as a carbon dioxide valorization process when captured carbon dioxide and renewable hydrogen are converted into methane (Laguillaumie et al., 2022; Sieborg et al., 2020). Regardless of the process configuration employed, one of the key parameters for defining BM efficiency is the Specific Hydrogenotrophic Methanogenic Activity (SHMA). The specific methanogenic activity represents the capacity of a defined microbial strain or community to produce methane (Hussain & Dubey, 2017). It is calculated as the maximum methane production rate per volatile suspended solids present in the anaerobic biomass, as a rough estimation of the microbial concentration (Ripoll et al., 2020). Unlike other biological processes, such as AD, DF, and PF,

the determination of the volume of gas produced by hydrogenotrophic methanogens requires specific strategies. In this case, in fact, a total of five moles of reagents (four of hydrogen and one of carbon dioxide) are converted into one mole of methane, as reported in Eq. 14 (section 2.6.1). Since the reagents are typically supplied as gases and are consumed during the process, the bio-methanation reaction leads to a decrease in headspace pressure rather than an increase, as usually occurs in other biological processes, making gas collection and measurement more challenging. One approach consists of the periodic determination of headspace pressure along with analysis of headspace composition by gas chromatography (Dolfing & Bloemen, 1985). However, this determination method has been reported to be time-consuming, labor-intensive, and hindered by potential gas leaks and pressure drops associated with gas sampling (Ripoll et al., 2020). An alternative approach is the manometric method, proposed by (Coates et al., 1996), in which gas sampling and GC analysis are avoided, and the estimation of methane production is based solely on the determination of the reactor headspace pressure. Based on the stoichiometry of the bio-methanation reaction, the recorded pressure drop is used to estimate methane production, according to Eq. 28 (Ripoll et al., 2020).

$$\Delta n_{CH4} = -\frac{\Delta n_{HS}}{4} = \frac{\Delta P V_{HS}}{4RT} \qquad \text{Eq. 28}$$

where $\Delta n_{HS}$ is the difference in the number of moles in the headspace between two time-points, $\Delta P$ is the consequent difference in pressure, $V_{HS}$ is the headspace volume, $R$ is the molar gas constant, and $T$ the test temperature in Kelvin. By relying solely on pressure determination, this method has been reported to be easier to perform, less labor-intensive, and capable of facilitating multiple replicate analyses, reducing bias associated with gas removal and leaks during sampling, and minimizing operator errors (Coates et al., 1996). The moles of methane produced are then generally converted into COD based on its complete stoichiometry conversion (64 $g_{COD}$ $mol_{CH4}^{-1}$) and then used for the determination of the biomass SHMA, according to Eq. 29

$$SHMA = \frac{\Delta n_{CH4} \times C}{g_{VSS} \times \Delta t} \quad \text{Eq. 29}$$

where *C* is the methane conversion factor from moles to COD, *gVSS* is the amount of volatile suspended solids present in the tested biomass, and *Δt* is the interval between two time-points.

SHMA determination has been employed by several authors for the definition of BM process performances, both regarding reactor configuration and biomass efficiency. Different parameters may affect the achieved SHMA, including pH, temperature, hydrogen partial pressure, gas-liquid mass transfer efficiency, and the composition of the microbial community. The temperature in BM systems must meet levels suitable for hydrogenotrophic methanogen growth, typically falling within the mesophilic (30 – 45 °C) or thermophilic (50 – 70 °C) ranges (Jensen et al., 2021). Despite increasing temperatures should adversely affect hydrogen solubility and gas-liquid mass transfer, under thermophilic conditions BM generally results in higher conversion yields, driven by the higher activity of hydrogenotrophic methanogens within this range of temperatures (Jensen et al., 2021; Kozak et al., 2022). Hydrogen partial pressure is a key driving force in hydrogen solubilization and, therefore, its bioavailability for hydrogenotrophic methanogens (Jensen et al., 2021). Higher hydrogen partial pressure improves hydrogen solubility, enhancing BM process yields (Ebrahimian et al., 2022). However, excessive values can lead to microbial inhibition, especially under in-situ configurations, where an increase in this parameter can lead to VFA accumulation and a pH drop within the reactor (Sieborg et al., 2020). Another parameter affecting gas-liquid mass transfer is agitation, which, when increased, promotes the dispersion and retention of gas bubbles, thereby enhancing the production rates (Jensen et al., 2021). Finally, microbial community composition and structure play an important role in defining SHMA, as a higher abundance of hydrogenotrophic methanogens enhances process yields. Additionally, biomass immobilization, increasing cell density, has been reported to improve interphase contact and, consequently, substrate utilization (González et al., 2023). Table 7 provides a comparison of SHMA values achieved by suspended and immobilized biomass. Ripoll et al., (2020), for instance, compared the SHMA of different anaerobic biomass typologies, reporting

a value of 72 ± 7 $mg_{COD(CH4)}\ g_{VSS}^{-1}\ d^{-1}$ for suspended biomass, from 3 to 6 times lower than the one achieved employing granular sludge (260 – 480 $mg_{COD(CH4)}\ g_{VSS}^{-1}\ d^{-1}$). This outcome is supported by several other authors, reporting higher SHMA values for granular sludge (570 - 790 $mg_{COD(CH4)}\ g_{VSS}^{-1}\ d^{-1}$, Gonzalez-Estrella et al., 2013; Regueiro et al., 2012) compared to those achieved by suspended biomass (18 – 60 $mg_{COD(CH4)}\ g_{VSS}^{-1}\ d^{-1}$, Hao et al., 2017; C. Liu et al., 2016; Pokorna et al., 2019). However, SHMA values comparable to those obtained with granular sludge were achieved by Regueiro et al., (2012) for several biomass types, ranging between 370 and 840 $mg_{COD(CH4)}\ g_{VSS}^{-1}\ d^{-1}$. This evidence further highlights that biomass structure and community composition are not the only factors affecting process yields but rather one of the many aspects to consider when aiming for process optimization.

*Table 7, Examples of SHMA values achieved by suspended biomass and granular sludge*

| Biomass type | Inoculum source \| waste treated | SHMA ($mg_{COD(CH4)}$ $g_{VSS}^{-1}$ $d^{-1}$) | Reference |
|---|---|---|---|
| Suspended biomass | Laboratory-scale CSTR (high TS content) \| Municipal wastewater | 18 ± 1 | (C. Liu et al., 2016) |
| | Laboratory-scale CSTR (low TS content) \| Municipal wastewater | 21 ± 4 | |
| | Full-scale CSTR \| Municipal wastewater | 45 ± 2 | (Hao et al., 2017) |
| | Laboratory-scale CSTR (mesophilic) \| Sewage sludge | 37 | (Pokorna et al., 2019) |
| | Laboratory-scale CSTR (thermophilic) \| Sewage sludge | 60 | |
| | Bench-scale CSTR \| Manure | 72 ± 7 | (Ripoll et al., 2020) |
| | Laboratory-scale CSTR \| Manure and glycerine | 370 ± 70 | (Regueiro et al., 2012) |
| | CSTR \| Sugar industry wastewater | 450 ± 60 | |
| | CSTR \| Sewage sludge | 550 ± 150 | |
| | CSTR \| Yeast industry wastewater | 830 ± 80 | |
| | CSTR \| Dairy and fish waste | 840 ± 80 | |
| Granular sludge | Pilot-scale EGSB \| Beverage wastewater | 260 ± 10 | (Ripoll et al., 2020) |
| | Laboratory-scale EGSB \| Beverage wastewater | 310 ± 10 | |
| | Pilot-scale UASB \| Dairy waste | 350 ± 10 | |
| | Full-scale UASB \| Dairy waste | 480 ± 30 | |
| | Laboratory-scale EGSB \| Protein-rich wastewater | 480± 30 | |
| | Full-scale UASB \| Brewery wastewater | 570 ± 30 | (Gonzalez-Estrella et al., 2013) |
| | UASB \| Brewery wastewater | 790 ± 40 | (Regueiro et al., 2012) |

## 2.7. References

Abdin, Z., Zafaranloo, A., Rafiee, A., Mérida, W., Lipiński, W., & Khalilpour, K. R. (2020). Hydrogen as an energy vector. In *Renewable and Sustainable Energy Reviews* (Vol. 120). Elsevier Ltd. https://doi.org/10.1016/j.rser.2019.109620

Acar, C., & Dincer, I. (2019). Review and evaluation of hydrogen production options for better environment. *Journal of Cleaner Production*, *218*, 835–849. https://doi.org/10.1016/j.jclepro.2019.02.046

Adessi, A., & De Philippis, R. (2012). Hydrogen production: Photofermentation. In *Springer 4* (Vol. 9781461412083, pp. 53–75). TUT Press. https://doi.org/10.1007/978-1-4614-1208-3_4

Adessi, A., & De Philippis, R. (2014). Photobioreactor design and illumination systems for H2 production with anoxygenic photosynthetic bacteria: A review. In *International Journal of Hydrogen Energy* (Vol. 39, Issue 7, pp. 3127–3141). Elsevier Ltd. https://doi.org/10.1016/j.ijhydene.2013.12.084

Adessi, Alessandra. (2013). *Hydrogen production using Purple Non-Sulfur Bacteria (PNSB) cultivated under natural or artificial light conditions with synthetic or fermentation derived substrates*. Firenze University Press.

Agyekum, E. B., Nutakor, C., Agwa, A. M., & Kamel, S. (2022). A Critical Review of Renewable Hydrogen Production Methods: Factors Affecting Their Scale-Up and Its Role in Future Energy Generation. In *Membranes* (Vol. 12, Issue 2). MDPI. https://doi.org/10.3390/membranes12020173

Ajanovic, A., Sayer, M., & Haas, R. (2022). The economics and the environmental benignity of different colors of hydrogen. *International Journal of Hydrogen Energy*. https://doi.org/10.1016/j.ijhydene.2022.02.094

Akhlaghi, N., & Najafpour-Darzi, G. (2020). A comprehensive review on biological hydrogen production. In *International Journal of Hydrogen Energy* (Vol. 45, Issue 43, pp. 22492–22512). Elsevier Ltd. https://doi.org/10.1016/j.ijhydene.2020.06.182

Alexandropoulou, M., Antonopoulou, G., Trably, E., Carrere, H., & Lyberatos, G. (2018). Continuous biohydrogen production from a food industry waste: Influence of operational parameters and microbial community analysis. *Journal of Cleaner Production*, *174*, 1054–1063. https://doi.org/10.1016/j.jclepro.2017.11.078

Alibardi, L., & Cossu, R. (2015). Composition variability of the organic fraction of municipal solid waste and effects on hydrogen and methane production potentials. *Waste Management*, *36*, 147–155. https://doi.org/10.1016/j.wasman.2014.11.019

Allegue, L. D., Puyol, D., & Melero, J. A. (2020). Novel approach for the treatment of the organic fraction of municipal solid waste: Coupling thermal hydrolysis with anaerobic digestion and photo-fermentation. *Science of the Total Environment*, *714*. https://doi.org/10.1016/j.scitotenv.2020.136845

American Chemistry Society. (2020, June 22). *Hydrogen*. Molecule of the Week Archive. https://www.acs.org/molecule-of-the-week/archive/h/hydrogen.html

Androga, D. D., Ozgur, E., Eroglu, I., Gunduz, U., & Yucel, M. (2012). Photofermentative Hydrogen Production in Outdoor Conditions. In *Hydrogen Energy - Challenges and Perspectives*. InTech. https://doi.org/10.5772/50390

Angelidaki, I., Treu, L., Tsapekos, P., Luo, G., Campanaro, S., Wenzel, H., & Kougias, P. G. (2018). Biogas upgrading and utilization: Current status and perspectives. In *Biotechnology Advances* (Vol. 36, Issue 2, pp. 452–466). Elsevier Inc. https://doi.org/10.1016/j.biotechadv.2018.01.011

Anjum, S., Aslam, S., Hussain, N., Bilal, M., Boczkaj, G., Smułek, W., Jesionowski, T., & Iqbal, H. M. N. (2023). Bioreactors and biophoton-driven biohydrogen production strategies. *International Journal of Hydrogen Energy*, *48*(55), 21176–21188. https://doi.org/10.1016/j.ijhydene.2023.01.363

Antonelli, M., Giordano, C., Chiriacò, M. V., Casari, S., Cadel, E., Chen, P. J., Magnani, A., Pizzileo, G., Falasconi, L., Alboni, F., & Cicatiello, C. (2024). Assessing the Monetary Value and Environmental Impact of Household Food Waste in Italy. *Sustainability (Switzerland)*, *16*(23). https://doi.org/10.3390/su162310614

Argun, H., & Kargi, F. (2011). Bio-hydrogen production by different operational modes of dark and photo-fermentation: An overview. In *International Journal of Hydrogen Energy* (Vol. 36, Issue 13, pp. 7443–7459). https://doi.org/10.1016/j.ijhydene.2011.03.116

Assawamongkholsiri, T., Reungsang, A., & Sittijunda, S. (2019). Photo-hydrogen and lipid production from lactate, acetate, butyrate, and sugar manufacturing wastewater with an alternative nitrogen source by rhodobacter sp. kku-ps1. *PeerJ*, *2019*(4). https://doi.org/10.7717/peerj.6653

Baldi, F., Pecorini, I., & Iannelli, R. (2019). Comparison of single-stage and two-stage anaerobic co-digestion of food waste and activated sludge for hydrogen and methane production. *Renewable Energy*, *143*, 1755–1765. https://doi.org/10.1016/j.renene.2019.05.122

Bao, M. D., Su, H. J., & Tan, T. W. (2013). Dark fermentative bio-hydrogen production: Effects of substrate pre-treatment and addition of metal ions or L-cysteine. *Fuel*, *112*, 38–44. https://doi.org/10.1016/j.fuel.2013.04.063

Barbosa, M. J., Rocha, J. M. S., Tramper, J., & Wijffels, R. H. (2001). Acetate as a carbon source for hydrogen production by photosynthetic bacteria. In *Journal of Biotechnology* (Vol. 85). www.elsevier.com/locate/jbiotec

Basak, N., Jana, A. K., Das, D., & Saikia, D. (2014). Photofermentative molecular biohydrogen production by purple-non-sulfur (PNS) bacteria in various modes: The present progress and future perspective. In *International Journal of Hydrogen Energy* (Vol. 39, Issue 13, pp. 6853–6871). Elsevier Ltd. https://doi.org/10.1016/j.ijhydene.2014.02.093

Beyazit, N. I. (2025). Journey to a sustainable future: The importance of renewable hydrogen in industrial and domestic applications. In *International Journal of Hydrogen Energy* (Vol. 99, pp. 836–851). Elsevier Ltd. https://doi.org/10.1016/j.ijhydene.2024.12.065

Bimestre, T. A., Júnior, J. A. M., Canettieri, E. V., & Tuna, C. E. (2022). Hydrodynamic cavitation for lignocellulosic biomass pretreatment: a review of recent developments and future perspectives. In *Bioresources and Bioprocessing* (Vol. 9, Issue 1). Springer Science and Business Media Deutschland GmbH. https://doi.org/10.1186/s40643-022-00499-2

Cao, K., Zhi, R., & Zhang, G. (2020). Photosynthetic bacteria wastewater treatment with the production of value-added products: A review. In *Bioresource Technology* (Vol. 299). Elsevier Ltd. https://doi.org/10.1016/j.biortech.2019.122648

Cao, Y., Liu, H., Liu, W., Guo, J., & Xian, M. (2022). Debottlenecking the biological hydrogen production pathway of dark fermentation: insight into the impact of strain improvement. In *Microbial Cell Factories* (Vol. 21, Issue 1). BioMed Central Ltd. https://doi.org/10.1186/s12934-022-01893-3

Capson-Tojo, G., Batstone, D. J., Grassino, M., & Hülsen, T. (2022). Light attenuation in enriched purple phototrophic bacteria cultures: Implications for modelling and reactor design. *Water Research*, *219*. https://doi.org/10.1016/j.watres.2022.118572

Capson-Tojo, G., Batstone, D. J., Grassino, M., Vlaeminck, S. E., Puyol, D., Verstraete, W., Kleerebezem, R., Oehmen, A., Ghimire, A., Pikaar, I., Lema, J. M., & Hülsen, T. (2020). Purple phototrophic bacteria for resource recovery: Challenges and opportunities. In *Biotechnology Advances* (Vol. 43). Elsevier Inc. https://doi.org/10.1016/j.biotechadv.2020.107567

Carmona-Cabello, M., Garcia, I. L., Leiva-Candia, D., & Dorado, M. P. (2018). Valorization of food waste based on its composition through the concept of biorefinery. In *Current Opinion in Green and Sustainable Chemistry* (Vol. 14, pp. 67–79). Elsevier B.V. https://doi.org/10.1016/j.cogsc.2018.06.011

Chatzis, A., Gkotsis, P., & Zouboulis, A. (2024). Biological methanation (BM): A state-of-the-art review on recent research advancements and practical implementation in full-scale BM units. In *Energy Conversion and Management* (Vol. 314). Elsevier Ltd. https://doi.org/10.1016/j.enconman.2024.118733

Chen, W., Li, T., Ren, Y., Wang, J., Chen, H., & Wang, Q. (2023). Biological hydrogen with industrial potential: Improvement and prospection in biohydrogen production. In *Journal of Cleaner Production* (Vol. 387). Elsevier Ltd. https://doi.org/10.1016/j.jclepro.2022.135777

Cheng, D., Ngo, H. H., Guo, W., Chang, S. W., Nguyen, D. D., Bui, X. T., Wei, W., Ni, B., Varjani, S., & Hoang, N. B. (2022). Enhanced photo-fermentative biohydrogen production from biowastes: An overview. In *Bioresource Technology* (Vol. 357). Elsevier Ltd. https://doi.org/10.1016/j.biortech.2022.127341

Cheng, Q., Zhang, R., Shi, Z., & Lin, J. (2024). Review of common hydrogen storage tanks and current manufacturing methods for aluminium alloy tank liners. *International Journal of*

*Lightweight Materials and Manufacture*, *7*(2), 269–284. https://doi.org/10.1016/j.ijlmm.2023.08.002

Chu, C. F., Xu, K. Q., Li, Y. Y., & Inamori, Y. (2012). Hydrogen and methane potential based on the nature of food waste materials in a two-stage thermophilic fermentation process. *International Journal of Hydrogen Energy*, *37*(14), 10611–10618. https://doi.org/10.1016/j.ijhydene.2012.04.048

Coates, J. D., Coughlanb, M. F., & Colleranb, E. (1996). Methods Simple method for the measurement of the hydrogenotrophic methanogenic activity of anaerobic sludges. In *Journal ofMicrobiological Journal of Microbiological Methods* (Vol. 26).

Conrad, R. (2020). Importance of hydrogenotrophic, aceticlastic and methylotrophic methanogenesis for methane production in terrestrial, aquatic and other anoxic environments: A mini review. In *Pedosphere* (Vol. 30, Issue 1, pp. 25–39). Soil Science Society of China. https://doi.org/10.1016/S1002-0160(18)60052-9

Corona-Martínez, D. A., Martínez-Amador, S. Y., Rodríguez-De la Garza, J. A., Laredo-Alcalá, E. I., & Pérez-Rodríguez, P. (2025). Recent Advances in Scaling up Bioelectrochemical Systems: A Review. *BioTech*, *14*(1), 8. https://doi.org/10.3390/biotech14010008

Correa-Villa, C., Moreno-Cárdenas, E., & de Bruijn, J. (2024). Presence of lactic acid bacteria in hydrogen production by dark fermentation: competition or synergy. In *World Journal of Microbiology and Biotechnology* (Vol. 40, Issue 12). Springer Science and Business Media B.V. https://doi.org/10.1007/s11274-024-04167-9

Das, D. (2009). Advances in biohydrogen production processes: An approach towards commercialization. *International Journal of Hydrogen Energy*, *34*(17), 7349–7357. https://doi.org/10.1016/j.ijhydene.2008.12.013

dena. (2021). *Powerfuels: Missing link to a successful global energy transition*. www.powerfuels.de

Detman, A., Laubitz, D., Chojnacka, A., Wiktorowska-Sowa, E., Piotrowski, J., Salamon, A., Kaźmierczak, W., Błaszczyk, M. K., Barberan, A., Chen, Y., Łupikasza, E., Yang, F., & Sikora, A. (2021). Dynamics and Complexity of Dark Fermentation Microbial Communities Producing Hydrogen From Sugar Beet Molasses in Continuously Operating Packed Bed Reactors. *Frontiers in Microbiology*, *11*. https://doi.org/10.3389/fmicb.2020.612344

Diekert, G., & Wohlfarth, G. (1994). Metabolism of homoacetogens. In *Antonie van Leeuwenhoek* (Vol. 66).

Dolfing, J., & Bloemen, W. G. B. M. (1985). Activity measurements as a tool to characterize the microbial composition of methanogenic environments. In *Journal of Microbiological Methods* (Vol. 4).

Dong, L., Zhenhong, Y., Yongming, S., Xiaoying, K., & Yu, Z. (2009). Hydrogen production characteristics of the organic fraction of municipal solid wastes by anaerobic mixed culture fermentation. *International Journal of Hydrogen Energy*, *34*(2), 812–820. https://doi.org/10.1016/j.ijhydene.2008.11.031

Dou, B., Zhang, H., Song, Y., Zhao, L., Jiang, B., He, M., Ruan, C., Chen, H., & Xu, Y. (2019). Hydrogen production from the thermochemical conversion of biomass: Issues and challenges. In *Sustainable Energy and Fuels* (Vol. 3, Issue 2, pp. 314–342). Royal Society of Chemistry. https://doi.org/10.1039/c8se00535d

Dzulkarnain, E. L. N., Audu, J. O., Wan Dagang, W. R. Z., & Abdul-Wahab, M. F. (2022). Microbiomes of biohydrogen production from dark fermentation of industrial wastes: current trends, advanced tools and future outlook. In *Bioresources and Bioprocessing* (Vol. 9, Issue 1). Springer Science and Business Media Deutschland GmbH. https://doi.org/10.1186/s40643-022-00504-8

Ebrahimian, F., De Bernardini, N., Tsapekos, P., Treu, L., Zhu, X., Campanaro, S., Karimi, K., & Angelidaki, I. (2022). Effect of pressure on biomethanation process and spatial stratification of microbial communities in trickle bed reactors under decreasing gas retention time. *Bioresource Technology*, *361*. https://doi.org/10.1016/j.biortech.2022.127701

Elbeshbishy, E., Dhar, B. R., Nakhla, G., & Lee, H. S. (2017). A critical review on inhibition of dark biohydrogen fermentation. In *Renewable and Sustainable Energy Reviews* (Vol. 79, pp. 656–668). Elsevier Ltd. https://doi.org/10.1016/j.rser.2017.05.075

European Biogas Association. (2023). *Decarbonising Europe's hydrogen production with biohydrogen. The role of sustainable biohydrogen in the total energy mix*.

Fang, H. H. P., Liu, H., & Zhang, T. (2005). Phototrophic hydrogen production from acetate and butyrate in wastewater. *International Journal of Hydrogen Energy*, *30*(7), 785–793. https://doi.org/10.1016/j.ijhydene.2004.12.010

Faye, O., Szpunar, J., & Eduok, U. (2022). A critical review on the current technologies for the generation, storage, and transportation of hydrogen. In *International Journal of Hydrogen Energy* (Vol. 47, Issue 29, pp. 13771–13802). Elsevier Ltd. https://doi.org/10.1016/j.ijhydene.2022.02.112

Fradinho, J., Allegue, L. D., Ventura, M., Melero, J. A., Reis, M. A. M., & Puyol, D. (2021). Up-scale challenges on biopolymer production from waste streams by Purple Phototrophic Bacteria mixed cultures: A critical review. In *Bioresource Technology* (Vol. 327). Elsevier Ltd. https://doi.org/10.1016/j.biortech.2021.124820

García-Depraect, O., Castro-Muñoz, R., Muñoz, R., Rene, E. R., León-Becerril, E., Valdez-Vazquez, I., Kumar, G., Reyes-Alvarado, L. C., Martínez-Mendoza, L. J., Carrillo-Reyes, J., & Buitrón, G. (2021). A review on the factors influencing biohydrogen production from lactate: The key to unlocking enhanced dark fermentative processes. In *Bioresource Technology* (Vol. 324). Elsevier Ltd. https://doi.org/10.1016/j.biortech.2020.124595

Gbiete, D., Narra, S., Mani Kongnine, D., Narra, M. M., & Nelles, M. (2024). Insights into Biohydrogen Production Through Dark Fermentation of Food Waste: Substrate Properties, Inocula, and Pretreatment Strategies. In *Energies* (Vol. 17, Issue 24). Multidisciplinary Digital Publishing Institute (MDPI). https://doi.org/10.3390/en17246350

Ghaib, K., & Ben-Fares, F. Z. (2018). Power-to-Methane: A state-of-the-art review. In *Renewable and Sustainable Energy Reviews* (Vol. 81, pp. 433–446). Elsevier Ltd. https://doi.org/10.1016/j.rser.2017.08.004

Ghimire, A. (2015). *Dark fermentative biohydrogen production from organic waste and application of by-products in a biorefinery concept*. https://tel.archives-ouvertes.fr/tel-01404689

Ghosh, S., Chowdhury, R., & Bhattacharya, P. (2018). A review on single stage integrated dark-photo fermentative biohydrogen production: Insight into salient strategies and scopes. In *International Journal of Hydrogen Energy* (pp. 2091–2107). Elsevier Ltd. https://doi.org/10.1016/j.ijhydene.2017.12.018

Ghosh, S., Dairkee, U. K., Chowdhury, R., & Bhattacharya, P. (2017). Hydrogen from food processing wastes via photofermentation using Purple Non-sulfur Bacteria (PNSB) – A review. In *Energy Conversion and Management* (Vol. 141, pp. 299–314). Elsevier Ltd. https://doi.org/10.1016/j.enconman.2016.09.001

Global Carbon Budget. (2023). *Global Carbon Budget*. With major processing by Our World in Data. "Annual $CO_2$ emissions – GCB" [dataset]. Global Carbon Project, "Global Carbon Budget" [original data]. https://ourworldindata.org/co2-and-greenhouse-gas-emissions#co2-and-greenhouse-gas-emissions-country-profiles

González, R., Cabeza, I. O., Casallas-Ojeda, M., & Gómez, X. (2023). Biological Hydrogen Methanation with Carbon Dioxide Utilization: Methanation Acting as Mediator in the Hydrogen Economy. In *Environments - MDPI* (Vol. 10, Issue 5). MDPI. https://doi.org/10.3390/environments10050082

Gonzalez-Estrella, J., Sierra-Alvarez, R., & Field, J. A. (2013). Toxicity assessment of inorganic nanoparticles to acetoclastic and hydrogenotrophic methanogenic activity in anaerobic granular sludge. *Journal of Hazardous Materials*, *260*, 278–285. https://doi.org/10.1016/j.jhazmat.2013.05.029

Gopalakrishnan, B., Khanna, N., & Das, D. (2019). Dark-Fermentative Biohydrogen Production. In *Biomass, Biofuels, Biochemicals: Biohydrogen, Second Edition* (pp. 79–122). Elsevier. https://doi.org/10.1016/B978-0-444-64203-5.00004-6

Gottardo, M., Dosta, J., Cavinato, C., Crognale, S., Tonanzi, B., Rossetti, S., Bolzonella, D., Pavan, P., & Valentino, F. (2023). Boosting butyrate and hydrogen production in acidogenic fermentation of food waste and sewage sludge mixture: a pilot scale demonstration. *Journal of Cleaner Production*, *404*. https://doi.org/10.1016/j.jclepro.2023.136919

Govindaraju, A., McKinlay, J. B., & LaSarre, B. (2019). Phototrophic lactate utilization by Rhodopseudomonas palustris is stimulated by coutilization with additional substrates. *Applied and Environmental Microbiology*, *85*(11). https://doi.org/10.1128/AEM.00048-19

Guo, X. M., Trably, E., Latrille, E., Carrre, H., & Steyer, J. P. (2010). Hydrogen production from agricultural waste by dark fermentation: A review. *International Journal of Hydrogen Energy*, *35*(19), 10660–10673. https://doi.org/10.1016/j.ijhydene.2010.03.008

Halder, P., Babaie, M., Salek, F., Shah, K., Stevanovic, S., Bodisco, T. A., & Zare, A. (2024). Performance, emissions and economic analyses of hydrogen fuel cell vehicles. In *Renewable and Sustainable Energy Reviews* (Vol. 199). Elsevier Ltd. https://doi.org/10.1016/j.rser.2024.114543

Hallenbeck, P. C., Ghosh, D., Skonieczny, M. T., & Yargeau, V. (2009). Microbiological and engineering aspects of biohydrogen production. *Indian Journal of Microbiology*, *49*(1), 48–59. https://doi.org/10.1007/s12088-009-0010-4

Hammi, Z., Labjar, N., Dalimi, M., El Hamdouni, Y., Lotfi, E. M., & El Hajjaji, S. (2024). Green hydrogen: A holistic review covering life cycle assessment, environmental impacts, and color analysis. In *International Journal of Hydrogen Energy* (Vol. 80, pp. 1030–1045). Elsevier Ltd. https://doi.org/10.1016/j.ijhydene.2024.07.008

Hao, X., Liu, R., van Loosdrecht, M. C. M., & Cao, D. (2017). Batch influences of exogenous hydrogen on both acidogenesis and methanogenesis of excess sludge. *Chemical Engineering Journal*, *317*, 544–550. https://doi.org/10.1016/j.cej.2017.02.093

Hawkes, F. R., Hussy, I., Kyazze, G., Dinsdale, R., & Hawkes, D. L. (2007). Continuous dark fermentative hydrogen production by mesophilic microflora: Principles and progress. *International Journal of Hydrogen Energy*, *32*(2), 172–184. https://doi.org/10.1016/j.ijhydene.2006.08.014

Hay, J. X. W., Wu, T. Y., Juan, J. C., & Md. Jahim, J. (2013). Biohydrogen production through photo fermentation or dark fermentation using waste as a substrate: Overview, economics, and future prospects of hydrogen usage. *Biofuels, Bioproducts and Biorefining*, *7*(3), 334–352. https://doi.org/10.1002/bbb.1403

Hitam, C. N. C., & Jalil, A. A. (2023). A review on biohydrogen production through photo-fermentation of lignocellulosic biomass. *Biomass Conversion and Biorefinery*, *13*, 8465–8483. https://doi.org/10.1007/s13399-020-01140-y/Published

Hu, C., Choy, S. Y., & Giannis, A. (2018). Evaluation of Lighting Systems, Carbon Sources, and Bacteria Cultures on Photofermentative Hydrogen Production. *Applied Biochemistry and Biotechnology*, *185*(1), 257–269. https://doi.org/10.1007/s12010-017-2655-5

Hülsen, T., Barry, E. M., Lu, Y., Puyol, D., & Batstone, D. J. (2016). Low temperature treatment of domestic wastewater by purple phototrophic bacteria: Performance, activity, and community. *Water Research*, *100*, 537–545. https://doi.org/10.1016/j.watres.2016.05.054

Hussain, A., & Dubey, S. K. (2017). Specific methanogenic activity test for anaerobic degradation of influents. In *Applied Water Science* (Vol. 7, Issue 2, pp. 535–542). Springer Verlag. https://doi.org/10.1007/s13201-015-0305-z

Hussy, I., Hawkes, F. R., Dinsdale, R., & Hawkes, D. L. (2003). Continuous Fermentative Hydrogen Production from a Wheat Starch Co-Product by Mixed Microflora. *Biotechnology and Bioengineering*, *84*(6), 619–626. https://doi.org/10.1002/bit.10785

Hustede, E., Steinbiichel, A., & Schlegel, H. G. (1993). Relationship between the photoproduction of hydrogen and the accumulation of PHB in non-sulphur purple bacteria. *Appl Microbiol Biotechnol*, *39*, 87–93.

Incer-Valverde, J., Korayem, A., Tsatsaronis, G., & Morosuk, T. (2023). "Colors" of hydrogen: Definitions and carbon intensity. In *Energy Conversion and Management* (Vol. 291). Elsevier Ltd. https://doi.org/10.1016/j.enconman.2023.117294

International Energy Agency. (2019). *The Future of Hydrogen*.

International Energy Agency. (2020). *Technology Perspectives Energy Special Report on Carbon Capture Utilisation and Storage CCUS in clean energy transitions*. www.iea.org/t&c/

International Energy Agency, I. (2023). *Global Hydrogen Review 2023*. www.iea.org

Jain, R., Panwar, N. L., Jain, S. K., Gupta, T., Agarwal, C., & Meena, S. S. (2024). Bio-hydrogen production through dark fermentation: an overview. In *Biomass Conversion and Biorefinery* (Vol. 14, Issue 12, pp. 12699–12724). Springer Science and Business Media Deutschland GmbH. https://doi.org/10.1007/s13399-022-03282-7

Jayathilake, C., Piyumika, G., Nazeer, Z., Wijayawardene, N., Rajakaruna, S., Kumla, J., & Fernando, E. (2024). Recent progress in the characterization and application of exo-electrogenic microorganisms. In *Antonie van Leeuwenhoek, International Journal of General and Molecular Microbiology* (Vol. 117, Issue 1). Springer Science and Business Media Deutschland GmbH. https://doi.org/10.1007/s10482-023-01916-y

Jensen, M. B., Ottosen, L. D. M., & Kofoed, M. V. W. (2021). H2 gas-liquid mass transfer: A key element in biological Power-to-Gas methanation. In *Renewable and Sustainable Energy Reviews* (Vol. 147). Elsevier Ltd. https://doi.org/10.1016/j.rser.2021.111209

Jeong, T. Y., Cha, G. C., Yoo, I. K., & Kim, D. J. (2007). Hydrogen production from waste activated sludge by using separation membrane acid fermentation reactor and photosynthetic reactor. *International Journal of Hydrogen Energy*, *32*(5), 525–530. https://doi.org/10.1016/j.ijhydene.2006.09.028

Jiao, H., Tsigkou, K., Elsamahy, T., Pispas, K., Sun, J., Manthos, G., Schagerl, M., Sventzouri, E., Al-Tohamy, R., Kornaros, M., & Ali, S. S. (2024). Recent advances in sustainable hydrogen production from microalgae: Mechanisms, challenges, and future perspectives. In *Ecotoxicology and Environmental Safety* (Vol. 270). Academic Press. https://doi.org/10.1016/j.ecoenv.2023.115908

Junghare, M., Subudhi, S., & Lal, B. (2012). Improvement of hydrogen production under decreased partial pressure by newly isolated alkaline tolerant anaerobe, Clostridium butyricum TM-9A: Optimization of process parameters. *International Journal of Hydrogen Energy*, *37*(4), 3160–3168. https://doi.org/10.1016/j.ijhydene.2011.11.043

Karki, R., Chuenchart, W., Surendra, K. C., Shrestha, S., Raskin, L., Sung, S., Hashimoto, A., & Kumar Khanal, S. (2021). Anaerobic co-digestion: Current status and perspectives. In

*Bioresource Technology* (Vol. 330). Elsevier Ltd. https://doi.org/10.1016/j.biortech.2021.125001

Kars, G., & Gündüz, U. (2010). Towards a super H2 producer: Improvements in photofermentative biohydrogen production by genetic manipulations. In *International Journal of Hydrogen Energy* (Vol. 35, Issue 13, pp. 6646–6656). Elsevier Ltd. https://doi.org/10.1016/j.ijhydene.2010.04.037

Keçebaş, A., & Kayfeci, M. (2019). Hydrogen properties. In *Solar Hydrogen Production: Processes, Systems and Technologies* (pp. 3–29). Elsevier. https://doi.org/10.1016/B978-0-12-814853-2.00001-1

Khanal, S. K., Chen, W. H., Li, L., & Sung, S. (2004). Biological hydrogen production: Effects of pH and intermediate products. *International Journal of Hydrogen Energy*, *29*(11), 1123–1131. https://doi.org/10.1016/j.ijhydene.2003.11.002

Kim, D. H., Kim, S. H., Kim, H. W., Kim, M. S., & Shin, H. S. (2011). Sewage sludge addition to food waste synergistically enhances hydrogen fermentation performance. *Bioresource Technology*, *102*(18), 8501–8506. https://doi.org/10.1016/j.biortech.2011.04.089

Kim, D. H., Son, H., & Kim, M. S. (2012). Effect of substrate concentration on continuous Photo-fermentative hydrogen production from lactate using Rhodobacter sphaeroides. *International Journal of Hydrogen Energy*, *37*(20), 15483–15488. https://doi.org/10.1016/j.ijhydene.2012.02.039

Kim, S. H., Han, S. K., & Shin, H. S. (2004). Feasibility of biohydrogen production by anaerobic co-digestion of food waste and sewage sludge. *International Journal of Hydrogen Energy*, *29*(15), 1607–1616. https://doi.org/10.1016/j.ijhydene.2004.02.018

Kofoed, M. V. W., Jensen, M. B., & Ottosen, L. D. M. (2021). Biological upgrading of biogas through CO2 conversion to CH4. In *Emerging Technologies and Biological Systems for Biogas Upgrading* (pp. 321–362). Elsevier. https://doi.org/10.1016/B978-0-12-822808-1.00012-X

Kozak, M., Köroğlu, E. O., Cirik, K., & Zaimoğlu, Z. (2022). Evaluation of ex-situ hydrogen biomethanation at mesophilic and thermophilic temperatures. *International Journal of Hydrogen Energy*, *47*(34), 15434–15441. https://doi.org/10.1016/j.ijhydene.2022.02.072

Laguillaumie, L., Rafrafi, Y., Moya-Leclair, E., Delagnes, D., Dubos, S., Spérandio, M., Paul, E., & Dumas, C. (2022). Stability of ex situ biological methanation of H2/CO2 with a mixed microbial culture in a pilot scale bubble column reactor. *Bioresource Technology*, *354*. https://doi.org/10.1016/j.biortech.2022.127180

Lanfranchi, A., Tassinato, G., Valentino, F., Martinez, G. A., Jones, E., Gioia, C., Bertin, L., & Cavinato, C. (2022). Hydrodynamic cavitation pre-treatment of urban waste: Integration with acidogenic fermentation, PHAs synthesis and anaerobic digestion processes. *Chemosphere*, *301*. https://doi.org/10.1016/j.chemosphere.2022.134624

Laurinavichene, T. V., Belokopytov, B. F., Laurinavichius, K. S., Tekucheva, D. N., Seibert, M., & Tsygankov, A. A. (2010). Towards the integration of dark- and photo-fermentative waste

treatment. 3. Potato as substrate for sequential dark fermentation and light-driven H 2 production. *International Journal of Hydrogen Energy*, *35*(16), 8536–8543. https://doi.org/10.1016/j.ijhydene.2010.02.063

Li, C., & Fang, H. H. P. (2007). Fermentative hydrogen production from wastewater and solid wastes by mixed cultures. In *Critical Reviews in Environmental Science and Technology* (Vol. 37, Issue 1, pp. 1–39). https://doi.org/10.1080/10643380600729071

Li, Y., Zhang, Z., Jiang, D., Jing, Y., Lu, C., Zhang, H., & Zhang, Q. (2021). Continuous dark and photo biohydrogen production in a baffled bioreactor and electrons distribution analysis. *Bioresource Technology*, *337*. https://doi.org/10.1016/j.biortech.2021.125440

Li, Z., Chen, Z., Ye, H., Wang, Y., Luo, W., Chang, J. S., Li, Q., & He, N. (2018). Anaerobic co-digestion of sewage sludge and food waste for hydrogen and VFA production with microbial community analysis. *Waste Management*, *78*, 789–799. https://doi.org/10.1016/j.wasman.2018.06.046

Lin, C. Y., & Chen, H. P. (2006). Sulfate effect on fermentative hydrogen production using anaerobic mixed microflora. *International Journal of Hydrogen Energy*, *31*(7), 953–960. https://doi.org/10.1016/j.ijhydene.2005.07.009

Liu, C., Li, H., Zhang, Y., & Chen, Q. (2016). Characterization of methanogenic activity during high-solids anaerobic digestion of sewage sludge. *Biochemical Engineering Journal*, *109*, 96–100. https://doi.org/10.1016/j.bej.2016.01.010

Liu, D., Zeng, R. J., & Angelidaki, I. (2008). Effects of pH and hydraulic retention time on hydrogen production versus methanogenesis during anaerobic fermentation of organic household solid waste under extreme-thermophilic temperature (70°C). *Biotechnology and Bioengineering*, *100*(6), 1108–1114. https://doi.org/10.1002/bit.21834

Liu, W., Zuo, H., Wang, J., Xue, Q., Ren, B., & Yang, F. (2021). The production and application of hydrogen in steel industry. In *International Journal of Hydrogen Energy* (Vol. 46, Issue 17, pp. 10548–10569). Elsevier Ltd. https://doi.org/10.1016/j.ijhydene.2020.12.123

Liu, X., Li, R., Ji, M., & Han, L. (2013). Hydrogen and methane production by co-digestion of waste activated sludge and food waste in the two-stage fermentation process: Substrate conversion and energy yield. *Bioresource Technology*, *146*, 317–323. https://doi.org/10.1016/j.biortech.2013.07.096

Lo, Y. C., Chen, C. Y., Lee, C. M., & Chang, J. S. (2011). Photo fermentative hydrogen production using dominant components (acetate, lactate, and butyrate) in dark fermentation effluents. *International Journal of Hydrogen Energy*, *36*(21), 14059–14068. https://doi.org/10.1016/j.ijhydene.2011.04.148

Łukajtis, R., Hołowacz, I., Kucharska, K., Glinka, M., Rybarczyk, P., Przyjazny, A., & Kamiński, M. (2018). Hydrogen production from biomass using dark fermentation. In *Renewable and Sustainable Energy Reviews* (Vol. 91, pp. 665–694). Elsevier Ltd. https://doi.org/10.1016/j.rser.2018.04.043

Lund, P. A., De Biase, D., Liran, O., Scheler, O., Mira, N. P., Cetecioglu, Z., Fernández, E. N., Bover-Cid, S., Hall, R., Sauer, M., & O'Byrne, C. (2020). Understanding How Microorganisms Respond to Acid pH Is Central to Their Control and Successful Exploitation. *Frontiers in Microbiology*, *11*. https://doi.org/10.3389/fmicb.2020.556140

Luo, G., Karakashev, D., Xie, L., Zhou, Q., & Angelidaki, I. (2011). Long-term effect of inoculum pretreatment on fermentative hydrogen production by repeated batch cultivations: Homoacetogenesis and methanogenesis as competitors to hydrogen production. *Biotechnology and Bioengineering*, *108*(8), 1816–1827. https://doi.org/10.1002/bit.23122

Luo, L., Sriram, S., Johnravindar, D., Louis Philippe Martin, T., Wong, J. W. C., & Pradhan, N. (2022). Effect of inoculum pretreatment on the microbial and metabolic dynamics of food waste dark fermentation. *Bioresource Technology*, *358*. https://doi.org/10.1016/j.biortech.2022.127404

Madigan, M. T., & Jung, D. O. (2009). *An Overview of Purple Bacteria: Systematics, Physiology, and Habitats* (pp. 1–15). https://doi.org/10.1007/978-1-4020-8815-5_1

Martins, I., Surra, E., Ventura, M., & Lapa, N. (2022). BioH2 from Dark Fermentation of OFMSW: Effect of the Hydraulic Retention Time and Organic Loading Rate. *Applied Sciences (Switzerland)*, *12*(9). https://doi.org/10.3390/app12094240

Mateus, S., Carvalheira, M., Cassidy, J., Freitas, E., Oehmen, A., & Reis, M. A. M. (2020). Two-stage anaerobic digestion system treating different seasonal fruit pulp wastes: Impact on biogas and hydrogen production and total energy recovery potential. *Biomass and Bioenergy*, *141*. https://doi.org/10.1016/j.biombioe.2020.105694

McCully, A. L., & McKinlay, J. B. (2016). Disrupting Calvin cycle phosphoribulokinase activity in Rhodopseudomonas palustris increases the H2 yield and specific production rate proportionately. *International Journal of Hydrogen Energy*, *41*(7), 4143–4149. https://doi.org/10.1016/j.ijhydene.2016.01.003

Metcalf & Eddy. (2014). *Wastewater Engineering: Treatment and Resource Recovery* (McGraw-Hill, Ed.; 5th ed.).

Mohanraj, S., Pandey, A., Venkata Mohan, S., Anbalagan, K., Kodhaiyolii, S., & Pugalenthi, V. (2019). Metabolic Engineering and Molecular Biotechnology of Biohydrogen Production. In *Biomass, Biofuels, Biochemicals: Biohydrogen, Second Edition* (pp. 413–434). Elsevier. https://doi.org/10.1016/B978-0-444-64203-5.00017-4

Monroy, I., & Buitrón, G. (2020). Production of polyhydroxybutyrate by pure and mixed cultures of purple non-sulfur bacteria: A review. In *Journal of Biotechnology* (Vol. 317, pp. 39–47). Elsevier B.V. https://doi.org/10.1016/j.jbiotec.2020.04.012

Moreno-Andrade, I., Berrocal-Bravo, M. J., & Valdez-Vazquez, I. (2023). Biohydrogen production from food waste and waste activated sludge in codigestion: influence of organic loading rate and changes in microbial community. *Journal of Chemical Technology and Biotechnology*, *98*(1), 230–237. https://doi.org/10.1002/jctb.7238

Moscoviz, R., Trably, E., Bernet, N., & Carrère, H. (2018). The environmental biorefinery: State-of-the-art on the production of hydrogen and value-added biomolecules in mixed-culture fermentation. *Green Chemistry*, *20*(14), 3159–3179. https://doi.org/10.1039/c8gc00572a

Nemmour, A., Inayat, A., Janajreh, I., & Ghenai, C. (2023). Green hydrogen-based E-fuels (E-methane, E-methanol, E-ammonia) to support clean energy transition: A literature review. In *International Journal of Hydrogen Energy* (Vol. 48, Issue 75, pp. 29011–29033). Elsevier Ltd. https://doi.org/10.1016/j.ijhydene.2023.03.240

Ngu, V., Fletcher, D. F., Kavanagh, J. M., Rafrafi, Y., Dumas, C., Morchain, J., & Cockx, A. (2023). H2 mass transfer – A key factor for efficient biological methanation: Comparison between pilot-scale experimental data, 1D and CFD models. *Chemical Engineering Science*, *268*. https://doi.org/10.1016/j.ces.2022.118382

Nikolaidis, P., & Poullikkas, A. (2017). A comparative overview of hydrogen production processes. In *Renewable and Sustainable Energy Reviews* (Vol. 67, pp. 597–611). Elsevier Ltd. https://doi.org/10.1016/j.rser.2016.09.044

Niño-Navarro, C., Chairez, I., Christen, P., Canul-Chan, M., & García-Peña, E. I. (2020). Enhanced hydrogen production by a sequential dark and photo fermentation process: Effects of initial feedstock composition, dilution and microbial population. *Renewable Energy*, *147*, 924–936. https://doi.org/10.1016/j.renene.2019.09.024

Palanivel, P. D., Jovita S, A., Babu, K., & Naina Mohamed, S. (2025). Harnessing dark fermentation: Mechanisms, metabolic pathways, and nanoparticle innovations for biohydrogen enhancement. In *International Journal of Hydrogen Energy* (Vol. 109, pp. 383–396). Elsevier Ltd. https://doi.org/10.1016/j.ijhydene.2025.02.033

Park, W., Hyun, S. H., Oh, S. E., Logan, B. E., & Kim, I. S. (2005). Removal of headspace CO2 increases biological hydrogen production. *Environmental Science and Technology*, *39*(12), 4416–4420. https://doi.org/10.1021/es048569d

Pokorna, D., Varga, Z., Andreides, D., & Zabranska, J. (2019). Adaptation of anaerobic culture to bioconversion of carbon dioxide with hydrogen to biomethane. *Renewable Energy*, *142*, 167–172. https://doi.org/10.1016/j.renene.2019.04.076

Prado, C. A., Antunes, F. A. F., Rocha, T. M., Sánchez-Muñoz, S., Barbosa, F. G., Terán-Hilares, R., Cruz-Santos, M. M., Arruda, G. L., da Silva, S. S., & Santos, J. C. (2022). A review on recent developments in hydrodynamic cavitation and advanced oxidative processes for pretreatment of lignocellulosic materials. In *Bioresource Technology* (Vol. 345). Elsevier Ltd. https://doi.org/10.1016/j.biortech.2021.126458

Precedence Research. (2024). *Blue Hydrogen Market Size, Share, and Trends 2024 to 2033*. https://www.precedenceresearch.com/blue-hydrogen-market

Qureshi, F., Yusuf, M., Tahir, M., Haq, M., Mohamed, M. M. I., Kamyab, H., Nguyen, H. H. T., Vo, D. V. N., & Ibrahim, H. (2023). Renewable hydrogen production via biological and thermochemical routes: Nanomaterials, economic analysis and challenges. In *Process Safety and Environmental Protection* (Vol. 179, pp. 68–88). Institution of Chemical Engineers. https://doi.org/10.1016/j.psep.2023.07.075

Rafieenia, R., Lavagnolo, M. C., & Pivato, A. (2018). Pre-treatment technologies for dark fermentative hydrogen production: Current advances and future directions. *Waste Management*, *71*, 734–748. https://doi.org/10.1016/j.wasman.2017.05.024

Rai, P. K., & Singh, S. P. (2016). Integrated dark- and photo-fermentation: Recent advances and provisions for improvement. In *International Journal of Hydrogen Energy* (Vol. 41, Issue 44, pp. 19957–19971). Elsevier Ltd. https://doi.org/10.1016/j.ijhydene.2016.08.084

Redondas, V., Gómez, X., García, S., Pevida, C., Rubiera, F., Morán, A., & Pis, J. J. (2012). Hydrogen production from food wastes and gas post-treatment by CO 2 adsorption. *Waste Management*, *32*(1), 60–66. https://doi.org/10.1016/j.wasman.2011.09.003

Reed-Berendt, B. G., Latham, D. E., Dambatta, M. B., & Morrill, L. C. (2021). Borrowing Hydrogen for Organic Synthesis. *ACS Central Science*, *7*(4), 570–585. https://doi.org/10.1021/acscentsci.1c00125

Regueiro, L., Veiga, P., Figueroa, M., Alonso-Gutierrez, J., Stams, A. J. M., Lema, J. M., & Carballa, M. (2012). Relationship between microbial activity and microbial community structure in six full-scale anaerobic digesters. *Microbiological Research*, *167*(10), 581–589. https://doi.org/10.1016/j.micres.2012.06.002

Ren, N. Q., Guo, W. Q., Wang, X. J., Xiang, W. S., Liu, B. F., Wang, X. Z., Ding, J., & Chen, Z. B. (2008). Effects of different pretreatment methods on fermentation types and dominant bacteria for hydrogen production. *International Journal of Hydrogen Energy*, *33*(16), 4318–4324. https://doi.org/10.1016/j.ijhydene.2008.06.003

Reungsang, A., Zhong, N., Yang, Y., Sittijunda, S., Xia, A., & Liao, Q. (2018). Hydrogen from photo fermentation. In *Green Energy and Technology* (Vol. 0, Issue 9789811076763, pp. 221–317). Springer Verlag. https://doi.org/10.1007/978-981-10-7677-0_7

Ripoll, E., López, I., & Borzacconi, L. (2020). Hydrogenotrophic activity: A tool to evaluate the kinetics of methanogens. *Journal of Environmental Management*, *270*. https://doi.org/10.1016/j.jenvman.2020.110937

Rogers, K. M., Turnbull, J. C., Dahl, J., Phillips, A., Bridson, J. H., Raymond, L. G., Liu, Z., Yuan, Y., & Hill, S. J. (2021). Authenticating bioplastics using carbon and hydrogen stable isotopes – An alternative analytical approach. *Rapid Communications in Mass Spectrometry*, *35*(9). https://doi.org/10.1002/rcm.9051

Rupprecht, J., Hankamer, B., Mussgnug, J. H., Ananyev, G., Dismukes, C., & Kruse, O. (2006). Perspectives and advances of biological H2 production in microorganisms. In *Applied Microbiology and Biotechnology* (Vol. 72, Issue 3, pp. 442–449). https://doi.org/10.1007/s00253-006-0528-x

Saratale, G. D., Chen, S.-D., Lo, Y.-C., Saratale, R. G., & Chang, J.-S. (2008). Outlook of biohydrogen production from lignocellulosic feedstock using dark fermentation-a review. In *Journal of Scientific & Industrial Research* (Vol. 67).

Sattar, A., Arslan, C., Ji, C., Sattar, S., Umair, M., Sattar, S., & Bakht, M. Z. (2016). Quantification of temperature effect on batch production of bio-hydrogen from rice crop wastes in an

anaerobic bio reactor. *International Journal of Hydrogen Energy*, *41*(26), 11050–11061. https://doi.org/10.1016/j.ijhydene.2016.04.087

Segovia-Hernández, J. G. (2025). Advancing E-fuels production through process intensification: overcoming challenges and seizing opportunities for a sustainable energy future - A critical review. In *Chemical Engineering and Processing - Process Intensification* (Vol. 208). Elsevier B.V. https://doi.org/10.1016/j.cep.2024.110107

Shaker, L. M., Mohammed, J. K., Basem, A., Halbos, R. J., Mahdi, R. R., Mohammed, S. A., Fayad, M. A., Al-Amiery, A., & Al Lami, M. H. (2024). Comparative analysis of solar cells and hydrogen fuel: A mini-review. In *Results in Engineering* (Vol. 23). Elsevier B.V. https://doi.org/10.1016/j.rineng.2024.102507

Sharma, A., & Arya, S. K. (2017). Hydrogen from algal biomass: A review of production process. In *Biotechnology Reports* (Vol. 15, pp. 63–69). Elsevier B.V. https://doi.org/10.1016/j.btre.2017.06.001

Sieborg, M. U., Jønson, B. D., Ashraf, M. T., Yde, L., & Triolo, J. M. (2020). Biomethanation in a thermophilic biotrickling filter using cattle manure as nutrient media. *Bioresource Technology Reports*, *9*. https://doi.org/10.1016/j.biteb.2020.100391

Sikora, A., Baszczyk, M., Jurkowski, M., & Zielenkiewicz, U. (2013). Lactic Acid Bacteria in Hydrogen-Producing Consortia: On Purpose or by Coincidence? In *Lactic Acid Bacteria - R & D for Food, Health and Livestock Purposes*. InTech. https://doi.org/10.5772/50364

Song, L., Yang, D., Liu, R., Liu, S., Dai, L., & Dai, X. (2022). Microbial production of lactic acid from food waste: Latest advances, limits, and perspectives. In *Bioresource Technology* (Vol. 345). Elsevier Ltd. https://doi.org/10.1016/j.biortech.2021.126052

Stolten, D., & Emonts, B. (2016). *Hydrogen Storage : New Materials for Future Energy Storage* (Vol. 1). Wiley-VCH [Imprint], John Wiley & Sons, Incorporated.

Su, H., Cheng, J., Zhou, J., Song, W., & Cen, K. (2010). Hydrogen production from water hyacinth through dark- and photo- fermentation. *International Journal of Hydrogen Energy*, *35*(17), 8929–8937. https://doi.org/10.1016/j.ijhydene.2010.06.035

Sun, X., Xu, H., Xuan, X., Manickam, S., Boczkaj, G., & Wang, B. (2024). Assessing the industrialization progress of hydrodynamic cavitation process intensification technology: a review. In *Current Opinion in Chemical Engineering* (Vol. 45). Elsevier Ltd. https://doi.org/10.1016/j.coche.2024.101037

Swainsbury, D. J. K., Qian, P., Hitchcock, A., & Hunter, C. N. (2023). The structure and assembly of reaction centre-light-harvesting 1 complexes in photosynthetic bacteria. In *Bioscience Reports* (Vol. 43, Issue 5). Portland Press Ltd. https://doi.org/10.1042/BSR20220089

Tan, W. H., Chong, S., Fang, H. W., Pan, K. L., Mohamad, M., Lim, J. W., Tiong, T. J., Chan, Y. J., Huang, C. M., & Yang, T. C. K. (2021). Microbial fuel cell technology—a critical review on scale-up issues. In *Processes* (Vol. 9, Issue 6). MDPI AG. https://doi.org/10.3390/pr9060985

Tedeeva, M. A., Kustov, A. L., Batkin, A. M., Garifullina, C., Zalyatdinov, A. A., Yang, D., Dai, Y., Yang, Y., & Kustov, L. M. (2024). Catalytic systems for hydrogenation of CO2 to methanol. In *Molecular Catalysis* (Vol. 566). Elsevier B.V. https://doi.org/10.1016/j.mcat.2024.114403

The Engineering ToolBox. (2009). *Combustion of Fuels - Carbon Dioxide Emission*. https://www.engineeringtoolbox.com/co2-emission-fuels-d_1085.html

Tsygankov, A. A., & Khusnutdinova, A. N. (2015). Hydrogen in metabolism of purple bacteria and prospects of practical application. In *Microbiology (Russian Federation)* (Vol. 84, Issue 1). Maik Nauka Publishing / Springer SBM. https://doi.org/10.1134/S0026261715010154

United Nations Environment Programme. (2024). *Think Eat Save Tracking Progress to Halve Global Food Waste*. https://www.unep.org/resources/publication/food-waste-index-report-2024

Vargas, S. R., Santos, P. V. dos, Zaiat, M., & Calijuri, M. do C. (2018). Optimization of biomass and hydrogen production by Anabaena sp. (UTEX 1448) in nitrogen-deprived cultures. *Biomass and Bioenergy*, *111*, 70–76. https://doi.org/10.1016/j.biombioe.2018.01.022

Verma, Y., Iqbal, J., Naushad, M., Bhaskaralingam, A., Kumar, A., Dhiman, P., Lai, C. W., & Sharma, G. (2025). Recent developments in photo-fermentative hydrogen evolution: Fundamental biochemistry and influencing factors a review. In *Journal of Environmental Management* (Vol. 374). Academic Press. https://doi.org/10.1016/j.jenvman.2024.123976

Vidal-Antich, C., Perez-Esteban, N., Astals, S., Peces, M., Mata-Alvarez, J., & Dosta, J. (2021). Assessing the potential of waste activated sludge and food waste co-fermentation for carboxylic acids production. *Science of the Total Environment*, *757*. https://doi.org/10.1016/j.scitotenv.2020.143763

Villanueva-Galindo, E., Vital-Jácome, M., & Moreno-Andrade, I. (2023). Dark fermentation for H2 production from food waste and novel strategies for its enhancement. In *International Journal of Hydrogen Energy* (Vol. 48, Issue 27, pp. 9957–9970). Elsevier Ltd. https://doi.org/10.1016/j.ijhydene.2022.11.339

Viscardi, R., Nigliaccio, G., Bassano, C., & Deiana, P. (2021). The potential of E-fuels as future fuels. *Energia, Ambiente e Innovazione*. https://doi.org/10.12910/EAI2021-022

Vita, A., & Italiano, C. (2019). Fuel and hydrogen related problems for conventional steam reforming of natural gas. In *Current Trends and Future Developments on (Bio-) Membranes: Membranes in Environmental Applications* (pp. 71–89). Elsevier Inc. https://doi.org/10.1016/B978-0-12-816778-6.00004-7

Wang, F., Swinbourn, R., & Li, C. (2023). Shipping Australian sunshine: Liquid renewable green fuel export. In *International Journal of Hydrogen Energy* (Vol. 48, Issue 39, pp. 14763–14784). Elsevier Ltd. https://doi.org/10.1016/j.ijhydene.2022.12.326

Wang, X., & Zhao, Y. cai. (2009). A bench scale study of fermentative hydrogen and methane production from food waste in integrated two-stage process. *International Journal of Hydrogen Energy*, *34*(1), 245–254. https://doi.org/10.1016/j.ijhydene.2008.09.100

Weijma, J., Gubbels, F., Hulshoff Pol, L. W., Stams, A. J. M., Lens, P., & Lettinga, G. (2002). *Competition for H 2 between sulfate reducers, methanogens and homoacetogens in a gas-lift reactor*. https://iwaponline.com/wst/article-pdf/45/10/75/425015/75.pdf

Woody, A., & Carlson, H. (2020). *State of Play: Hydrogen in 2020*.

Xu, F., Li, Y., Ge, X., Yang, L., & Li, Y. (2018). Anaerobic digestion of food waste – Challenges and opportunities. In *Bioresource Technology* (Vol. 247, pp. 1047–1058). Elsevier Ltd. https://doi.org/10.1016/j.biortech.2017.09.020

Xuan, J., He, L., Wen, W., & Feng, Y. (2023). Hydrogenase and Nitrogenase: Key Catalysts in Biohydrogen Production. In *Molecules* (Vol. 28, Issue 3). MDPI. https://doi.org/10.3390/molecules28031392

Yang, Y. N., Zhu, M. J., & Zhao, L. (2025). Enhanced thermophilic hydrogen production from co-substrate of pretreated waste activated sludge and food waste: Analysis from microbial growth and metabolism. *International Journal of Hydrogen Energy*, *97*, 431–443. https://doi.org/10.1016/j.ijhydene.2024.11.456

Yu, S., Fan, Y., Shi, Z., Li, J., Zhao, X., Zhang, T., & Chang, Z. (2023). Hydrogen-based combined heat and power systems: A review of technologies and challenges. In *International Journal of Hydrogen Energy* (Vol. 48, Issue 89, pp. 34906–34929). Elsevier Ltd. https://doi.org/10.1016/j.ijhydene.2023.05.187

Yukesh Kannah, R., Kavitha, S., Preethi, Parthiba Karthikeyan, O., Kumar, G., Dai-Viet, N. V., & Rajesh Banu, J. (2021). Techno-economic assessment of various hydrogen production methods – A review. In *Bioresource Technology* (Vol. 319). Elsevier Ltd. https://doi.org/10.1016/j.biortech.2020.124175

Zagrodnik, R., & Duber, A. (2024). Continuous dark-photo fermentative H2 production from synthetic lignocellulose hydrolysate with different photoheterotrophic cultures: Sequential vs. co-culture processes. *Energy*, *290*. https://doi.org/10.1016/j.energy.2023.130105

Zahedi, S., Solera, R., Micolucci, F., Cavinato, C., & Bolzonella, D. (2016). Changes in microbial community during hydrogen and methane production in two-stage thermophilic anaerobic co-digestion process from biowaste. *Waste Management*, *49*, 40–46. https://doi.org/10.1016/j.wasman.2016.01.016

Zhang, D., Wang, G., Wang, X., Zhao, J., Jia, B., & Dai, X. (2020). Co-fermentation of waste activated sludge and agricultural waste for hydrogen production: Effect of the carbon-to-nitrogen mass ratio. *Desalination and Water Treatment*, *173*, 57–64. https://doi.org/10.5004/dwt.2020.24701

Zhang, Q., Lee, D. J., Wang, Y., Zhang, Z., Lee, D. J., Zhou, X., Jing, Y., Jiang, D., Hu, J., & He, C. (2017). Photo-fermentative hydrogen production from crop residue: A mini review. In

*Bioresource Technology* (Vol. 229, pp. 222–230). Elsevier Ltd. https://doi.org/10.1016/j.biortech.2017.01.008

Zhang, Q., Zhang, Z., Wang, Y., Lee, D. J., Li, G., Zhou, X., Jiang, D., Xu, B., Lu, C., Li, Y., & Ge, X. (2018). Sequential dark and photo fermentation hydrogen production from hydrolyzed corn stover: A pilot test using 11 m3 reactor. *Bioresource Technology*, *253*, 382–386. https://doi.org/10.1016/j.biortech.2018.01.017

Zhao, Z. T., Ding, J., Wang, B. Y., Bao, M. Y., Liu, B. F., Pang, J. W., Ren, N. Q., & Yang, S. S. (2024). Advances in the biomass valorization in dark fermentation systems: A sustainable approach for biohydrogen production. In *Chemical Engineering Journal* (Vol. 481). Elsevier B.V. https://doi.org/10.1016/j.cej.2023.148444

Ziara, R. M. M., Miller, D. N., Subbiah, J., & Dvorak, B. I. (2019). Lactate wastewater dark fermentation: The effect of temperature and initial pH on biohydrogen production and microbial community. *International Journal of Hydrogen Energy*, *44*(2), 661–673. https://doi.org/10.1016/j.ijhydene.2018.11.045

Zong, W., Yu, R., Zhang, P., Fan, M., & Zhou, Z. (2009). Efficient hydrogen gas production from cassava and food waste by a two-step process of dark fermentation and photo-fermentation. *Biomass and Bioenergy*, *33*(10), 1458–1463. https://doi.org/10.1016/j.biombioe.2009.06.008

# 3. Materials and Methods

## 3.1. Experimental overview

This chapter describes the methods employed in the thesis to address the research objectives, with details on the experimental setups and analytical methodologies.

The main objective of the research was to investigate the feasibility of converting the organic matter present in waste streams into hydrogen through sustainable biological processes and, subsequently, exploit the generated hydrogen for the synthesis of e-fuels, aimed at transforming exhausted carbon dioxide back into an energy-rich molecule. To do so, the available technologies for sustainable and scalable biological hydrogen production were investigated, focusing on utilizing both Dark and Photo Fermentation to enhance the overall process yields.

The experimental work was structured in 3 main sections: Dark Fermentation, Photo Fermentation, and Bio-Methanation. While the initial goal was to gradually scale up all processes, due to timing and operative constrains only Dark Fermentation was moved to larger volumes, while Photo Fermentation and Bio-Methanation were tested only at laboratory scale.

Regarding Dark Fermentation (DF), four trials were conducted (Tests 1 – 4). All DF experiments focused on the valorisation of food waste and waste activated sludge utilizing mixed microbial consortia. In the first DF test, food waste and waste activated sludge were fermented in batch conditions in laboratory scale reactors (Test 1, section 3.2.1, 4.1). The second DF experiment tested a hydraulic cavitation pretreatment of the influent feedstock to assess its efficacy in enhancing production yields (Test 2, section 3.2.2, 4.2). The third DF test evaluated the stability of the process under semi-continuous conditions, on the same scale (Test 3, section 3.2.3, 4.3). In the fourth DF test, a pilot scale system was employed in semi-continuous mode, contingently evaluating the conversion to hydrogen of organic waste by DF, and the valorisation

of the Dark Fermentation Effluent (DFE) to biogas by Anaerobic Digestion (AD) (Test 4, section 3.2.4, 4.4).

In relation to Photo Fermentation (PF), two tests were performed (Tests 5 – 6). In the first PF test, two different wild type strains (*Rhodopseudomonas palustris* and *Rhodospirillum rubrum*) were utilized and evaluated for their hydrogen production capacity using the metabolites present in the DFE as the primary carbon source (Test 5, section 3.3.1, 5.1). In the second PF test, mutated strains of *Rps. palustris* were tested with the same goal. These mutated strains were specifically selected for their enhanced tolerance to elevated ammonium concentrations, one of the main challenges when coupling Dark and Photo Fermentation processes, and for alterations in their metabolic pathways that optimized hydrogen generation (Test 6, section 3.3.2, 5.2).

In regard to Bio-Methanation (BM), one test was carried out (Test 7). This BM experiment focused on producing methane by the biological conversion of hydrogen and carbon dioxide. In this test, suspended biomass and granular sludge were compared in terms of activity and production yields (Test 7, section 3.4.1, 6.1).

In Table 8, all the conducted tests are summarized.

*Table 8, List of experiments conducted in this thesis*

| Test | Biological Process | Feeding strategy | Scale | Substrate | Microorganisms | Section |
|---|---|---|---|---|---|---|
| 1 | DF | Batch | Lab scale | FW+WAS | Mixed microbial consortium | 3.2.1<br>4.1 |
| 2 | DF | Batch | Lab scale | HC pretreated FW+WAS | Mixed microbial consortium | 3.2.2<br>4.2 |
| 3 | DF | Semi-continuous | Lab scale | FW+WAS | Mixed microbial consortium | 3.2.3<br>4.3 |
| 4 | DF | Semi-continuous | Pilot scale | FW+WAS | Mixed microbial consortium | 3.2.4<br>4.4 |
| 5 | PF | Batch | Lab scale | DFE | *Rps. palustris*, *Rsp. rubrum* | 3.3.1<br>5.1 |
| 6 | PF | Batch | Lab scale | DFE | Mutated strains of *Rps. palustris* | 3.3.2<br>5.2 |
| 7 | BM | Batch | Lab scale | $H_2$+$CO_2$ | Suspended biomass and granular sludge | 3.4.1<br>6.1 |

## 3.2. Dark Fermentation

### 3.2.1. Test 1: Lab-scale Dark Fermentation of Food Waste and WAS mixture, in Batch Condition

In Test 1, a laboratory-scale reactor system was operated under batch conditions to evaluate the conversion of organic waste into hydrogen via Dark Fermentation (DF). Working under batch mode tests and on a small scale allows for a simplified process setup, ensuring control over key experimental variables such as pH, temperature, and substrate homogeneity, and helps in defining the operative parameters for the subsequent experimental trials.

Inoculum and substrates

In Test 1, a mixture of Organic Waste (OW) and Waste Activated Sludge (WAS) were used as substrates. The OW was a mixture of (% w/w): lettuce (56.7 %), beetroot (42.5 %), and toilet paper (0.8 %). These substrates were purchased at a grocery shop and then mixed using a kitchen blender until complete homogenization. The choice of substrates to use and their ratio (6:6:1 on a Total Solid basis) was based on the data from the MELiSSA project (contract No. 19297/05/NL/SFe) as a possible scenario of wastes generated by a crew of astronauts. This part of the experimental tests, in fact, was included into the Purple-B project (contract No. 4000137190), focused on developing biological immobilized systems for producing hydrogen from the organic waste generated by astronauts on the International Space Station (ISS). The WAS was collected from the static gravimetric thickener of the municipal Wastewater Treatment Plant (WWTP, VERITAS spa, Fusina, Italy). In this test, no digestate was added as microbial inoculum, considering the WAS as a biologically active substrate. The solid content of the substrates is reported in Table 9.

*Table 9, Total Solids and Total Volatile Solids content of the substrates used in Test 1*

| | TS [$g_{TS}$ $kg^{-1}$] | TVS [$g_{TVS}$ $kg^{-1}$] | TVS/TS ratio [%] |
|---|---|---|---|
| Lettuce | 89 ± 3 | 74 ± 7 | 83 ± 5 |
| Beetroot | 119 ± 1 | 111.1 ± 0.5 | 94 ± 1 |
| Toilet Paper | 990 ± 10 | 960 ± 40 | 96 ± 3 |
| OW | 83.5 ± 0.9 | 75.9 ± 0.7 | 90.9 ± 0.1 |
| WAS | 24.6 ± 0.2 | 19.4 ± 0.2 | 78.9 ± 0.2 |

Reactor Configuration and Experimental setup

Test 1 was run using the automatized lab-scale batch reactors (RES Reliable Environmental Solutions, Ravenna, Italy) showed in Figure 4.

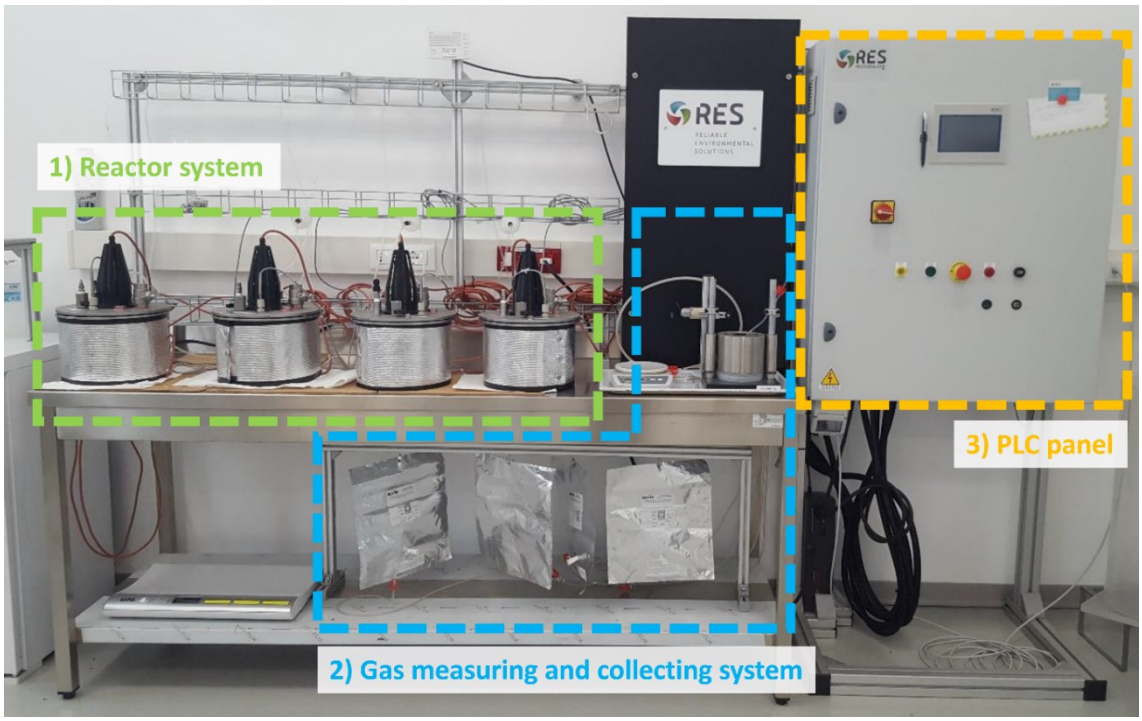


*Figure 4, Experimental setup used for Test 1. 1) Reactor system, made of four identical 6 L reactors equipped with electric heating bands, insulation jackets, temperature probes, and agitators; 2) Gas measuring and collecting system; 3) PLC panel to control operative parameters and data logging.*

The fermenter system is supplied with 4 identical reactors (6 L of total volume, 4 L of operative volume)

Each reactor consists of:

- a stainless steel (AISI-304) vessel with a removable cover flange
- ball valves on the cover flange for feeding, sampling, and gas flushing
- an electric heating band and insulation jacket for temperature control
- an electric motor-driven vertical mixer with an anchor-style agitator
- a temperature probe
- a pressure sensor
- a safety pressure relief valve
- a gas meter for measuring volumetric gas production
- a 10 L gas-sampling bag for gas collection
- electronically controlled solenoid valves for managing gas measurement and collection

All reactors are connected to an electric panel equipped with a PLC that manages temperature control, mixing, gas measurement and sampling, and data logging.

Each fermentation test was conducted with no initial inoculum, considering the WAS as a biologically active substrate. Six distinct organic loadings (0, 5, 10, 15, 20, 25 $kg_{TVS(OW)}$ $m^{-3}$) were tested, with increasing amount of OW corresponding to a proportional reduction in WAS, as showed in Figure 5. Each condition was tested in duplicate. Figure 6 provides a schematic overview of the experimental setup.

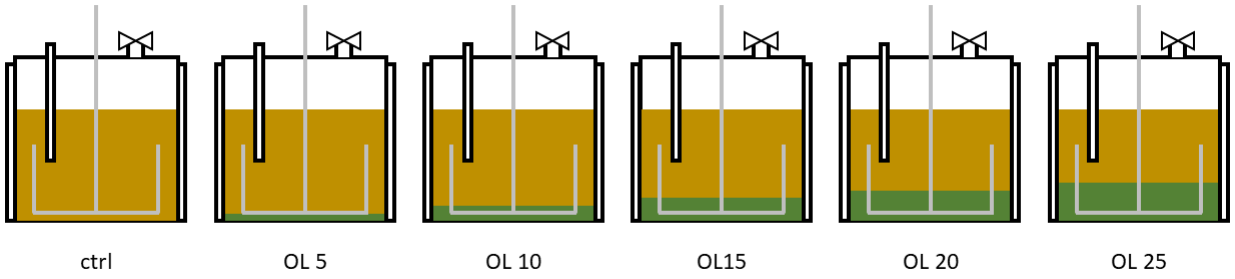


*Figure 5, Scheme of the tested conditions and the relative labels. In light brown the amount of WAS dosed, in dark green the amount of OW*

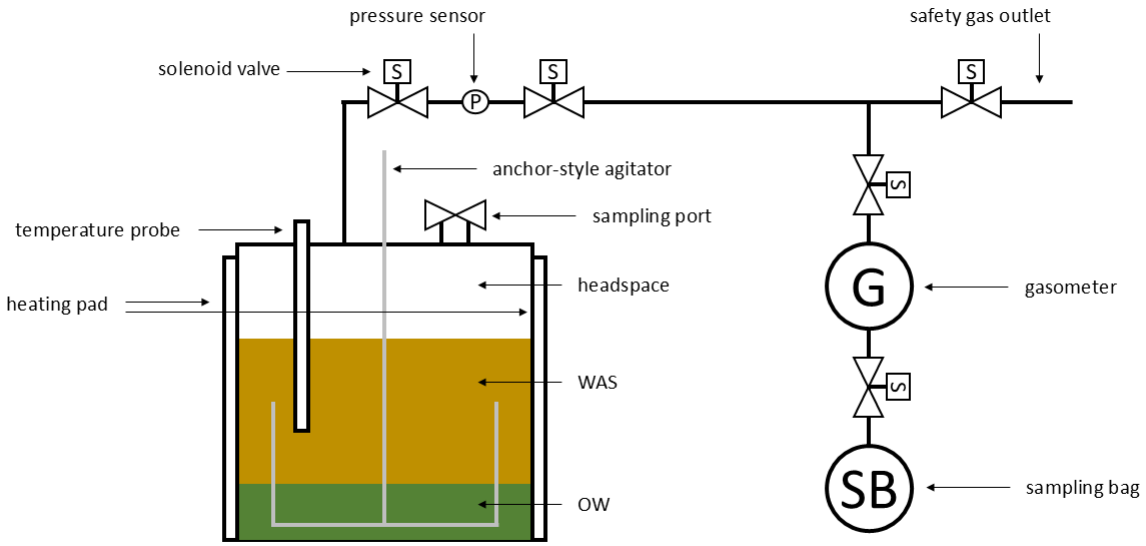


*Figure 6, Scheme of the components of the reactors involved in Test 1*

The percentage of substrates dosed in each condition and its relative OL are reported in Table 10.

*Table 10, Experimental setup of Test 1*

| Label | OW [% w/w] | WAS [% w/w] | OW [% tvs/tvs] | WAS [% tvs/tvs] | OL[a] [$kg_{TVS(OW)}$ $m^{-3}$] | OL[b] [$kg_{TVS(tot)}$ $m^{-3}$] |
|---|---|---|---|---|---|---|
| *ctrl* | 0 | 100 | 0 | 100 | 0 | 19.4 |
| *OL 5* | 5.8 | 94.2 | 19.4 | 80.6 | 5 | 22.7 |
| *OL 10* | 13.2 | 86.8 | 38.0 | 62.0 | 10 | 26.3 |
| *OL 15* | 20.4 | 79.6 | 51.6 | 48.4 | 15 | 30.0 |
| *OL 20* | 27.1 | 72.9 | 61.5 | 38.5 | 20 | 33.5 |
| *OL 25* | 33.9 | 66.1 | 69.5 | 30.5 | 25 | 37.0 |

OL[a] – organic loading considering the WAS as inoculum

OL[b] – organic loading considering the WAS as a substrate

The biogas production was continuously monitored to detect in time any potential methanogenic activity. The system was designed to measure the pressure in each reactor 30 minutes after the test began. Subsequent measurements were scheduled according to the pressure increase rate, calculated as pressure difference over time between consecutive readings. This allowed the system to estimate the pressure buildup within the reactor headspace and adjust the measurement frequency accordingly, preventing pressure levels that could negatively impact microbial activity. When the headspace pressure exceeded 1,350 mbar, solenoid valves automatically directed the produced biogas to the gasometer, logging the recorded volume in the data system. After the reading, the biogas was collected into the 10 L gas-sampling bag, reducing the headspace pressure. The measured gas volume was then standardized to normal temperature and pressure conditions (273.15 K, 1 atm) for accurate comparison and analysis. A sample of the fermentative broth was collected on a daily basis to analyze pH variations and VFA composition determination. The pH fluctuations were monitored throughout the experiment but were not regulated. Each fermentative test was conducted over a 10-days period.

Analytical methods

The total solids (TS) and total volatile solids (TVS) content of the substrates was determined using a gravimetric method according to the APHA Standard Methods for the Examination of Water and Wastewater (Baird et al., 2017). The chemical oxygen demand (COD) of the substrates was measured using a closed reflux titrimetric method according to APHA standard methods (Baird et al., 2017). Fermentation broth samples were centrifuged at 4,500 rpm for 5 min and filtrated through a 0.2 µm cellulose acetate membrane before pH and VFA analysis (section 3.5). The pH was determined using a pH electrode (HI1131B, Hanna Instruments, Italy) and a bench pH-meter (HI5522, Hanna Instruments, Italy). All VFA concentrations were expressed as COD, based on their complete stoichiometric conversion. The acidogenic yields ($g_{VFA(COD)}$ $kg_{TVS}^{-1}$) were calculated as the ratio between the produced VFAs to the TVS input under each experimental condition (section 3.6). Ammonium concentration was quantified at the end of the test using an Ion Selective Electrode (HI4101, Hanna Instruments, Italy). The composition of the produced biogas was analyzed with a biogas analyzer (ETG, MCA 100 Syn Biogas Multigas Analyzer) equipped with a thermal conductivity detector (TCD) for the hydrogen measurement, a non-dispersive infrared (NDIR) sensor for the methane and carbon dioxide measurement, and an electrochemical cell for oxygen quantification.

### 3.2.2. Test 2: Lab-scale Dark Fermentation of Hydrodynamic Cavitated Food Waste and WAS mixture, in Batch Condition

In Test 2, the batch mode DF process was integrated with a Hydrodynamic Cavitation (HC) pretreatment of the substrates. Pretreatments are typically employed to break down complex organic materials, as WAS flocs and FW fibers can be, by means of mechanical, physical, or chemical transformations, with the primary goal of increasing their bioavailability for microbial degradation and therefore their kinetics. For details on cavitation phenomenon and its application in organic waste pretreatment refer to Section 2.2.2.

Inoculum and substrates

In Test 2, a mixture of Food Waste (FW) and Waste Activated Sludge (WAS) were used as the substrate. The Food Waste was sourced from a municipal fruit and vegetable market (Mercato Ortofrutticolo Comunale, VERITAS spa, Mestre, Italy), which provided several boxes of mixed unsold products with the following composition (% w/w): onions (36 %), tomatoes (20 %), broccoli (16 %), parsley (11 %), chard (10 %), and apples (7 %) (Figure 7a). These waste materials were thoroughly mixed and shredded using an industrial mechanical grinder (Fruit Shredder 61903, WilTec Wildanger Technik GmbH, Germany) to obtain a homogeneous mixture (Figure 7b-c).

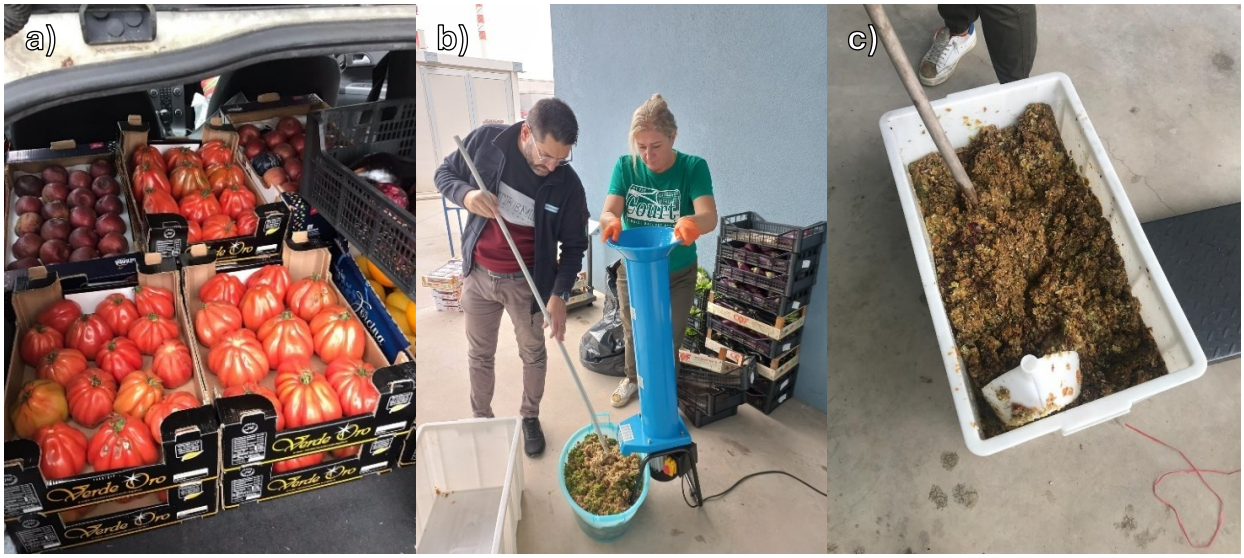


*Figure 7, Collection and homogenization of food waste. a) Unsold food boxes collected from the municipal fruit and vegetable market; b) shredding procedure using an industrial mechanical grinder; c) homogeneous mixture obtained after processing.*

The WAS was collected from the static gravimetric thickener of the municipal Wastewater Treatment Plant (WWTP, VERITAS spa, Fusina, Italy). The anaerobic digestate used as inoculum for the fermentation process was also sourced from the same WWTP. The digestate was used as such, with no thermal pretreatment or sieving. The physio-chemical characteristics of the FW, WAS, and inoculum are summarized in Table 12.

Hydrodinamic cavitation pretreatment of the substrates

A Hydrodynamic Cavitation (HC) process was tested as a pretreatment method to enhance substrate fermentability and improve hydrogen production yields. The HC reactor used for the pretreatment was a BioBang® cavitator (Three-es srl, Lazzate, Italy) (Figure 8).

*Figure 8, Hydrodynamic cavitator employed for the HC pretreatment*

The pretreatment aimed to increase the bioavailability of organic substrates by disrupting WAS flocs and breaking down FW fibers. The cavitation pretreatment was applied to 380 L of an organic waste mixture (40 kg of FW, 200 L of WAS, 140 L of tap water). The FW and WAS proportions were selected to achieve a 50:50 TVS ratio (corresponding to a 20:80 ratio on fresh matter basis). This ratio was determined based on the methodology outlined in Valentino et al. (2019) and Moretto et al. (2020), which also employed a 50:50 TVS ratio in similar tests. Dilution with water was necessary to meet the minimum operational volume required for HC pretreatment.

The organic waste mixture was placed in a cubic meter tank equipped with a stirring system and a closed-loop circuit was applied, continuously recirculating the organic mixture throughout the duration of the pretreatment.

The pretreatment parameters are summarized in Table 11.

*Table 11, Operative parameters of the HC pretreatment*

| | | |
|---|---|---|
| Inlet pressure | bars | 1.8–2 |
| Electrical power | kW | 17 |
| $Q_{recirculation}$ | L $min^{-1}$ | 80–100 |
| Rotor speed | rpm | 1450–1550 |
| Duration | min | 30 |

In Table 12 are reported the physio-chemical characteristics of the inoculum and the organic waste used during the test.

*Table 12, Physio-chemical characteristics of the inoculum and the organic wastes used in Test 2*

| | TS [$g_{TS}$ $kg^{-1}$] | TVS [$g_{TVS}$ $kg^{-1}$] | sCOD [$g_{O2}$ $L^{-1}$] | $NH_4^+$ [$mg_{NH4+}$ $L^{-1}$] | pH | Partial alkalinity [$mg_{CaCO3}$ $L^{-1}$] | Total alkalinity [$mg_{CaCO3}$ $L^{-1}$] |
|---|---|---|---|---|---|---|---|
| FW | 92 ± 3 | 82 ± 3 | 68 ± 1 | 152 ± 8 | 4.62 | - | - |
| WAS | 40.6 ± 0.1 | 28.4 ± 0.1 | 1.13 ± 0.01 | 148 ± 3 | 6.38 | 287 ± 9 | 627 ± 12 |
| Mix (not-pretreated) | 30.1 ± 0.1 | 23.2 ± 0.2 | 7.47 ± 0.02 | 139 ± 4 | 4.85 | - | - |
| Mix (HC pretreated) | 31.7 ± 0.1 | 24.7 ± 0.1 | 10.85 ± 0.03 | 176 ± 5 | 4.88 | - | - |
| Inoculum | 29.5 ± 0.1 | 19.2 ± 0.2 | 0.65 ± 0.01 | 720 ± 20 | 7.72 | 1787 ± 15 | 2500 ± 30 |

Reactor Configuration and Experimental setup

The fermentation batch tests were conducted on the pretreated (*HC*) and untreated (*ctrl*) organic mixture, in duplicate, using the same automatized lab-scale batch reactors (RES Reliable Environmental Solutions, Ravenna, Italy) described in Section 3.2.1 (Figure 4)

Each reactor was inoculated with 0.4 L of digestate, followed by the addition of 2.5 L of organic waste mixture and 1.1 L of tap water, resulting in an initial organic loading (OL) of 14.5 $kg_{TVS}$ $m^{-3}$ and a Feed-to-Microorganisms (F/M) ratio of 7.55 $g_{VS(feed)}$ $g_{VS(microorganisms)}^{-1}$. The reactors were maintained at a temperature of 37.0 ± 0.6 °C with continuous stirring at 14 rpm. Each reactor was flushed with nitrogen gas for 1 minute before starting the test, to establish anaerobic conditions within the reaction environment. Gas production was measured continuously, following the same automatic procedure described in Test 1 (Section 3.2.1), while the gas composition ($H_2$, $CO_2$, $O_2$, $CH_4$) was analyzed on a daily basis. Due to technical constraints, sampling of the fermentative mixed liquor was not conducted during the experiment, but only at the end of the test, to analyze solid content and pH. The test was carried out over a 6 d period and was interrupted once no further hydrogen production was detected.

Analytical methods

The total solids (TS) and total volatile solids (TVS) content of the substrates was determined using a gravimetric method according to the APHA Standard Methods for the Examination of Water and Wastewater (Baird et al., 2017). The chemical oxygen demand (COD) of the substrates was measured using a closed reflux titrimetric method according to APHA standard methods (Baird et al., 2017). The pH was determined using a pH electrode (HI1131B, Hanna Instruments, Italy) and a bench pH-meter (HI5522, Hanna Instruments, Italy). Partial and total alkalinity of WAS and digestate were determined using a trimetric method according to APHA standard methods (Baird et al., 2017). The composition of the produced biogas was analyzed with a biogas analyzer (ETG, MCA 100 Syn Biogas Multigas Analyzer) equipped with a thermal conductivity detector (TCD) for the hydrogen measurement, a non-dispersive infrared (NDIR)

sensor for the methane and carbon dioxide measurement, and an electrochemical cell for oxygen quantification.

### 3.2.3. Test 3: Lab-scale Dark Fermentation of Food Waste and WAS in Semi-continuous Condition

In Test 3, the DF process was shifted from batch mode to semi-continuous feeding. This transition is particularly valuable when aiming to scale up a process to industrial level, especially when the primary objective is waste treatment rather than the production of high-value products. While batch mode testing is useful for maintaining strict control over experimental variables and defining initial operative parameters, it cannot accurately represent the dynamic conditions of industrial scaled-up waste treatment. Working under semi-continuous operation offers a practical compromise, providing on one hand a more realistic simulation of industrial conditions while on the other hand maintaining operational simplicity.

#### Inoculum and substrates

Similarly to the previous experiments, Food Waste (FW) and Waste Activated Sludge (WAS) were used as substrates. The FW was sourced from the municipal fruit and vegetable market (Mercato Ortofrutticolo Comunale, VERITAS spa, Mestre, Italy) and, according to seasonal availability, consisted of the following unsold materials (% w/w): apples (42 %), tomatoes (34 %), citrus fruits (8 %), fennels (7 %), onions (6 %), lettuce (3 %), eggplants (0.9 %), and beans (0.1 %). These waste materials were thoroughly mixed and shredded with a kitchen blander to obtain a homogeneous mixture.

The WAS, as well as the digestate used as inoculum, was collected from the municipal Wastewater Treatment Plant (WWTP, VERITAS spa, Fusina, Italy). The digestate was used as such, without any thermal pretreatment or sieving.

The physio-chemical characteristics of the inoculum and the organic wastes used in the test are detailed in Table 13.

*Table 13, Physio-chemical characterization of the substrates and inoculum used in Test 3*

| | TS [$g_{TS}$ $kg^{-1}$] | TVS [$g_{TVS}$ $kg^{-1}$] | sCOD [$g_{O2}$ $L^{-1}$] | $NH_4^+$ [$mg_{NH4+}$ $L^{-1}$] | pH | Partial alkalinity [$mg_{CaCO3}$ $L^{-1}$] | Total alkalinity [$mg_{CaCO3}$ $L^{-1}$] |
|---|---|---|---|---|---|---|---|
| FW | 102 ± 2 | 99 ± 2 | 190 ± 10 | 44.7 ± 0.6 | 3.94 | - | - |
| WAS | 33 ± 3 | 21 ± 2 | 0.52 ± 0.01 | 122 ± 3 | 7.45 | 200 ± 6 | 550 ± 10 |
| Inoculum | 30 ± 1 | 18 ± 1 | 0.42 ± 0.01 | 690 ± 18 | 8.53 | 2025 ± 20 | 3050 ± 25 |

Reactor Configuration and Experimental setup

The semi-continuous test was conducted using the same lab-scale fermenter (RES Reliable Environmental Solutions, Ravenna, Italy) as in the previous experiment, but equipped with a modified vessel to accommodate the feeding procedure. The modified vessel, showed in Figure 9a is provided with a charge/discharge butterfly valve and a stainless steel (AISI-304) 400 mL syringe (Figure 9b) used for both the removal of the effluent and the addition of new substrate.


*Figure 9, Modified vessel employed in Test 3. a) detail of the charge/discharge valve; b) syringe used for effluent removal and substrate addition*

The start-up of the process was performed inoculating the reactor with 0.3 L of digestate, followed by the addition of 300 g of FW, 1.4 L of WAS, and 2.0 L of tap water, resulting in total operative volume of 4.0 L. Figure 10 provides a schematic overview of the experimental setup.

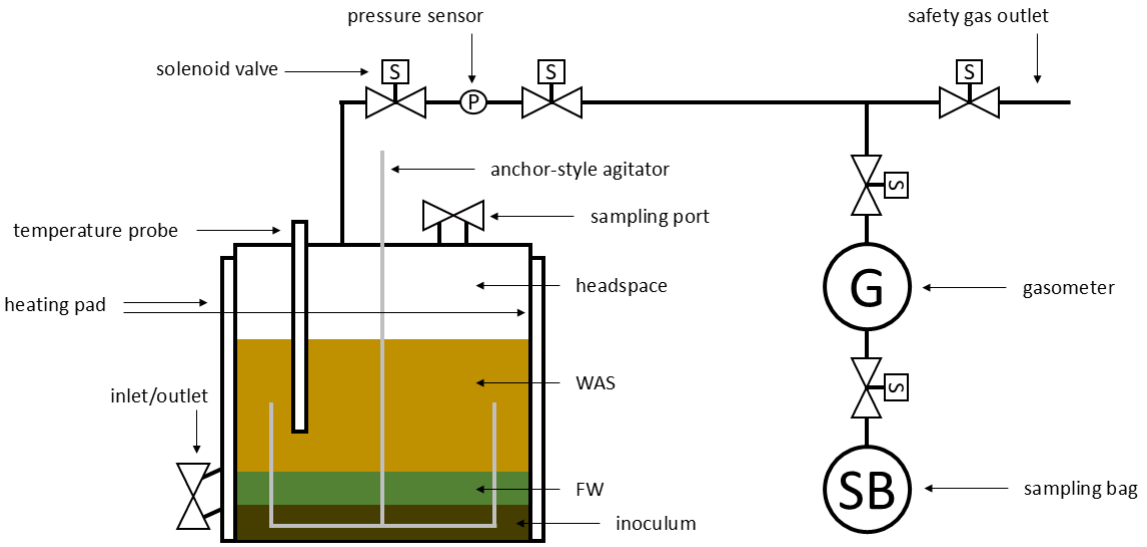


*Figure 10, Scheme of the components of the reactors involved in Test 3*

This setup resulted in an OL and F/M ratio of 15 $kg_{TVS}$ $m^{-3}$ and 11.0 $VS_{feed}$ $VS_{inoculum}^{-1}$, respectively. To ensure anaerobic conditions, the reactor was flushed with nitrogen for 3 minutes before the experiment began. The system was then maintained at a temperature of 37.0 ± 0.6 °C with continuous mixing at 14 rpm. During the first 4 days, no substrate was added, allowing the biomass sufficient time to acclimatize to the process conditions. From day 4 onward, the reactor was fed daily (5 days a week, with no feeding during the weekend) maintaining a Hydraulic Retention Time (HRT) of 3.1 d and an Organic Loading Ratio (OLR) of 12 $kg_{TVS}$ $m^{-3}$ $d^{-1}$ (corresponding to the addition of 270 g of FW and 1.0 L of WAS each feeding). The pH of the system was continuously monitored and automatically adjusted within the range of 5.20 to 5.50 using a peristaltic pump to dose a 3 N NaOH solution. The process was run under these conditions for a total duration of 42 days (6 weeks). The operative conditions of the test are summarized in Table 14.

*Table 14, Operative conditions set up during the semi-continuous DF test*

| | | |
|---|---|---|
| Start-up duration | d | 4 |
| Test duration | d | 43 |
| Temperature | °C | 37.0 ± 0.6 |
| pH | | 5.5 |
| HRT | d | 3.1 |
| OLR | $kg_{TVS}$ $m^{-3}$ $d^{-1}$ | 12 |

Gas production was measured continuously, following the same automatic procedure described in Test 1 (Section 3.2.1), while the gas composition ($H_2$, $CO_2$, $O_2$, $CH_4$) was analyzed on a daily basis. The fermentative broth was sampled daily during the feeding process, and was used to analyze solid content, pH, total alkalinity, $NH_4^+$ concentration, sCOD, and VFA composition.

Analytical methods

The total solids (TS) and total volatile solids (TVS) content of the substrates was determined using a gravimetric method according to the APHA Standard Methods for the Examination of Water and Wastewater (Baird et al., 2017). The soluble chemical oxygen demand (sCOD) of the samples was measured using a closed reflux colorimetric method according to APHA standard methods (Baird et al., 2017). Fermentation broth samples were centrifuged at 4,500 rpm for 5 min and filtrated through a 0.2 µm cellulose acetate membrane before pH, alkalinity, $NH_4^+$, and VFA analysis (section 3.5). The pH was determined using a pH electrode (HI1131B, Hanna Instruments, Italy) and a bench pH-meter (HI5522, Hanna Instruments, Italy). Partial and total alkalinity were determined using a trimetric method according to APHA standard methods (Baird et al., 2017). Ammonium concentration was quantified using an Ion Selective Electrode (HI4101, Hanna Instruments, Italy). All VFA concentrations were expressed as COD, based on their complete stoichiometric conversion. The composition of the produced biogas was analyzed with a biogas analyzer (ETG, MCA 100 Syn Biogas Multigas Analyzer) equipped with a thermal conductivity detector (TCD) for the hydrogen measurement, a non-dispersive infrared (NDIR) sensor for the methane and carbon dioxide measurement, and an electrochemical cell for oxygen quantification.

### 3.2.4. Test 4: Pilot-scale Dark Fermentation of Food Waste and WAS in Semi-continuous Condition, and Anaerobic Digestion of the Fermentative Effluent

In Test 4, a pilot-scale bioreactor system was employed in semi-continuous mode, evaluating the bioconversion efficiency of organic waste into hydrogen via Dark Fermentation (DF) and the subsequent valorization of the Dark Fermentation Effluent (DFE) into biogas through Anaerobic Digestion (AD). Figure 11 provides a schematic overview of the two-phase DF-AD process involved in this test. The integration of DF and AD processes into a two-phase system was

imperative for scaling up the operation, as it provided a possible valorization pathway for the generated DFE, enhancing the overall energy recovery from the wastes, and contributed to the stabilization and reduction in mass of the waste.

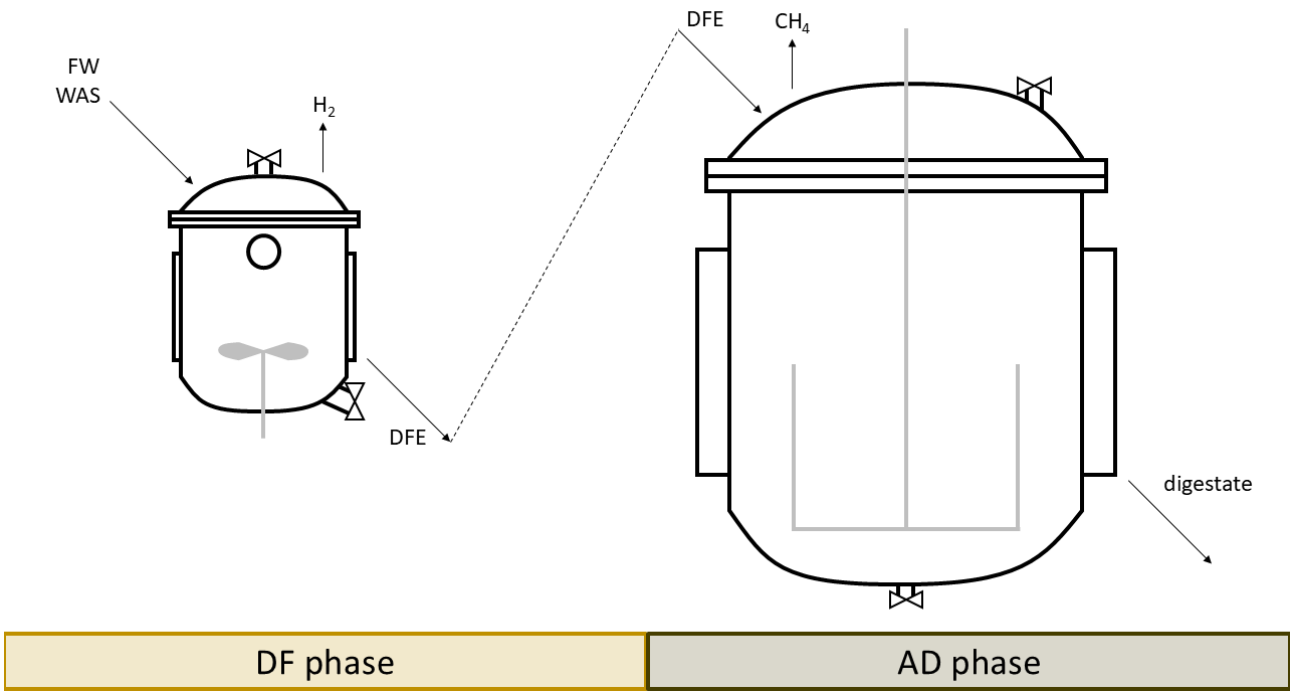


*Figure 11, Schematic representation of the two-phase DF-AD process conducted in Test 4*

Inoculum and substrates

In Test 4, the protocol employed in the previous test was adapted for pilot-scale operations. The substrates utilized for fermentation were Food Waste (FW), sourced from the municipal fruit and vegetable market (Mercato Ortofrutticolo Comunale, VERITAS spa, Mestre, Italy), and Waste Activated Sludge (WAS), collected from the municipal Wastewater Treatment Plant (WWTP, VERITAS spa, Fusina, Italy). Due to the overall quantity of substrates required for the entire experimental period and the constraints of the municipal fruit and vegetable market to provide all materials at once, together with the impossibility of storing properly that volume of

material over a long period, it was necessary to prepare the FW mixture in two separate batches. The first mixture (FW 1) was composed of the following materials (% w/w): eggplants (28.8 %), cauliflowers (26.7 %), apples (20.0 %), onions (16.6 %), and corn salad (7.9 %). The second mixture (FW 2) consisted of (% w/w): tomatoes (33.1 %), lettuce (20.5 %), onions (13.4 %), apples (12.3 %), bananas (12.0 %), eggplants (7.5 %), and broccoli (1.1 %). On both batches, the FW was thoroughly mixed and shredded using an industrial mechanical grinder (Fruit Shredder 61903, WilTec Wildanger Technik GmbH, Germany) to ensure uniformity of the mixture, as for Test 2 (Figure 7, section 3.2.2). These mixtures were then stored at -4 °C and thawed as required for the fermentation process.

The digestate used as inoculum was sourced from the same municipal Wastewater Treatment Plant (WWTP, VERITAS spa, Fusina, Italy) as for the WAS. The digestate was used as such, without undergoing any thermal pretreatment or sieving processes. The WAS was stored in a sealed external storage tank, subjected to environmental temperatures fluctuating between 3 °C and 15 °C throughout the duration of the experimental period. Monitoring the physio-chemical characteristics of the WAS over time revealed a substantial variation in its solids content after approximately two weeks (as reported in Table 15). This difference is likely due to an inadequate homogenization of the storage tank before sampling. The sampling was performed by mean of a membrane pump and followed a 10-minute recirculation of the storage tank contents at a flow rate of approximately 50 L $min^{-1}$ to ensure homogeneity.

Table 15 presents the physio-chemical characteristics of the inoculum and the organic waste materials used during the test. FW 1 and FW 2 refer to the two batches of food waste mixture prepared during the experimental period. WAS 1 and WAS 2 indicate the two observed characteristics of solid content in the same substrate storage tank.

*Table 15, Total Solids and Total Volatile Solids content of the inoculum and substrates used in Test 4*

| | TS [$g_{TS}$ $kg^{-1}$] | TVS [$g_{TVS}$ $kg^{-1}$] | TVS ratio [% TVS/TS] |
|---|---|---|---|
| FW 1 | 76 ± 1 | 71 ± 3 | 92 ± 2 |
| FW 2 | 84 ± 5 | 79 ± 6 | 93 ± 1 |
| WAS 1 | 35 ± 2 | 23 ± 2 | 65 ± 2 |
| WAS 2 | 13 ± 2 | 8 ± 1 | 64 ± 1 |
| Inoculum | 33.2 ± 0.4 | 19.3 ± 0.2 | 58.2 ± 0.3 |

Reactor Configuration and Experimental setup

The DF phase of Test 4 was conducted on the pilot-scale reactor (RES Reliable Environmental Solutions, Ravenna, Italia) showed in Figure 12 and Figure 13.

The reactor (67 L of total volume, 45 L of operative volume) includes:

- a stainless steel (AISI-304) vessel with a removable lid
- ball valves and fittings on the cover flange for feeding, pH correction, and nitrogen flushing
- a butterfly valve on the bottom side of the reactor for discharging and sampling
- an electric heating band for temperature control
- an electric motor-driven vertical mixer with a propeller agitator
- a temperature probe
- a pressure sensor
- a safety pressure relief valve
- a pH probe
- a gas meter for measuring volumetric gas production

- a 25 L gas-bag for gas collection
- a peristaltic pump to dose 10 N NaOH for pH control
- electronically controlled valves for managing gas measurement and collection

The reactor is connected to an electric panel equipped with a PLC that manages temperature control, mixing, gas measurement and sampling, and data logging.

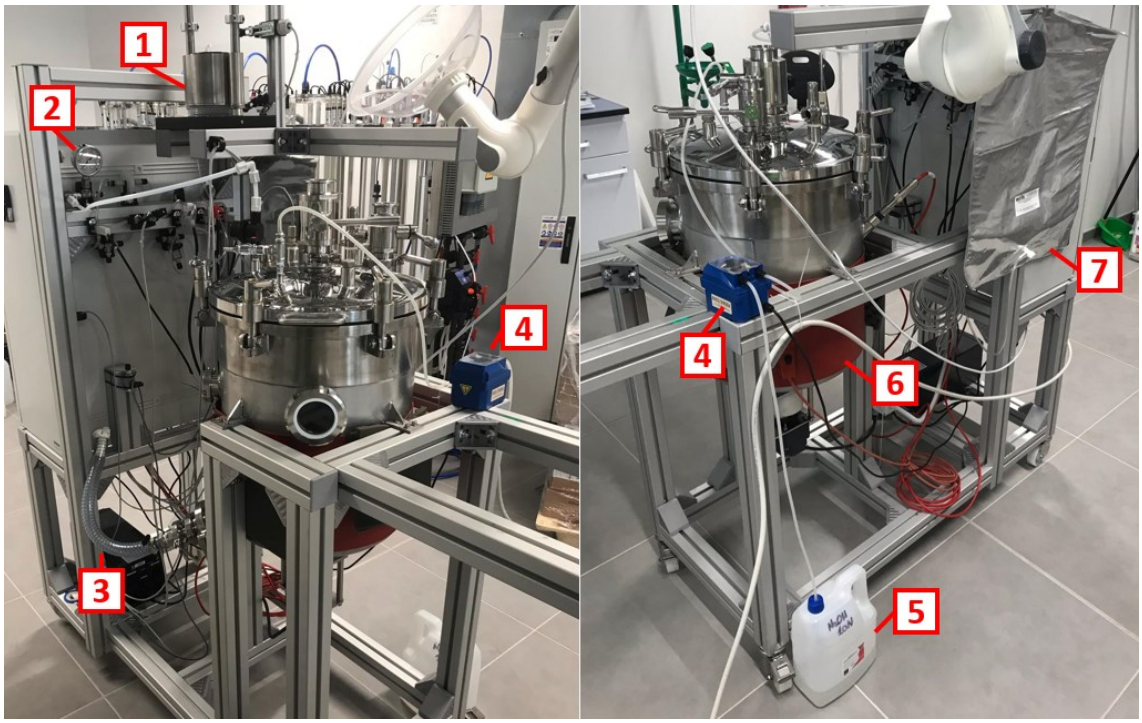


*Figure 12, Front and rear side of the pilot-scale reactor employed in the DF phase of Test 4. 1) volumetric gasometer; 2) pressure sensor; 3) DFE discharge outlet; 4) peristaltic pump for pH control; 5) 10 N NaOH solution for pH control; 6) electric heating band for temperature control; 7) 25 L gas-sampling bag for biogas collection*

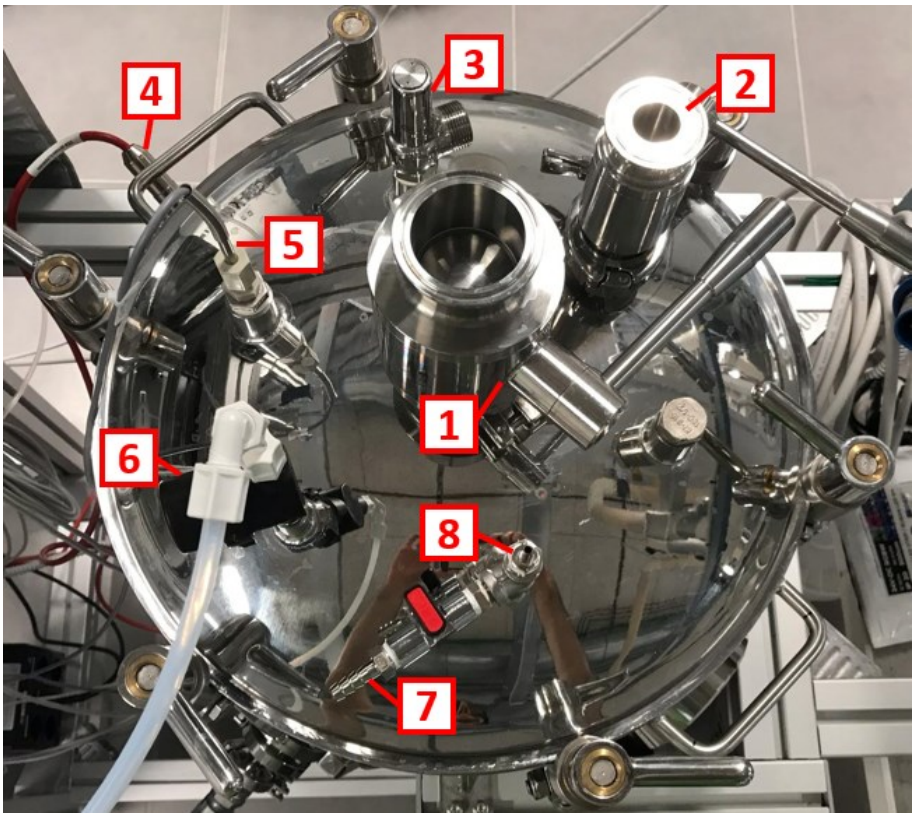


*Figure 13, Detail of the valves and fittings present in the cover flange of the pilot-scale reactor. 1) feeding inlet valve; 2) nitrogen flushing gas outlet; 3) safety pressure relief valve; 4) pH probe; 5) temperature probe; 6) humidity filter and gas sampling connection; 7) nitrogen flushing gas inlet / headspace sampling port; 8) pH control fitting*

The start-up of the test was conducted by setting an OL of 15 $kg_{TVS}$ $m^{-3}$ and an F/M ratio of 11. To adhere to these operational parameters, the reactor was inoculated with 3.18 L of digestate, loaded with 4.78 kg of FW and 14.48 kg of WAS, and brought to volume adding 22.5 L of water. The reactor's headspace was then flushed with nitrogen until a residual oxygen content lower than 0.2% was achieved, ensuring anaerobic conditions within the reaction space. The system was maintained at a temperature of 37.0 ± 0.6 °C with continuous mixing at 120 rpm. The pH was maintained within a range of 5.40 – 5.50 by automatically dosing a 10 N NaOH solution. Compared to previous laboratory scale tests, the mixing speed was increased to improve substrate homogenization and optimize gas-liquid mass transfer of dissolved hydrogen. This adjustment aimed at enhancing hydrogen release into the headspace, thereby minimizing its bioavailability and reducing the activity of hydrogenotrophic microorganisms, which could otherwise consume the produced hydrogen.

The experiment was conducted over a total duration of 23 days. During the first two weeks, the system was fed daily (5 days a week, with no feeding during the weekend) maintaining an HRT of 3.0 d and an OLR of 12.0 ± 0.5 $kg_{TVS}$ $m^{-3}$ $d^{-1}$ (corresponding to 3.71 kg of FW and 11.29 kg of WAS per feeding). After this initial phase, the same feeding procedure was maintained, but the feeding volume was adjusted to account for the observed fluctuations in WAS solids content, ensuring the maintenance of both the target OLR and the TVS ratio between FW and WAS. This allowed for a concomitant reduction of the HRT to 1.5 d, promoting the wash out of the hydrogenotrophic methanogens that had begun to establish in the system. Table 16 summarizes the variation in the DF operative parameters over the experimental period.

*Table 16, Variation in the HRT and feeding volume over the experimental period of the DF phase of Test 4*

| Period [d] | HRT [d] | FW [kg $d^{-1}$] | WAS [L $d^{-1}$] | OLR [$kg_{TVS}$ $m^{-3}$ $d^{-1}$] |
|---|---|---|---|---|
| 0 – 13 | 3 | 3.71 (FW1) | 11.29 (WAS 1) | 12.0 ± 0.5 |
| 14 – 17 | 1.5 | 3.71 (FW1) | 26.29 (WAS 2) | 12.0 ± 0.5 |
| 18 – 23 | 1.5 | 3.35 (FW2) | 26.65 (WAS 2) | 12.0 ± 0.5 |

Gas production was measured continuously, following the same automatic procedure described in Test 1 (Section 3.2.1). In this case, the pressure threshold for gas measurement was reduced to 1,200 mbar to accelerate the discharge of the produced hydrogen into the sampling bag. This adjustment aimed at limiting the operative headspace pressure and, consequently, the partial pressure of hydrogen, thereby reducing the concentration of dissolved hydrogen available for hydrogenotrophic methanogens and limiting their activity. The gas composition ($H_2$, $CO_2$, $O_2$, $CH_4$) was analyzed on a daily basis. The fermentative broth was sampled daily during the feeding process and was used for solid content determination.

The AD phase of Test 4 was conducted on the pilot-scale assembled reactor (GreenPropulsion Laboratory, Fusina, Italy) showed in Figure 14.


*Figure 14, Pilot-scale reactor employed in the AD phase of Test 4*

The reactor (450 L of total volume, 350 L of operative volume) includes:

- a stainless steel (AISI-304) vessel
- ball valves and fittings on the cover flange for feeding, gas sampling, and nitrogen flushing
- a ball valve on the bottom of the reactor for effluent discharging
- a ball valve on the mid-high side of the reactor for mixed liquor sampling
- an electric motor-driven vertical mixer with an anchor-style agitator
- a temperature probe
- a reactor jacket with glycerol as heat transfer fluid
- a boiler for glycerol heating, and electronically controlled pumps for fluid recirculation in the reactor jacket
- a nitrogen cylinder for headspace flushing

- a pressure sensor
- a safety pressure relief valve
- a pH probe
- a electronically controlled solenoid valve for gas discharge
- a drum-type gas meter for measuring volumetric gas production

The reactor is connected to an electric panel equipped with a PLC that manages temperature control, mixing, headspace pressure thresholds, and data logging.

The start-up of the pilot-scale digester was conducted by introducing 350 L of digestate as inoculum. The operational parameters were set to maintain mesophilic conditions at 37 ± 1 °C, with continuous mixing at 30 rpm. The reactor headspace was then purged with nitrogen gas until the residual oxygen concentration fell below 0.2 %, thereby establishing a strict anaerobic condition within the reaction space. The pH was monitored continuously but not regulated. The reactor was inoculated two weeks before the start of the test, thereby allowing the microbial consortium to acclimatize to the process conditions.

The experiment was conducted contingently with the DF phase over a total duration of 23 days. In the first period, while the DF phase was maintained at an HRT of 3 d, the AD system was fed daily (5 days a week, with no feeding on weekends) with the entire 15 L of DFE generated in the first fermentative phase, corresponding to an HRT of 23.3 d and an OLR of 0.7 $kg_{TVS}\ m^{-3}\ d^{-1}$. In the second period, when the HRT of the DF phase was reduced to 1.5 d, the AD system continued to be fed following the same procedure but with an increased volume of 20 L per feeding, corresponding to an HRT of 17.5 d and an OLR of 1.0 $kg_{TVS}\ m^{-3}\ d^{-1}$. Table 17 describes the variation in the AD operative parameters over the experimental period.

*Table 17, Variation in the HRT and feeding volume over the experimental period of the AD phase of Test 4*

| Period [d] | HRT [d] | DFE [L $d^{-1}$] | OLR [$kg_{TVS}$ $m^{-3}$ $d^{-1}$] |
|---|---|---|---|
| 0 – 13 | 23.3 | 15.0 (FW1) | 0.7 ± 0.1 |
| 14 – 23 | 17.5 | 20.0 (FW2) | 1.0 ± 0.1 |

Gas production was measured continuously by mean of a drum-type gas meter connected to the solenoid valve for biogas discharge of the reactor. The valve was set to automatically open once reached 0.02 bar of pressure, channeling the produced gas to the measurement system. The gas composition ($H_2$, $CO_2$, $O_2$, $CH_4$) was analyzed on a daily basis by directly sampling the biogas present in the headspace of the reactor. The digestate was sampled daily after the feeding process and was used for solid content determination.

Analytical methods

The total solids (TS) and total volatile solids (TVS) content of the substrates was determined using a gravimetric method according to the APHA Standard Methods for the Examination of Water and Wastewater (Baird et al., 2017). The soluble chemical oxygen demand (sCOD) of the samples was measured using a closed reflux colorimetric method according to APHA standard methods (Baird et al., 2017). DFE and digestate samples were centrifuged at 4,500 rpm for 5 min and filtrated through a 0.2 µm cellulose acetate membrane before $NH_4^+$ and VFA analysis (section 3.5). Ammonium concentration was quantified using an Ion Selective Electrode (HI4101, Hanna Instruments, Italy). All VFA concentrations were expressed as COD, based on their complete stoichiometric conversion. The composition of the biogas produced in the DF phase was analyzed with a biogas analyzer (ETG, MCA 100 Syn Biogas Multigas Analyzer) equipped with a thermal conductivity detector (TCD) for the hydrogen measurement, a non-dispersive infrared (NDIR) sensor for the methane and carbon dioxide measurement, and an electrochemical cell for oxygen quantification. For the AD phase, biogas composition was analyzed with a portable biogas analyzer (Biogas 5000, Geotechnical Italia, Italy) featuring the same sensors as the one used in the DF phase, except for the TCD for hydrogen determination.

## 3.3. Photo Fermentation

### 3.3.1. Test 5: Preliminary test of PPB growth on Fermentative Broth

Test 5 focused on investigating the valorization of the DFE produced in the previous fermentative steps through PF processes. During DF, only a portion of the substrates is converted into hydrogen, while a significant portion remains in the effluent in the form of short-chain organic acids. By the integration of DF and PF, these organic acids could further be converted into hydrogen, enhancing the overall yield of the process. In this test, a batch-scale PF system was employed to evaluate PPB's adaptation to a DFE-based medium and their ability to convert the supplied organic compounds into hydrogen.

Inoculum and substrates

In Test 5, the PF test was carried out using *Rhodopseudomonas palustris* and *Rhodospirillum rubrum*, both supplied by BCCM (Belgian Coordinated Collections of Microorganisms, Ghent, Belgium).

Initially, the two Purple Phototrophic Bacteria (PPB) inocula were maintained axenically and moved from immobilized culture on Petri dishes to suspended culture thorough sequential acclimatation in RPN culture medium, as outlined in Bianchi et al., (2010), under continuous illumination (3,000 lux, incandescent lamp). Figure 15 and Figure 16 show the PPB inocula throughout the acclimatation process.

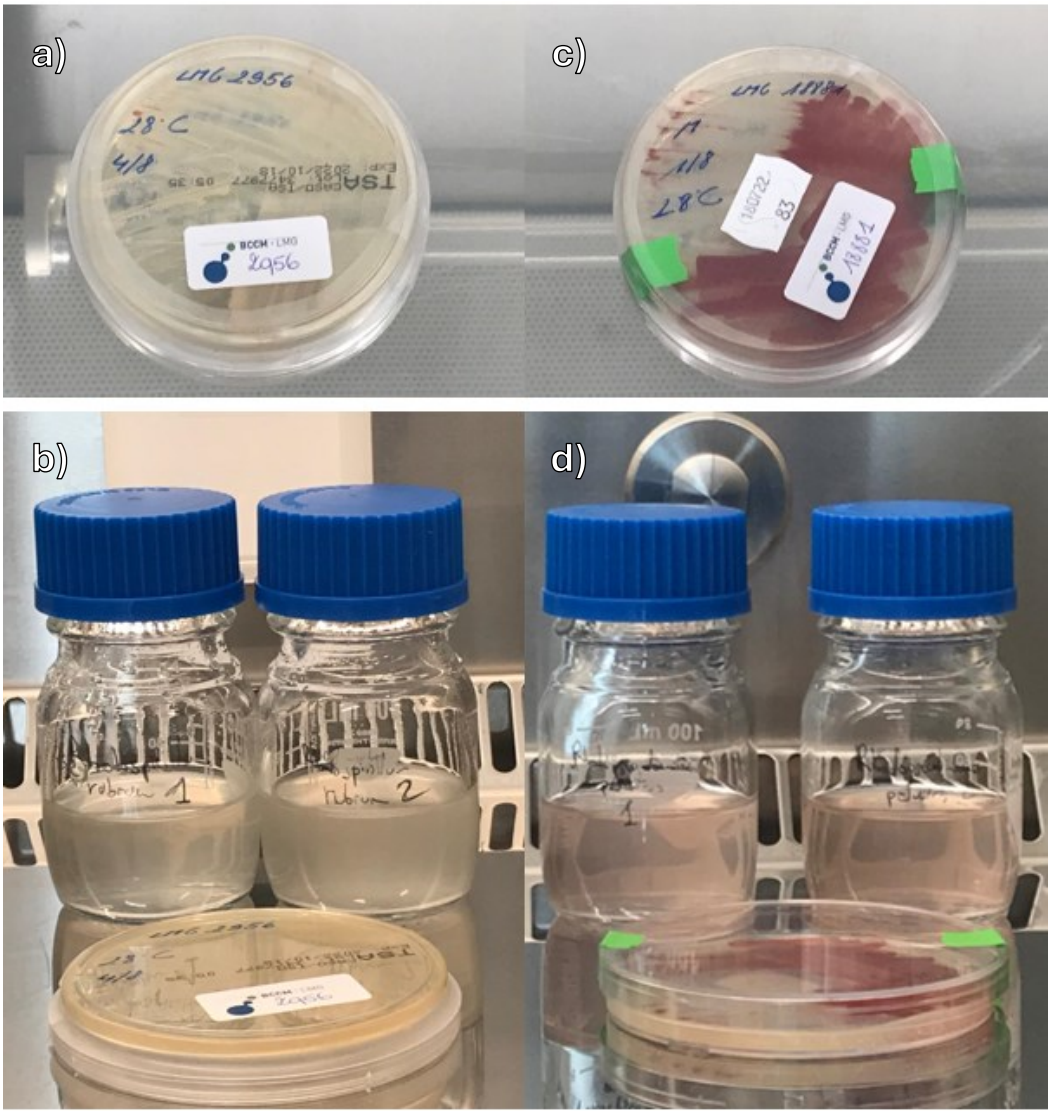


*Figure 15, PPB inocula on immobilized culture and on suspended culture at the beginning of the acclimatation phase. a) Rsp. rubrum on Petri dish and b) on suspended culture; c) Rps. palustris on Petri dish and d) on suspended culture*

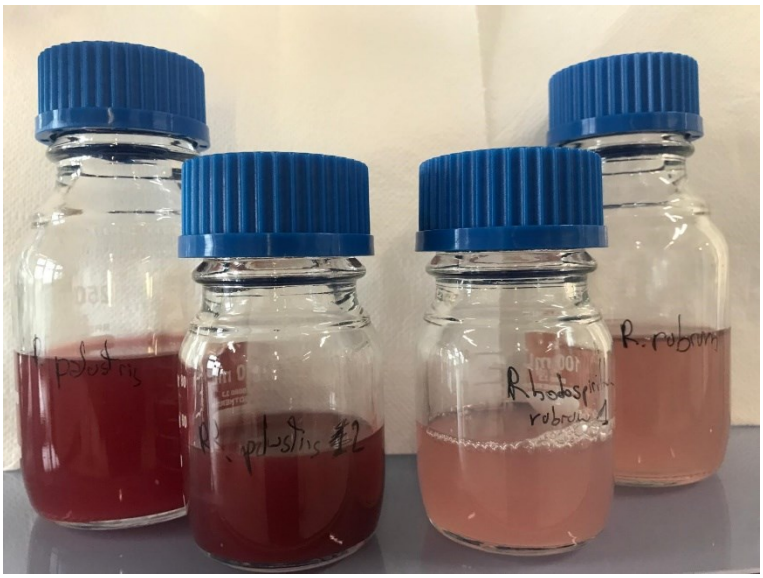

*Figure 16, PPB inocula at the end of the acclimatation phase on RPN medium. On the left Rps. palustris, on the right Rsp. rubrum*

The acclimatation phase took place over a total duration time of 30 days. At the end of the acclimatation phase, the biomass content of the two strains growth on RPN medium were of 0.65 ± 0.04 and 0.22 ± 0.03 $g_{PPB}$ $L^{-1}$ for *Rps. palustris* and *Rsp. rubrum*, respectively.

The Dark Fermentation Effluent (DFE) generated during previous DF phases (Test 1) was processed and pretreated to obtain a medium (Fermentative Broth medium, labeled as FB medium) enriched in VFA to be used for PPB growth. The DFE was first adjusted at 6.8 pH with NaOH 6 N, then centrifuged at 9,000 rpm for 10 min and filtered through a 0.2 µm sterile cellulose acetate membrane, for sterilization. The fermentation broth was then diluted 1:5 with an RPP medium prepared without the addition of malic acid; thus, maintaining the overall composition of the medium and replacing with VFA the carbon source for PPB metabolism.

Both strains were maintained under axenic conditions operating under a Class II Biological Safety Cabinet (BioVanguard, Baker, Netherlands). Culture media were sterilized either by autoclaving at 121 °C and 1.2 bar for 20 min or by filtration through 0.2 µm sterile cellulose acetate membranes.

The experimental PF phase was carried out comparing the growth yields of both strains on an RPP medium containing 4.0 g $L^{-1}$ of malic acid (Bianchi et al., 2010) and on FB medium. The composition of the different culture media is reported in Table 18.

*Table 18, Chemical composition of the culture media RPN, RPP, and FB*

| | | RPN | RPP | FB |
|---|---|---|---|---|
| pH | | 6.8 [a] | 6.8 [a] | 6.8 [a] |
| DL-malic acid | $g_{COD}$ $L^{-1}$ | 1.43 | 2.86 | - |
| acetic acid | $g_{COD}$ $L^{-1}$ | - | - | 0.75 ± 0.06 |
| propionic acid | $g_{COD}$ $L^{-1}$ | - | - | 0.38 ± 0.05 |
| butyric acid | $g_{COD}$ $L^{-1}$ | - | - | 0.30 ± 0.08 |
| valeric acid | $g_{COD}$ $L^{-1}$ | - | - | 0.32 ± 0.02 |
| caproic acid | $g_{COD}$ $L^{-1}$ | - | - | 0.84 ± 0.04 |
| heptanoic acid | $g_{COD}$ $L^{-1}$ | - | - | 0.24 ± 0.01 |
| total carbon source | $g_{COD}$ $L^{-1}$ | 1.43 | 2.86 | 2.8 ± 0.2 |
| $NH_4^+$ | $mg_{NH4+}$ $L^{-1}$ | - | - | 87 ± 9 |
| $NH_4Cl$ | $mg_{NH4+}$ $L^{-1}$ | 168.4 | - | - |
| Na-glutamate | g $L^{-1}$ | - | 0.4 | - |
| $K_2HPO_4$ | g $L^{-1}$ | 0.5 | 0.5 | 0.4 |
| $KH_2PO_4$ | g $L^{-1}$ | 0.3 | 0.3 | 0.24 |
| $MgSO_4 \cdot 7H_2O$ | g $L^{-1}$ | 0.4 | 0.4 | 0.32 |
| NaCl | g $L^{-1}$ | 0.4 | 0.4 | 0.32 |
| $CaCl \cdot 2H_2O$ | g $L^{-1}$ | 0.075 | 0.075 | 0.06 |
| Yeast extract | g $L^{-1}$ | 0.4 | - | - |

| | | | | |
|---|---|---|---|---|
| 4 mM Iron(III) citrate | mL $L^{-1}$ | 5 | 5 | 4 |
| Trace elements [b] | mL $L^{-1}$ | 1 | 1 | 0.8 |
| Vitamins [c] | mL $L^{-1}$ | 1 | 1 | 0.8 |

[a] pH adjusted to target value dosing a NaOH 6N solution

[b] Composition (g $L^{-1}$): $H_3BO_3$ (0.30), $MnCL_2 \cdot 4H_2O$ (0.03), $ZnSO_4 \cdot 7H_2O$ (0.10), $Na_2MoO_4 \cdot 2H_2O$ (0.30), $CuCL_2 \cdot 2H_2O$ (0.01), $NiCL_2 \cdot 6H_2O$ (0.02), $CoCL_2 \cdot 6H_2O$ (0.2)

[c] Composition (g $L^{-1}$): biotin (0.10), niacinamide (0.35), thiamin dichloride (0.30), p-aminobenzoic acid (0.20), pyridoxine hydrochloride (0.10), Ca-pantothenate (0.10), cobalamin (0.05)

Reactor Configuration and Experimental setup

The PF test was run in 250 mL serum bottles, with 200 mL of working volume. Each PPB strain was tested on RPP medium and on FB medium, in duplicate, as reported in Table 19.

*Table 19, Experimental setup of the PF phase conducted in Test 5*

| Test | PPB strain | Medium |
|---|---|---|
| ctrl-p | *Rps. palustris* | RPP |
| FB-p | *Rps. palustris* | FB |
| ctrl-r | *Rsp. rubrum* | RPP |
| FB-r | *Rsp. rubrum* | FB |

Each bottle started with a biomass concentration of 0.020 ± 0.003 $g_{(PPB)}$ $L^{-1}$. The inoculation protocol involved sampling an aliquot of volume from the acclimated PPB cultures, calculated accordingly to its concentration to achieve the target biomass concentration at the end of the preparation. The sampled volume underwent centrifugation at 9,000 rpm for 10 min to separate the biomass from the spent medium. The resulting biomass pellet was resuspended in sterile tap water and centrifugated again, to ensure the complete removal of the previous

medium components, that could otherwise inhibit the process. Finally, the biomass pellet was resuspended in the appropriate medium for each test condition. The bottles were sealed with butyl rubber stoppers and sealed with aluminum crimp caps, then flushed with argon to remove oxygen and nitrogen from the headspace. The PPB bottles were then incubated at 30 °C under continuous illumination (3,000 lux, incandescent lamps). The test lasted 25 d. Figure 17 shows the experimental setup at the beginning and at the end of the test.

*Figure 17, Test bottles at the beginning and at the end of the growth period in Test 5*

Every two days, samples of the culture solutions were collected for OD determination. Sampling was performed by withdrawing 1 mL of culture collecting through the butyl rubber stopper using a sterile syringe and needle, ensuring the maintenance of axenic condition within the test bottles. Before sampling, gas production was assessed by connecting each bottle gas-tight to a water displacement cylinder, interposing a 0.2 µm sterile cellulose acetate membrane in between to prevent contaminations.

Analytical methods

The biomass concentration of the PPB cultures at the end of the acclimatation phase was determined by dry weight measurement (section 3.5). To minimize sample volume withdrawal

during the test, biomass concentration was monitored by optical density (OD) at 660 nm. Absorbance measurements were performed on diluted culture samples by a UV-VIS spectrophotometer (Spectrosmart Basic, Zetalab, Italy) with 1 cm path-length optical glass cuvettes. To avoid interference caused by difference in medium turbidity, the dilution was performed using for each sample the appropriate test medium. Calibration curves ranging from 3 to 200 $mg_{PPB}$ $L^{-1}$ were used to convert OD values to biomass concentrations. The calibration curves were prepared for *Rps. palustris* and for *Rsp. rubrum*, both on RPP and on FB medium, preparing solution of known biomass concentration following the same inoculation protocol previously described. Light intensity was measured by lux meter (LX1330B, Dr. Meter, USA).

### 3.3.2. Test 6: Biological Hydrogen Production from Organic Wastes Fermentation Effluent: Testing Mutant Strains of *Rhodopseudomonas palustris*

Test 6 examined the potentiality of mutant PPB strains application in DF-PF systems. Genetically engineered PPB have gathered the attention of several authors as a promising approach for boosting biological hydrogen production. Deepening the knowledge on their efficiency in valorising a DFE-based medium could offer valuable insights for process integration. In this test, batch-scale operations have been conducted to investigate the role of different mutations in promoting microbial metabolic efficiency, with the main goal of maximizing hydrogen production from DFE. The experiments were conducted at the Dipartimento di Scienze e Tecnologie Agrarie, Alimentari, Ambientali e Forestali (DAGRI) of Università degli Studi di Firenze under the supervision of Professor Alessandra Adessi, to whom I express my sincere gratitude for the support and hospitality.

Inoculum and substrates

In Test 6, four strains of *Rhodospeudomonas plaustris* were tested. A wild-type *Rps. palustris* CGA009 from the collection of the Department of Microbiology, University of Washington, Seattle (WA, USA), compared with three mutated strains belonging to the Department of Biology, University of Indiana, Bloomington (IN, USA) collection: *Rps. palustris* CGA4001 (*Δhup*S), a wild-type CGA009 with the structural gene of the uptake hydrogenase deleted; *Rps. palustris* CGA4003 (*Δhup*S, NifA*), a CGA4001 with the *nif*A gene carrying a deletion that makes NifA*, the transcriptional activator of *nif* genes, constitutively active; *Rps. palustris* CGA4017 (*Δhup*S, NifA*, Δ*cbb*M, Δ*cbb*LS, Δ*cbb*P::*kmR*), a CGA4003 lacking enzymes of the Calvin cycle: RuBisCO and phosphoribulokinase. The strains were maintained axenically in RPN culture medium, prepared as described in Bianchi et al. (2010). Figure 18 shows the strains grown on RPN medium.


*Figure 18, Rps. palustris strains growing on RPN medium a) immediately after inoculation and b) before transferring the strains onto RPP. In each picture, from left to right: Rps. palustris 42OL, not used in this experiment; Rps. palustris CGA009; Rps. palustris CGA4001; Rps. palustris CGA4013; and Rps. palustris CGA4017.*

All strains were acclimated to the test condition growing for 17 days on RPP medium and then for 18 days on Fermentative Broth (FB) medium, under a continuous illumination (150 µmol $m^{-2}$ $s^{-1}$, 3000 K white LEDs, 38 W). The RPP medium (Bianchi et al., 2010) was prepared using 3.84 $g_{COD}$ $L^{-1}$ of acetic acid as carbon source. The FB medium was prepared

using the DFE from Test 1. The DFE was adjusted at 6.8 pH with NaOH 6 N, centrifuged at 9,000 rpm for 10 min, diluted (1:6 for acclimatation and 1:4 for the tests), and autoclaved. During the preparation, FB medium concentration was supplemented with (g $L^{-1}$): $K_2HPO_4$ (0.5), $KH_2PO_4$ (0.5), $MgSO_4 \cdot 7H_2O$ (0.4), and Fe(III) citrate (0.005). The chemical composition of the different media used is reported in Table 20.

*Table 20, Chemical composition of the culture media RPN, $RPP_{(acetic)}$, $FB_{(acclimatation)}$, and $FB_{(test)}$*

| | | RPN | $RPP_{(acetic)}$ | $FB_{(acclimatation)}$ | $FB_{(test)}$ |
|---|---|---|---|---|---|
| pH | | 6.8 [a] | 6.8 [a] | 6.8 [a] | 6.8 [a] |
| DL-malic acid | $g_{COD}$ $L^{-1}$ | 1.43 | - | - | - |
| acetic acid | $g_{COD}$ $L^{-1}$ | - | 3.84 | 0.77 ± 0.03 | 1.16 ± 0.05 |
| propionic acid | $g_{COD}$ $L^{-1}$ | - | - | 0.05 ± 0.01 | 0.08 ± 0.01 |
| butyric acid | $g_{COD}$ $L^{-1}$ | - | - | 0.35 ± 0.02 | 0.52 ± 0.03 |
| valeric acid | $g_{COD}$ $L^{-1}$ | - | - | 0.30 ± 0.03 | 0.45 ± 0.05 |
| caproic acid | $g_{COD}$ $L^{-1}$ | - | - | 1.9 ± 0.1 | 2.9 ± 0.1 |
| heptanoic acid | $g_{COD}$ $L^{-1}$ | - | - | 0.4 ± 0.1 | 0.6 ± 0.2 |
| total carbon source | $g_{COD}$ $L^{-1}$ | 1.43 | 3.84 | 3.8 ± 0.3 | 5.7 ± 0.4 |
| $NH_4^+$ | $mg_{NH4+}$ $L^{-1}$ | - | - | 49 ± 1 | 74 ± 1 |
| $NH_4Cl$ | $mg_{NH4+}$ $L^{-1}$ | 168.4 | - | - | - |
| Na-glutamate | g $L^{-1}$ | - | 0.4 | - | - |
| $K_2HPO_4$ | g $L^{-1}$ | 0.5 | 0.5 | 0.5 | 0.5 |
| $KH_2PO_4$ | g $L^{-1}$ | 0.3 | 0.3 | 0.5 | 0.5 |
| $MgSO_4 \cdot 7H_2O$ | g $L^{-1}$ | 0.4 | 0.4 | 0.4 | 0.4 |
| NaCl | g $L^{-1}$ | 0.4 | 0.4 | - | - |
| $CaCl_2 \cdot 2H_2O$ | g $L^{-1}$ | 0.075 | 0.075 | - | - |

| | | | | | |
|---|---|---|---|---|---|
| Yeast extract | g $L^{-1}$ | 0.4 | - | - | - |
| Iron(III) citrate 4 mM | mL $L^{-1}$ | 5 | 5 | 5 | 5 |
| Trace elements [b] | mL $L^{-1}$ | 1 | 1 | - | - |
| Vitamins [c] | mL $L^{-1}$ | 1 | 1 | - | - |

[a] pH adjusted to target value dosing a NaOH 6N solution

[b] Composition (g $L^{-1}$): $H_3BO_3$ (0.30), $MnCL_2 \cdot 4H_2O$ (0.03), $ZnSO_4 \cdot 7H_2O$ (0.10), $Na_2MoO_4 \cdot 2H_2O$ (0.30), $CuCL_2 \cdot 2H_2O$ (0.01), $NiCL_2 \cdot 6H_2O$ (0.02), $CoCL_2 \cdot 6H_2O$ (0.2)

[c] Composition (g $L^{-1}$): biotin (0.10), niacinamide (0.35), thiamin dichloride (0.30), p-aminobenzoic acid (0.20), pyridoxolium hydrochloride (0.10), Ca-pantothenate (0.10), cobalamin (0.05)

Reactor Configuration and Experimental setup

The test was carried out in glass bottles with a working volume of 280 mL to limit the headspace volume as much as possible, minimizing nitrogen inhibition and facilitating gas collection. Each bottle was provided with a silicon septum on the cap for culture sampling and a gas-tight fitting (1 mL syringe barrel filled with absorbent cotton, as seen in Figure 19a) connected to a gas-trap for hydrogen measurement.


*Figure 19, a) detail of the cap to allow culture sampling and gas outflow; b) gas-trap for volumetric hydrogen quantification, with detail of the one-way valve installed in between the bottles and the gas-trap during phase 2*

The gas-trap consists of a glass cylinder (300 mm in length and 40 mm internal diameter, Figure 19b), open at the bottom and closed at the top, with the top part equipped with a pierceable septum. To set up the gas-trap, the cylinder was completely filled with a slightly basic solution and then placed upside down into a beaker filled with the same solution. The test bottle was then connected to the trap with a Tygon tube, as showed in Figure 20. The solution of the gas-trap was adjusted to basic pH with a few drops of NaOH 6N to dissolve the $CO_2$ produced during the process, ensuring that only hydrogen could be accumulated in the trap's headspace for measurement. Before inoculation, the entire system was checked for gas leaks. Once ensured that, all components (bottle, cap, septum, and fitting) were individually autoclaved for 15 minutes at 121 °C for sterilization.

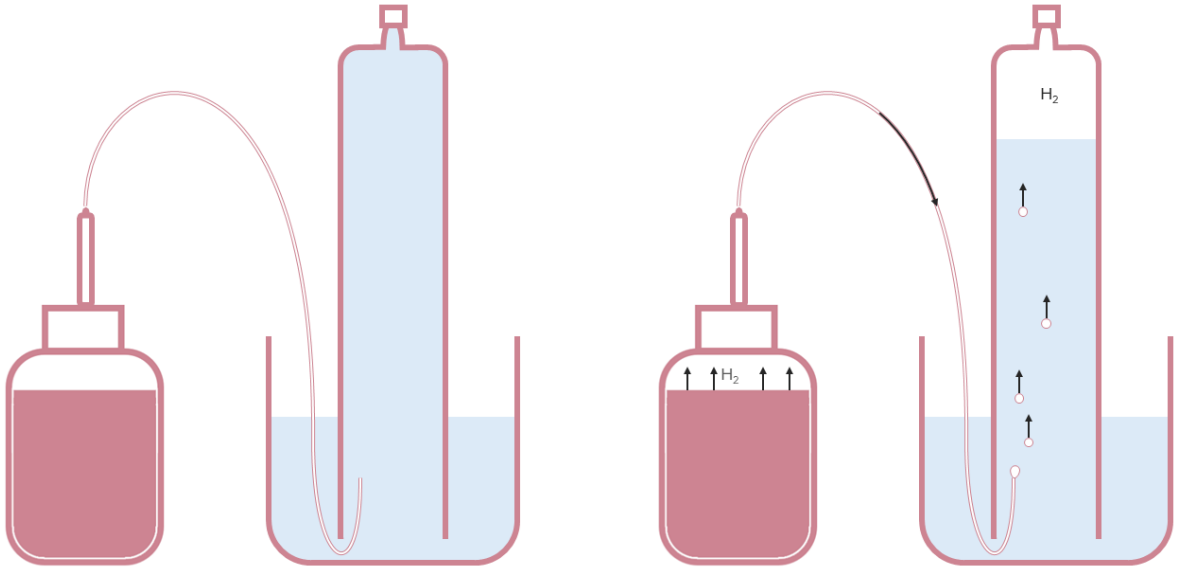


*Figure 20, Schematic representation of the volumetric hydrogen measurement using gas-traps*

The test was divided into three main phases, as summarized in Table 21.

*Table 21, Growth medium and duration of the different phases conducted in Test 6*

| | Medium | Duration [days] |
|---|---|---|
| *phase 1* | $RPP_{(acetic)}$ | 17 |
| *phase 2* | $FB_{(acclimatation)}$ | 18 |
| *phase 3* | $FB_{(test)}$ | 52 |

During *phase 1*, the four bacterial strains were cultivated in an $RPP_{(acetic)}$ medium to qualitatively evaluate their ability to hydrogen production potential under synthetic conditions. Each strain was tested with a single replicate, and gas-traps were not connected to the bottles. The inoculation process was conducted adding 10 mL of strain culture to 270 mL of synthetic medium, followed by incubation at room temperature (26 °C) under continuous illumination (150 µmol $m^{-2}$ $s^{-1}$, 3000 K white LEDs, 38 W), for 17 days. In this first phase, neither biomass

growth nor hydrogen production were quantitatively monitored. The monitoring process involved solely the observation of the bacterial culture for visible hydrogen formation (Figure 21), and the determination of the DW at the end of the growth phase.

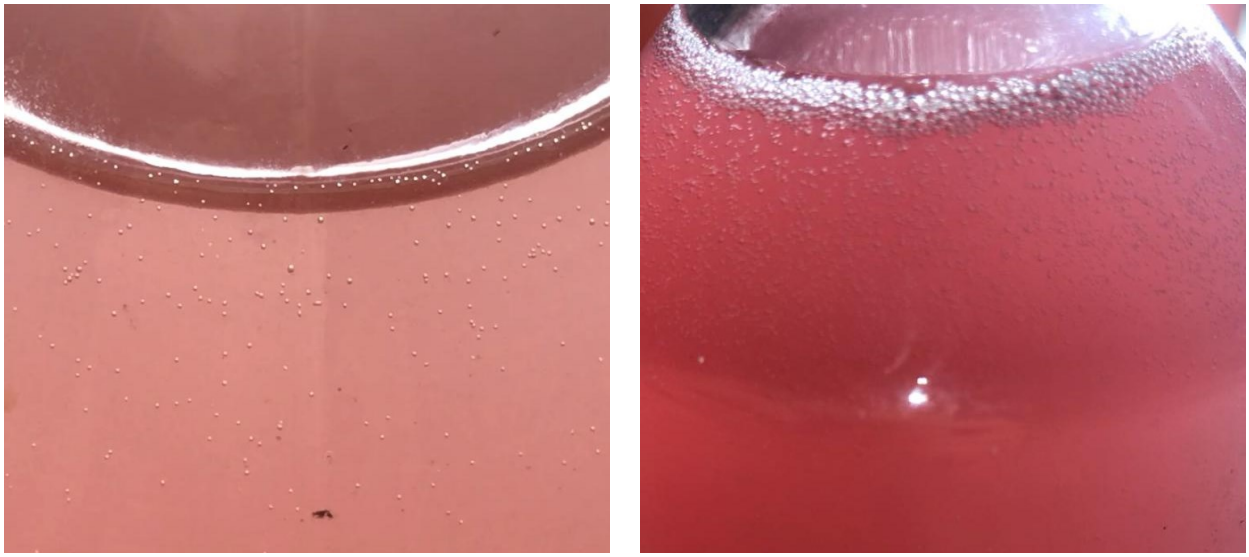

*Figure 21, Detail of hydrogen bubbles formation in the test bottles during phase 1*

*Phase 2* aimed to acclimate the PPB strains to the heterogeneous carbon source presents in the DFE. Each strain was inoculated in triplicate.

The inoculation process started with the centrifugation (4500 rpm for 15 min) of an aliquot of PPB culture from *phase 1*, to remove the spent growth medium. The retrieved PPB biomass pellet was then washed with sterilized water and centrifugated again, finally resuspending it in 25 mL of $FB_{(acclimatation)}$ medium, obtaining a highly-concentrated inoculum solution. The concentration of this solution was calculated according to Eq. 30

$$C_{HCI} = C_{phase1} \times \frac{V_C}{V_R} \quad \text{Eq. 30}$$

where $C_{HCl}$ is the concentration the highly-concentrated inoculum, $V_R$ the resuspension volume, $C_{phase1}$ the concentrations reached at the end of *phase 1*, and $V_C$ the centrifugated volume during the inoculation process.

A defined volume of the highly-concentrated inoculum solution was then added to each of the test replicates, ensuring an initial PPB concentration of 100 ± 20 $mg_{PPB}\ L^{-1}$ when filling the bottles to a total volume of 280 mL. The bottles were incubated following the same operative parameters used in *phase 1* (26 °C, 24 h illumination, 150 µmol $m^{-2}\ s^{-1}$, 3000 K white LEDs, 38 W) In this phase, each bottle was individually connected to a gas-trap for hydrogen measurement. To prevent the backflow of liquid from the trap into the culture bottles, one-way valves were placed in between the bottles and the gas-traps (Figure 19b). The acclimatation phase lasted 18 days. On day 8$^{th}$ and at the end of the experiment, 3 mL samples were withdrawn from each bottle to determine OD, BChl *a* content, and $NH_4^+$ concentration. DW analysis was performed only at the end of the test to minimize sample volume withdrawal, while for the intermediate time point, DW was estimated according to the OD calibration curve. Sampling and monitoring of the cultures were minimized during the test to prevent depressurization of the headspace and avoid disturbances in the gas collection system. Figure 22 shows the experimental setup and bottle configuration at the beginning and end of *phase 2*.

*Figure 22, Bottle configuration at the beginning (left) and end (right) of phase 2*

*Phase 3* was run using the $FB_{(test)}$ medium and following the same protocol employed in the previous phase. The inoculation process involved the use of the acclimated PPB biomass obtained at the end of *phase 2*. Due to concerns about potential leaks observed in *phase 2*, the one-way valves were omitted. The experiment lasted 52 days, maintaining the same operative parameters used in the previous phases (26 °C, 24 h illumination, 150 µmol $m^{-2}$ $s^{-1}$, 3000 K white LEDs, 38 W). The monitoring of OD, BChl *a* content, and $NH_4^+$ concentration was performed at day $8^{th}$, $17^{th}$, $31^{st}$, and at the end of the test. DW was measured only at the end of the test and estimated using the OD calibration curve for intermediate time-points, following the same approach and reasons explained in phase 2.

Analytical methods

The biomass concentration of the PPB cultures was determined either by DW measurement (section 3.5) when sufficient sample volume was available for a disruptive analysis or, when

this was not a viable option, estimated from OD values using a calibration curve. The OD analysis was performed at 660 nm on diluted culture samples. To avoid interference caused by difference in medium turbidity, the dilution was performed using the same medium tested in each phase. Calibration curves ranging from 3 to 200 $mg_{PPB}$ $L^{-1}$ were used to convert OD values to biomass concentrations. The calibration curves were prepared for each tested strain, with $FB_{(acclimatation)}$ and $FB_{(test)}$ media, preparing solution of known biomass concentration following the same inoculation protocol previously described. BChl *a* concentration was determined by extracting the pigments with a cold acetone:methanol (7:2, v/v) solution and reading the absorbance at 775 nm (section 3.5). OD and BChl *a* determination was performed by a UV-VIS spectrophotometer (UV-3100PC UV-Vis, Varian, Australia) using 1 cm path-length optical glass cuvettes. $NH_4^+$ concentration was determined by the Nessler method using high scale ammonia reagents kits (HI93733-01, Hanna Instruments, Italy) and a photometer (HI97733, Hanna Instruments, Italy). The photosynthetic photon flux density at the culture surface was determined with a quantum/radiometer/photometer (DO9721, Delta Ohm, Italy) equipped with a quantum sensor (LP9021, Delta Ohm, Italy). Hydrogen production was measured by the water displacement method, using an alkaline solution to ensure $CO_2$ solubilization.

## 3.4. Bio-Methanation

### 3.4.1. Test 7: Evaluation of Hydrogenotrophic Bio-Methanation on suspended biomass and granular sludge

In Test 7, a laboratory scale experiment was conducted in batch mode to assess the feasibility of biological conversion of hydrogen and carbon dioxide into methane. The process aimed at exploring sustainable alternative routes for biological hydrogen utilization, while enabling the conversion of carbon dioxide back to an energy-rich compound as a tool to extend the temporal gap between carbon production and actual emission. Testing the methanogenic activity of two morphologically distinct inocula, specifically suspended biomass and granular sludge,

provided insights into the identification of the optimal reactor configuration for process optimization.

Inoculum and substrates

In Test 7, the hydrogenotrophic methanogenic activity of suspended biomass and granular sludge were compared. The digestate used as inoculum of suspended biomass was sourced from the full-scale anaerobic digester of a municipal Wastewater Treatment Plant (WWTP, VERITAS spa, Fusina, Italy) treating civil wastewaters. The digestate was sieved through a 2 mm mesh to remove residual solid organic compounds and inert materials. It was then kept at mesophilic temperature at 39 °C for one week to allow the complete degradation of residual organic compounds. Granular sludge was provided by GreenPropulsion Laboratory (GPLab, Fusina, Italy) and sourced from a full-scale UASB reactor treating industrial wastewater at high COD concentration at a partner paper production company. To remove the storage liquid in which the granules were kept, the granular sludge was sieved through a 0.75 mm mesh and gently dabbed three times with absorbent paper towels from the bottom of the mesh to remove any residual liquid adhering to the granules. The granules were then placed in BA medium and kept at 39 °C for one week to ensure the complete degradation of residual organic compounds. The TS and TVS of both the inocula are reported in Table 22.

*Table 22, Total Solids and Total Volatile Solids content of the anaerobic inocula used in Test 7*

| | TS [$g_{TS}$ $kg^{-1}$] | TVS [$g_{TVS}$ $kg^{-1}$] | TVS ratio [% TVS/TS] |
|---|---|---|---|
| Digestate | 34.9 ± 0.2 | 19.2 ± 0.1 | 54.8 ± 0.3 |
| Granular sludge | 87.2 ± 0.2 | 73.9 ± 0.5 | 84.7 ± 0.1 |

Granular sludge was maintained in BA medium, prepared according to Angelidaki & Sanders (2004) as described in Table 23. To avoid methane production from different carbon

sources and restrict it to the sole conversion of the carbon dioxide and hydrogen supplied to the system, the test medium was modified (labeled BA-C, Table 23) by removing carbonates and, consequently, adjusting phosphate concentration to ensure adequate buffer capacity.

*Table 23, Chemical composition of the maintaining medium BA and the test medium BA-C*

| | | BA | BA-C |
|---|---|---|---|
| $NH_4Cl$ | g $L^{-1}$ | 1 | 1 |
| NaCl | g $L^{-1}$ | 0.1 | 0.1 |
| $MgSO_4 \cdot 7H_2O$ | mg $L^{-1}$ | 121.2 | 121.2 |
| $CaCl_2 \cdot 2H_2O$ | mg $L^{-1}$ | 50 | 50 |
| $K_2HPO_4 \cdot 3H_2O$ | g $L^{-1}$ | 0.4 | 2 |
| $NaHCO_3$ | g $L^{-1}$ | 2.6 | - |
| Resazurin | mg $L^{-1}$ | 0.5 | 0.5 |
| Trace elements [a] | mL $L^{-1}$ | 1 | 1 |
| Vitamins [b] | mL $L^{-1}$ | 0.25 | 0.25 |

[a] Composition (mg $L^{-1}$): $FeCl_2 \cdot 4H_2O$ (2363.2), $H_3BO_3$ (50), $MnCL_2 \cdot 4H_2O$ (50), $ZnSO_4 \cdot 7H_2O$ (59.2), $(NH_4)_6Mo_7O_{24} \cdot 4H_2O$ (50), $CuCL_2 \cdot 2H_2O$ (38), $NiCL_2 \cdot 6H_2O$ (92), $CoCL_2 \cdot 6H_2O$ (50), EDTA (500), HCl 36% (1 mL $L^{-1}$)

[b] Composition (mg $L^{-1}$): biotin (4), folic acid (4), pyridoxine hydrochloride (20), riboflavin (10), thiamin dichloride (10), cyanocobalamin (0.2), nicotinic acid (5), p-aminobenzoic acid (10), lipoic acid (10)

The $CO_2$ used as substrate was obteined from a carbon dioxide 4.5 cylinder, while $H_2$ was produced with over 99.99999 % purity from a hydrogen generator (AD-180, Cinel Gas Generators s.r.l., Padova, Italy).

Reactor Configuration and Experimental setup

During this test, a total of six batch trials were conducted, three for suspended biomass and three for granular sludge. Figure 23 shows the 1 L glass bottles provided with an additional opening on the neck-side that were used throughout the experiment. On the top opening each bottle was provided with an automatic system for pressure measurements (BOD RESPIROMETRIC Sensor, VELP Scientifica srl, Italy). The additional opening was closed with a silicon septum and used for headspace flushing and for substrate feeding.

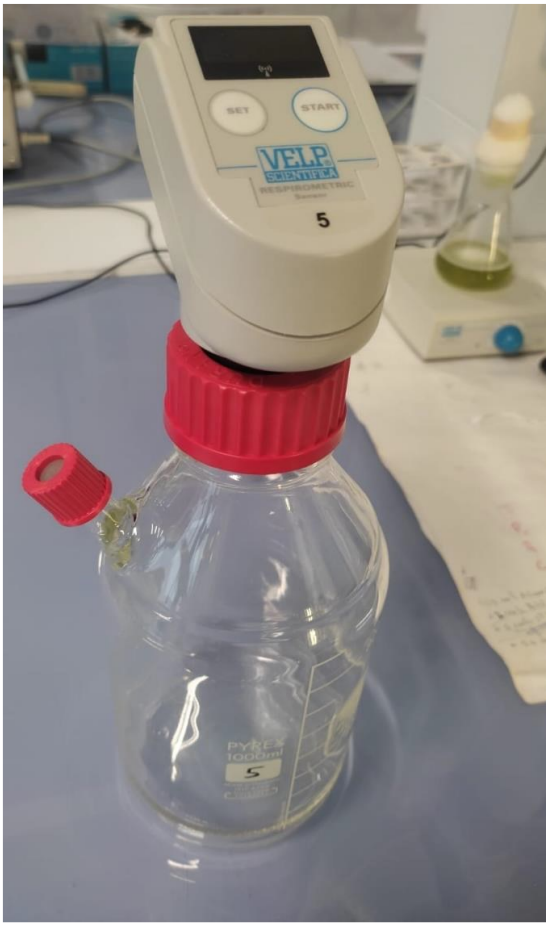


*Figure 23, Test bottles and pressure sensor employed in Test 7*

Each experimental trial consisted in dosing a predetermined quantity of inoculum into the test bottle, flushing the system with nitrogen to ensure anaerobic conditions, and pressurizing it by feeding a precise volume of hydrogen and carbon dioxide. In the tests with suspended biomass

(trials S1, S2a, and S2b), the bottles were inoculated with 400 mL of digestate. For the granular sludge tests (trials G1, G2a, and G2b), the bottles were inoculated with 100 g of granules, followed by dilution to a final volume of 400 mL using BA-C medium. This ensured consistency between headspace volumes throughout the experiment and provided an adequate liquid phase for gases dissolution. Nitrogen flushing of the headspace was performed at the beginning of the first trial for each inoculum type. For the subsequent ones, test bottles were pressurized with fresh substrate in a fed-batch mode, without opening them, thereby maintaining anaerobic conditions. Each test was conducted in triplicate, alongside duplicate blank controls without substrate introduction. Hydrogen and carbon dioxide were supplied to the system to reach a 4:1 molar ratio at the beginning of each trial, according to the stochiometric proportion of bio-methanation (Eq. 14).

$$CO_2 + 4H_2 \rightarrow CH_4 + 2H_2O \qquad \text{Eq. 14}$$

In the absence of a standard gas mixture containing both components, hydrogen and carbon dioxide were introduced separately into the test bottles. The volume of gas added into the system was calculated based on: i) the predefined 4:1 molar ratio between $H_2$ and $CO_2$; ii) the residual concentration of carbon dioxide in the headspace; iii) the absolute pressure limit of 2,000 mbar imposed by the pressure sensors employed in the experiments. The gas feeding procedure involved connecting a three-way valve to the test bottle's headspace by piercing the silicon septum with a needle. One outlet of the valve was then connected to a gas-bag containing the desired gas to add, while the other to a 100 mL gas-tight syringe. A schematic representation of the gas feeding procedure is provided in Figure 24.

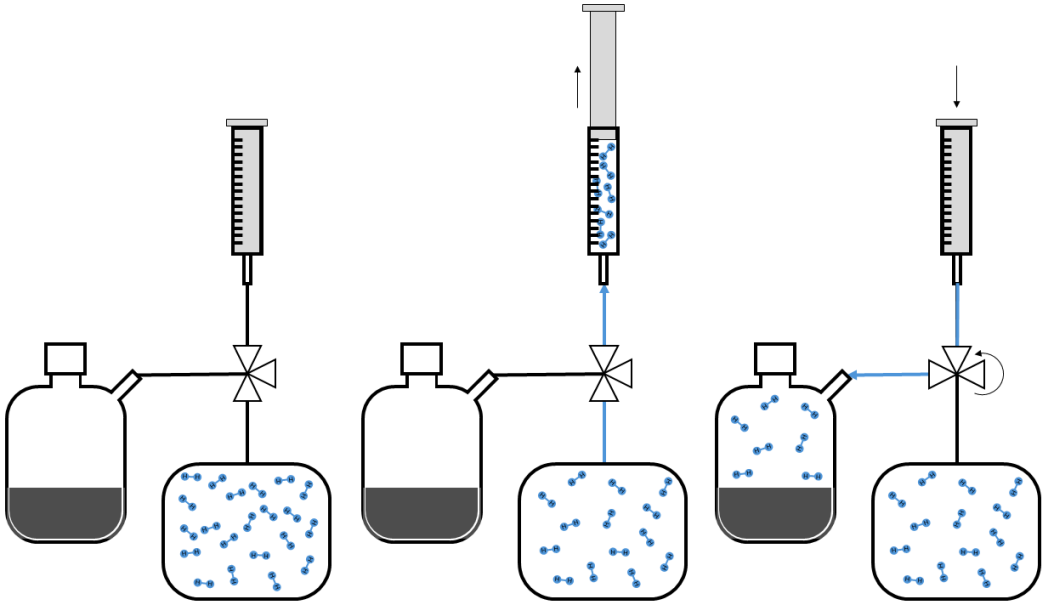

*Figure 24, Schematic representation of the gas feeding procedure. From left to right, the sequence includes a) connecting the three-way valve to the test bottle; b) withdrawing a known volume of gas from the gas-bag using a gas-tight syringe; c) injecting the gas into the test bottle. This process was repeated several times when the introduction of larger volumes of gas was needed*

Following the gas feeding procedure, the test bottles were incubated at mesophilic temperature at 39 °C with continuous mixing at 180 rpm, by a magnetic and an orbital mixer for suspended biomass and granular sludge, respectively. Table 24 summarizes the operative conditions of each trial.

*Table 24, Operative conditions and amount of substrate fed to each trial*

| Trial | Inoculum | T (°C) | $N_2$ flushing | $H_2$ (mmol) | $CO_2$ [a] (mmol) | $CO_2$ [b] (mmol) |
|---|---|---|---|---|---|---|
| S1 | Suspended biomass | 39 | + | 16.5 | 0.00 | 4.1 |
| S2a | Suspended biomass | 39 | - | 24.8 | 1.0 | 5.2 |
| S2b | Suspended biomass | 39 | - | 24.8 | 1.4 | 4.8 |
| G1 | Granular sludge | 39 | + | 16.5 | 0.00 | 4.1 |
| G2a | Granular sludge | 39 | - | 24.8 | 0.8 | 5.4 |
| G2b | Granular sludge | 39 | - | 24.8 | 0.3 | 5.9 |

[a] unconsumed carbon dioxide present in the test bottle's headspace from the previous trial

[b] carbon dioxide injected into the test bottles, calculated to obtain a 4:1 $H_2$:$CO_2$ molar ratio taking into account the residual concentration of $CO_2$ present in the headspace

Methane production was monitored following the manometric method, adapted from Coates et al. (1996) and Ripoll et al. (2020) (section 2.6.1). During hydrogenotrophic bio-methanation, 5 moles of dissolved gaseous reagents are consumed for every 1 mole of methane produced (Eq. 14, section 3.4.1); thus, causing a decrease in the headspace pressure when the reaction takes place in a confined system under controlled temperature. As described by Ripoll et al. (2020), considering the stoichiometric reaction ratio, the ideal gas law can be used to calculate the number of moles of produced methane between two time-points ($\Delta n_{CH4}$) as detailed in Eq. 31

$$\Delta n_{CH4} = -\frac{\Delta n_{HS}}{4} = \frac{\Delta P V_{HS}}{4RT} \qquad \text{Eq. 31}$$

where $\Delta n_{HS}$ is the difference in number of moles in the headspace between two time-points, $\Delta P$ is the consequent difference in pressure, $V_{HS}$ is the headspace volume, R is the molar gas constant, and T the test temperature in Kelvin.

The pressure sensors were connected to a wireless data logger (Wireless DataBox, VELP Scientifica srl, Italy) for automatically record pressure values every 2 h. Each trial lasted until no significant change in pressure was detected, typically taking between 3 to 4 days.

Analytical methods

The total solids (TS) and total volatile solids (TVS) content of the substrates was determined using a gravimetric method according to the APHA Standard Methods for the Examination of Water and Wastewater (Baird et al., 2017). The composition of the biogas produced in the DF phase was analyzed with a biogas analyzer (ETG, MCA 100 Syn Biogas Multigas Analyzer)

equipped with a thermal conductivity detector (TCD) for the hydrogen measurement, a non-dispersive infrared (NDIR) sensor for the methane and carbon dioxide measurement, and an electrochemical cell for oxygen quantification.

## 3.5. Physio-chemical analyses

This section presents all internal analytical methods used that differ from standard application methods.

### Volatile Fatty Acids (VFA) quantification

VFAs were determined by High Performance Liquid Chromatography (HPLC) using a chromatographer (1100 series, Agilent Technologies, USA) equipped with a 0.5 µm x 4.0 mm x 150 mm (Acclaim™ Organic Acid column, Thermo Scientific, USA) and a diode array detector (DAD). A 2.5 mM methansulfonic acid (Sigma-Aldrich, ≥ 99.0 % purity) aqueous solution and acetonitrile (Sigma-Aldrich, gradient grade, ≥ 99.9 % purity) were used as mobile phases A and B, respectively, in a ratio 45/55 (A/B). The column was maintained at 30 °C and the detection wavelength was set at 210 nm. VFAs concentration was calculated using a calibration curve ranging from 1 to 10 mM obtained by diluting a Volatile Free Acid Mix (Sigma Aldrich, certified reference material). All VFAs concentrations were presented as COD based on their complete stoichiometric conversion.

### Biomass concentration: Dry Weight (DW) and Optical Density)

The Dry Weight (DW) of the PPB samples was measured gravimetrically by filtering a known volume of PPB culture (ranging between 3 to 5 mL, based on the cell density and the available amount of sample) through a cellulose acetate filter with mesh porosity of 0.22 µm. Filters were previously dried at 105 °C for at least 4 hours and weighted. After filtering, the biomass was rinsed with distilled water to eliminate residual medium, then the filters were dried at

105 °C for at least 4 hours and weighted. Weighting was performed on a high-resolution analytical balance (0.1 mg readability, AB204-S, Mettler Toledo, Italy).

Optical density (OD) was used as a not-disruptive method for the determination of biomass concentration when only limited sample volume was available for monitoring. OD was measured at 660 nm by a UV-VIS spectrophotometer (Spectrosmart Basic, Zetalab, Italy; UV-3100PC UV-Vis, Varian, Australia) with 1 cm path-length optical glass cuvettes. Readings were performed on 3 mL of properly diluted samples. To minimize discrepancies caused by medium turbidity, particularly pronounced in FB medium, dilutions were performed using the same culture medium. Additionally, the absorbance of a blank containing only the same culture medium was subtracted from each reading. Known concentrations (ranging from 3 to 200 $mg_{PPB}$ $L^{-1}$, determined by DW measurement) of each PPB strain were used to construct a calibration curve for estimating DW values from OD readings, according to Eq. 32. The calibration curves were constructed using five points and were forced to pass through zero.

$$DW\ [g_{PPB}\ L^{-1}] = OD \times c \qquad \text{Eq. 32}$$

The calibration coefficient *c* of each PPB strain is reported in Table 25.

*Table 25, Calibration coefficient determined for estimating DW values from OD readings. $R^2 > 0.998$*

| | (Test 5, Section 3.3.1) | | (Test 6, Section 3.3.2) | |
|---|---|---|---|---|
| | RPP | FB | $FB_{(acclimatation)}$ | $FB_{(test)}$ |
| *Rps. palustris* | 0.3659 | 0.3927 | - | - |
| *Rsp. rubrum* | 0.4780 | 0.4567 | - | - |
| *Rps. palustris* CGA009 | - | - | 0.3886 | 0.5064 |
| *Rps. palustris* CGA4001 | - | - | 0.4028 | 0.6359 |
| *Rps. palustris* CGA4003 | - | - | 0.3744 | 0.6119 |
| *Rps. palustris* CGA4017 | - | - | 0.4884 | 0.5743 |

Bacteriochlorophyll *a* (BChl *a*) content

The Bacteriochlorophyll *a* (BChl *a*) content was estimated spectrophotometrically after pigment extraction. A known volume of PPB culture (2 mL) was centrifuged at 12,000 rpm for 5 minutes, the supernatant was discarded, and the biomass pellet resuspended in 2 mL of acetone:methanol (7:2, v/v) solution. The sample vials were then stored at 4 °C and protected from light to prevent pigment denaturation. After 30 min, the vials were centrifuged again at 12,000 rpm for 5 minutes, following the reading of the supernatant absorbance at 775 nm by a UV-VIS spectrophotometer (UV-3100PC UV-Vis, Varian, Australia) with 1 cm path-length optical glass cuvettes. The absorbance of a blank containing only the extracting solution was subtracted from each reading. The BChl *a* content was determined as in Eq. 33

$$BChl\ a\ [\mu g_{BChl\ a}\ mL^{-1}] = \frac{A - A_b}{e \times l} \times MW_{BChl\ a} \times D \times \frac{V_s}{V_e} \qquad \text{Eq. 33}$$

where $A$ and $A_b$ are the absorbance of the sample and the blank, respectively, $e$ is the extinction coefficient of BChl *a* in acetone:methanol (7:2, v/v) (75 $mM^{-1}$, Clayton, 1963), $l$ is the path-length of the optical glass cuvettes (1 cm), $MW_{BChl\ a}$ is the molecular weight of bacteriochlorophyll *a* (911.49 g $mol^{-1}$), $D$ is the applied dilution factor, $V_s$ and $V_e$ are the volumes of microbial culture sampled and extraction solution, respectively.

## 3.6. Data analysis

### 3.6.1. Dark Fermentation Tests

The conversion efficiency of organic compounds through DF process was assessed by the calculation of various yield parameters, including Specific Gas Production (SGP), Specific Hydrogen Production (SHP), Specific Methane Production (SMP), Gas Production Rate (GPR), Hydrogen Production Rate (HPR), and Acidification Yield (AY).

The Specific Gas Production (SGP, Eq. 34) was calculated as the amount of overall gas produced per unit of substrate supplied to the system, expressed as TVS. The Specific

Hydrogen Production (SHP, Eq. 35) and Specific Methane Production (SMP, Eq. 36) were determined with a similar approach, based on the total hydrogen and methane produced, respectively.

$$SGP\ [NL\ kg_{TVS}{}^{-1}] = \frac{V_{tot}\ [NL]}{S\ [kg_{TVS}]} \quad \text{Eq. 34}$$

$$SHP\ [NL_{H2}\ kg_{TVS}{}^{-1}] = \frac{V_{H2}\ [NL_{H2}]}{S\ [kg_{TVS}]} \quad \text{Eq. 35}$$

$$SGP\ [NL_{CH4}\ kg_{TVS}{}^{-1}] = \frac{V_{CH4}\ [NL_{CH4}]}{S\ [kg_{TVS}]} \quad \text{Eq. 36}$$

where $V_{tot}$ is the total volume of gas produced by the system during the experimental period, $V_{H2}$ and $V_{CH4}$ represent the total volumes of hydrogen and methane produced, respectively, and $S$ is the amount of substrate supplied to the system.

The Hydrogen Production Rate (HPR, Eq. 37) was calculated as the amount of hydrogen produced per unit time and per unit reactor volume. The Gas Production Rate (GPR, Eq. 38) was determined solely for the AD process coupled with DF system, based on the overall biogas production.

$$HPR\ [NmL_{H2}\ L_{reactor}{}^{-1}\ h^{-1}] = \frac{V_{H2}\ [NmL_{H2}]}{V_{reactor}\ [L] \times \Delta t} \quad \text{Eq. 37}$$

$$GPR\ [NL_{biogas}\ m^{-3}\ d^{-1}] = \frac{V_{biogas}\ [NL_{biogas}]}{V_{reactor}\ [m^{-3}] \times \Delta t} \quad \text{Eq. 38}$$

where $V_{reactor}$ is the operative volume of the tested system, $V_{H2}$ and $V_{biogas}$ represent the total volumes of hydrogen and biogas produced, respectively, and $\Delta t$ is the interval between two time-points. Depending on the period of time period considered, the rates may be expressed as $NmL_{H2}\ L_{reactor}{}^{-1}\ h^{-1}$, typically for laboratory-scale setups and short durations, as $NL_{H2}\ L_{reactor}{}^{-1}\ d^{-1}$, or $NL_{biogas}\ m^{-3}{}_{reactor}\ d^{-1}$, generally for pilot-scale setups or longer timeframes.

The Acidification Yield (AY, Eq. 39) was calculated to assess the system efficiency in converting the supplied substrate into VFAs.

$$AY\ [g_{VFA(COD)}\ g_{TVS}{}^{-1}] = \frac{C_{VFA}[g_{VFA(COD)}\ L^{-1}]}{OL\ [kg_{TVS}\ m^{-3}]} \quad \text{Eq. 39}$$

where $C_{VFA}$ is the concentration of VFAs obtained at the end of the experiment, expressed as COD based on the complete stoichiometric conversion, and *OL* is the Organic Loading tested.

### 3.6.2. Photo Fermentation Tests

The efficiency of the PF processes was determined by calculating biomass productivity ($P_{max}$), growth coefficient ($\mu_{max}$), and Hydrogen Yield (HY).

The biomass productivity ($P_{max}$, Eq. 40) and growth coefficient ($\mu_{max}$, Eq. 41) were determined during the exponential growth phase of the microbial cultures. $P_{max}$ was calculated as the difference in biomass concentrations between two subsequent time points, while $\mu_{max}$ was derived from the difference in the natural logarithm of the biomass concentration.

$$P_{max}[mg_{PPB}\ L^{-1}\ d^{-1}] = \frac{\Delta X_{PPB}\ [mg_{PPB}\ L^{-1}]}{\Delta t} \quad \text{Eq. 40}$$

$$\mu_{max}[\ d^{-1}] = \frac{\ln(X_i) - \ln(X_{i-1})}{\Delta t} \quad \text{Eq. 41}$$

where $\Delta X$ is the difference in biomass concentration $X_i$ and $X_{i-1}$, and $\Delta t$ is the interval between the two time-points $t_i$ and $t_{i-1}$.

The hydrogen production yield (HY, Eq. 42) was calculated as the amount of hydrogen produced per unit of VFA supplied to the system.

$$HY\ [NmL_{H2}\ g_{VFA(COD)}{}^{-1}] = \frac{V_{H2}\ [NL_{H2}]}{VFA\ [g_{VFA(COD)}]} \quad \text{Eq. 42}$$

where $V_{H2}$ is the total volume of hydrogen produced by the system during the experimental period, and *VFA* is the amount of VFAs supplied to the system, expressed as COD based on their complete stoichiometric conversion.

### 3.6.3. Biological Methanation Tests

The biomass efficiency in converting hydrogen into methane during the BM tests was defined by calculating the total volume of methane produced, the bio-methanation yield both as moles of methane produced per moles of hydrogen supplied to the system ($\gamma_{BM}$), and as percentage based on the maximum theoretic conversion ($\gamma_{BM\%}$), and the Specific Hydrogenotrophic Methanogenic Activity (SHMA).

Once determined the number of moles of methane produced, according to Eq. 31 (section 3.4.1), the volume of methane produced was determined based on the ideal gas law (Eq. 43) and standardized at normal pressure (1 bar) and temperature (0 °C).

$$\Delta V_{CH4}\ [NmL_{CH4}] = \Delta n_{CH4} \times \frac{R \times T^N}{P^N} \quad \text{Eq. 43}$$

where $\Delta n_{CH4}$ is the difference in moles of methane produced between two time-points, *R* is the ideal gas constant, and $T^N$ and $P^N$ the temperature (273.15 K) and pressure (1 bar) at normal condition, respectively.

The conversion efficiency $\gamma_{BM}$ (Eq. 44) was calculated as the moles of methane produced per unit of moles of hydrogen supplied, while $\gamma_{BM\%}$ (Eq. 45) based on the maximum theoretical amount of methane that could be produced from the supplied hydrogen.

$$\gamma_{BM}[mol_{CH4}\, mol_{H2}{}^{-1}] = \frac{n_{CH4}}{n_{H2}} \quad \text{Eq. 44}$$

$$\gamma_{BM\%}[\%] = \frac{n_{CH4}}{n_{CH4-max}} \quad \text{Eq. 45}$$

where $n_{CH4}$ is the overall cumulative number of moles of methane produced, $n_{H2}$ the number of moles of hydrogen supplied, and $n_{CH4\text{-}max}$ the maximum theoretical number of moles of methane that could be produced from the supplied hydrogen based on the complete stoichiometric conversion of the bio-methanation reaction (1 mole of methane for each mole of hydrogen, Eq. 14, section 3.4.1).

The Specific Hydrogenotrophic Methanogenic Activity (SHMA, Eq. 29) was determined as the amount of methane produced by the system per unit of time per volatile suspended solids present in the anaerobic biomass, as a rough estimation of the microbial concentration (Ripoll et al., 2020).

$$SHMA\ [mg_{CH4(COD)} g_{VSS}{}^{-1} h^{-1}] = \frac{\Delta n_{CH4}}{\Delta t} \times C \times \frac{1}{g_{VSS}} \quad \text{Eq. 29}$$

where $\Delta n_{CH4}$ is the number of moles of methane produced, $C$ is the methane conversion factor from moles to COD (64 $mg_{COD}$ $mmol_{CH4}{}^{-1}$), $g_{VSS}$ is the amount of volatile suspended solids present in the tested biomass, and $\Delta t$ is the interval between two time-points.

## 3.7. References

Angelidaki, I., & Sanders, W. (2004). Assessment of the anaerobic biodegradability of macropollutants. *Rev Environ Sci Biotechnol*, *3*, 117–129. https://doi.org/https://doi.org/10.1007/s11157-004-2502-3

Baird, R., Bridgewater, L., American Public Health Association, American Water Works Association, & Water Environmental Federation. (2017). *Standard methods for the examination of water and wastewater* (23rd ed., Vol. 1). American Public Health Association.

Bianchi, L., Mannelli, F., Viti, C., Adessi, A., & De Philippis, R. (2010). Hydrogen-producing purple non-sulfur bacteria isolated from the trophic lake Averno (Naples, Italy). *International Journal of Hydrogen Energy*, *35*(22), 12216–12223. https://doi.org/10.1016/j.ijhydene.2010.08.038

Clayton, R. K. (1963). Toward the isolation of a photochemical reaction center in Rhodopseudomonas palustris. *Biochimica et Biophysica Acta, 75, 312*–323. https://doi.org/10.1016/0006-3002(63)90618-8

Coates, J. D., Coughlanb, M. F., & Colleranb, E. (1996). Methods Simple method for the measurement of the hydrogenotrophic methanogenic activity of anaerobic sludges. In *Journal of Microbiological Journal of Microbiological Methods* (Vol. 26).

Moretto, G., Russo, I., Bolzonella, D., Pavan, P., Majone, M., & Valentino, F. (2020). An urban biorefinery for food waste and biological sludge conversion into polyhydroxyalkanoates and biogas. *Water Research*, *170*. https://doi.org/10.1016/j.watres.2019.115371

Ripoll, E., López, I., & Borzacconi, L. (2020). Hydrogenotrophic activity: A tool to evaluate the kinetics of methanogens. *Journal of Environmental Management*, *270*. https://doi.org/10.1016/j.jenvman.2020.110937

Valentino, F., Moretto, G., Gottardo, M., Pavan, P., Bolzonella, D., & Majone, M. (2019). Novel routes for urban bio-waste management: A combined acidic fermentation and anaerobic digestion process for platform chemicals and biogas production. *Journal of Cleaner Production*, *220*, 368–375. https://doi.org/10.1016/j.jclepro.2019.02.102

# 4. Results: Dark Fermentation Tests

## 4.1. Test 1: Lab-scale Dark Fermentation of Food Waste and WAS mixture, in Batch Condition

In Test 1, a small-scale batch DF system was tested with the goal of, firstly, ensuring $H_2$ production in the first days of fermentation and, secondly, optimizing VFA production and the acidification yields of the treated substrates. Working under batch conditions in this first test allowed an initial evaluation of the process performances, providing insights into substrate degradation efficiency and the potential operative parameters influencing hydrogen yields. For details on the methodological approach and experimental setup of the test, refer to section 3.2.1.

Figure 25 shows the Specific Gas Production observed during Test 1. The control condition (*ctrl*), where only WAS with no OW addition was fermented, resulted in the lowest SGP, with a final value of 48 ± 2 NL $kg_{TVS}^{-1}$. The *OL 5* condition did not result in any detectable biogas production over the 10 experimental days and is therefore not included in Figure 25. Given the biological process involved, this outcome is unexpected, as the combination of supplied organic substrate, inoculum, and other operative conditions such as pH and temperature should have supported hydrogen or carbon dioxide production, with potential methane generation in the later stages of the test, as observed in all other conditions. This suggests a possible failure in the gas measurement or storage system during this test, that did not ensure the monitoring of gas production under this specific condition.

Among other tested conditions, the highest SGP was observed at the end of the test at *OL 20*, with 119 ± 8 NL $kg_{TVS}^{-1}$. Increasing the organic loading to 25 $kg_{TVS}$ $m^{-3}$ caused a severe decline in the SGP, dropping to 82 ± 4 NL $kg_{TVS}^{-1}$. The difference in SGP between *OL 20* and *OL 25* was particularly pronounced during the first 5 – 6 days of the experiment, as noticeable from Figure 25. At *OL 25*, in fact, the high substrate loading likely caused excessive acidification of the

fermentative broth, possibly due to the accumulation of acetate, butyrate, and lactate, which are the primary metabolites generated during FW anaerobic fermentation (Gu et al., 2018; Jariyaboon et al., 2023). This resulted in a pH drop to values as low as 3.76 (Figure 28), leading to an initial inhibition of the microbial consortium and an overall decrease in gas production yields.

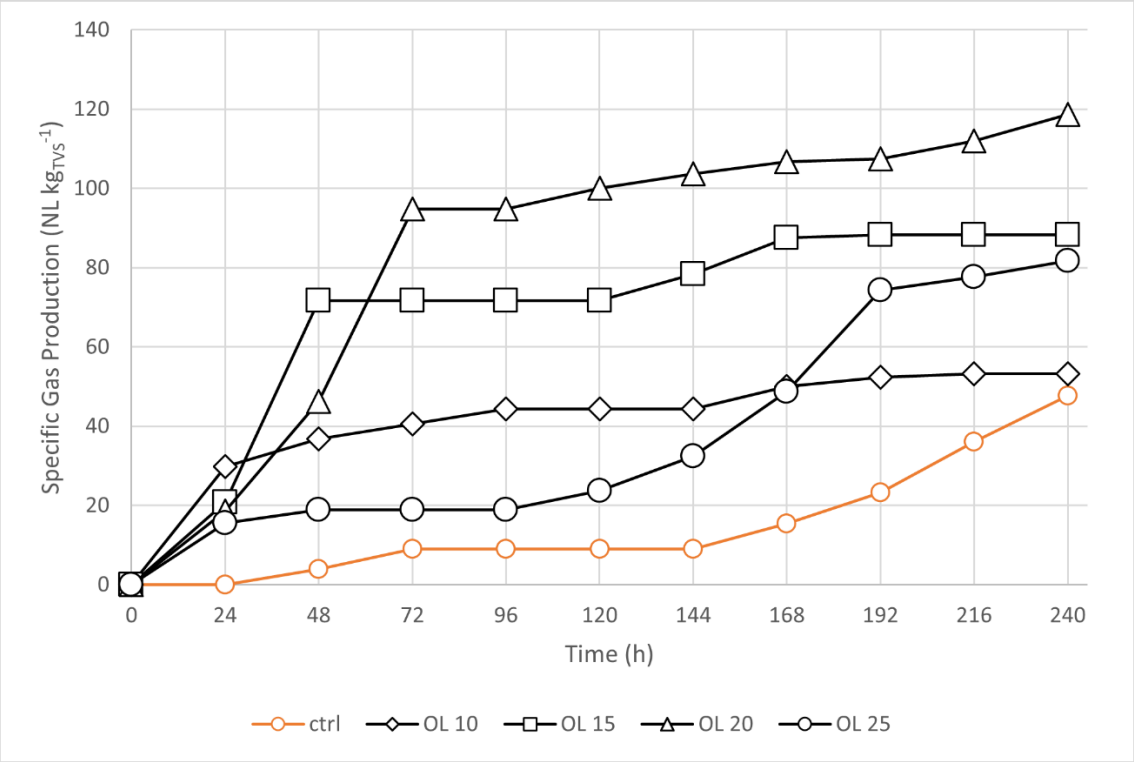


*Figure 25, Specific Gas Production of the conditions tested during Test 1*

Figure 26 shows the Specific Hydrogen Production observed under the different experimental conditions. *OL 5* and *ctrl* are not included in the figure, as no hydrogen production was detected in these conditions. The highest value of Specific Hydrogen Production was observed at *OL 20*, with 16 ± 1 $NL_{H2}\ kg_{TVS}^{-1}$, followed by *OL 15* and *OL 10*, with 15 ± 1 and 13 ± 1 $NL_{H2}\ kg_{TVS}^{-1}$, respectively. *OL 25* resulted in the lowest SHP (10 ± 1 $NL_{H2}\ kg_{TVS}^{-1}$), due to the excessive acidification of the fermentative broth that occurred in the first days of fermentation, as stated above. The decrease in the SHP at increasing OL values aligns with findings from

other authors. Higher OLs are often associated with a more severe VFA accumulation, which may result in a decrease in pH values and consequent inhibition of HPB (Jariyaboon et al., 2023; Rangel et al., 2020), as observed in this test. However, the obtained SHP values were lower compared to those obtained by other authors for the treatment of these substrates, ranging generally between 60 and 190 $L_{H2}$ $kg_{VS}^{-1}$ (Kim et al., 2011; Li et al., 2018; Yang et al., 2025). A key difference between these studies and the conducted Test 1 is that in those experiments the substrates were pretreated to enhance the bioavailability of the organic compounds. Such pretreatments are, most likely, one of the reasons for the lower yield obtained. Moreno-Andrade et al. (2023) tested the co-fermentation of not-pretreated FW and WAS, working at 10 $kg_{TVS}$ $m^{-3}$ and obtaining a maximum hydrogen yield of 65 $L_{H2}$ $kg_{VS}^{-1}$, four times higher than the yield resulting from this test. This result was obtained by mixing FW and WAS with a co-substrate ratio of 90:10 based on VS. When decreasing the co-substrate ratio in favor of WAS, until up to 30:70, they observed a severe decrease in the process yield. Comparable findings were obtained in similar studies by other authors (Kim et al., 2011; Li et al., 2018; X. Liu et al., 2013). This suggests that, in addition to other parameters, the tested co-substrate ratios (ranging between 20:80 and 70:30 based on VS) may not have been optimal for maximizing process efficiency, as higher yields were generally associated with higher FW:WAS ratios (Table 3, section 2.4.343).

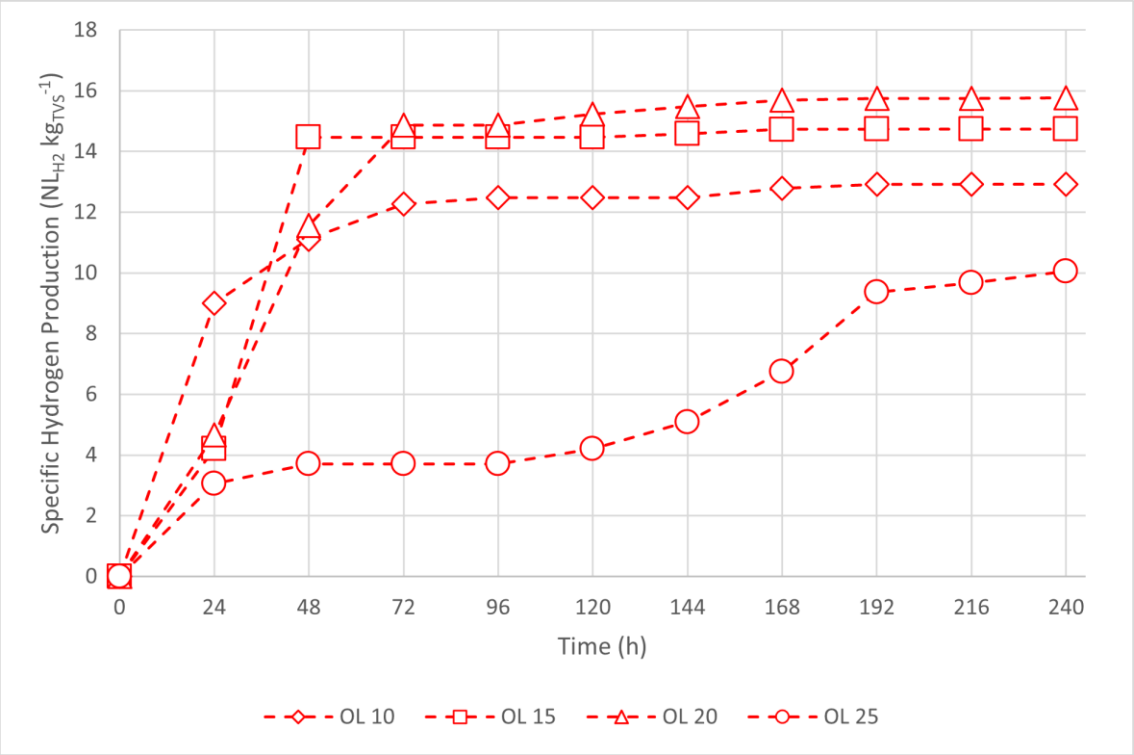


*Figure 26, Specific Hydrogen Production of the conditions tested during Test 1*

Figure 27 shows the composition of the produced gas during the test and reveals how the majority of hydrogen was produced during the early days of fermentation. This observation is consistent with the metabolic activity of the fermentative microorganisms, which typically shows peak activity of hydrogenase enzyme and higher substrate conversion efficiency during the early phases of fermentation (Ghimire, 2015; Gopalakrishnan et al., 2019).

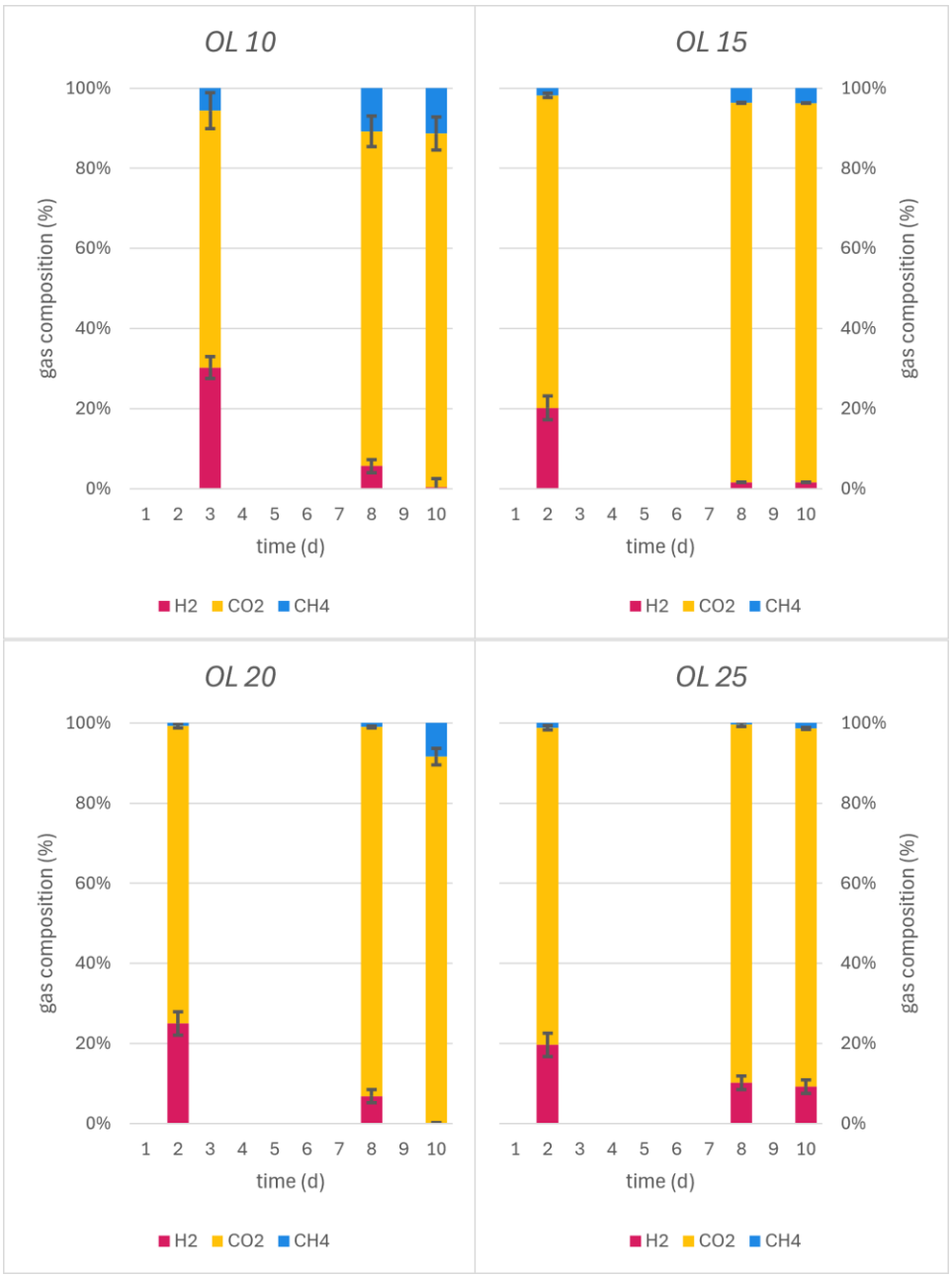


*Figure 27, Composition of the produced biogas during Test 1*

In all conditions, the maximum concentration of hydrogen was recorded between days 2 and 3, with the highest values observed at *OL 10* (30 ± 3 $\%_{H2}$) and *OL 20* (25 ± 3 $\%_{H2}$). These values are in line with the percentage of hydrogen found by many other authors treating these substrates (Baldi et al., 2019; Gottardo et al., 2023; Zahedi et al., 2016). As the test proceeded, hydrogen concentration decreased considerably in all conditions with OL values beneath

20 $kg_{TVS}$ $m^{-3}$, indicating a shift towards different metabolic pathways resulting in less hydrogen production, if not its consumption, carried by propionate-producers or hydrogenotrophic methanogens, as in Eq. 12 and Eq. 14 (Ghimire, 2015).

| | | |
|---|---|---|
| Propionic acid | $C_6H_{12}O_6 + 2H_2 \rightarrow 2CH_3CH_2COOH + 2H_2O$ | Eq. 12 |
| Hydrogenotrophic methanogens | $CO_2 + 4H_2 \rightarrow CH_4 + 2H_2O$ | Eq. 14 |

The activity of hydrogenotrophic methanogens was spotted by the presence of methane in the produced gas. In all conditions, methane was found in the gas produced at the end of the test, with the highest concentration at OL 10 (11 ± 4 %) and the lowest at OL 25 (1.3 ± 0.2 %). The occurrence of hydrogenotrophic methanogens in the reaction environment was unsurprising under the specific test conditions, as they were indigenous in the supplied unsterilized substrates, particularly the WAS, and no pretreatment for their inactivation was performed. However, their activity was mostly inhibited by the acidic pH reached in every condition, ranging between 4 and 5.5 (Figure 28). The maintenance of lower pH values during the fermentative phase at OL 25 is the most reasonable explanation for the lower concentration of methane obtained under this condition at the end of the test. Additionally, *OL 25* was the only condition that maintained a higher hydrogen concentration until the end of the test, with 9 ± 2 $\%_{H2}$, while all other conditions resulted in concentrations < 2 $\%_{H2}$ as the test ended. This is most likely associated with the low pH values during the initial days of fermentation at OL 25, which may have caused an inhibition of the system and a delay in HPB activity. Despite maintaining this relatively higher hydrogen concentration until the end of the test, this condition resulted in the overall lowest SHP (Figure 26).

Table 26 summarizes the main yield parameters discussed above.

*Table 26, Gas production yields obtained at the end of Test 1*

| | | *OL 10* | *OL 15* | *OL 20* | *OL 25* |
|---|---|---|---|---|---|
| Gas Production | NL | 5.6 ± 0.3 | 10.6 ± 0.6 | 16 ± 1 | 12.1 ± 0.6 |
| $H_2$ Production | $NL_{H2}$ | 1.2 ± 0.1 | 1.8 ± 0.1 | 2.1 ± 0.1 | 1.5 ± 0.1 |
| SGP | $NL_{biogas}\ kg_{TVS}^{-1}$ | 53 ± 3 | 88 ± 7 | 119 ± 8 | 82 ± 4 |
| SHP | $NL_{H2}\ kg_{TVS}^{-1}$ | 13 ± 1 | 15 ± 1 | 16 ± 1 | 10 ± 1 |
| maximum $H_2$ activity | $NL_{H2}\ kg_{TVS}^{-1}\ h^{-1}$ | 0.37 ± 0.03 | 0.43 ± 0.04 | 0.29 ± 0.05 | 0.13 ± 0.03 |
| maximum HPR | $NmL_{H2}\ L_{reactor}^{-1}\ h^{-1}$ | 10 ± 1 | 13 ± 1 | 10 ± 1 | 4 ± 1 |
| maximum $H_2$ content | % | 30 ± 3 | 20 ± 2 | 25 ± 2 | 20 ± 2 |

Figure 28 shows the pH trend of all conditions during the fermentation test. As mentioned, the pH was only monitored and not adjusted to target values; thus, leading to significant fluctuation of this value, especially at high organic loadings. The higher the organic loading, the more significant the initial drop in pH, with values as low as 3.95 and 3.76 for *OL 20* and *OL 25*, respectively. Moreover, despite all conditions finally stabilized at pH values in the range 4.9–5.5, higher organic loadings required longer times for pH to become stable: *OL 5*, *OL 10*, and *OL 15* showed a stable pH value after just 2–3 days, while *OL 20* and *OL 25* required 6 and 8 days, respectively. The pH drop observed in *OL 20* and *OL 25* can have a direct effect in inhibiting microorganisms' growth. VFAs, in fact, are weak acids with a pKa of 4.8 – 4.9 (C2 – C7) (Elbeshbishy et al., 2017). At pH below 4, VFAs remain in their undissociated form. Being more fat-soluble, they can diffuse through the plasma membrane, dissociate in the cytosol, and lower its pH, thereby inhibiting microbial growth and activity (Lund et al., 2020). When there was no addition of OW (in the *ctrl* condition), pH did not change notably, as there was no availability of easily fermentable organic compounds, no significant production of VFA, and no change in pH.

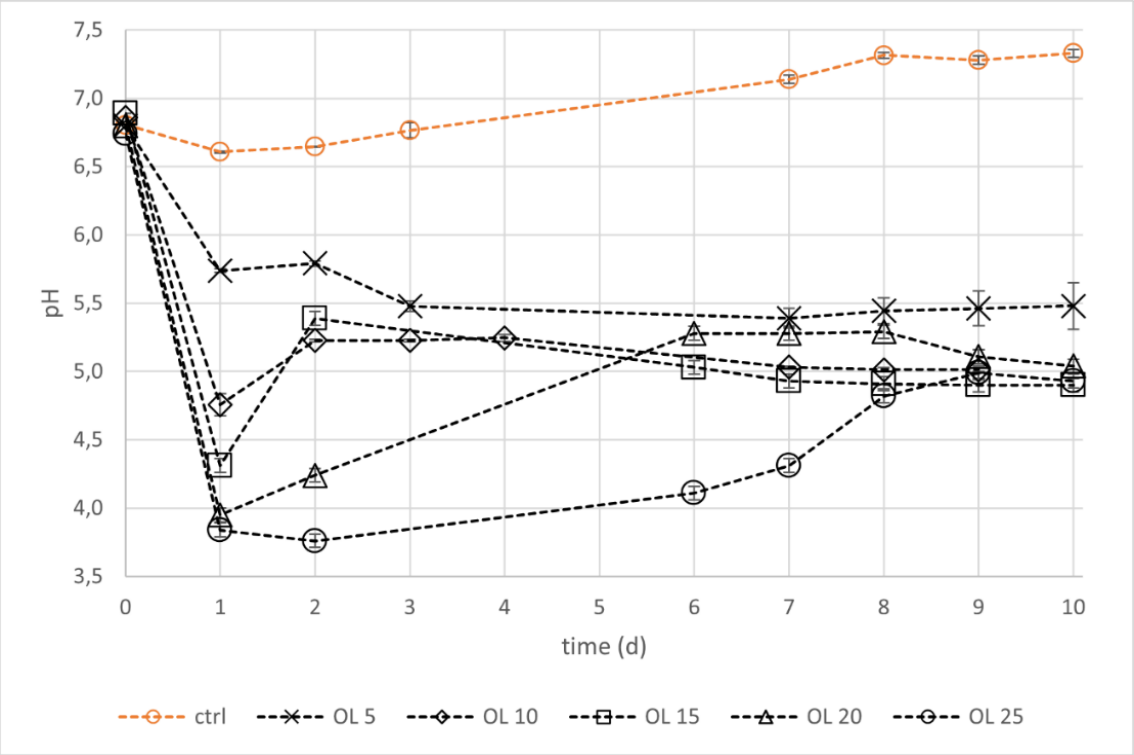


*Figure 28, pH fluctuations during Test 1*

The production of VFA and their profile (C1 – C7) in all the tested conditions is reported in Figure 29. At the end of the 10 days of fermentation, the majority of the conditions stabilized at a concentration of $11.4 \pm 0.3\ g_{COD(VFA)}\ L^{-1}$, except for *OL 5* ($7.7 \pm 0.4\ g_{COD(VFA)}\ L^{-1}$) and *ctrl* ($3.7 \pm 0.3\ g_{COD(VFA)}\ L^{-1}$), which exhibited lower values. Conditions with an organic loading higher than $10\ kg_{TVS}\ m^{-3}$ showed a similar VFA profile at the end of the test, with a fermentative broth predominantly composed of acetic acid (C2, 30–40 %), propionic acid (C3, 20–30 %), butyric acid (C4, ~10 %), and valeric acid (C5, 20–30 %). The presence of acetic acid and butyric acid can be a good indicator of the process's correct progression, as they may result from acetic and butyric fermentation, both metabolic reactions that led to a net hydrogen production (4 and $2\ mol_{H2}\ mol_{hexose}^{-1}$, respectively) (Ghimire, 2015). The presence and accumulation of propionic and valeric acid in all the tested conditions, instead, can be a sign of an unbalanced, or at least not yet fully optimized, process. Propionic fermentation, in fact, has a negative effect

on DF, as the reaction causes the consumption of one mole of hydrogen for each mole of propionate produced (Eq. 12, Section 2.4.1), and should then be avoided to optimize the process yield. The high levels of propionic acid may justify the occurrence of valeric acid in the fermentate, potentially resulting from chain elongation processes in which propionate is elongated to odd-carbon acids (Wu et al., 2019).

*OL 25* was characterized by the overall highest concentrations, reached at day 2 with a peak concentration of 18.1 ± 0.9 $g_{COD(VFA)}$ $L^{-1}$, mainly composed of acetic acid (~95 %). It's worth mentioning that the analytical method employed (Section 3.5) is limited to the identification of VFA and does not allow the detection of lactic acid. Consequently, it cannot be excluded that some of the samples might contain lactic acid along with the identified VFA, especially in those samples with higher organic loading and pH values below 4.

In general, increasing the organic loading to values higher than 15 $kg_{TVS}$ $m^{-3}$ caused a pH drop to ≤ 4 after 24 hours (Figure 28), corresponding to high acid production primarily consisting of acetic acid (Figure 29) and possibly, lactic acid. This is likely due to an unbalanced ratio between the organic substrate and WAS content (less than 50% on a TVS basis, Table 10 Section 3.2.1) which is no longer able to provide sufficient alkalinity to buffer the pH of the system. Itoh et al., (2012) indicated that acidogenic fermentation without pH control results in a pH drop below 4 (down to 3.5) within 24 hours, with an accumulation of lactic acid. The authors found that LAB, which are tolerant to extremely low pH, became dominant in acidogenic fermentation, suggesting heterolactic fermentation as the main metabolic pathway, with the conversion of the supplied organic carbon source to lactic acid, ethanol or acetic acid, and carbon dioxide (Itoh et al., 2012). Thanks to their versatile metabolic processes and ability to survive in adverse conditions, LAB are ubiquitous in the environment (Villanueva-Galindo et al., 2023) and are reported to be a part of the native microbial community of FW (Villanueva-Galindo et al., 2023). Their presence in the mixed DF consortium can be a determinant factor affecting process yields and inhibiting $H_2$ production from FW (Canto-Robertos et al., 2023; Sikora et al., 2013).


*Figure 29, Profile of the VFA produced during Test 1*

These bacteria, in fact, can compete with HPB for substrate assimilation and, being characterized by higher growth rates (Rombouts et al., 2020), may cause a shift in the process balance, replacing $H_2$-fermentation with lactic acid fermentation, which causes lactic acid to

take over as the main product of the reaction, with a loss in hydrogen (Asunis et al., 2019; Jo et al., 2007). This is most likely what happened in the first days of *OL 25*, where hydrogen production was inhibited for the first 5 days of fermentation (Figure 26), in line with the period in which the pH was below 4 and the microbial metabolism was probably shifted towards lactic acid fermentation. Lactic acid presence may have also contributed to the synthesis of valeric acid, found in increasing concentrations across all conditions, as high initial concentration of lactate can lead to an increase of odd-carbon fatty acids such as propionate and valerate (Y. Liu et al., 2024; Wu et al., 2019).

However, there is no unanimity across the scientific community on the role of LAB in DF processes (Correa-Villa et al., 2024), as several authors found that the high acidification caused by LAB can result in higher hydrogen yields (García-Depraect et al., 2021; Xue et al., 2024), and that lactate can be used as a storage strategy for subsequent hydrogen production (Roslan et al., 2024).

All the above observations suggest that the process was not fully optimized for $H_2$ production, as fermentation to propionate and lactate produce no $H_2$, and neither does chain elongation to valerate. Nonetheless, the goal of Test 1 was not solely the production of hydrogen, but also the generation of a VFA-rich DFE to be directed to a PF process, making high acidification yield a positive outcome.

The best Acidification Yields (AY), reported in Table 27, were obtained at *OL 10* and *OL 15*, with 0.42 ± 0.04 and 0.39 ± 0.02 $g_{VFA(COD)}\ g_{TVS}^{-1}$, respectively. This value aligns with those reported by other authors for similar processes: 0.41 – 0.44 $g_{VFA(COD)}\ g_{TVS}^{-1}$ for the fermentation of OFMSW and WAS (Valentino et al., 2019), and 0.32 – 0.46 $g_{VFA(COD)}\ g_{TVS}^{-1}$ for the fermentation of FW and WAS (Vidal-Antich et al., 2021). The lowest AY (0.19 ± 0.02 $g_{VFA(COD)}\ g_{TVS}^{-1}$) was obtained in the control condition with the mono-fermentation of only WAS. Mono-fermentation of FW and WAS, in fact, is reported to have a lower fermentation yield compared to the co-fermentation of the two substrates (Vidal-Antich et al., 2021).

*Table 27, Acidification Yields (AY), VFA, and $NH_4^+$ concentration of the effluent at the end of Test 1*

| | OL[a] [$kg_{TVS(OW)}\ m^{-3}$] | OL[b] [$kg_{TVS}\ m^{-3}$] | Ammonium [$mg_{NH4+}\ L^{-1}$] | VFA [$g_{VFA(COD)}\ L^{-1}$] | AY [$g_{VFA(COD)}\ g_{TVS}^{-1}$] |
|---|---|---|---|---|---|
| *ctrl* | 0 | 19.4 | 284 ± 14 | 3.7 ± 0.3 | 0.19 ± 0.02 |
| *OL 5* | 5 | 22.7 | 701 ± 35 | 7.7 ± 0.4 | 0.34 ± 0.02 |
| *OL 10* | 10 | 26.3 | 253 ± 13 | 11 ± 1 | 0.42 ± 0.04 |
| *OL 15* | 15 | 30.0 | 107 ± 5 | 11.6 ± 0.6 | 0.39 ± 0.02 |
| *OL 20* | 20 | 33.5 | 136 ± 7 | 11.4 ± 0.6 | 0.34 ± 0.02 |
| *OL 25* | 25 | 37.0 | 260 ± 14 | 11.6 ± 0.6 | 0.31 ± 0.02 |

OL[a] – organic loading considering the WAS as inoculum

OL[b] – organic loading considering the WAS as a substrate

The ammonium concentration in the effluent, measured at the end of the test, is reported in Table 27. *OL 15* and *OL 20* were the conditions characterized by the lowest ammonium concentration, with 107 ± 5 and 137 ± 7 $mg_{NH4+}\ L^{-1}$, respectively. *OL 5* showed the overall highest concentration, with 701 ± 35 $mg_{NH4+}\ L^{-1}$, probably resulting from a more complete degradation of the fed substrates, leading to the release of the nitrogen bonded to the organic matter. Such high ammonium concentration can be a contributing factor in hindering hydrogen production at OL 5, as it is reported to negatively affect DF systems (Salerno et al., 2006), with an estimated threshold of 670 $mg_{NH4+}\ L^{-1}$ (Gottardo et al., 2013).

## 4.2. Test 2: Lab-scale Dark Fermentation of Hydrodynamic Cavitated Food Waste and WAS mixture, in Batch Condition

Test 2 evaluated the effect of a Hydrodynamic Cavitation pretreatment of the substrate in a batch-mode DF process, as detailed in Section 3.2.2. In Figure 30, the cumulative biogas and hydrogen production are reported. The gas production in the HC pretreated substrates, at the end of the test, resulted slightly higher compared to the one obtained for the *ctrl* test: 4.86 ± 0.04 NL compared to 4.24 ± 0.04 NL (14.6 % higher).

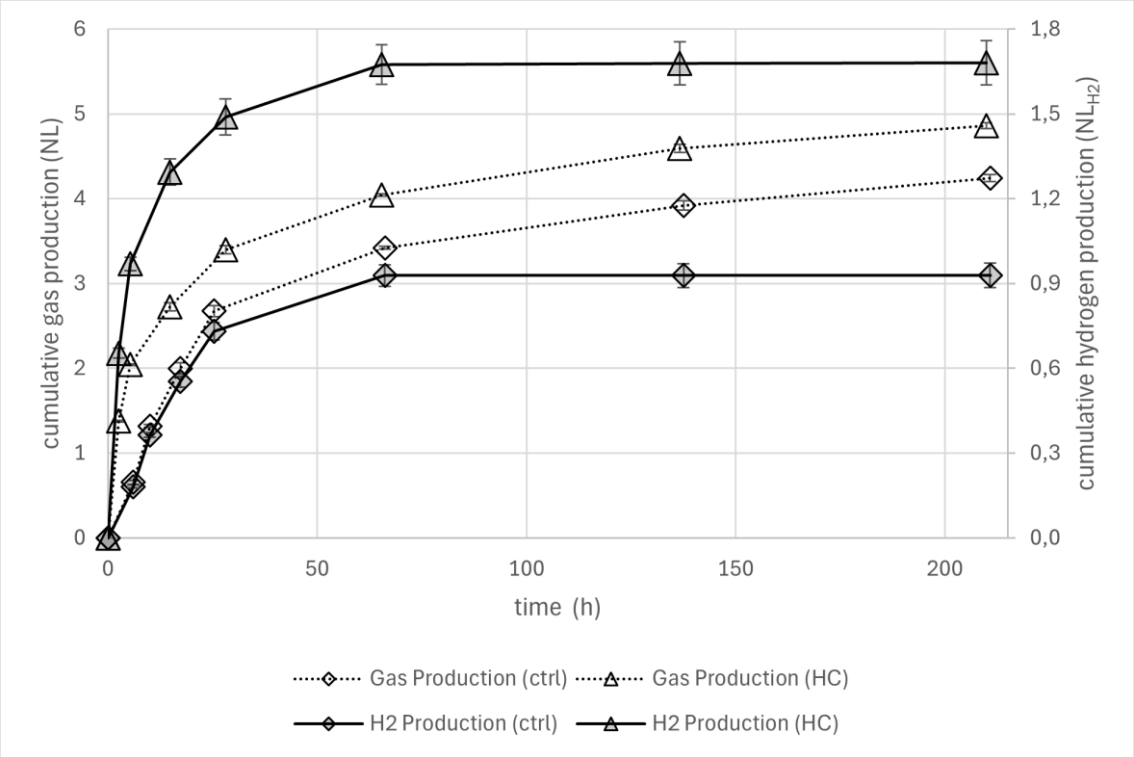


*Figure 30, Cumulative gas and hydrogen production during Test 2*

This improvement becomes more evident when only hydrogen production is considered, with a final cumulative hydrogen production of 1.68 ± 0.08 $NL_{H2}$ and 0.93 ± 0.04 $NL_{H2}$ (81 % higher) for *HC* and *ctrl* tests, respectively. The overall increase in gas production observed in the *HC*

tests (+ 0.6 ± 0.1 NL) is, then, mostly due to an increase in hydrogen production (+ 0.8 ± 0.1 NL) rather than other gases. This led to a notable increase in the SHP, as shown in Figure 31, that resulted in 29 ± 1 $NL_{H2}\,kg_{TVS}^{-1}$ and 16 ± 1 $NL_{H2}\,kg_{TVS}^{-1}$ (81 % higher) for *HC* and *ctrl* tests, respectively. The yield obtained under *ctrl* conditions, despite the differences in the FW composition, are in line with those obtained during Test 1 (15 ± 1 $NL_{H2}\,kg_{TVS}^{-1}$, at a similar co-substrate ratio). As discussed in the previous test, the obtained yields are inconsistent with those obtained by other authors under similar conditions, which typically range between 60 and 190 $NL_{H2}\,kg_{TVS}^{-1}$ (Kim et al., 2011; Li et al., 2018; X. Liu et al., 2013; Moreno-Andrade et al., 2023; Yang et al., 2025). This discrepancy can be attributed to the suboptimal co-substrate ratio and composition of the microbial community utilized in the test. The hydrogen production reached a plateau after around 66 h. After this point, a significant rise in methane production (dotted lines in Figure 31) was observed in both conditions, suggesting the end of the hydrogen production phase and the establishment of conditions favorable for hydrogenotrophic methanogens. Similarly to the previous test, the use of unsterilized substrates and a not-pretreated inoculum allowed for hydrogenotrophic methanogens proliferation in the reaction environment. In the *HC* test, however, methane production was limited during the first days of the experiment, and this is possibly associated with the HC pretreatment of the substrate, which could have partially inactivated the indigenous microbial community of FW and WAS (Blagojević et al., 2025).

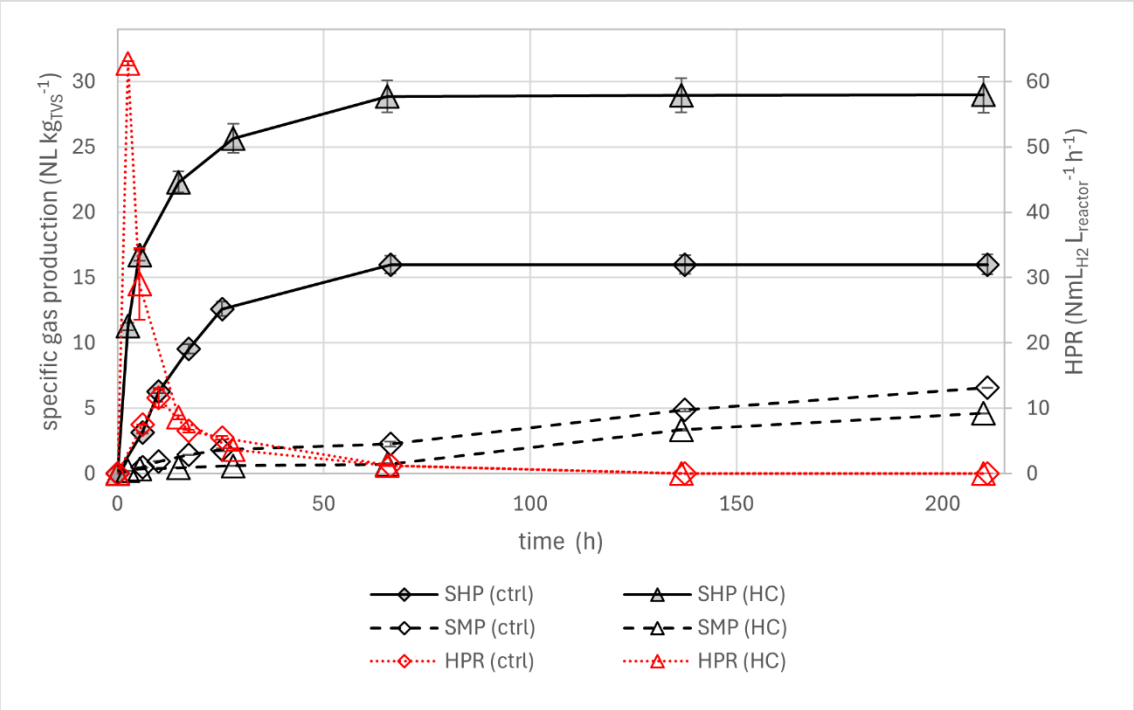


*Figure 31, Specific Hydrogen and Methane Production (SHP and SMP) and Hydrogen Production Rate (HPR) obtained during Test 2*

It's interesting to take into consideration HPR, shown as red dotted lines in Figure 31. The maximum HPR (62.8 ± 0.3 NmL $L_{reactor}^{-1}$ $h^{-1}$) was recorded under *HC* condition immediately after the beginning of the test, after 2.6 hours, while for the *ctrl* the maximum rate was considerably lower (7.5 ± 0.1 NmL $L_{reactor}^{-1}$ $h^{-1}$) and was reached later on during the test, after 10 hours. After around 24 hours, the HPR of the two conditions decreased steadily, settling at values close to zero, further evidence of the end of the hydrogen production phase. The peak HPR observed in the *HC* test was consistent with the values obtained by other authors in similar experiments, which typically report values ranging between 50 and 100 $mL_{H2}$ $L_{reactor}^{-1}$ $h^{-1}$ (X. Liu et al., 2013; Yang et al., 2025). The improvement compared to the *ctrl* condition can likely be attributed to the HC pretreatment of the substrate before DF, which may have enhanced substrate disintegration and solubilization, increasing its bioavailability and, thereby, accelerating its conversion to hydrogen.

Figure 32 shows the composition of the produced biogas over time. In both conditions, the highest hydrogen concentration was reached after the first day, 47 ± 1 $\%_{H2}$ and 28 ± 2 $\%_{H2}$ in *HC* and *ctrl* conditions, respectively. The percentage obtained under *ctrl* condition is in line with the values found by other authors in similar processes, typically ranging between 18 and 36 % (Baldi et al., 2019; Gottardo et al., 2023; Zahedi et al., 2016), while the one obtained under *HC* condition resulted slightly higher, further demonstrating the potential of the pretreatment in improving the process performances. However, percentages close to 60 % in hydrogen were reported by Li et al., (2018) in co-fermentation experiments with FW and WAS.

From the observation of both the SMP curves (dotted lines, Figure 31) and the methane concentration shown in Figure 32, HC pretreatment seems to have inhibited hydrogenotrophic methanogen activity, delaying methane evolution in the early days of the fermentation and allowing for the production of biogas richer in hydrogen and with minor traces of methane (< 1 $\%_{CH4}$ during the first 2 days of fermentation for the *HC* test, compared to 3–4 $\%_{CH4}$ for *ctrl* test), suggesting that the HC pretreatment enhanced the metabolic efficiency of the process. The high concentration of methane obtained at the end of the test (27 ± 1 % and 30 ± 1 %, for *HC* and *ctrl* conditions, respectively), and the near-zero amount of hydrogen detected in the produced gas, is further evidence of the end of hydrogen production and the shift toward a methanogenic phase.

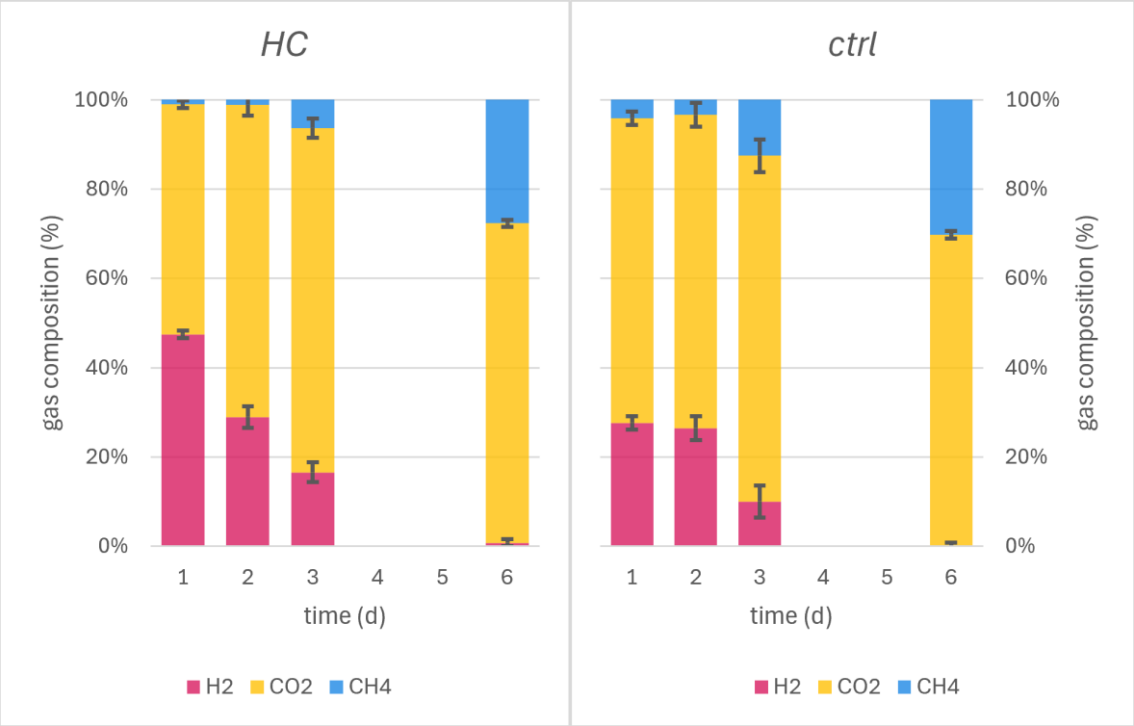


*Figure 32, Composition of the produced biogas during Test 2*

Table 28 summarizes the main yield parameters discussed above.

*Table 28, Yield parameters obtained at the end of Test 2*

| | | *HC* test | *ctrl* test |
|---|---|---|---|
| Gas Production | NL | 4.86 ± 0.04 | 4.24 ± 0.04 |
| $H_2$ Production | $NL_{H2}$ | 1.68 ± 0.08 | 0.93 ± 0.04 |
| SGP | $NL_{biogas}\ kg_{TVS}^{-1}$ | 84 ± 1 | 73 ± 1 |
| SHP | $NL_{H2}\ kg_{TVS}^{-1}$ | 29 ± 1 | 16 ± 1 |
| maximum HPR | $NmL_{H2}\ L_{reactor}^{-1}\ h^{-1}$ | 62.8 ± 0.3 | 7.5 ± 0.1 |
| maximum $H_2$ content | % | 47 ± 1 | 28 ± 2 |

Under the selected operative parameters for the HC pretreatment (Table 11), the energy requirement of the process was estimated to be around 22 kWh/ton, based on the 17 kW electrical power of the hydrodynamic cavitator, the 30-minute pretreatment duration, and the 380 L of organic waste mixture treated. This value is considerably lower than the energy requirement of conventional pretreatment methods, such as thermal pretreatment, which may require approximately 49 kWh/ton when heating the substrate from 20 to 80 °C (Barth et al., 2024). However, the additional hydrogen generated due to the HC pretreatment in this test was not sufficient to compensate for the energy consumed, hindering the economic viability of the approach. For this reason, the pretreatment step was omitted from subsequent tests. To better evaluate the potential feasibility of the HC pretreatment, a throughout set of tests would be necessary, investigating different pretreatment operative conditions and substrate compositions.

## 4.3. Test 3: Lab-scale Dark Fermentation of Food Waste and WAS in Semi-continuous Condition

Test 3 was conducted to evaluate the performance of a Dark Fermentation semi-continuous system treating a mixture of WAS and FW, as detailed in Section 3.2.3. Figure 33 shows the Total Solids (TS) and Total Volatile Solids (TVS) content in the DFE during the test. It is possible to observe that the solid content of the DFE increased during the first two weeks, settling at stable values from the 3$^{rd}$ week onwards. At stability, the effluent was characterized by a total solid content and total volatile solid content of 41 ± 2 $g_{TS}$ $kg^{-1}$ and 29 ± 2 $g_{TVS}$ $kg^{-1}$, respectively, and a TVS/TS ratio of 71 ± 4 %.

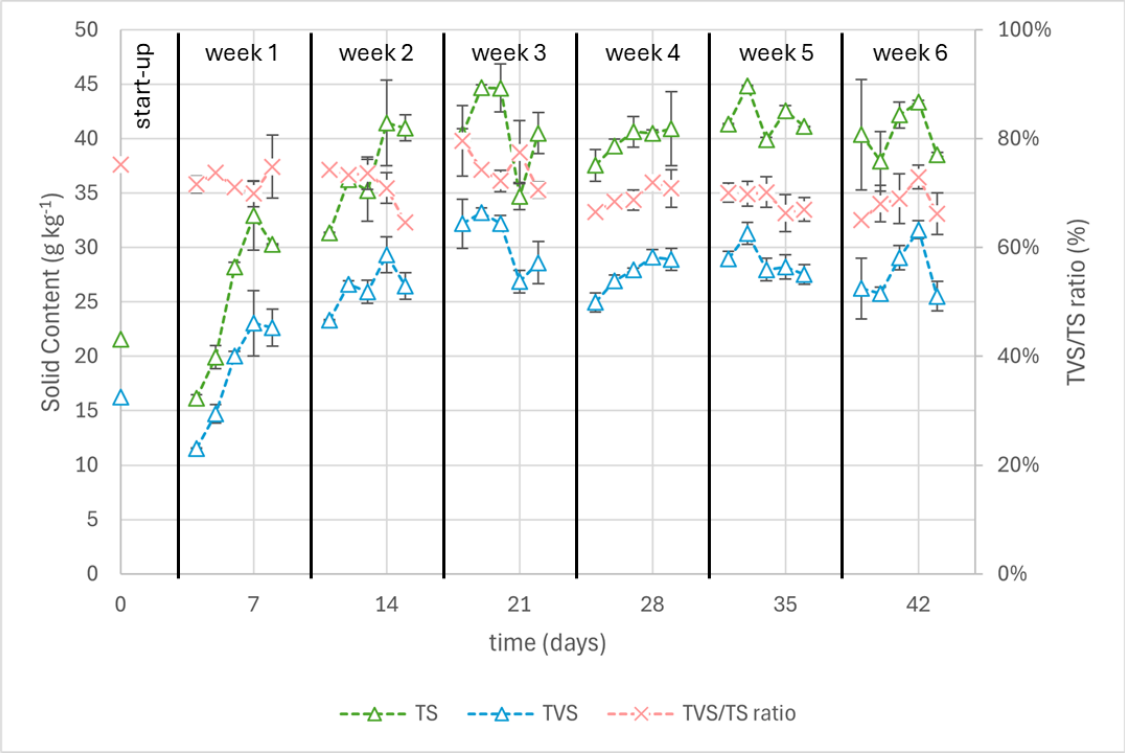


*Figure 33, Fluctuations of Total Solids (TS) and Total Volatile Solids (TVS) content during Test 3*

Figure 34 shows the pH, the alkalinity, and the ammonium concentration of the system during the experiment.

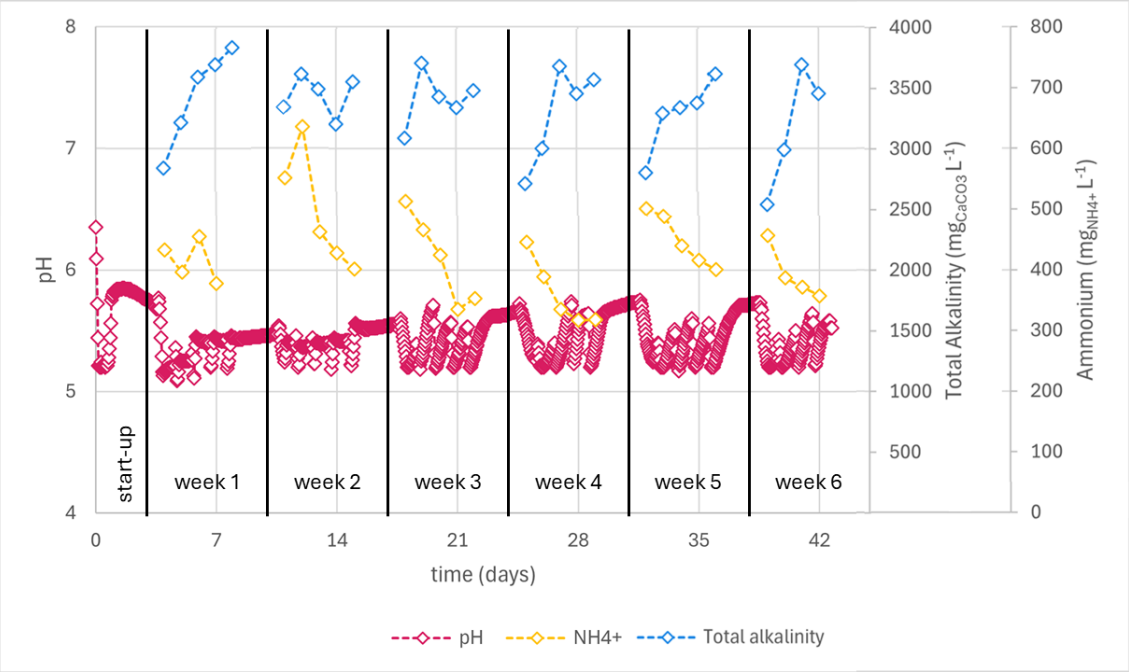


*Figure 34, Fluctuations of the pH values within the reactor, and the ammonium concentration and total alkalinity of the DFE during Test 3*

The pH, controlled by a peristaltic pump dosing a 3 N NaOH solution, fluctuated within the set range of 5.20 and 5.50 throughout the experiment. The total alkalinity of the DFE did not exhibit considerable fluctuations between weeks, but showed rather an internal fluctuation within each week, with lower values on Mondays and higher values on the following days, followed by a decrease during the weekends. In contrast, the ammonium concentration of the DFE showed an inverse trend, with higher values obtained at the beginning of the week and lower in the subsequent days, followed by an increase during the weekends. The ammonium decrease during the weekdays is most likely due to: (I) the mixed liquor dilution connected to the feeding procedure, and (II) the low HRT which hinders the complete degradation of nitrogen-rich organic compounds (e.g., amino acids, proteins), limiting the release of ammonium in the system. Conversely, during the weekends, the temporary suspension of the feeding procedure provided more time for the microbial community to decompose the supplied nitrogenous organic compounds; thus, resulting in the release of a higher quantity of ammonium.

In Figure 35, the daily Specific Gas Production, Specific Hydrogen Production, and Specific Methane Production (SGP, SHP, and SMP) are reported, together with $H_2$ and $CH_4$ concentrations in the produced gas.

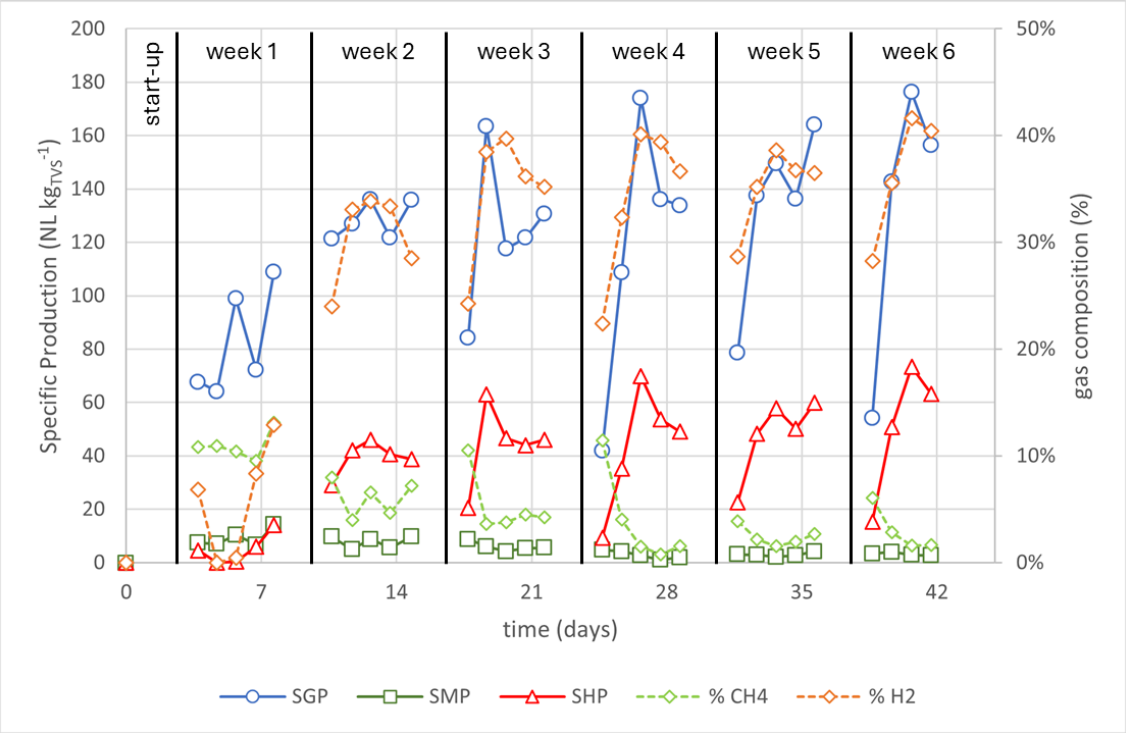


*Figure 35, Specific Gas Production (SGP), Specific Hydrogen Production (SHP), Specific Methane Production (SMP), and gas composition during Test 3. The remaining fraction of gas to reach 100% was $CO_2$, not explicitly reported in the figure*

From the observation of Figure 35, it is evident how all parameters were strongly affected by the two-days feeding pause over the weekend, which led to a severe drop in process yields at the beginning of each week. The SGP and SHP values recorded every Monday were considerably lower than the average of the other days of the week and were therefore not considered for the calculation of the weekly averages (Figure 38). Moreover, the gas produced after Monday's feeding showed a marked increase in the $CH_4$ content, with values as high as 8.0, 10.5, and 11.5 % at the beginning of the 2$^{nd}$, 3$^{rd}$, and 4$^{th}$ week, respectively. The combination of all these factors suggests that the weekend feeding pause provided more time for the proliferation of slow-growing microorganisms within the microbial consortium, particularly

hydrogenotrophic methanogens. This led on one hand to the decrease in the hydrogen content of the produced gas, and on the other to the increase in methane. This hypothesis is further supported by the observation of the fluctuation in the headspace pressure during the weekends (Figure 36). The hydrogenotrophic pathway led to the production of 1 mole of $CH_4$ for every 5 moles of reagents consumed (4 moles of $H_2$ and 1 mole of $CO_2$) causing system pressure to decrease, when volume is a fixed parameter (Ripoll et al., 2020). This decrease is particularly evident at the end of weeks 1 and 2, both events associated with high methane content and low hydrogen concentration in the subsequent day. This behavior seems less evident in weeks 3 to 5, where the pressure drops caused by hydrogen and carbon dioxide consumption were probably compensated by higher overall gas production and increased stability of the microbial consortium.

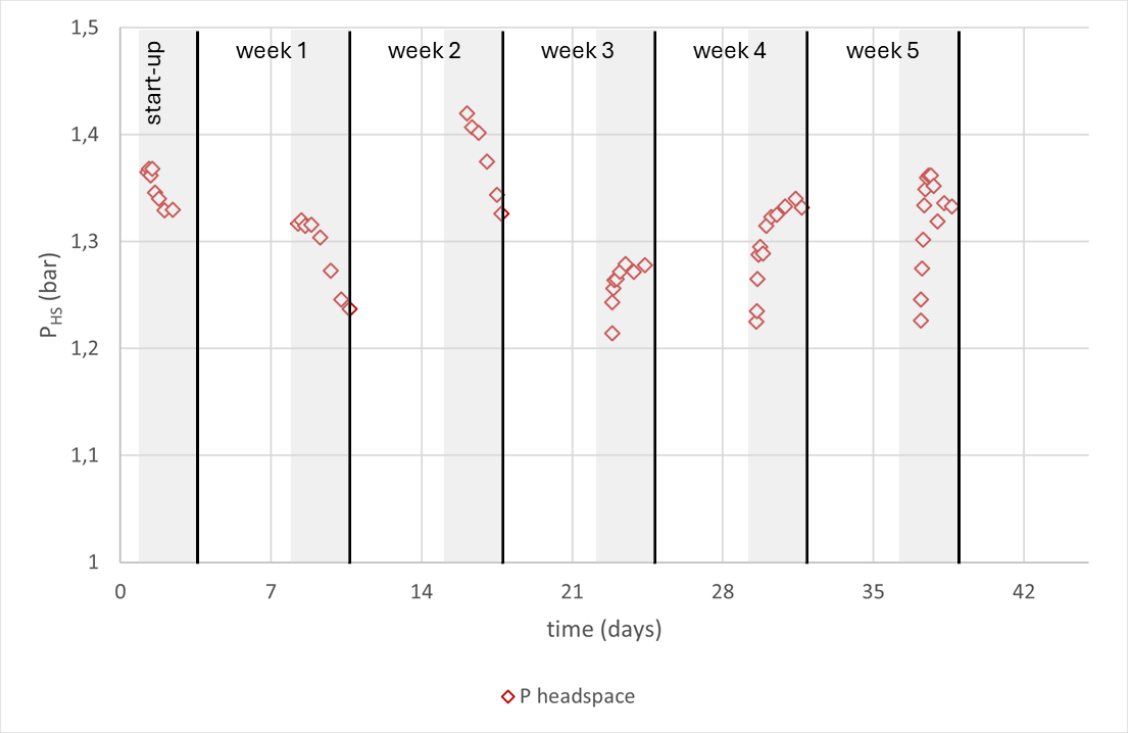


*Figure 36, Reactor headspace pressure fluctuations during weekend feeding pause. Weekends are highlighted in grey.*

Figure 37 illustrates the composition of the produced gas throughout the experiment. During the 1st week, microbial biomass was not effectively selected for hydrogen production, resulting in the production of gas poor in hydrogen and relatively rich in methane, with carbon dioxide being the predominant component. In the subsequent weeks, the methane content progressively decreases, reaching values as low as 1–2 %, while the hydrogen content stabilizes at 37.5 ± 2.5 %, consistent with the composition ranges reported by other authors for similar experimental conditions (Baldi et al., 2019; Gottardo et al., 2023; Zahedi et al., 2016). Even from this perspective, the impact of feeding interruption during the weekend appears clear, resulting in a drop in hydrogen content and a rise in methane at the beginning of each week, as detailed above.

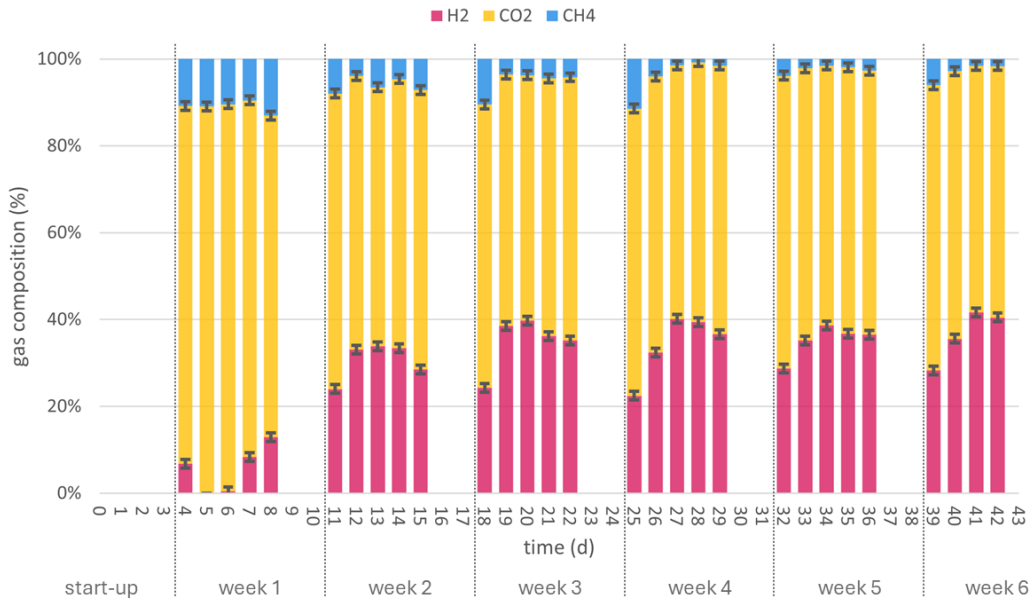


*Figure 37, Composition of the produced gas during Test 3*

To prevent discrepancies, data collected on Mondays were excluded from the computation of weekly averages of yield parameters and compositions showed in Figure 38.

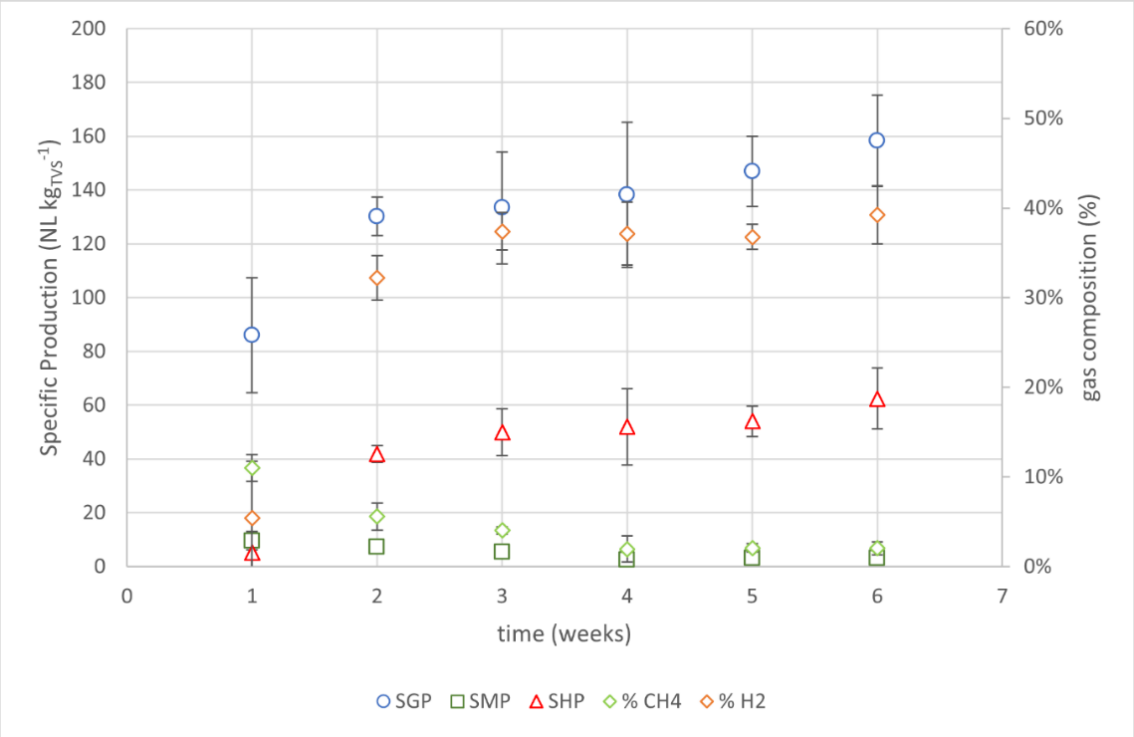


*Figure 38, Weekly average values of Specific Gas Production (SGP), Specific Hydrogen Production (SHP), Specific Methane Production (SMP), and gas composition during Test 3. The remaining fraction of gas to reach 100% was $CO_2$, not explicitly reported in the figure*

The yield parameters obtained at the end of the test are reported in Table 29

*Table 29, Average yield parameters obtained at the end of Test 3*

| | | |
|---|---|---|
| SGP | NL $kg_{TVS}^{-1}$ | 143 ± 20 |
| % $H_2$ | $\%_{H2}$ | 37.5 ± 2.5 |
| SHP | $NL_{H2}$ $kg_{TVS}^{-1}$ | 54 ± 10 |
| % $CH_4$ | $\%_{CH4}$ | 2.6 ± 1.2 |
| SMP | $NL_{CH4}$ $kg_{TVS}^{-1}$ | 3.5 ± 1.4 |
| HPR | $NL_{H2}$ $L_{reactor}^{-1}$ $d^{-1}$ | 0.65 ± 0.12 |

The SHP value obtained at the end of Test 3 (54 ± 10 $NL_{H2}$ $kg_{TVS}^{-1}$) was slightly higher than the ones reported by other authors under similar conditions (Baldi et al., 2019; Gottardo et al., 2023; Zahedi et al., 2016). The closest value was obtained by Gottardo et al., (2023), that reported a hydrogen yield of 46 $L_{H2}$ $kg_{VS}^{-1}$, obtained by the semi-continuous co-fermentation of hydrolyzed FW and WAS under thermophilic conditions at HRT of 4 d and OLR of 4.6 $kg_{VS}$ $m^{-3}$ $d^{-1}$. The obtained HPR value (0.65 ± 0.12 $NL_{H2}$ $L_{reactor}^{-1}$ $d^{-1}$), as well, resulted higher than the ones reported in similar studies ($NL_{H2}$ $L_{reactor}^{-1}$ $d^{-1}$): 0.10 – 0.21(Gottardo et al., 2023), 0.13 – 0.18 (Baldi et al., 2019), and 0.43 (Zahedi et al., 2016). The higher yield obtained in the present study can be attributed to the shorter HRT, the more precise control of the pH during the experimental period, and the smaller scale of the test. Higher HPR were instead reported by Moreno-Andrade et al., (2023), who obtained 0.73 $NL_{H2}$ $L_{reactor}^{-1}$ $d^{-1}$ with not-pretreated substrates at a shorter HRT of 8 h d and a higher OLR of 22 $kg_{VS}$ $m^{-3}$ $d^{-1}$, both parameters that are known for improving the production rate (García-Depraect et al., 2021) at the expenses of the conversion efficiency (15.6 $L_{H2}$ $kg_{VS}^{-1}$), which was lower than the one obtained in the present experiment.

## 4.4. Test 4: Pilot-scale Dark Fermentation of Food Waste and WAS in Semi-continuous Condition and Anaerobic Digestion of the Fermentative Effluent

Test 4 was conducted to scale-up the results obtained in the previous test to the pilot scale. As detailed in Section 3.2.4, the DF system was coupled with an AD reactor for DFE valorization, following a two-phase approach.

In the DF phase, 3 d and 1.5 d of HRT were tested. The HRT value was shortened after the first two weeks of the experiment based on yield results and evidence of hydrogenotrophic methanogens proliferation, as a measure to facilitate their washout.

Figure 39 shows the fluctuation in pH and temperature that occurred within the DF reactor throughout the experiment. At both 3 d and 1.5 d of HRT, the feeding procedure caused an abrupt decrease in temperature, particularly pronounced under the shorter HRT operation. This effect is mostly due to the employed semi-continuous feeding strategy, consisting of introducing the entire feed volume once per day (one-third of the total operational volume at 3 d HRT and two-third at 1.5 d HRT), with WAS at around 15 °C and FW at room temperature after the over-night thaw. The pH was controlled by a peristaltic pump automatically dosing a 10 N NaOH solution, to maintain it within a range of 5.4 – 5.6. The impact of feeding on pH stability was more pronounced at HRT of 1.5 d, due to the higher volume of substrate introduced daily, as mentioned above. Each feeding resulted in an initial pH increase, caused by the higher pH of the substrate fed, followed by a subsequent sharp pH drop associated with the conversion of the substrate to organic acids by HPB, along with hydrogen evolution.

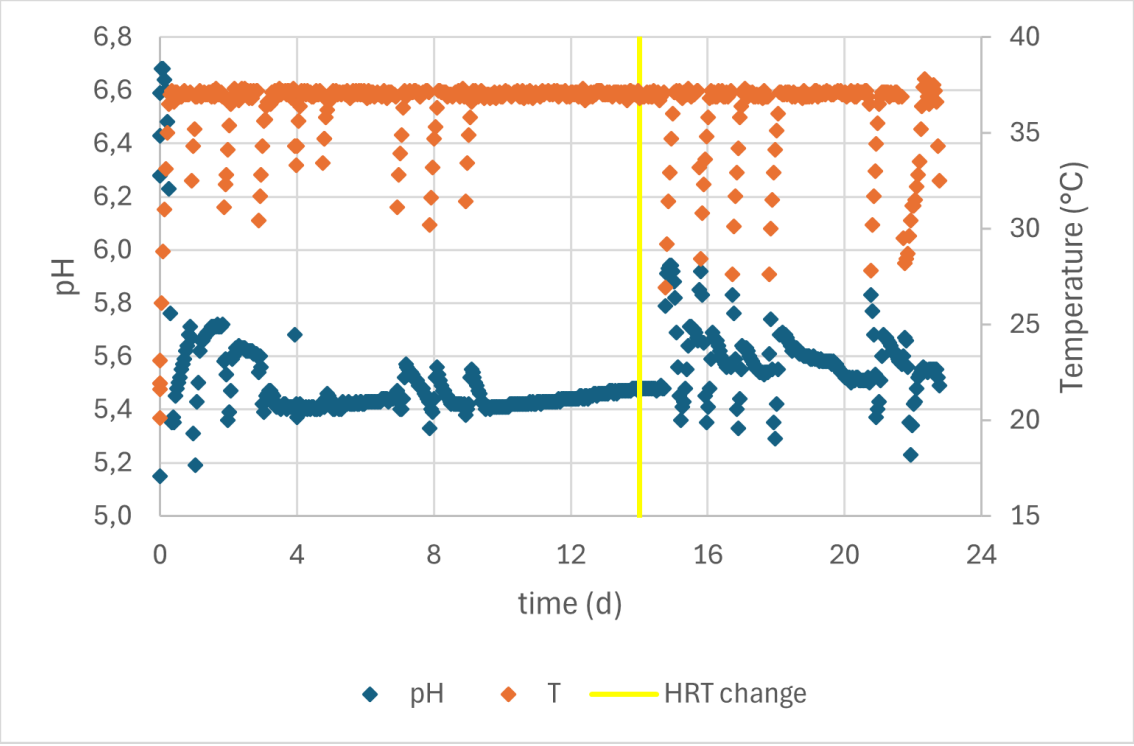


*Figure 39, Fluctuations in pH and temperature during the semi-continuous operations of the DF phase of Test 4. The yellow line indicates the transition in HRT from 3 d (left) to 1.5 d (right)*

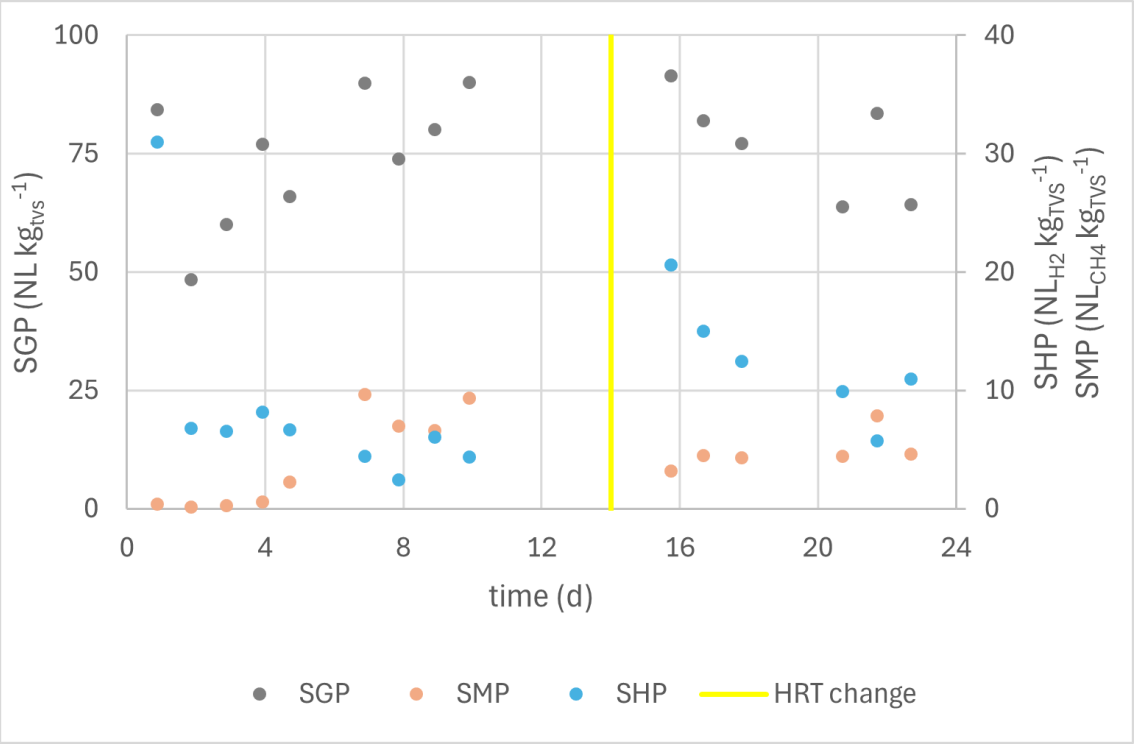


*Figure 40, Specific Gas Production (SGP), Specific Hydrogen Production (SHP), and Specific Methane Production (SMP) obtained during the DF phase of Test 4. The yellow line indicates the transition in HRT from 3 d (left) to 1.5 d (right)*

Figure 40 illustrates the specific conversion yields obtained throughout the experiment. The SGP resulted stable throughout the experiment, with 73 ± 14 NL $kg_{TVS}^{-1}$ and 77 ± 11 NL $kg_{TVS}^{-1}$ reported for HRT of 3 d and 1.5 d, respectively. In contrast, a much evident fluctuation appears in the SHP. The overall highest SHP value was obtained after the first day of the experiment, with 31 ± 3 $NL_{H2}$ $kg_{TVS}^{-1}$. However, a sharp decline was observed in the following days, resulting in an average SHP value of 6 ± 2 $NL_{H2}$ $kg_{TVS}^{-1}$ under an HRT of 3 d. This yield was substantially lower than the one obtained at a smaller scale during Test 3 (54 ± 10 $NL_{H2}$ $kg_{TVS}^{-1}$) under similar conditions, and lower than the expected yield values reported in the literature, ranging between 8.6 to 46 $NL_{H2}$ $kg_{TVS}^{-1}$ (Baldi et al., 2019; Gottardo et al., 2023; Zahedi et al., 2016). Additionally, a significant increase in methane production was detected, rising from near-zero methane production during the first week, to 8 ± 2 $NL_{CH4}$ $kg_{TVS}^{-1}$ in the following one. These data suggested the emergence of a potential shift in the microbial community in favor of hydrogen-consuming

bacteria, associated with the growth and adaptation of hydrogenotrophic methanogens within the fermentative environment. Based on these observations, the HRT was shortened to 1.5 d to facilitate the washout of the undesired microorganisms and support the proliferation of HPB (Palanivel et al., 2025). This adjustment led to a slight improvement in the SHP, particularly in the first week, where an average of 16 ± 4 $NL_{H2}\ kg_{TVS}^{-1}$ was achieved. The overall average SHP under HRT of 1.5 d was 12 ± 5 $NL_{H2}\ kg_{TVS}^{-1}$, though process stability was not achieved within the experimental period. Although shortening the HRT effectively reduced the activity of hydrogen-consuming microorganisms, it did not completely eliminate their presence, as evidenced by the observed SMP of 5 ± 2 $NL_{CH4}\ kg_{TVS}^{-1}$. The proliferation of hydrogen-consuming microorganisms is most likely associated with: i) the initially higher HRT, as HRTs below 2 d are generally recommended to effectively wash out methanogens from the system (Guo et al., 2010); ii) the feeding-pause occurred during the weekend, which provided favorable conditions for methanogens to proliferate; iii) the absence of inoculum pretreatment, which allowed undesired microorganisms to remain active in the system (Rafieenia et al., 2018); and iv) the scaling up to a larger reactor volume, which may have introduced mixing issues and heterogeneity, causing the generation of poorly-mixed regions within the reactor, that could have provided favorable conditions for slow-growing microorganisms, such as methanogens.

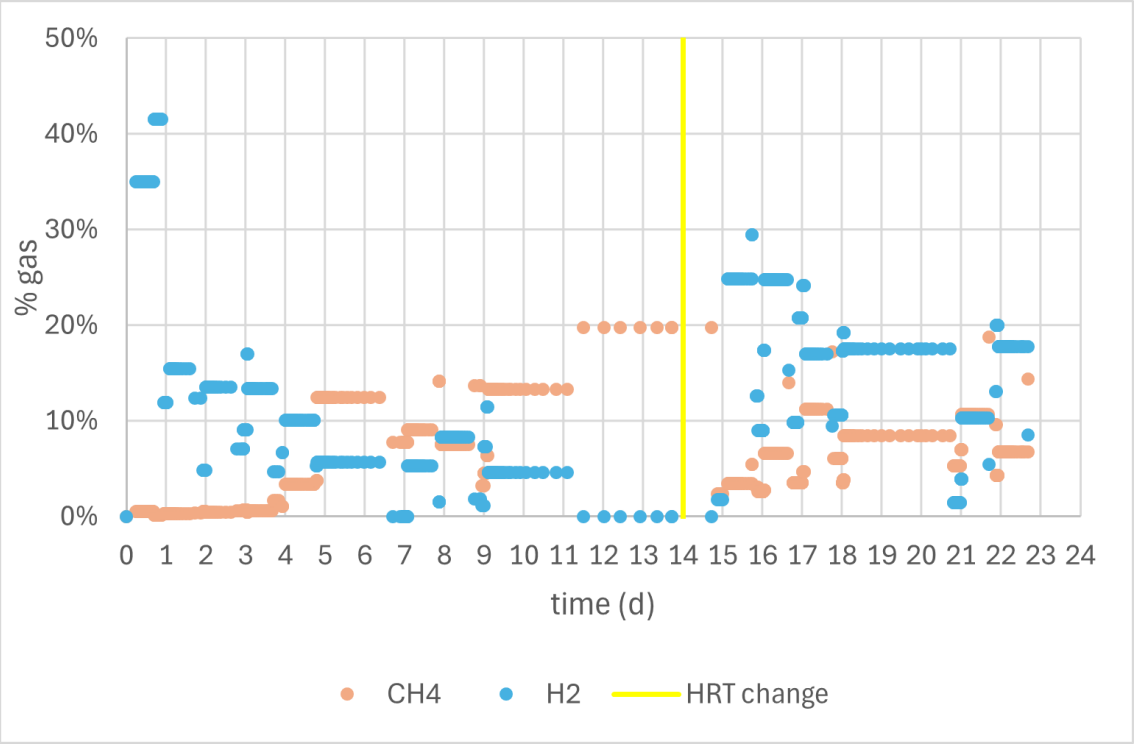


*Figure 41, Composition of the produced gas during the DF phase of Test 4. The remaining fraction of gas to reach 100% was carbon dioxide, not explicitly reported in the figure. The yellow line indicates the transition in HRT from 3 d (left) to 1.5 d (right)*

Figure 41 shows the composition of the produced gas during Test 4. The improvement in process efficiency associated with shortening the HRT to 1.5 d is noticeable from this perspective as well. The highest hydrogen content was achieved after the first day of fermentation, with a peak composition of 41.5 $\%_{H2}$, reached in the first 20 hours. After this point, the composition of the gas substantially decreased reaching values around 10 $\%_{H2}$ in the first week and 5 $\%_{H2}$ in the second one, while methane content increased from 3 $\%_{CH4}$ to 9 $\%_{CH4}$ in the same timeframe. At the end of the period maintained at an HRT of 3 d, the produced gas was composed only of 20 $\%_{CH4}$, with no detectable hydrogen. The transition to an HRT of 1.5 d improved the quality of the gas produced, which resulted on average characterized by 16 $\%_{H2}$ and 6 $\%_{CH4}$. Higher hydrogen levels and lower methane content reached under this condition indicate reduced activity of hydrogen-consuming microorganisms, although the detectable

methane content in the gas suggests these undesired microorganisms were not completely eliminated from the reactor.

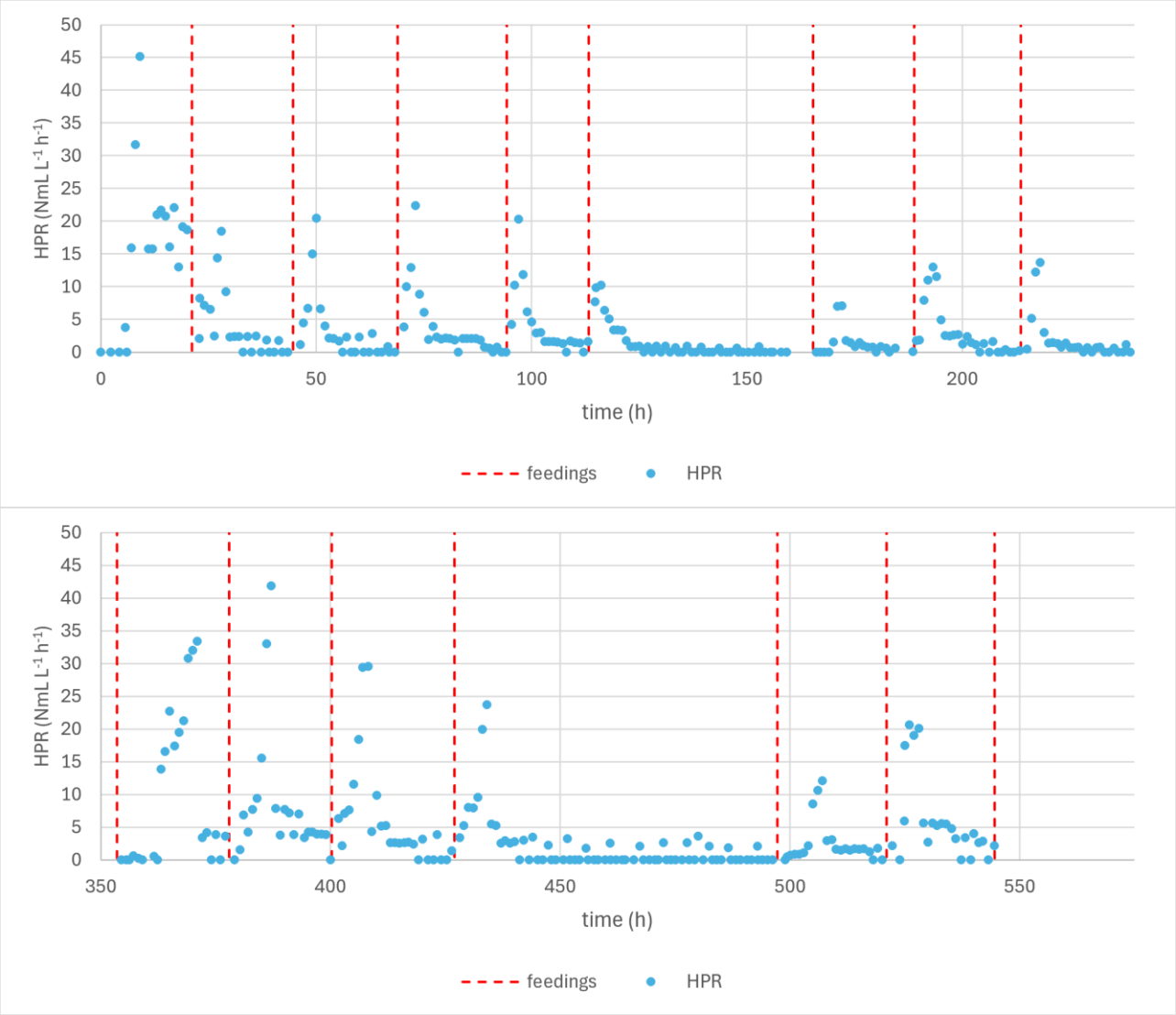


*Figure 42, Fluctuations in Hydrogen Production Rate (HPR) during the DF phase of Test 4, under HRT of 3 d (top) and 1.5 d (bottom). The red dotted lines represent the timing of feedings*

Figure 42 shows the fluctuation in HPR throughout the experiment. The highest HPR value (45.2 $NmL_{H2}$ $L_{reactor}^{-1}$ $h^{-1}$) was achieved at an HRT of 3 d, after 9 h from the beginning of the test. In the subsequent days of the first week, the maximum HPR recorded after each feeding ranged

around 18 ± 5 $NmL_{H2}\ L_{reactor}^{-1}\ h^{-1}$, decreasing to 11 ± 4 $NmL_{H2}\ L_{reactor}^{-1}\ h^{-1}$ in the second week, suggesting a shift in the microbial community that impacted the HPB. Reducing the HRT to 1.5 d enhanced the system efficiency, with maximum HPRs ranging around 32 ± 8 $NmL_{H2}\ L_{reactor}^{-1}\ h^{-1}$ in the first week after the HRT was adjusted, and 16 ± 6 $NmL_{H2}\ L_{reactor}^{-1}\ h^{-1}$ in the second one. In both the HRTs tested, the maximum HPR was achieved within the first 10 h after feeding (on average after 5 ± 2 h under 3 d of HRT, and 8 ± 1 h under 1.5 d of HRT). The sole exception was observed after the first feeding of HRT 1.5 d, where maximum HPR was reached after more than 17 h, most likely due to the long feeding-pause of the previous days and the perturbation caused by the change in the operative conditions. In most cases, HPR values rapidly declined to near-zero values a few hours after reaching their peak, indicating the end of the hydrogen evolution phase. This finding suggests that further reduction of the HRT could be feasible without substantially compromising either production rates or substrate conversion efficiency, provided that the OLR remains unchanged. However, due to the semi-continuous daily feeding regime employed, this parameter could not be shortened without causing significant disruption to the microbial consortium.

Table 30 summarizes the yield parameters obtained in the DF phase of Test 4. Under both the tested HRT, the achieved process yields resulted substantially lower than the ones obtained in the previous experiment, including conversion efficiency, production rate, and gas composition (Test 3, SHP of 54 ± 10 $NL_{H2}\ kg_{TVS}^{-1}$, HPR of 0.65 ± 0.12 $NL_{H2}\ L^{-1}\ d^{-1}$, 37.5 ± 2.5 $\%_{H2}$, section 4.3), and lower than the yields expected from literature findings under similar operative conditions (Table 4, Section 2.4.3, Baldi et al., 2019; Gottardo et al., 2023; Zahedi et al., 2016). This, combined with the fluctuations observed between consecutive weeks throughout the experiment, suggests that process stability was not achieved, either for the operative parameters employed or for the reactor configuration, which did not allow an optimal DF process. Modifications to the reactor setup to enhance mixing and ensure greater homogeneity within the reactor, along with the implementation of different feeding strategies represent the

most recommended approaches for optimizing this specific DF system, in the perspective of future experiments.

*Table 30, Yield parameters obtained throughout Test 4*

| | | | |
|---|---|---|---|
| HRT | d | 3.0 | 1.5 |
| SGP | NL $kg_{TVS}^{-1}$ | 73 ± 14 | 77 ± 11 |
| % $H_2$ | $\%_{H2}$ | 12.5 | 16 |
| SHP | $NL_{H2}$ $kg_{TVS}^{-1}$ | 6 ± 2 | 12 ± 5 |
| % $CH_4$ | $\%_{CH4}$ | 5.0 * | 6 |
| SMP | $NL_{CH4}$ $kg_{TVS}^{-1}$ | 4 ± 4 ** | 5 ± 2 |
| mHPR[a] | $NL_{H2}$ $L_{reactor}^{-1}$ $h^{-1}$ | 16 ± 5 | 27 ± 10 |
| HPR | $NL_{H2}$ $L_{reactor}^{-1}$ $d^{-1}$ | 0.07 ± 0.03 | 0.14 ± 0.08 |

* below 3 $\%_{CH4}$ in the first week, 9 $\%_{CH4}$ in the second one

** below 1 $NL_{CH4}$ $kg_{TVS}^{-1}$ in the first week, 8 ± 2 $NL_{CH4}$ $kg_{TVS}^{-1}$ in the second one

[a] average of the maximum HPR achieved after each feeding

The DFE generated during the DF phase was subsequently fed into an AD process to ensure effluent valorization through biogas production. During the test, the operative parameters of the AD system were slightly modified in response to the DF HRT adjustment, from an HRT of 23.3 d and an OLR of 0.7 ± 0.1 $kg_{TVS}$ $m^{-3}$ $d^{-1}$ during the first two weeks, to 17.5 d and 1.0 ± 0.1 $kg_{TVS}$ $m^{-3}$ $d^{-1}$ during the last two weeks.

Figure 43 shows the fluctuations in pH and alkalinity observed during the AD phase. Although the overall timeframe of the experiment does not allow relevant speculation over the stability of the process, no significant fluctuations in pH and alkalinity were detected. The pH was stable at 7.8 ± 0.2 throughout the experiment and was not affected by the HRT and OLR

modification. In the first two weeks, under longer HRT and lower OLR, an increasing trend of total alkalinity was reported (from 2750 to 3100 $mg_{CaCO3}\,L^{-1}$), while partial alkalinity resulted stable at $2130 \pm 80\ mg_{CaCO3}\,L^{-1}$. The increase in the difference between total and partial alkalinity suggests that the concentration of compounds with a buffer capacity at pH values of around 4 (i.e., VFAs) was increasing in the system. The stability of partial alkalinity indicates that this accumulation was buffered by the carbonates present in the system, making excessive acidification of the reactor unlikely. After HRT and OLR were slightly increased, both partial ($2500 \pm 120\ mg_{CaCO3}\,L^{-1}$) and total alkalinity ($3520 \pm 80\ mg_{CaCO3}\,L^{-1}$) were stable. This outcome was unsurprising, as the applied high HRT and low OLR were within the optimal operational range for AD (Rabii et al., 2019).

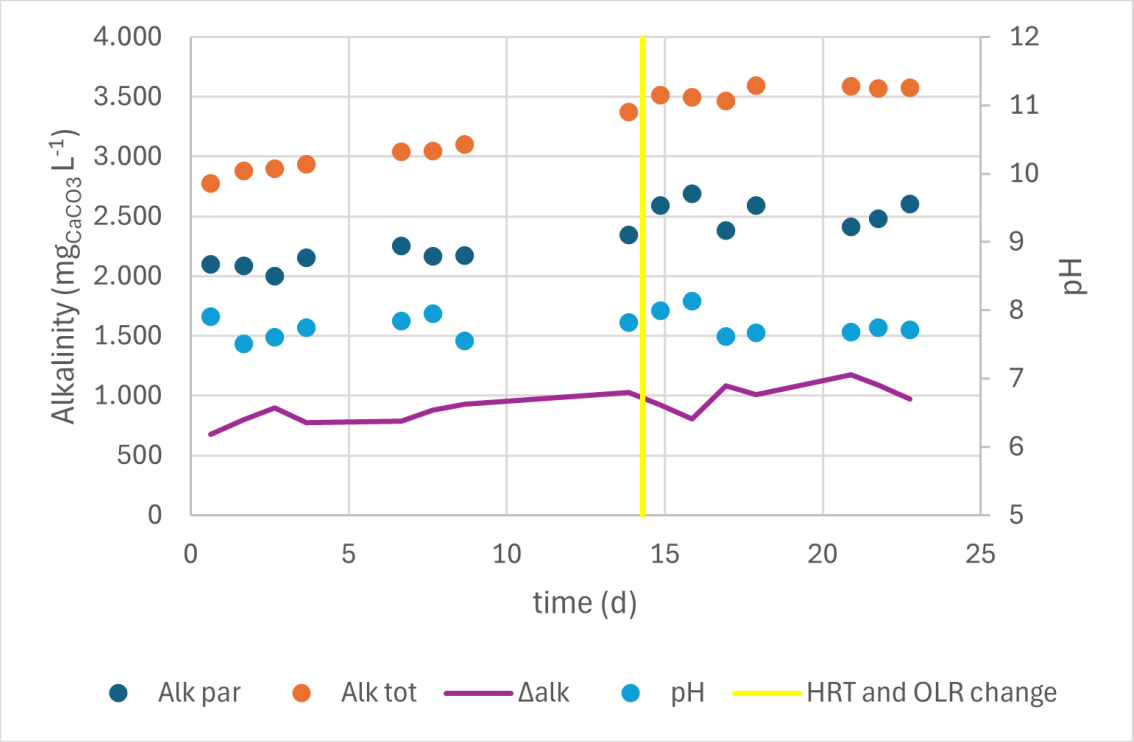


*Figure 43, Fluctuations in pH and alkalinity during the AD phase of Test 4. The yellow line indicates HRT and OLR adjustment*

Figure 44 shows the yield parameters achieved during the AD treatment of the DFE. During the first two weeks of the experiment, the system faced lower stability, most likely associated with

the start-up of the system. After this period, and with the adjustment of HRT and OLR to 17.5 d and 1.0 ± 0.1 $kg_{TVS}$ $m^{-3}$ $d^{-1}$, the yield parameters of the process stabilized at an SGP of 460 ± 80 NL $kg_{TVS}^{-1}$ and an SMP of 270 ± 50 $NL_{CH4}$ $kg_{TVS}^{-1}$, consistent with the yield achieved in the methanogenic phase by Zahedi et al., (2016) under similar conditions (287 ± 36 $NL_{CH4}$ $kg_{TVS}^{-1}$, under an HRT of 16 d and an OLR of 3 $kg_{TVS}$ $m^{-3}$ $d^{-1}$). The achieved GPR exhibits lower stability, most likely due to the weekend feeding interruptions and the short overall experimental period investigated. Moreover, the GPR obtained was considerably lower than those reported by Zahedi et al., (2016), with an average value of 360 ± 100 NL $m^{-3}_{reactor}$ $d^{-1}$ during the last weeks of the experiment compared to 1000 ± 100 NL $m^{-3}_{reactor}$ $d^{-1}$ achieved in the referenced study. This outcome was likely related to the low OLR applied in the present work, forced to a maximum value of 1.0 ± 0.1 $kg_{TVS}$ $m^{-3}$ $d^{-1}$ due to the low solid concentration of the DFE generated in the DF phase.

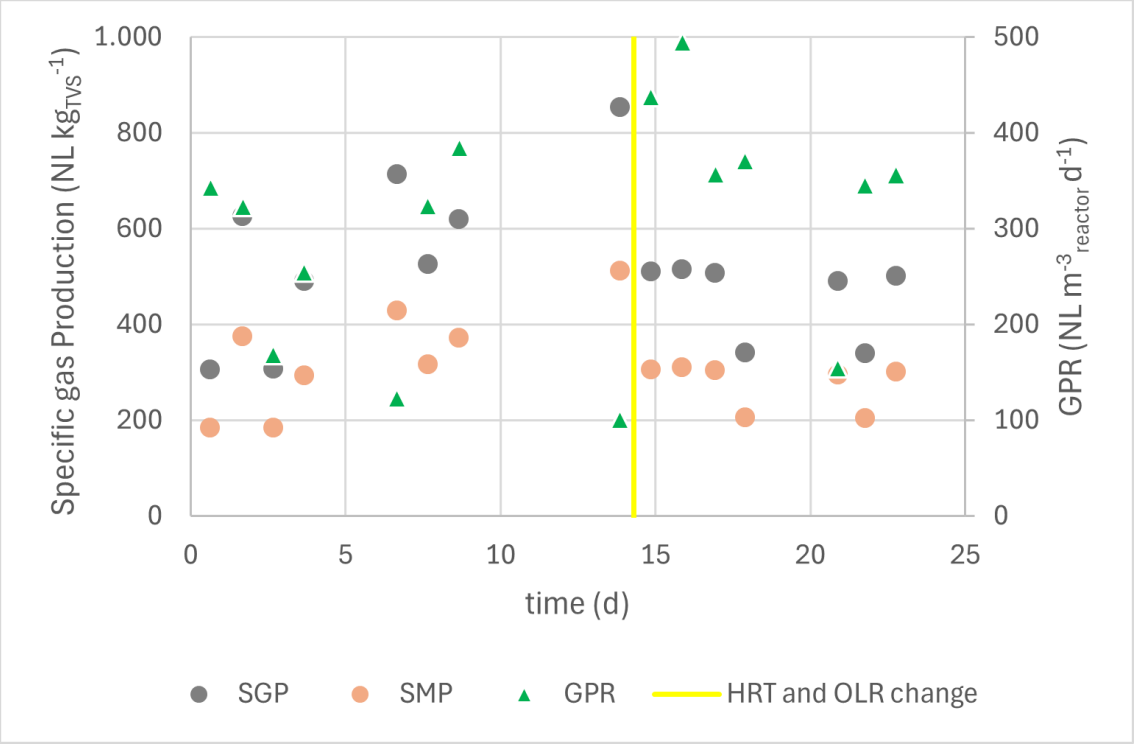


*Figure 44, Specific Gas Production (SGP), Specific Methane Production (SMP), and Gas Production Rate (GPR) achieved during the AD phase of Test 4. The yellow line indicates HRT and OLR adjustment*

## 4.5. General Conclusions

The experiments conducted confirmed the feasibility of a DF co-fermentation system treating FW and WAS.

Under batch-mode conditions, the OL resulted as a key parameter in determining hydrogen production yields and VFA accumulation. The highest hydrogen yield was obtained at an OL 20 $kg_{TVS}\ m^{-3}$ (16 $NL_{H2}\ kg_{TVS}^{-1}$), while higher loadings (*OL 25*) resulted in system acidification and HPB inhibition. The achieved yields, substantially lower than those reported in the literature, ranging generally between 60 and 190 $L_{H2}\ kg_{VS}^{-1}$ (Kim et al., 2011; Li et al., 2018; Yang et al., 2025), indicated that optimal process conditions were unattained. A key difference between the referenced study and the first batch test conducted (Test 1) lay in the substrate pretreatment, a well-acknowledge strategy for boosting process efficiency (Rafieenia et al., 2018). The effect of this parameter was tested in the second batch test (Test 2), where a hydrodynamic cavitation pretreatment of the co-substrate was performed. The tested pretreatment significantly enhanced the conversion efficiency of the process, almost doubling the achieved SHP (+81 % compared to the fermentation of untreated substrate). This outcome is likely associated with the positive effect of the HC pretreatment in enhancing the substrate bioavailability and hindering the activity of the indigenous microorganisms present in the two co-substrates.

Testing the system under semi-continuous operation resulted in improved process yields, with a peak SHP of 54 ± 10 $NL_{H2}\ kg_{TVS}^{-1}$, HPR of 0.65 ± 0.12 $NL_{H2}\ L^{-1}\ d^{-1}$, and hydrogen concentrations of 37.5 ± 2.5 % when working at laboratory-scale (Test 3). The achieved yields were higher than those reported by several other authors at similar operative conditions (Baldi et al., 2019; Gottardo et al., 2023; Zahedi et al., 2016). Scaling up to pilot-scale (Test 4), however, resulted in lower yields (SHP of 6 – 12 $NL_{H2}\ kg_{TVS}^{-1}$) and stability issues, with evidence of a more severe hydrogenotrophic methanogens proliferation under both the tested HRTs (3 d and 1.5 d). Shortening the HRT to 1.5 d partially mitigated methanogens activity, though it did not ensure their complete elimination from the system. The outcomes achieved in Test 4 suggested that process stability was unattained, most likely due to a proliferation of hydrogen-consuming

bacteria, most likely caused by: i) the initially higher HRT applied; ii) the employed feeding strategy with pauses during the weekend; ii) the lack of inoculum pretreatment; iv) and the scale-up of the system, which may have introduced mixing challenges and heterogeneity.

The valorization of the generated DFE through an AD process was investigated and did not present significant challenges, primarily due to the long HRT (17.5 – 23.3 d) and low OLR (0.7 – 1.0 $kg_{TVS}$ $m^{-3}$ $d^{-1}$) applied. The AD process resulted in an SMP of 270 ± 50 $NL_{CH4}$ $kg_{TVS}^{-1}$, consistent with the yield achieved in literature for similar processes (287 ± 36 $NL_{CH4}$ $kg_{TVS}^{-1}$, (Zahedi et al., 2016). However, the relatively low GPR obtained (360 ± 100 NL $m^{-3}_{reactor}$ $d^{-1}$) suggested that the process may be further optimized, in particular by improving process integration to allow for an increased OLR in the AD phase.

## 4.6. References

Asunis, F., De Gioannis, G., Isipato, M., Muntoni, A., Polettini, A., Pomi, R., Rossi, A., & Spiga, D. (2019). Control of fermentation duration and pH to orient biochemicals and biofuels production from cheese whey. *Bioresource Technology*, *289*. https://doi.org/10.1016/j.biortech.2019.121722

Baldi, F., Pecorini, I., & Iannelli, R. (2019). Comparison of single-stage and two-stage anaerobic co-digestion of food waste and activated sludge for hydrogen and methane production. *Renewable Energy*, *143*, 1755–1765. https://doi.org/10.1016/j.renene.2019.05.122

Barth, M., Werner, M., Otto, P., Richwien, B., Bahramsari, S., Krause, M., Schwan, B., & Abendroth, C. (2024). Microwave-assisted organic acids and green hydrogen production during mixed culture fermentation. Biotechnology for Biofuels and Bioproducts, 17(1). https://doi.org/10.1186/s13068-024-02573-7

Blagojevič, M., Zupanc, M., Gostiša, J., Stres, B., Šmid, A., Dular, M., Slemenik Perše, L., Gradišar Centa, U., Bizjan, B., Rak, G., Novak, U., Likozar, B., & Kolbl Repinc, S. (2025). The impact of radicals on physicochemical properties of waste activated sludge during hydrodynamic cavitation treatment. *Ultrasonics Sonochemistry*, *115*, 107291. https://doi.org/10.1016/j.ultsonch.2025.107291

Canto-Robertos, M., Quintal-Franco, C., Ponce-Caballero, C., Vega-De Lille, M., & Moreno-Andrade, I. (2023). Inhibition of hydrogen production by endogenous microorganisms from

food waste. *Brazilian Journal of Chemical Engineering*, *40*(1), 137–150. https://doi.org/10.1007/s43153-022-00235-5

Correa-Villa, C., Moreno-Cárdenas, E., & de Bruijn, J. (2024). Presence of lactic acid bacteria in hydrogen production by dark fermentation: competition or synergy. In *World Journal of Microbiology and Biotechnology* (Vol. 40, Issue 12). Springer Science and Business Media B.V. https://doi.org/10.1007/s11274-024-04167-9

Elbeshbishy, E., Dhar, B. R., Nakhla, G., & Lee, H. S. (2017). A critical review on inhibition of dark biohydrogen fermentation. In *Renewable and Sustainable Energy Reviews* (Vol. 79, pp. 656–668). Elsevier Ltd. https://doi.org/10.1016/j.rser.2017.05.075

García-Depraect, O., Castro-Muñoz, R., Muñoz, R., Rene, E. R., León-Becerril, E., Valdez-Vazquez, I., Kumar, G., Reyes-Alvarado, L. C., Martínez-Mendoza, L. J., Carrillo-Reyes, J., & Buitrón, G. (2021). A review on the factors influencing biohydrogen production from lactate: The key to unlocking enhanced dark fermentative processes. In *Bioresource Technology* (Vol. 324). Elsevier Ltd. https://doi.org/10.1016/j.biortech.2020.124595

Ghimire, A. (2015). *Dark fermentative biohydrogen production from organic waste and application of by-products in a biorefinery concept*. https://tel.archives-ouvertes.fr/tel-01404689

Gopalakrishnan, B., Khanna, N., & Das, D. (2019). Dark-Fermentative Biohydrogen Production. In *Biomass, Biofuels, Biochemicals: Biohydrogen, Second Edition* (pp. 79–122). Elsevier. https://doi.org/10.1016/B978-0-444-64203-5.00004-6

Gottardo, M., Cavinato, C., Bolzonella, D., & Pavan, P. (2013). *Dark Fermentation Optimization by Anaerobic Digested Sludge Recirculation: Effects on Hydrogen Production*. *32*. www.aidic.it/cet

Gottardo, M., Dosta, J., Cavinato, C., Crognale, S., Tonanzi, B., Rossetti, S., Bolzonella, D., Pavan, P., & Valentino, F. (2023). Boosting butyrate and hydrogen production in acidogenic fermentation of food waste and sewage sludge mixture: a pilot scale demonstration. *Journal of Cleaner Production*, *404*. https://doi.org/10.1016/j.jclepro.2023.136919

Gu, X. Y., Liu, J. Z., & Wong, J. W. C. (2018). Control of lactic acid production during hydrolysis and acidogenesis of food waste. *Bioresource Technology*, *247*, 711–715. https://doi.org/10.1016/j.biortech.2017.09.166

Guo, X. M., Trably, E., Latrille, E., Carrre, H., & Steyer, J. P. (2010). Hydrogen production from agricultural waste by dark fermentation: A review. *International Journal of Hydrogen Energy*, *35*(19), 10660–10673. https://doi.org/10.1016/j.ijhydene.2010.03.008

Itoh, Y., Tada, K., Kanno, T., & Horiuchi, J. I. (2012). Selective production of lactic acid in continuous anaerobic acidogenesis by extremely low pH operation. *Journal of Bioscience and Bioengineering*, *114*(5), 537–539. https://doi.org/10.1016/j.jbiosc.2012.05.020

Jariyaboon, R., Hayeeyunu, S., Usmanbaha, N., Ismail, S. Bin, O-Thong, S., Mamimin, C., & Kongjan, P. (2023). Thermophilic Dark Fermentation for Simultaneous Mixed Volatile Fatty

Acids and Biohydrogen Production from Food Waste. *Fermentation*, *9*(7). https://doi.org/10.3390/fermentation9070636

Jo, J. H., Jeon, C. O., Lee, D. S., & Park, J. M. (2007). Process stability and microbial community structure in anaerobic hydrogen-producing microflora from food waste containing kimchi. *Journal of Biotechnology*, *131*(3), 300–308. https://doi.org/10.1016/j.jbiotec.2007.07.492

Kim, D. H., Kim, S. H., Kim, H. W., Kim, M. S., & Shin, H. S. (2011). Sewage sludge addition to food waste synergistically enhances hydrogen fermentation performance. *Bioresource Technology*, *102*(18), 8501–8506. https://doi.org/10.1016/j.biortech.2011.04.089

Li, Z., Chen, Z., Ye, H., Wang, Y., Luo, W., Chang, J. S., Li, Q., & He, N. (2018). Anaerobic co-digestion of sewage sludge and food waste for hydrogen and VFA production with microbial community analysis. *Waste Management*, *78*, 789–799. https://doi.org/10.1016/j.wasman.2018.06.046

Liu, X., Li, R., Ji, M., & Han, L. (2013). Hydrogen and methane production by co-digestion of waste activated sludge and food waste in the two-stage fermentation process: Substrate conversion and energy yield. *Bioresource Technology*, *146*, 317–323. https://doi.org/10.1016/j.biortech.2013.07.096

Liu, Y., Chen, L., Duan, Y., Li, R., Yang, Z., Liu, S., & Li, G. (2024). Recent progress and prospects for chain elongation of transforming biomass waste into medium-chain fatty acids. *Chemosphere*, *355*. https://doi.org/10.1016/j.chemosphere.2024.141823

Lund, P. A., De Biase, D., Liran, O., Scheler, O., Mira, N. P., Cetecioglu, Z., Fernández, E. N., Bover-Cid, S., Hall, R., Sauer, M., & O'Byrne, C. (2020). Understanding How Microorganisms Respond to Acid pH Is Central to Their Control and Successful Exploitation. *Frontiers in Microbiology*, *11*. https://doi.org/10.3389/fmicb.2020.556140

Moreno-Andrade, I., Berrocal-Bravo, M. J., & Valdez-Vazquez, I. (2023). Biohydrogen production from food waste and waste activated sludge in codigestion: influence of organic loading rate and changes in microbial community. *Journal of Chemical Technology and Biotechnology*, *98*(1), 230–237. https://doi.org/10.1002/jctb.7238

Palanivel, P. D., Jovita S, A., Babu, K., & Naina Mohamed, S. (2025). Harnessing dark fermentation: Mechanisms, metabolic pathways, and nanoparticle innovations for biohydrogen enhancement. In *International Journal of Hydrogen Energy* (Vol. 109, pp. 383–396). Elsevier Ltd. https://doi.org/10.1016/j.ijhydene.2025.02.033

Rabii, A., Aldin, S., Dahman, Y., & Elbeshbishy, E. (2019). A review on anaerobic co-digestion with a focus on the microbial populations and the effect of multi-stage digester configuration. *Energies*, *12*(6). https://doi.org/10.3390/en12061106

Rafieenia, R., Lavagnolo, M. C., & Pivato, A. (2018). Pre-treatment technologies for dark fermentative hydrogen production: Current advances and future directions. *Waste Management*, *71*, 734–748. https://doi.org/10.1016/j.wasman.2017.05.024

Rangel, C., Sastoque, J., Calderon, J., Mosquera, J., Velasquez, P., Cabezab, I., & Acevedo, P. (2020). Hydrogen production by dark fermentation process: Effect of initial organic load. *Chemical Engineering Transactions*, *79*, 133–138. https://doi.org/10.3303/CET2079023

Ripoll, E., López, I., & Borzacconi, L. (2020). Hydrogenotrophic activity: A tool to evaluate the kinetics of methanogens. *Journal of Environmental Management*, *270*. https://doi.org/10.1016/j.jenvman.2020.110937

Rombouts, J. L., Kranendonk, E. M. M., Regueira, A., Weissbrodt, D. G., Kleerebezem, R., & van Loosdrecht, M. C. M. (2020). Selecting for lactic acid producing and utilising bacteria in anaerobic enrichment cultures. *Biotechnology and Bioengineering*, *117*(5), 1281–1293. https://doi.org/10.1002/bit.27301

Roslan, E., Mohamed, H., Abu Hassan, S. H., Carrere, H., & Trably, E. (2024). Coupling lactic acid fermentation of food waste at various concentrations as storage strategy with dark fermentation for biohydrogen production. *International Journal of Hydrogen Energy*, *88*, 358–368. https://doi.org/10.1016/j.ijhydene.2024.09.134

Salerno, M. B., Park, W., Zuo, Y., & Logan, B. E. (2006). Inhibition of biohydrogen production by ammonia. *Water Research*, *40*(6), 1167–1172. https://doi.org/10.1016/j.watres.2006.01.024

Sikora, A., Baszczyk, M., Jurkowski, M., & Zielenkiewicz, U. (2013). Lactic Acid Bacteria in Hydrogen-Producing Consortia: On Purpose or by Coincidence? In *Lactic Acid Bacteria - R & D for Food, Health and Livestock Purposes*. InTech. https://doi.org/10.5772/50364

Valentino, F., Moretto, G., Gottardo, M., Pavan, P., Bolzonella, D., & Majone, M. (2019). Novel routes for urban bio-waste management: A combined acidic fermentation and anaerobic digestion process for platform chemicals and biogas production. *Journal of Cleaner Production*, *220*, 368–375. https://doi.org/10.1016/j.jclepro.2019.02.102

Vidal-Antich, C., Perez-Esteban, N., Astals, S., Peces, M., Mata-Alvarez, J., & Dosta, J. (2021). Assessing the potential of waste activated sludge and food waste co-fermentation for carboxylic acids production. *Science of the Total Environment*, *757*. https://doi.org/10.1016/j.scitotenv.2020.143763

Villanueva-Galindo, E., Vital-Jácome, M., & Moreno-Andrade, I. (2023). Dark fermentation for H2 production from food waste and novel strategies for its enhancement. In *International Journal of Hydrogen Energy* (Vol. 48, Issue 27, pp. 9957–9970). Elsevier Ltd. https://doi.org/10.1016/j.ijhydene.2022.11.339

Wu, Q., Bao, X., Guo, W., Wang, B., Li, Y., Luo, H., Wang, H., & Ren, N. (2019). Medium chain carboxylic acids production from waste biomass: Current advances and perspectives. In *Biotechnology Advances* (Vol. 37, Issue 5, pp. 599–615). Elsevier Inc. https://doi.org/10.1016/j.biotechadv.2019.03.003

Xue, S., Chen, H., Wang, F., Lv, G., Tan, L., & Liu, G. (2024). The effect of substrate acidification on the biohydrogen production by dark fermentation. *International Journal of Hydrogen Energy*, *49*, 177–188. https://doi.org/10.1016/j.ijhydene.2023.07.183

Yang, Y. N., Zhu, M. J., & Zhao, L. (2025). Enhanced thermophilic hydrogen production from co-substrate of pretreated waste activated sludge and food waste: Analysis from microbial growth and metabolism. *International Journal of Hydrogen Energy*, *97*, 431–443. https://doi.org/10.1016/j.ijhydene.2024.11.456

Zahedi, S., Solera, R., Micolucci, F., Cavinato, C., & Bolzonella, D. (2016). Changes in microbial community during hydrogen and methane production in two-stage thermophilic anaerobic co-digestion process from biowaste. *Waste Management*, *49*, 40–46. https://doi.org/10.1016/j.wasman.2016.01.016

# 5. Results: Photo Fermentation Tests

## 5.1. Test 5: Preliminary test of PPB growth on Fermentative Broth

In Test 5, a batch PF system was tested to valorize the DFE generated in the previously conducted DF phase for growing PPB and producing hydrogen, thus maximizing the overall conversion efficiency of the integrated process. The test was conducted by comparing the performance of two PPB strains (*Rhodopseudomonas palustris* and *Rhodospirillum rubrum*) in growing on synthetic medium (RPP medium) and on diluted DFE (labeled FB medium). For further details on the methodological approach and experimental setup of the test, refer to section 3.3.1.

In Figure 45, the biomass growth of the different conditions is reported.

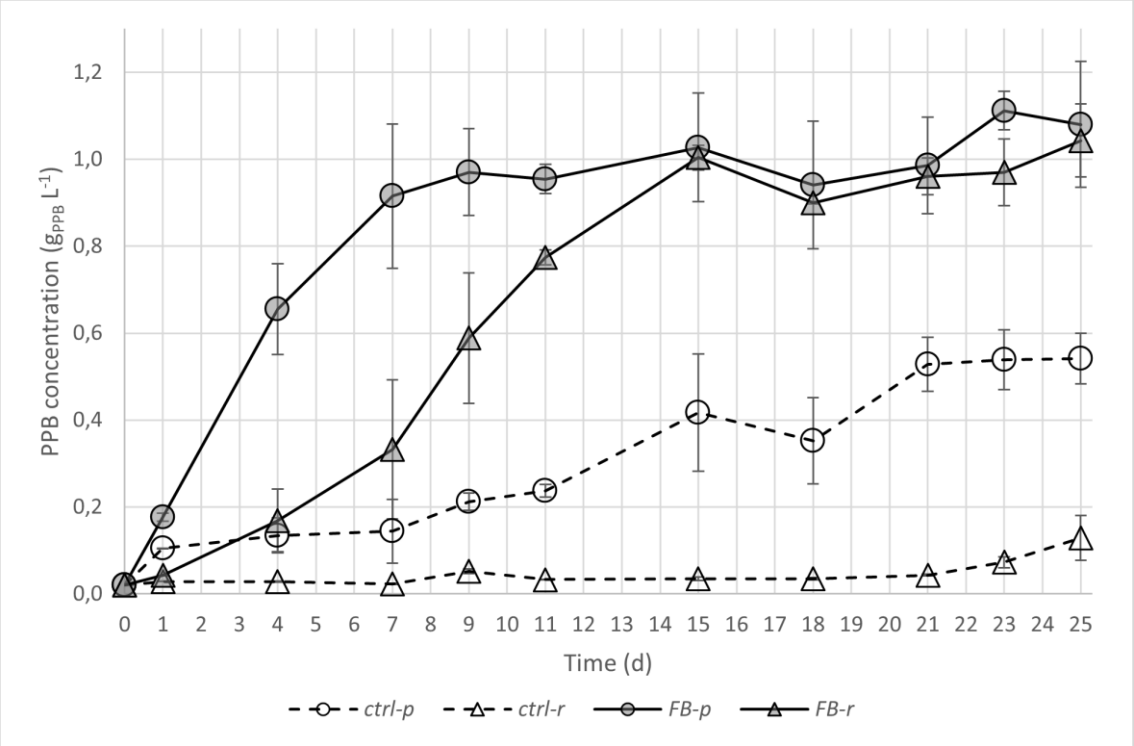


*Figure 45, Biomass concentration of Rps. palustris and Rsp. rubrum on RPP and FB media*

Both the PPB strains reached a higher biomass concentration when fed with the FB medium (1.08 and 1.04 $g_{PPB}$ $L^{-1}$, for *FB-p* and *FB-r* conditions, respectively) compared with RPP medium (0.54 and 0.13 $g_{PPB}$ $L^{-1}$, for *ctrl-p* and *ctrl-r*, respectively). Maximum productivity and maximum growth rate (reported in Table 31) also improved when growing under FB medium. Being all kinetic parameters higher in *FB* conditions, both strains demonstrated the capability to successfully exploit a heterogenous carbon source for their growth. Similar findings were reported by Hu et al. (2018), who observed that, while other strains selectively consume specific carbon sources, *Rsp. rubrum* and *Rps. palustris* could metabolize a variety of carbon sources (acetate, butyrate, lactate, and malate) for growth and hydrogen production. Additionally, their study found that *Rps. palustris* grew faster than the other tested PPB and showed high efficiency across a broad range of light and carbon sources, consistent with the results of this test.

*Table 31, Growth yields obtained throughout Test 5*

| Test | PPB concentration [$g_{PPB}$ $L^{-1}$] | Productivity [$mg_{PPB}$ $L^{-1}$ $d^{-1}$] | μ [$d^{-1}$] |
|---|---|---|---|
| ctrl-p | 0.54 ± 0.06 | 84.31 | 4.43 |
| FB-p | 1.08 ± 0.14 | 159.53 | 5.05 |
| ctrl-r | 0.13 ± 0.05 | 28.09 | 2.16 |
| FB-r | 1.04 ± 0.08 | 128.32 | 3.76 |

Figure 46 illustrates the trend in carbon source consumption throughout the experiment. Under control conditions (left panel of Figure 46), both strains exhibit malic acid consumption, with concentrations decreasing from the initial 2.86 $g_{COD}$ $L^{-1}$ to 0.85 and 1.94 $g_{COD}$ $L^{-1}$, for *Rps. palustris* and *Rsp. rubrum*, respectively. Malic acid consumption was more pronounced in *Rps. palustris* (70 % consumed) rather than in *Rsp. rubrum* (32 % consumed). This is consistent with the higher biomass production observed for the former, where the decrease in malic acid concentration is most likely associated with the metabolization of this compound as a carbon

source for biomass production. When the strains were cultivated on FB medium (right panel of Figure 46), although a decrease in the VFA concentration was observed (1.45 $g_{COD}$ $L^{-1}$ at the end of the test in both conditions, corresponding to a 48 % decrease), the consumption pattern is less consistent, as substantial fluctuations in both VFA profile and concentration were reported.

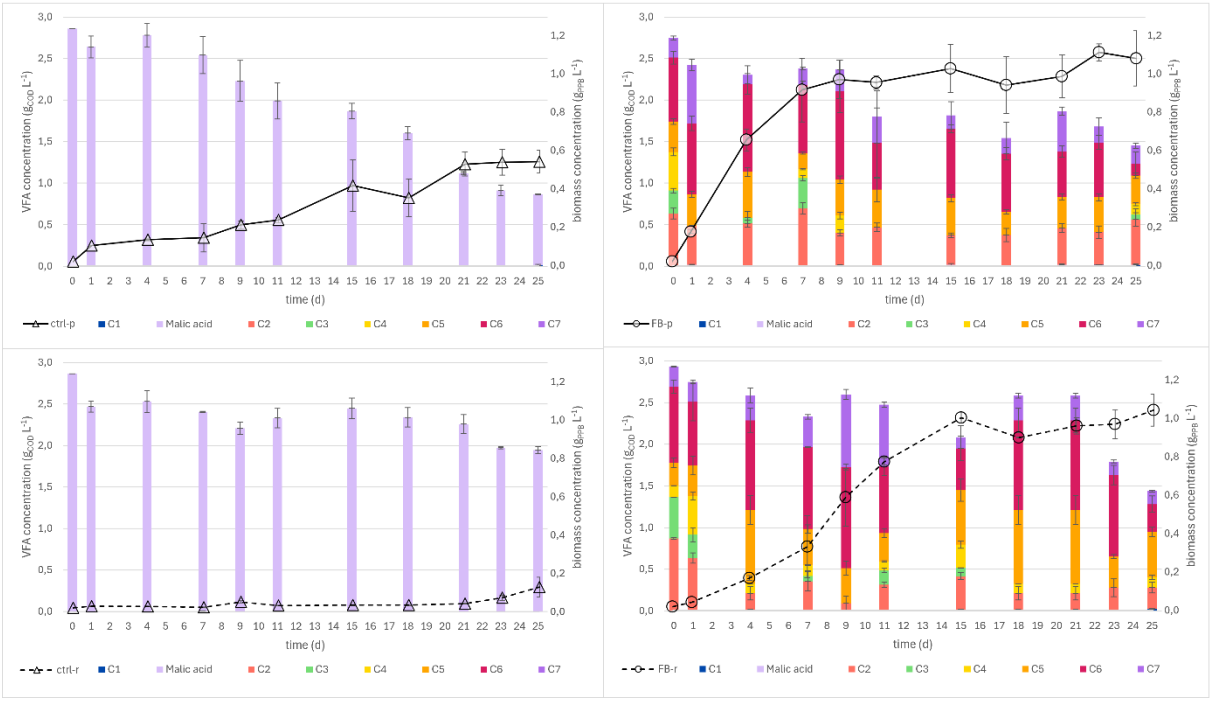


*Figure 46, Profile of the VFA and malic acid consumption throughout Test 5. In the top row, Rps. Palustris on RPP medium (left) and FB medium (right), on the bottom row Rsp. rubrum on RPP medium (left) and FB medium (right)*

Additionally, no significant gas production was detected throughout the test. The most likely reason for this outcome lies in the high ammonium concentration of the FB medium (87 ± 9 $mg_{NH4+}$ $L^{-1}$). Despite hydrogen production by PPB being reported even at higher ammonium concentrations (180 $mg_{NH4+}$ $L^{-1}$, Waligórska et al., 2009), optimal hydrogen production is only achievable at concentrations below 13 – 26 $mg_{NH4+}$ $L^{-1}$ (Capson-Tojo et al., 2020). Ammonium, in fact, is a well-known limiting factor affecting nitrogenase activity and synthesis, effectively shifting the microbial metabolism from hydrogen evolution to ammonium

assimilation and biomass growth (Adessi & De Philippis, 2014). Given that hydrogen production was the main goal of the test, a higher dilution rate of the DFE should have been considered to reduce its inhibitory effect. However, no hydrogen production was observed under control conditions either, suggesting that ammonium concentration was not the primary reason why this outcome remained unattained, or at least not the sole one. Another possible explanation may be related to the employed monitoring methodology, particularly the frequency of sampling for biomass concentration determination. Although each sampling involved the withdrawal of only a few milliliters, its frequency could have led to undesired gas leakage, air infiltration within the system, or perturbances in headspace pressure, potentially compromising the effectiveness of the gas measurement procedure.

The test, however, highlights the feasibility of cultivating these strains on a medium with mixed VFA as the carbon source, consistent with the results of several other studies (Adessi, 2013; Hu et al., 2018; Zhang et al., 2017, 2018).

Further tests should be carried out to correct the operative conditions (lighting system and illuminated surface) or to establish a more effective pretreatment of the fermentative broth, to ensure PPB growth as well as hydrogen production.

## 5.2. Test 6: Biological Hydrogen Production from Organic Wastes Fermentation Effluent: Testing Mutant Strains of *Rhodopseudomonas palustris*

Test 6 evaluated the performance of mutated strains of *Rhodopseudomonas palustris* in converting the previously generated DFE into hydrogen. Four strains were tested: a wild-type *Rps. palustris* CGA009; *Rps. palustris* CGA4001 (*Δhup*S); *Rps. palustris* CGA4003 (*Δhup*S, NifA*); and *Rps. palustris* CGA4017 (*Δhup*S, NifA*, Δ*cbb*M, Δ*cbb*LS, Δ*cbb*P::*kmR*). All strains

were acclimated to synthetic medium (*phase 1*) and then inoculated with diluted DFE (*phase 2* and *phase 3*). For details on the strains and methods employed, refer to section 3.2.2.

During *phase 1*, the monitoring process was limited to observing the bacterial culture for any visible hydrogen production; thus, no quantitative data was recorded. The first strain to show hydrogen production was CGA4001 (at day 4), followed by CGA4003 (at day 7). CGA4017 showed some hydrogen production around day 14, but the amount was relatively low compared to the other strains. CGA009 did not exhibit any hydrogen formation. All the mutant strains appeared to adapt to the medium faster compared to the wild-type strain and were able to exhibit some gas production. All strains grew successfully in the $RPP_{(acetic)}$ medium, resulting in a final biomass concentration of 456 ± 51 (CGA009), 600 ± 58 (CGA4001), 633 ± 58 (CGA4003), and 489 ± 19 (CGA4017) $mg_{PPB}\ L^{-1}$. It can be observed that the two strains that resulted in a more abundant and early gas production were the ones that reached a higher biomass concentration at the end of the test (CGA4001 and CGA4003). However, since the monitoring in this phase provided only qualitative data, with no determination of hydrogen production or substrate consumption, it is not possible to draw further and more detailed conclusions.

*Phase 2* was designed as an initial adaptation stage to the growth medium derived from the DFE. As shown in Figure 47, all strains grew successfully in the $FB_{(acclimatation)}$ medium during this phase. The figure shows the DW of the strains, the BChl *a* content of the biomass, and the $NH_4^+$ concentration recorded during this experimental phase.

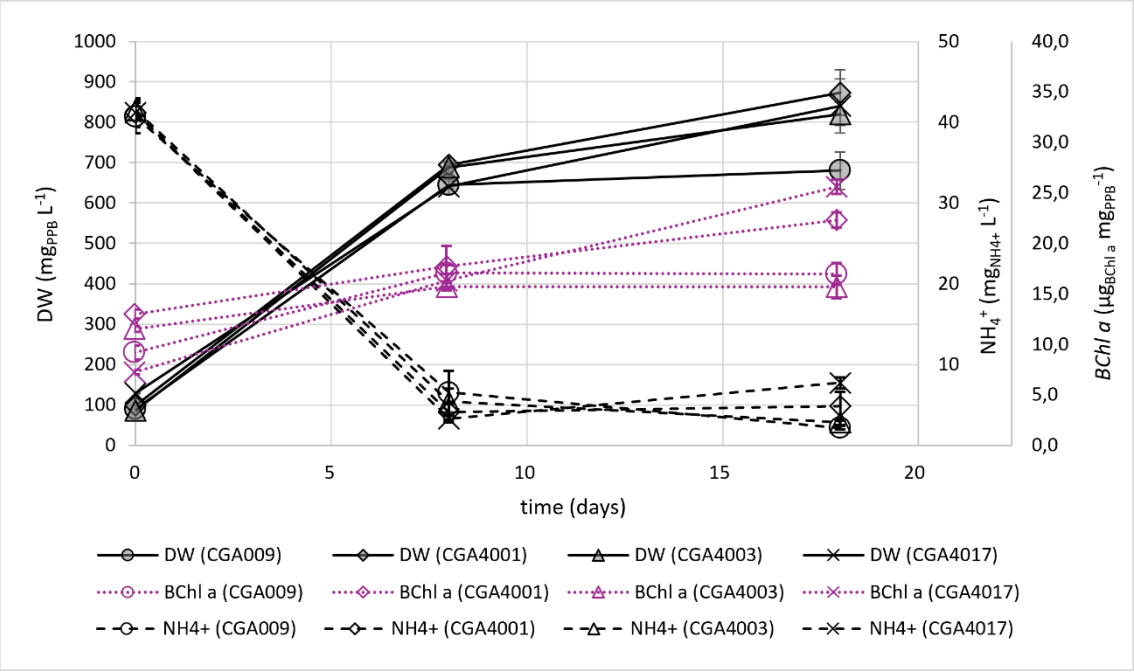


*Figure 47, Biomass growth, ammonium concentration, and bacteriochlorophyll a content of the tested strains during phase 2 of Test 6*

All tested strains show similar behavior both in terms of growth rates and ammonium consumption. Ammonium was significantly consumed in the first days of the test, with nitrogen removal yields ranging from 84 to 92 % on day 8$^{th}$. The same timeframe was associated with a substantial increase in biomass concentration across all strains, highlighting the direct relationship between nitrogen assimilation and microbial growth, as reported by several authors (Androga et al., 2011; Capson-Tojo et al., 2020). Unfortunately, due to the limited number of samples withdrawn during the test, it was not possible to accurately track the kinetics of bacterial growth and ammonium removal. Throughout the experimental period, all strains exhibited an increase in bacteriochlorophyll a content. This rise in BChl *a* content is most likely associated with the concurrent increase in biomass concentration, which leads to a self-shading effect. This phenomenon occurs when biomass density increases in a culture, driving PPB to produce more pigments in response to reduced light availability (Carlozzi & Sacchi, 2001). As biomass concentration rises in a reactor, the self-shading effect intensifies,

leading to reduced light availability and lowering system efficiency (Capson-Tojo et al., 2022). Therefore, these parameters need to be carefully monitored and optimized to achieve higher hydrogen production, especially when scaling the system to continuous or semi-continuous processes. The main issue encountered during this phase, however, was related to hydrogen production itself. Hydrogen evolution was relatively low both in produced volume and in reproducibility, with only two bottles of CGA4017 and one of CGA4001 collecting some hydrogen (49 ± 2 and 34 $NmL_{H2}$, respectively). This outcome suggested potential issues with the reactor setup that led to gas leaks. A thorough inspection of all components revealed that the employed one-way valves, despite proper installation, were unable to provide a completely gas-thigh environment. Consequently, the test was interrupted, and the reactor setup was modified by removing the one-way valves and connecting the test bottles directly to the gas-traps, thus minimizing potential gas losses in the subsequent phase.

Figure 48 illustrates the behavior of PPB cultures during *phase 3*. As reported in the previous phase, all strains grew successfully with the diluted DFE, achieving a biomass concentration of 1344 ± 51 and 1156 ± 51 $mg_{PPB}\ L^{-1}$, in CGA4003 and CGA4017, respectively. In most of the tested conditions, an initial decline in BChl *a* concentration was observed, most likely due to the new environmental operative conditions, particularly the greater light availability resulting from the decreased biomass concentration. However, unlike in the previous phase, no clear relationship between BChl *a* content and biomass concentration was observed. Despite a significant increase in biomass concentration, BChl *a* content showed no increasing trend during the test, with values remaining relatively stable within a range of 10 – 20 $\mu g_{BChl\ a}\ mg_{PPB}^{-1}$. Another important difference between the two phases is the reported decreasing trend in ammonium concentrations. Although the ammonium concentration did decrease during the test, the consumption was lower compared to *phase 2*, with removal efficiency ranging around 50–55 % in CGA009 and CGA4001, and 70–75 % in CGA4001 and CGA4017.

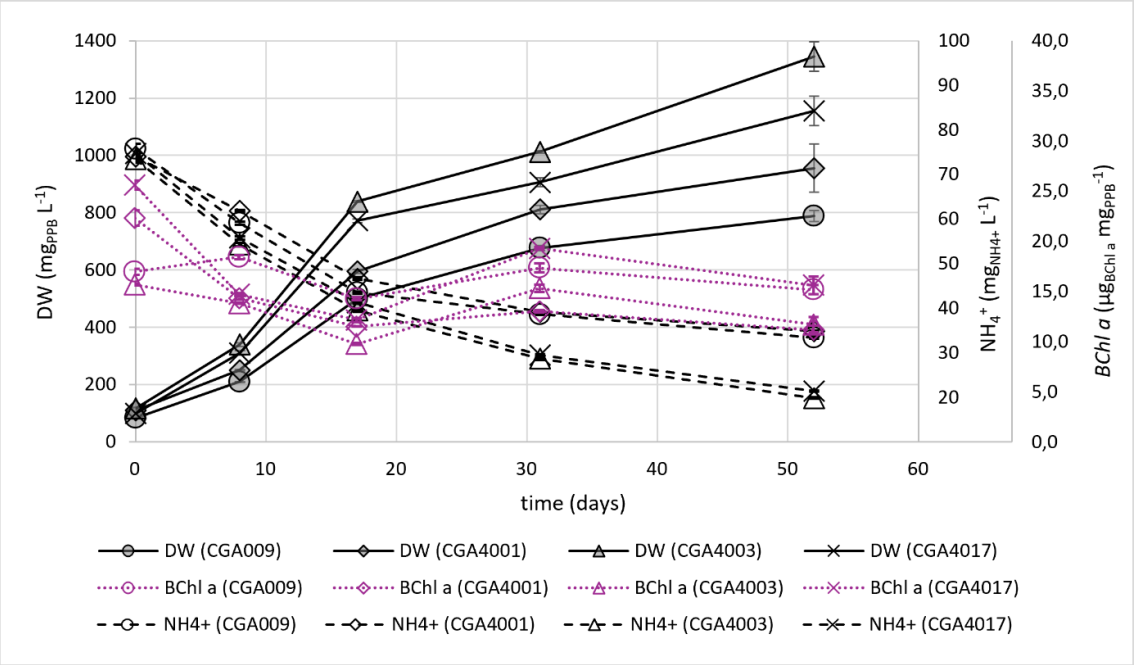


*Figure 48, Biomass growth, ammonium concentration, and bacteriochlorophyll a content of the tested strains during phase 3 of Test 6*

Table 32 summarizes the characteristics of the PPB cultures at the end of each tested phase, regarding biomass concentration, BChl *a* content, ammonium concentration, and its removal.

*Table 32, Physio-chemical characteristics of the PPB cultures at the end of each phase of Test 6*

| | | | *phase 1* | *phase 2* | *phase 3* |
|---|---|---|---|---|---|
| DW | $mg_{PPB}\ L^{-1}$ | CGA009 | 456 ± 51 | 680 ± 46 | 789 ± 19 |
| | | CGA4001 | 600 ± 58 | 873 ± 53 | 956 ± 84 |
| | | CGA4003 | 633 ± 58 | 820 ± 28 | 1344 ± 51 |
| | | CGA4017 | 489 ± 19 | 840 ± 67 | 1156 ± 51 |
| BChl *a* | $\mu g_{BChl\ a}\ mg_{PPB}^{-1}$ | CGA009 | - | 17.0 ± 1.0 | 15.2 ± 0.5 |
| | | CGA4001 | - | 22.3 ± 0.7 | 11.2 ± 0.4 |
| | | CGA4003 | - | 15.7 ± 1.3 | 11.7 ± 0.8 |
| | | CGA4017 | - | 25.6 ± 0.7 | 15.6 ± 0.9 |
| $NH_4^+$ | $mg_{NH4+}\ L^{-1}$ | CGA009 | - | 2.2 ± 0.2 | 33.4 ± 0.3 |
| | | CGA4001 | - | 4.9 ± 0.8 | 34.9 ± 0.1 |
| | | CGA4003 | - | 2.8 ± 0.3 | 19.9 ± 0.2 |
| | | CGA4017 | - | 7.7 ± 0.7 | 21.4 ± 0.1 |
| $NH_4^+$ removal | % | CGA009 | - | 95 ± 6 | 56 ± 2 |
| | | CGA4001 | - | 88 ± 10 | 53 ± 1 |
| | | CGA4003 | - | 93 ± 4 | 73 ± 2 |
| | | CGA4017 | - | 81 ± 7 | 71 ± 1 |

Despite the persistently higher ammonium levels reported during *phase 3*, hydrogen production was detected (Figure 49) and was characterized by substantially higher volumes and reproducibility compared to what was observed in the previous phase. This suggests that the previously reported low hydrogen yields may have been, at least partially, related to gas leakages through the one-way valves, as previously hypothesized.

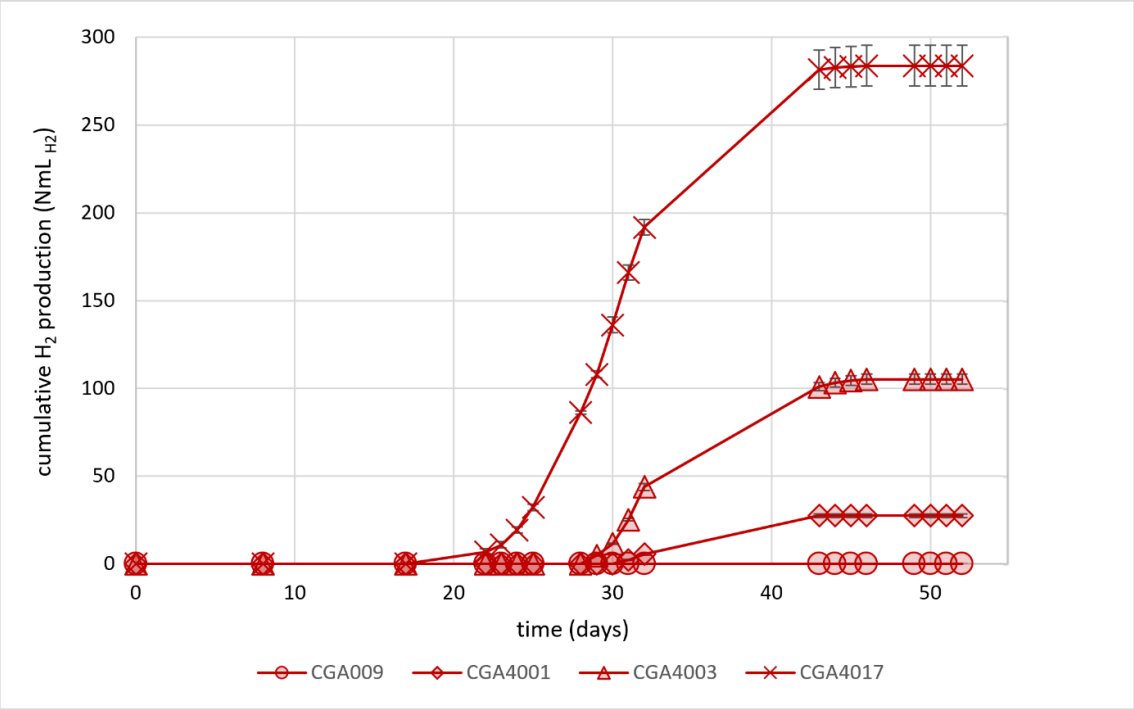


*Figure 49, Biological cumulative hydrogen evolution and substrate conversion efficiency throughout phase 3 of Test 6*

The only strain that did not show any hydrogen production throughout the test was the wild-type CGA009, which lacks specific genetic mutations to cope with ammonium concentrations present in the medium, leading to inhibition of the nitrogenase enzyme and hydrogen production. In contrast, all other strains reported hydrogen production, with the highest hydrogen cumulative production achieved by the two strains characterized by mutations in the *nif*A gene (105 ± 3 $NmL_{H2}$ and 284 ± 12 $NmL_{H2}$, for CGA4003 and CGA4017, respectively). The mutation consists of a deletion that makes NifA*, the transcriptional activator of *nif* genes, constitutively active, enabling the bacteria to activate nitrogenase without being affected by the presence of ammonium. Among the *nif*A-mutated strains, CGA4017 resulted further advantaged by the additional mutations that eliminate Calvin cycle's enzymes RuBisCO and phosphoribulokinase, thereby preventing the competitive pathway of $CO_2$ fixation and allowing for higher hydrogen production. Conversely, *Rps. palustris* CGA4001, which is characterized by the sole deletion of the structural gene of the uptake hydrogenase,

showed an advantage in producing hydrogen over the wild-type, but resulted in lower hydrogen production when compared to the other mutated strains, reaching 27 ± 1 $NmL_{H2}$ at the end of the test.

All the mutated strains faced a long delay before hydrogen evolution, with CGA4017 starting hydrogen production after 23 days, and CGA4003 and CGA4001 after 29 and 31 days, respectively. This delay, which was less evident in *phase 2* where CGA4001 began producing hydrogen after 4 days and CGA4017 after 11, might be due to the higher initial ammonium concentration set up in this phase, which was 74 ± 1 $mg_{NH4+}$ $L^{-1}$ instead of 49 ± 1 $mg_{NH4+}$ $L^{-1}$. Another potential factor contributing to this prolonged delay may be the occurrence of a malfunction caused by the removal of the one-way valves. On day 7$^{th}$, in fact, some of the liquid contained in the gas-traps unintentionally entered the test bottles, causing the pH to rise to values close to 9. This liquid backflow was likely caused by the combination of two factors: the absence of one-way valves, which would have prevented liquid from rising back into the bottles, and the absence of an initial flushing of the headspace of the bottles with inert gas, such as argon, which was not available at the time. PPB, in fact, are capable of fixing gaseous nitrogen as ammonium. The consumption of the nitrogen present in the headspace of the bottles, which, not being flushed with a suitable gas, was initially composed by air, caused a reduction in pressure and, with no one-way valves to stop the flow, led to the backflow of some of the solution from the gas-trap into the bottle. To restore the operative conditions of the test, the pH of each bottle was brought back to 6.8 by dosing an HCl 1N solution. Then, to avoid this issue from recurring, the connections to the gas-traps were sealed with Mohr pipe clamps and reopened only after confirming a slight overpressure in the headspace of the test bottles.

*Table 33, Hydrogen production yields obtained in each phase of Test 6*

| | | | *phase 1* | *phase 2* | *phase 3* |
|---|---|---|---|---|---|
| total $H_2$ produced | $NmL_{H2}$ | CGA009 | - | 0 ± 0 | 0 ± 0 |
| | | CGA4001 | - | 34[a] | 27 ± 1 |
| | | CGA4003 | - | 0 ± 0 | 105 ± 3 |
| | | CGA4017 | - | 49 ± 2 | 284 ± 12 |
| HPR | $NmL_{H2}\ L_{reactor}^{-1}\ d^{-1}$ | CGA009 | - | 0 ± 0 | 0 ± 0 |
| | | CGA4001 | - | 13[a] | 13 ± 1 |
| | | CGA4003 | - | 0 ± 0 | 75 ± 2 |
| | | CGA4017 | - | 32 ± 1 | 120 ± 5 |
| $H_2$ yield | $NmL_{H2}\ g_{COD}^{-1}$ | CGA009 | - | 0 ± 0 | 0 ± 0 |
| | | CGA4001 | - | 37[a] | 19 ± 1 |
| | | CGA4003 | - | 0 ± 0 | 74 ± 2 |
| | | CGA4017 | - | 53 ± 2 | 200 ± 8 |

[a] no standard deviation available due to failure in the gas collecting system

The maximum HPR of 120 ± 5 $NmL_{H2}\ L_{reactor}^{-1}\ d^{-1}$ was reported for *Rps. palustris* CGA4017 and was achieved on day 31st during phase 3. When testing DF processes, significantly higher production rates were reported, with 200 $NmL_{H2}\ L_{reactor}^{-1}\ h^{-1}$ and 650 $NmL_{H2}\ L_{reactor}^{-1}\ d^{-1}$ achieved under batch and continuous conditions, respectively (Test 2 and Test3, Section 4.2 and 4.3). It is well known, in fact, that PF is characterized by much lower substrate utilization and product formation rates compared to DF (Ghosh et al., 2018). However, the PF process allows for a substantially higher conversion of organic compounds into hydrogen (Ghosh et al., 2017). During phase 3, for instance, *Rps. palustris* CGA4017 achieved a conversion efficiency of 200 ± 8 $NmL_{H2}\ g_{COD}^{-1}$, higher than the yields obtained during the abovementioned DF phases, corresponding to 29 ± 1 and 54 ± 10 $NmL_{H2}\ g_{TVS}^{-1}$, under batch and continuous conditions, respectively (Test 2 and Test3, Section 4.2 and 4.3). Despite highlighting the potential role of

mutated strains in enhancing process efficiency, the yields achieved under each tested strain were lower than those reported in literature, generally ranging between 400 and 800 $NmL_{H2}\ g_{COD}^{-1}$ for the PF phase of integrated DF–PF systems (see Table 5, Section 2.5.3, Laurinavichene et al., 2010; Niño-Navarro et al., 2020; Su et al., 2010; Zong et al., 2009). A possible explanation for this outcome is associated with the VFA profile of the DFE, which could have possibly facilitated PHA accumulation rather than hydrogen production (Hustede et al., 1993; Kim et al., 2012). The determination of the PHA content accumulated in the PPB biomass would have provided deeper insights into the dominant metabolic pathways of the process and is consequently recommended for further investigation. Another possible reason for this discrepancy, as previously mentioned, could be the abrupt pH increase caused by the malfunction linked with the removal of the one-way valves that, although promptly addressed, may have affected microbial activity and overall process efficiency.

In the speculative scenario of direct integration of the DF process for FW and WAS valorization (Test 3, Section 4.3) with a PF phase employing *Rps. palustris* CGA4017, the coupling of the system would enhance the overall yield of the process. The initial DF phase of the substrates would possibly yield 54 ± 10 $NL_{H2}\ kg_{TVS}^{-1}$, while producing a DFE containing 0.31 – 0.42 $kg_{VFA(COD)}\ kg_{TVS}^{-1}$ (according to the AY obtained during Test 1, Section 4.1). The subsequent PF phase would convert these residual organic compounds into hydrogen, with a yield of 200 ± 8 $NL_{H2}\ kg_{COD}^{-1}$, corresponding to 62 – 84 $NL_{H2}\ kg_{TVS}^{-1}$ when considering the volatile solids initially fed into the DF reactor. The sequential integration of the two phases would result in a total hydrogen yield of 116 – 138 $NL_{H2}\ kg_{TVS}^{-1}$, thus enhancing the individual yield achievable with the single processes.

## 5.3. General Conclusions

The experiments confirmed the feasibility of growing PPB on DFE, potentially enabling the conversion into hydrogen of the residual fraction of organic carbon sources remaining after DF. Under the first batch experiment, two strains of PPB, namely *Rps. palustris* and *Rsp. rubrum*, were compared in terms of their adaptation to a DFE-based medium and their capability to produce hydrogen. The results of this first test emphasized the potential utilization of PPB for DFE treatment, as both strains reported substantially higher growth yields compared to those achieved when growing on a synthetic medium. However, no hydrogen production was detected, suggesting the presence of some inhibitory compound in the treated effluent which hindered the process. High ammonium concentration in the effluent was identified as the main factor contributing to this outcome. Although proper dilution pretreatment, ammonium concentration remained at around 87 $mg_{NH4+}$ $L^{-1}$, much higher than the suggested ammonium threshold for PF (13–26 $mg_{NH4+}$ $L^{-1}$ Capson-Tojo et al., 2020). Given these results, ammonium-resistant PPB strains were investigated. Four *Rps. palustris* strains were employed to assess how different mutations affected the process yields. The mutations included uptake hydrogenase deletion, constitutive activation of nitrogenase, and the removal of RuBisCO and phosphoribulokinase enzymes. The mutated strains were capable of producing hydrogen despite the high ammonium concentration of the DFE, highlighting their potential role in improving DF–PF integration.

## 5.4. References

Adessi, A., & De Philippis, R. (2014). Photobioreactor design and illumination systems for H2 production with anoxygenic photosynthetic bacteria: A review. In *International Journal of Hydrogen Energy* (Vol. 39, Issue 7, pp. 3127–3141). Elsevier Ltd. https://doi.org/10.1016/j.ijhydene.2013.12.084

Adessi, Alessandra. (2013). *Hydrogen production using Purple Non-Sulfur Bacteria (PNSB) cultivated under natural or artificial light conditions with synthetic or fermentation derived substrates*. Firenze University Press.

Androga, D. D., Özgür, E., Eroglu, I., Gündüz, U., & Yücel, M. (2011). Significance of carbon to nitrogen ratio on the long-term stability of continuous photofermentative hydrogen production. *International Journal of Hydrogen Energy*, *36*(24), 15583–15594. https://doi.org/10.1016/j.ijhydene.2011.09.043

Capson-Tojo, G., Batstone, D. J., Grassino, M., & Hülsen, T. (2022). Light attenuation in enriched purple phototrophic bacteria cultures: Implications for modelling and reactor design. *Water Research*, *219*. https://doi.org/10.1016/j.watres.2022.118572

Capson-Tojo, G., Batstone, D. J., Grassino, M., Vlaeminck, S. E., Puyol, D., Verstraete, W., Kleerebezem, R., Oehmen, A., Ghimire, A., Pikaar, I., Lema, J. M., & Hülsen, T. (2020). Purple phototrophic bacteria for resource recovery: Challenges and opportunities. In *Biotechnology Advances* (Vol. 43). Elsevier Inc. https://doi.org/10.1016/j.biotechadv.2020.107567

Carlozzi, P., & Sacchi, A. (2001). Biomass production and studies on Rhodopseudomonas palustris grown in an outdoor, temperature controlled, underwater tubular photobioreactor. In *Journal of Biotechnology* (Vol. 88). www.elsevier.com/locate/jbiotec

Ghosh, S., Chowdhury, R., & Bhattacharya, P. (2018). A review on single stage integrated dark-photo fermentative biohydrogen production: Insight into salient strategies and scopes. In *International Journal of Hydrogen Energy* (pp. 2091–2107). Elsevier Ltd. https://doi.org/10.1016/j.ijhydene.2017.12.018

Ghosh, S., Dairkee, U. K., Chowdhury, R., & Bhattacharya, P. (2017). Hydrogen from food processing wastes via photofermentation using Purple Non-sulfur Bacteria (PNSB) – A review. In *Energy Conversion and Management* (Vol. 141, pp. 299–314). Elsevier Ltd. https://doi.org/10.1016/j.enconman.2016.09.001

Hu, C., Choy, S. Y., & Giannis, A. (2018). Evaluation of Lighting Systems, Carbon Sources, and Bacteria Cultures on Photofermentative Hydrogen Production. *Applied Biochemistry and Biotechnology*, *185*(1), 257–269. https://doi.org/10.1007/s12010-017-2655-5

Hustede, E., Steinbiichel, A., & Schlegel, H. G. (1993). Relationship between the photoproduction of hydrogen and the accumulation of PHB in non-sulphur purple bacteria. *Appl Microbiol Biotechnol*, *39*, 87–93.

Kim, D. H., Son, H., & Kim, M. S. (2012). Effect of substrate concentration on continuous Photo-fermentative hydrogen production from lactate using Rhodobacter sphaeroides. *International Journal of Hydrogen Energy*, *37*(20), 15483–15488. https://doi.org/10.1016/j.ijhydene.2012.02.039

Laurinavichene, T. V., Belokopytov, B. F., Laurinavichius, K. S., Tekucheva, D. N., Seibert, M., & Tsygankov, A. A. (2010). Towards the integration of dark- and photo-fermentative waste treatment. 3. Potato as substrate for sequential dark fermentation and light-driven H 2

production. *International Journal of Hydrogen Energy*, *35*(16), 8536–8543. https://doi.org/10.1016/j.ijhydene.2010.02.063

Niño-Navarro, C., Chairez, I., Christen, P., Canul-Chan, M., & García-Peña, E. I. (2020). Enhanced hydrogen production by a sequential dark and photo fermentation process: Effects of initial feedstock composition, dilution and microbial population. *Renewable Energy*, *147*, 924–936. https://doi.org/10.1016/j.renene.2019.09.024

Su, H., Cheng, J., Zhou, J., Song, W., & Cen, K. (2010). Hydrogen production from water hyacinth through dark- and photo- fermentation. *International Journal of Hydrogen Energy*, *35*(17), 8929–8937. https://doi.org/10.1016/j.ijhydene.2010.06.035

Waligórska, M., Seifert, K., Górecki, K., Moritz, M., & Łaniecki, M. (2009). Kinetic model of hydrogen generation by Rhodobacter sphaeroides in the presence of NH4+ ions. *Journal of Applied Microbiology*, *107*(4), 1308–1318. https://doi.org/10.1111/j.1365-2672.2009.04314.x

Zhang, Q., Lee, D. J., Wang, Y., Zhang, Z., Lee, D. J., Zhou, X., Jing, Y., Jiang, D., Hu, J., & He, C. (2017). Photo-fermentative hydrogen production from crop residue: A mini review. In *Bioresource Technology* (Vol. 229, pp. 222–230). Elsevier Ltd. https://doi.org/10.1016/j.biortech.2017.01.008

Zhang, Q., Zhang, Z., Wang, Y., Lee, D. J., Li, G., Zhou, X., Jiang, D., Xu, B., Lu, C., Li, Y., & Ge, X. (2018). Sequential dark and photo fermentation hydrogen production from hydrolyzed corn stover: A pilot test using 11 m3 reactor. *Bioresource Technology*, *253*, 382–386. https://doi.org/10.1016/j.biortech.2018.01.017

Zong, W., Yu, R., Zhang, P., Fan, M., & Zhou, Z. (2009). Efficient hydrogen gas production from cassava and food waste by a two-step process of dark fermentation and photo-fermentation. *Biomass and Bioenergy*, *33*(10), 1458–1463. https://doi.org/10.1016/j.biombioe.2009.06.008

# 6. Results: Biological Methanation Tests

## 6.1. Test 7: Evaluation of Hydrogenotrophic Bio-Methanation on suspended biomass and granular sludge

Test 7 explored the potential utilization of hydrogen for biological methanation. The experiment compared the performance of two biomass typologies: suspended biomass (trials S1, S2a, and S2b) and granular sludge (trials G1, G2a, and G2b). Both inocula were tested under batch conditions, suppling hydrogen and carbon dioxide in a 4:1 ratio, according to the stochiometric proportion of bio-methanation. Three trials were conducted for each inoculum: one with a lower hydrogen supply (16.5 $mmol_{H2}$, S1 and G1) and two with a higher hydrogen feeding (24.8 $mmol_{H2}$, S2a, S2b, G2a, and G2b). Refer to section 3.4.1 for a detailed description of the methodological approach and the experimental setup of the test.

Figure 50 shows the cumulative methane produced during the three trials of suspended anaerobic biomass, expressed as volume at normal conditions of pressure (1 atm) and temperature (0 °C).

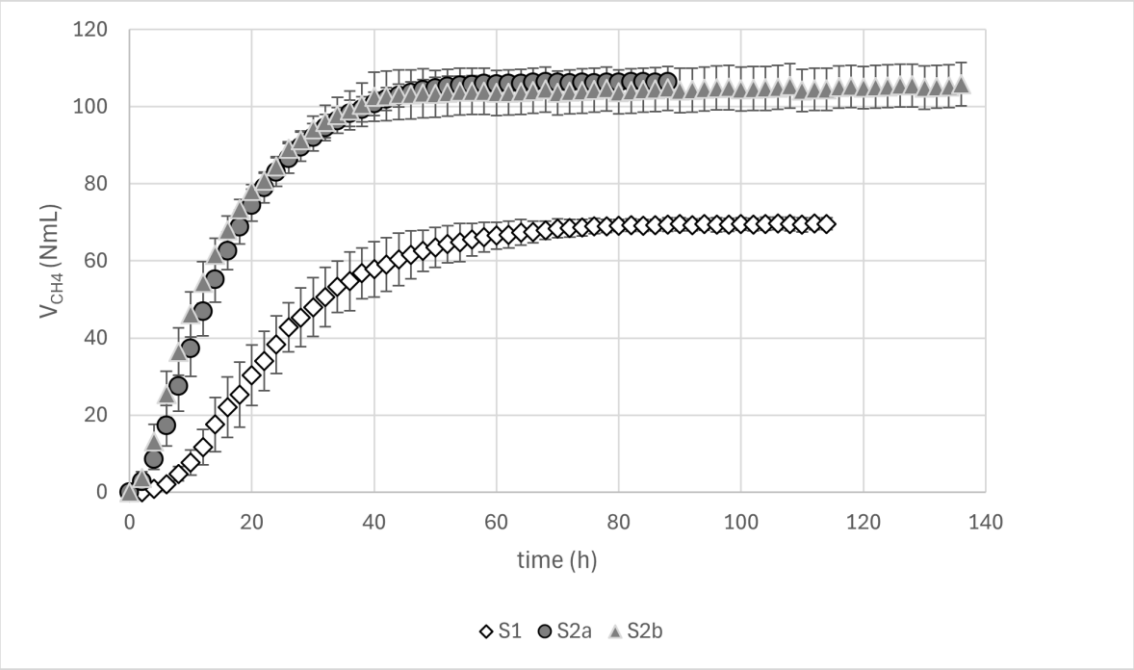


*Figure 50, Cumulative methane production from suspended biomass through bio-methanation during Test 7*

It is important to note that, differently from the DF and PF tests conducted, the volume of gas produced in these experiments is not directly measured and stored in gas-sampling bags (as in DF tests) or gas-traps (as in PF tests) but rather calculated based on the pressure difference recorded throughout the process. This methodology, as proposed by (Coates et al., 1996) and (Ripoll et al., 2020), relies on the stoichiometry of the bio-methanation reaction, where 5 moles of gaseous substrates are consumed for each mole of methane produced. Since the reaction occurs within a fixed headspace volume and at a constant temperature, the difference in moles of the gaseous mixture results in a pressure drop, which is used to estimate methane production.

Given the lower hydrogen supply provided as a substrate during trial S1, the resulting methane production was lower (70 ± 1 $NmL_{CH4}$) compared to trials S2a and S2b (106 ± 1 and 105 ± 4 $NmL_{CH4}$, respectively). These latter two trials, which received a higher hydrogen input, followed similar production trends with no substantial differences.

Figure 51 illustrates the methane production yields, further highlighting the weight of the amount of substrate supplied in defining the cumulative production.

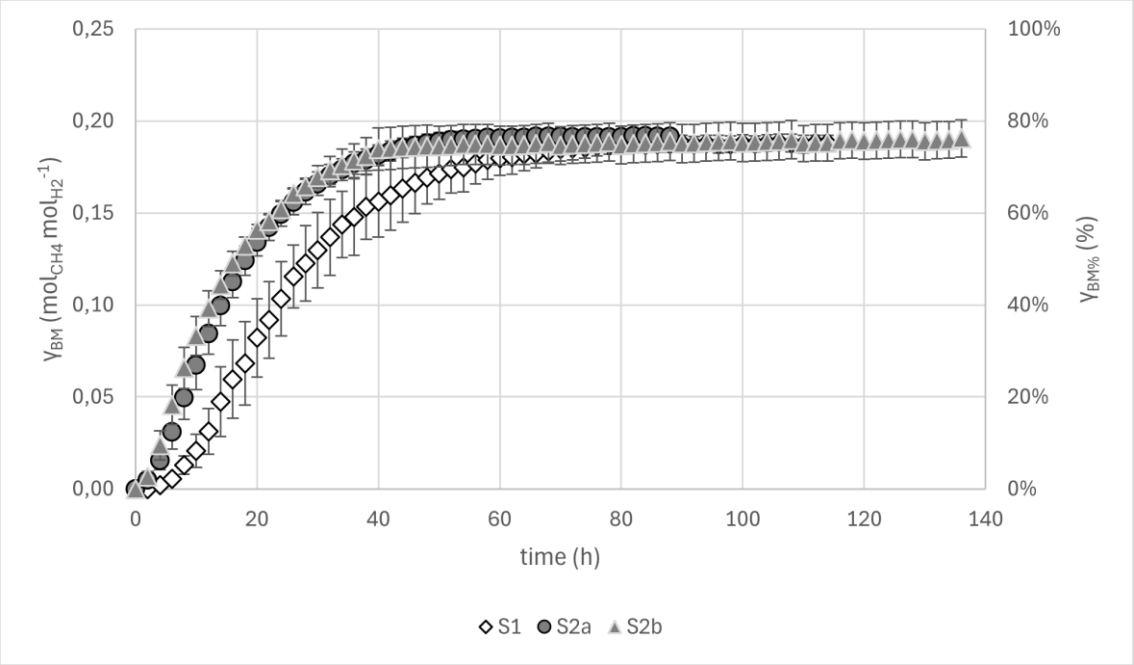


*Figure 51, Methane production yield achieved by suspended biomass during Test 7*

The yields are expressed as moles of methane produced per mole of hydrogen supplied ($mol_{CH4}\, mol_{H2}^{-1}$) and as a percentage of the maximum theoretical conversion efficiency, corresponding to one mole of methane produced for every four moles of hydrogen supplied. From this perspective, all the conducted trials reported similar yields, ranging at the end of the test between 0.188 – 0.192 $mol_{CH4}\, mol_{H2}^{-1}$, corresponding to 75 – 77 % of the maximum theoretical conversion efficiency.

Figure 52 shows the Specific Hydrogenotrophic Methanogenic Activity (SHMA) of the suspended biomass.

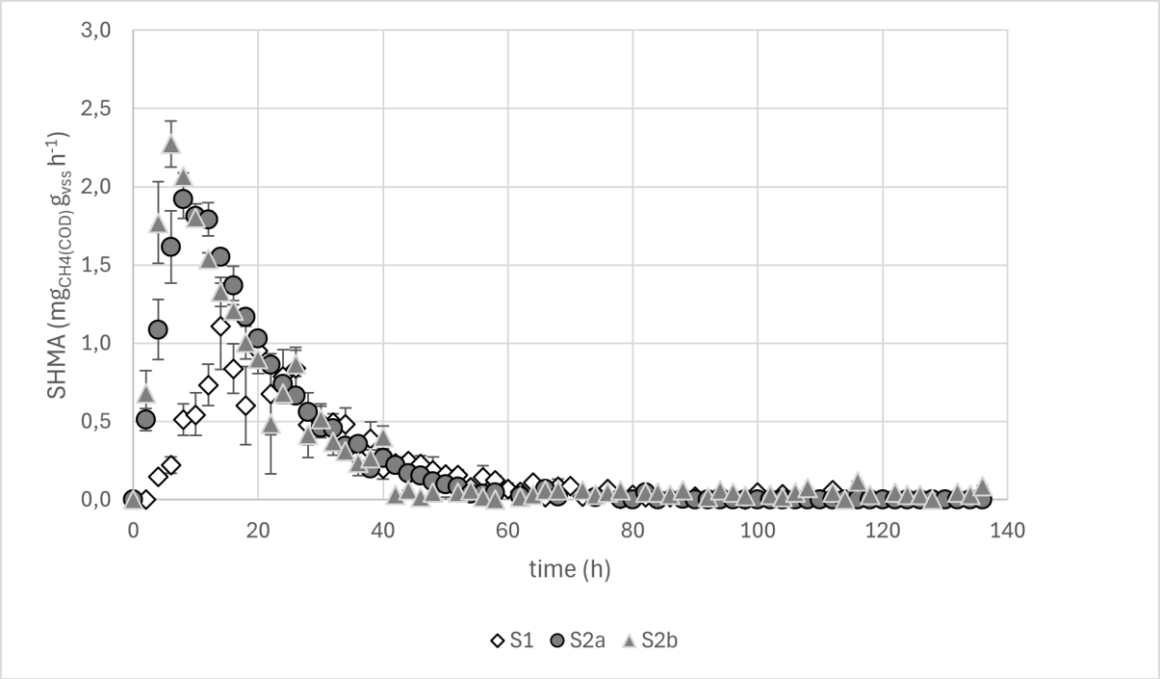


*Figure 52, Specific Hydrogenotrophic Methanogenic Activity (SHMA) achieved by suspended biomass during Test 7*

Among the different trials, S1 resulted in the lowest value of maximum SHMA, corresponding to 1.1 ± 0.3 $mg_{CH4(COD)}$ $g_{VSS}^{-1}$ $h^{-1}$, while in S2a and S2b this value progressively increased, from 1.9 ± 0.1 to 2.3 ± 0.1 $mg_{CH4(COD)}$ $g_{VSS}^{-1}$ $h^{-1}$. The achieved values are consistent with those reported by Liu et al., (2016), Hao et al., (2017), and Pokorna et al., (2019), reporting SHMA values for suspended biomass ranging between 0.8 to 2.5 $mg_{CH4(COD)}$ $g_{VSS}^{-1}$ $h^{-1}$. The lower biomass activity observed during trial S1 is most likely primarily associated with the limited substrate availability, which led to a lower partial pressure of hydrogen in the headspace and, thereby, to a slower dissolution of the substrate in the liquid phase, reducing its bioavailability. Additionally, the inoculum was sourced from a full-scale anaerobic digester treating municipal WAS and, therefore, consisted of a mixed consortium not specifically acclimated to utilizing only hydrogen and carbon dioxide as substrates. The progressive enrichment of hydrogenotrophic methanogens within the biomass between trials is likely the reason for the higher SHMA achieved in the last trial conducted.

Similar behaviors were observed in trials conducted with granular sludge, as shown in Figure 53. The first trial (G1) led to overall lower methane production (73 ± 1 $NmL_{CH4}$), mostly due to the lower hydrogen supply. The subsequent two trials (G2a and G2b), given the higher amount of hydrogen fed to the system, resulted in a cumulative production of 112 ± 2 $NmL_{CH4}$.

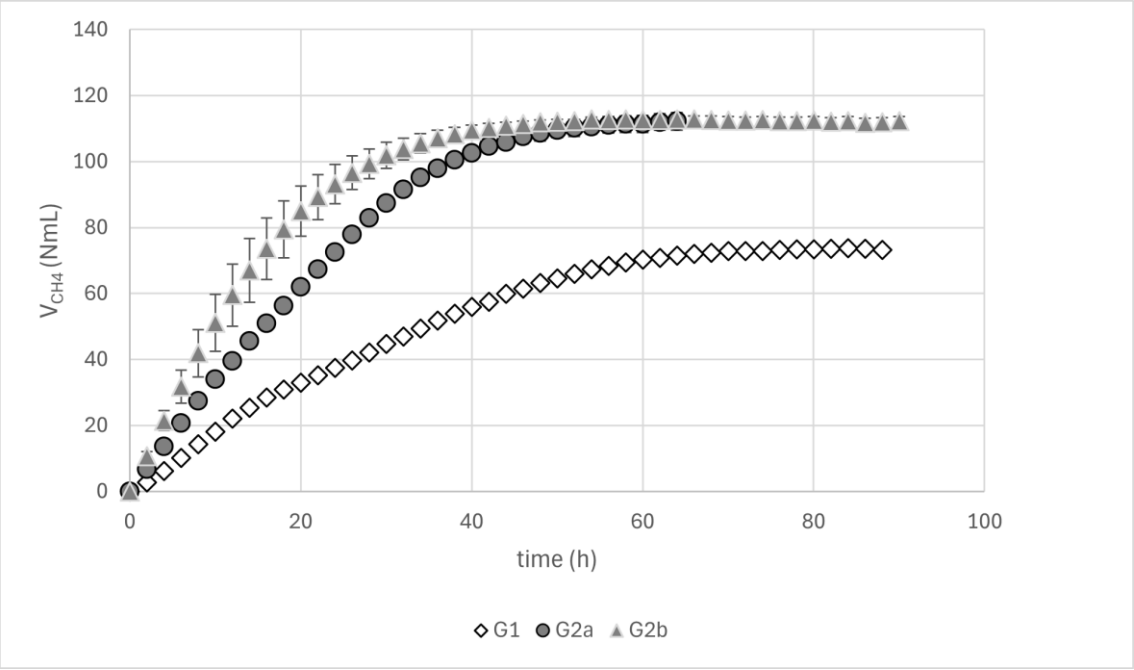


*Figure 53, Cumulative methane production from granular sludge through bio-methanation during Test 7*

When comparing the conversion efficiency, as reported in Figure 54, no significant differences were observed among the yields obtained at the end of each trial. In all conditions, a conversion yield ranging between 0.198 and 0.202 $mol_{CH4}\ mol_{H2}^{-1}$ was achieved, corresponding to 79 – 81 % of the maximum theoretical conversion efficiency. The conversion yields achieved are consistent with those reported by Kozak et al., (2022) and Bassani et al., (2017), who reported 0.18 and 0.19 $mol_{CH4}\ mol_{H2}^{-1}$, respectively.

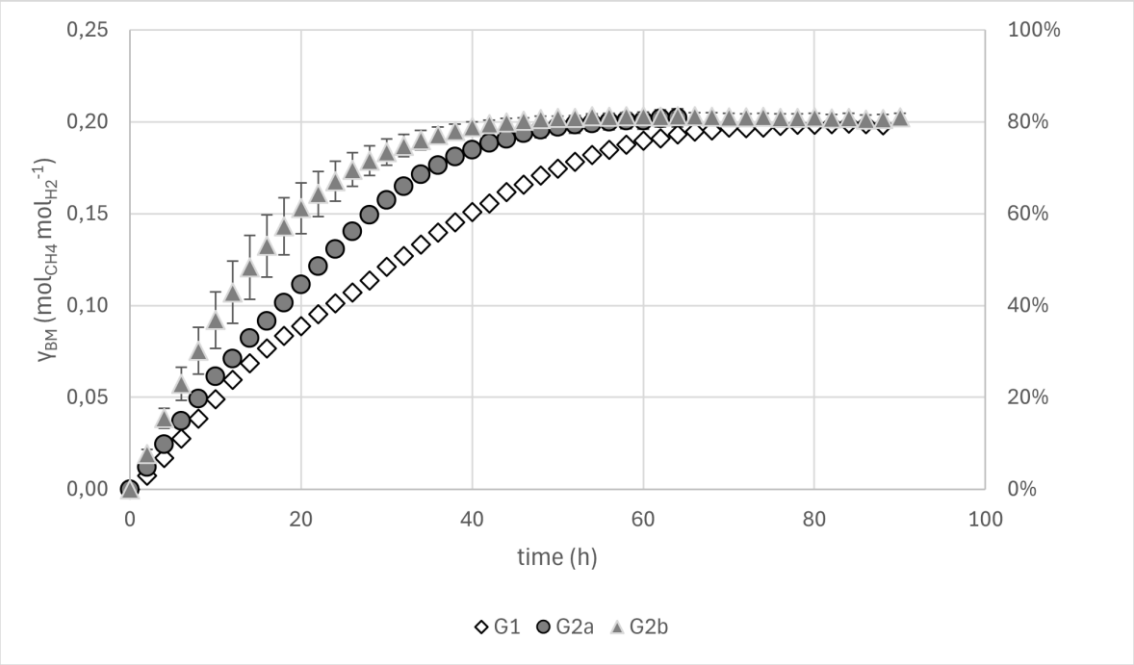


*Figure 54, Methane production yield achieved by granular sludge during Test 7*

Rather than in the yield, each trial differs from the kinetic of the conversion process. This finding is particularly highlighted in Figure 55, which illustrates the SHMA of granular sludge biomass throughout the test. A progressive increase in the SHMA value was observed from trial to trial, rising from $0.8 \pm 0.1$ $mg_{CH4(COD)}$ $g_{VSS}^{-1}$ $h^{-1}$ achieved during G1, to $1.3 \pm 0.1$ and $2.0 \pm 0.3$ $mg_{CH4(COD)}$ $g_{VSS}^{-1}$ $h^{-1}$ achieved in G2a and G2b, respectively. While the lower activity recorded in G1 can be attributed to the lower amount of hydrogen supplied to the system, similarly to what was observed in trial S1, the differences in SHMA value between trials G2a and G2b, given the same substrate was provided, are most likely associated with the progressive enrichment in hydrogenotrophic methanogens within the granular sludge.

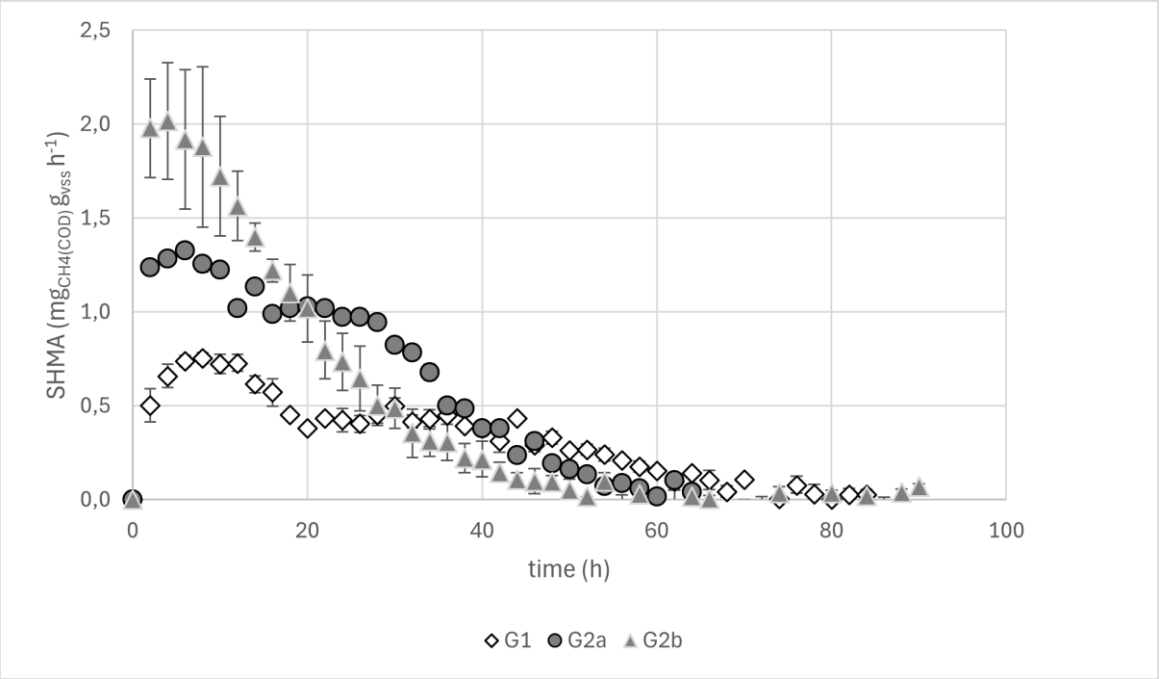


*Figure 55, Specific Hydrogenotrophic Methanogenic Activity (SHMA) achieved by granular sludge during Test 7*

## 6.2. General Conclusions

Table 34 summarizes the yields and activities obtained in each trial conducted.

*Table 34, Cumulative methane production and conversion efficiency parameters for the trials testing suspended biomass (S1, S2a, and S2b) and granular sludge (G1, G2a, and G2b)*

| | | V ($NmL_{CH4}$) | $\gamma_{BM}$ ($mol_{CH4}\ mol_{H2}^{-1}$) | $\gamma_{BM\%}$ (%) | SHMA ($mg_{CH4(COD)}\ g_{VSS}^{-1}\ h^{-1}$) |
|---|---|---|---|---|---|
| Suspended biomass | S1 | 70 ± 1 | 0.188 ± 0.004 | 75 ± 2 | 1.1 ± 0.3 |
| | S2a | 106 ± 1 | 0.192 ± 0.002 | 76.6 ± 1.0 | 1.9 ± 0.1 |
| | S2b | 105 ± 4 | 0.190 ± 0.002 | 75.9 ± 0.8 | 2.3 ± 0.1 |
| Granular sludge | G1 | 73 ± 1 | 0.198 ± 0.001 | 79.4 ± 0.4 | 0.8 ± 0.1 |
| | G2a | 112 ± 2 | 0.201 ± 0.004 | 80 ± 1 | 1.3 ± 0.1 |
| | G2b | 112 ± 1 | 0.202 ± 0.001 | 80.7 ± 0.2 | 2.0 ± 0.3 |

Both suspended and granular sludge resulted in similar yields, with granular sludge yielding slightly higher values in terms of conversion efficiency compared to suspended biomass, but generally slightly lower SHMA. However, while the SHMA values observed for the suspended biomass are consistent with those reported by several authors, typically ranging between 0.8 to 2.5 $mg_{CH4(COD)}$ $g_{VSS}^{-1}$ $h^{-1}$ (Hao et al., 2017; Liu et al., 2016; Pokorna et al., 2019), granular sludge exhibits substantially lower activity compared to the literature. Several authors, in fact, achieved SHMA values ranging between 10 to 30 $mg_{CH4(COD)}$ $g_{VSS}^{-1}$ $h^{-1}$ (Gonzalez-Estrella et al., 2013; Regueiro et al., 2012; Ripoll et al., 2020) when testing granular sludge. Several factors may have contributed to this outcome. The suboptimal gas-liquid mass transfer in the system is most likely one of the main aspects that hindered the process conversion rate. This parameter could have been improved by increasing the agitation or by recirculating the headspace gas through sparging. Additionally, the ratio between the substrate fed and the microorganisms present may have been insufficient to observe the true maximum SHMA for the tested microbial consortia, thereby the lower values achieved may not only be due to substrate solubilization but also to its overall availability. This suggests that the maximum SHMA values for the tested inocula could have been significantly improved by a more precise definition of the operative parameters and reactor configurations.

## 6.3. References

Bassani, I., Kougias, P. G., Treu, L., Porté, H., Campanaro, S., & Angelidaki, I. (2017). Optimization of hydrogen dispersion in thermophilic up-flow reactors for ex situ biogas upgrading. *Bioresource Technology*, *234*, 310–319. https://doi.org/10.1016/j.biortech.2017.03.055

Coates, J. D., Coughlanb, M. F., & Colleranb, E. (1996). Methods Simple method for the measurement of the hydrogenotrophic methanogenic activity of anaerobic sludges. In *Journal ofMicrobiological Journal of Microbiological Methods* (Vol. 26).

Gonzalez-Estrella, J., Sierra-Alvarez, R., & Field, J. A. (2013). Toxicity assessment of inorganic nanoparticles to acetoclastic and hydrogenotrophic methanogenic activity in anaerobic granular sludge. *Journal of Hazardous Materials*, *260*, 278–285. https://doi.org/10.1016/j.jhazmat.2013.05.029

Hao, X., Liu, R., van Loosdrecht, M. C. M., & Cao, D. (2017). Batch influences of exogenous hydrogen on both acidogenesis and methanogenesis of excess sludge. *Chemical Engineering Journal*, *317*, 544–550. https://doi.org/10.1016/j.cej.2017.02.093

Kozak, M., Köroğlu, E. O., Cirik, K., & Zaimoğlu, Z. (2022). Evaluation of ex-situ hydrogen biomethanation at mesophilic and thermophilic temperatures. *International Journal of Hydrogen Energy*, *47*(34), 15434–15441. https://doi.org/10.1016/j.ijhydene.2022.02.072

Liu, C., Li, H., Zhang, Y., & Chen, Q. (2016). Characterization of methanogenic activity during high-solids anaerobic digestion of sewage sludge. *Biochemical Engineering Journal*, *109*, 96–100. https://doi.org/10.1016/j.bej.2016.01.010

Pokorna, D., Varga, Z., Andreides, D., & Zabranska, J. (2019). Adaptation of anaerobic culture to bioconversion of carbon dioxide with hydrogen to biomethane. *Renewable Energy*, *142*, 167–172. https://doi.org/10.1016/j.renene.2019.04.076

Regueiro, L., Veiga, P., Figueroa, M., Alonso-Gutierrez, J., Stams, A. J. M., Lema, J. M., & Carballa, M. (2012). Relationship between microbial activity and microbial community structure in six full-scale anaerobic digesters. *Microbiological Research*, *167*(10), 581–589. https://doi.org/10.1016/j.micres.2012.06.002

Ripoll, E., López, I., & Borzacconi, L. (2020). Hydrogenotrophic activity: A tool to evaluate the kinetics of methanogens. *Journal of Environmental Management*, *270*. https://doi.org/10.1016/j.jenvman.2020.110937

# 7. Conclusions and future perspectives

This thesis investigated the conversion of Food Waste (FW) and Waste Activated Sludge (WAS) into hydrogen through the integration of biological production processes (i.e., Dark and Photo Fermentation) to enhance the production yields and ultimately assess the potential for converting the produced hydrogen into bio-methane through biological methanation. The activities conducted were divided into three main processes: Dark Fermentation tests (DF, **Chapter 4**), Photo Fermentation tests (PF, **Chapter 5**), and Biological Methanation tests (BM, **Chapter 6**). Regarding the DF process (**Chapter 4**), batch and semi-continuous tests, both at laboratory and pilot scale, were conducted to determine the optimal process parameters and assess the scalability of the process. The experiments conducted confirmed the feasibility of a DF co-fermentation system treating FW and WAS. The best process efficiencies were achieved under semi-continuous laboratory scale, where, at stability, a peak SHP of 54 ± 10 $NL_{H2}\ kg_{TVS}^{-1}$, HPR of 0.65 ± 0.12 $NL_{H2}\ L^{-1}\ d^{-1}$, and hydrogen concentrations of 37.5 ± 2.5 % were achieved (Test 3, Section 4.3). These results were obtained at a co-substrate ratio between FW and WAS of 50:50 based on TVS, an OLR of 12 $kg_{TVS}\ m_{-3}\ d_{-1}$, an HRT of 3.1 d, and a pH of 5.5. The achieved yields were higher than those reported by several other authors at similar operative conditions. However, maintaining the same operative parameters while scaling-up the process to pilot scale (Test 4, Section 4.4) resulted in lower yields (SHP of 6 ± 2 $NL_{H2}\ kg_{TVS}^{-1}$, HPR of 0.07 ± 0.03 $NL_{H2}\ L_{reactor}^{-1}\ d^{-1}$) and stability issues, with evidence of a more severe hydrogenotrophic methanogens proliferation. The proliferation of hydrogen-consuming microorganisms was probably due to a combination of different factors, including the selected HRT, the feeding-pause that occurred during the weekend, the absence of inoculum pretreatment, and the scaling-up to a larger reactor volume. To mitigate methanogens' influence on process efficiency, the HRT was shortened to 1.5 d, resulting in doubling the SHP (12 ± 5 $NL_{H2}\ kg_{TVS}^{-1}$) and the HPR (0.14 ± 0.08 $NL_{H2}\ L_{reactor}^{-1}\ d^{-1}$). However, the achieved process yields were substantially lower than those obtained at semi-continuous laboratory scale (Test 3, Section 4.3), and lower than the yields expected from literature

findings under similar operative conditions (Table 4, Section 2.4.3), suggesting the need for further improvements in either operative parameters or reactor configuration. Regarding the valorization of the Dark Fermentative Effluent (DFE) generated during DF processes, the coupling of the system with Anaerobic Digestion (AD) (Test 4, Section 4.4) and PF (Test 5 and Test 6, Section 5.1 and 5.2) was investigated. The integration of DF and AD processes was relatively straightforward and presented no significant challenges, primarily due to the long HRT (17.5 – 23.3 d) and low OLR (0.7 – 1.0 $kg_{TVS}$ $m^{-3}$ $d^{-1}$) applied in the AD phase. This resulted in an SMP of 270 ± 50 $NL_{CH4}$ $kg_{TVS}^{-1}$, consistent with the yield achieved in literature for similar processes. Yet, the relatively low GPR (360 ± 100 NL $m^{-3}_{reactor}$ $d^{-1}$) suggested that the process integration may be further optimized, especially by managing the employed operative volumes to increase the OLR in the AD phase. Coupling DF with PF (**Chapter 5**) proved to be a feasible strategy for valorizing the DFE. However, relying on wild-type Purple Phototrophic Bacteria (PPB), despite enhanced growth kinetics being observed, hindered the conversion of residual organic compounds present in the DFE into hydrogen (Test 5, Section 5.1). This outcome was mainly attributed to the high ammonium concentration in the DFE, which inhibits nitrogenase, the key enzyme responsible for photofermentative hydrogen evolution. Given this result, mutated strains of *Rhodopseudomonas palustris* were investigated to enhance photofermentative hydrogen production (Test 6, Section 5.2). The tested mutations, including uptake hydrogenase deletion, constitutive activation of nitrogenase, and the removal of RuBisCO and phosphoribulokinase enzymes, led to improved photofermentative performances. The highest conversion efficiency was observed in *Rps. palustris* CGA4017, which carried all the abovementioned mutations. Hydrogen production despite high ammonium concentrations presents a promising strategy for improving DF-PF integration. The subsequent conversion of hydrogen into methane through biological methanation (**Chapter 6**) was found technically feasible using both suspended and immobilized biomass (Test 7, Section 6.1). While the achieved Specific Hydrogenotrophic Methanogenic Activity (SHMA) for suspended biomass (1.1 – 2.3 $mg_{CH4(COD)}$ $g_{VSS}^{-1}$ $h^{-1}$) aligns with the values reported in the literature, the lower results observed for granular sludge (0.8 – 2.0 $mg_{CH4(COD)}$ $g_{VSS}^{-1}$ $h^{-1}$, compared to literature values of 10 – 30 $mg_{CH4(COD)}$ $g_{VSS}^{-1}$ $h^{-1}$) suggest the process could be

further optimized. Valuable strategies for enhancing biological methanation yields, such as improving the gas-liquid mass transfer and adjusting the ratio between the fed substrate and the microorganisms, could be evaluated in future experiments.

The activities conducted over three years aimed to assess the scalability of a DF process treating organic waste and to evaluate potential integration routes with other biological processes, such as AD, PF, or BM. While all processes have proven to be feasible, further research is required before applying the integrated system at a pilot or industrial scale. Using FW and WAS as co-substrates emerged as a promising approach for biological hydrogen production, as it allows tuning the organic loading rate of the system while balancing its buffer capacity. Additionally, their year-round availability supports the feasibility of scaling up the process. However, the heterogeneity and seasonal variability of municipal FW may pose some constraints on this application, potentially hindering the long-term stability of the process. Additionally, the proliferation of hydrogen-consuming microorganisms requires further investigation to develop strategies to minimize their impact on process yield. When the system is coupled with a PF process, DFE can be further converted into hydrogen, enhancing overall process yield due to the high efficiency of PPB in converting organic acids into hydrogen at near-theoretical yields, especially when mutated strains are used. However, in the perspective of process industrialization, several factors strongly affect feasibility and require a thorough techno-economic evaluation. While pure mutated PPB strains enhance production yields, the gains may not justify the costs of DFE sterilization, necessary to maintain axenic conditions in the PF reactor, or the increased system complexity required to manage mutated strains and prevent their accidental release into the environment. Moreover, despite artificial lighting being a useful tool for laboratory scale applications, it is not a viable option for industrial use due to severe economic and energy costs that are incompatible with hydrogen production. Alternatively, integrating DF and PPB systems to generate alternative byproducts could be considered, potentially focusing on high-value products such as carotenoids, coenzyme Q10 (CoQ10) and 5-aminolevulinic acid (5-ALA); thus, justifying the higher operative costs associated with DFE pretreatment and artificial lighting.

Producing hydrogen through sustainable methods opens the possibility of converting it into bio-methane, promoting carbon dioxide conversion into an energy-rich fuel. In this regard, bio-methanation offer a valuable alternative to catalytic processes, as it can utilize non-highly pure gases such as the ones produced through DF and PF. However, DF produces a gas that, under optimal reaction conditions, already contains 50 – 60 % carbon dioxide. Therefore, relying on this gas stream for carbon dioxide bio-methanation presents two main challenges: first, its hydrogen content must be increased to meet the 4:1 molar ratio required for optimal conversion yields; and second, its utilization for exogenous carbon dioxide conversion would require purification pretreatment steps, as it already contains excess carbon dioxide, undermining the cost and energy efficiency of the process. This limitation may be less significant when the process is coupled solely with PF, as it can produce a gas with substantially higher hydrogen and lower carbon dioxide content, allowing for the addition of exogenous carbon dioxide to meet bio-methanation stoichiometric requirements. However, further research should focus on determining the optimal operative parameters and reactor configurations; thus, to maximize process yields and enable system scale-up.

# 8. Acknowledgements

I would first like to thank my supervisor, Prof. Cristina Cavinato, for guiding me through various research activities from my master's degree to the conclusion of this PhD project, which she has supervised with interest in all these years.

I would also like to thank the GreenPropulsion Laboratory of VERITAS spa for their collaboration, and in particular Dr. Graziano Tassinato for his insightful suggestions, as well as Francesco Nisato and Margherita Turatello for their kind support.

My sincere thanks go to the revisors of this thesis, Prof. David Bolzonella and Prof. Lorenzo Bertin, for their valuable scientific contributions to this work.

This work was partially developed within the Purple-B project (contract No. 4000137190), "Purple-B: Hydrogen production from immobilized cells in photo-bioreactors", funded by the European Space Agency (ESA), and within the MODSEN project (contract No. CSEAB_00364), "MODel of Saving ENergy from organic waste fermentation" Funded by MITE, Ministry of the Ecological Transition.

As part of this PhD, I participated in several knowledge-exchange activities promoted by the COST Action PurpleGain, which allowed me to deepen my understanding of photofermentative processes and connect with peer researchers who significantly contributed to my scientific and personal growth. During one of these events, I had the pleasure of meeting Prof. Alessandra Adessi, who later kindly hosted and supervised me for a couple of months at the Dipartimento di Scienze e Tecnologie Agrarie, Alimentari, Ambientali e Forestali (DAGRI) of Università degli Studi di Firenze. A sincere thanks is also addressed to Prof. J.B. McKinlay of the University of Indiana Bloomington (USA), for kindly providing the *Rhodopseudomonas palustris* CGA4001, CGA4003, and CGA4017 strains.

I thank all my colleagues at the Università Ca' Foscari di Venezia, with whom I shared the difficulties and joys of everyday life in the office and laboratory.

Last, but not least, a special thanks to my family and friends for their love, presence, and support throughout this journey.